THE ROLE OF CYTOKINE SIGNALLING, CELLULAR SENESCENCE AND ITS SECRETORY PHENOTYPE IN NORMAL PITUITARY DEVELOPMENT AND TUMOURIGENESIS

By

José Mario González Meljem

Thesis submitted to University College London for the degree of

Doctor of Philosophy

2017

Developmental Biology and Cancer Programme

GOSH-UCL Institute of Child Health

University College London

DECLARATION

I, José Mario González Meljem confirm that the work presented in this thesis is my own. Where information has been derived from other sources, I confirm that this has been indicated in the thesis.

Jose Mario Gonzalez Meljem

UCL student number 110052843

ABSTRACT

Oncogene-induced senescence (OIS) is classically described as a potent anti-tumourigenic barrier that restrains the proliferation of pre-malignant cells. Senescent cells can also promote immune clearance by secreting a plethora of chemokines and inflammatory factors, collectively known as the Senescence-Associated Secretory Phenotype (SASP). However, the SASP can also promote tumourigenesis paracrinally. In this study, OIS and the SASP were studied in mouse models for adamantinomatous craniopharyngioma (ACP), which express oncogenic β-catenin in pituitary progenitors/stem cells. Surprisingly, oncogenic β-catenin-targeted cells did not give rise to the tumour mass in the majority of cases and stopped dividing after a short burst of proliferation to form β-catenin-accumulating cell clusters. Here it is demonstrated that β-catenin clusters undergo OIS as determined by a lack of proliferation markers, activation of the p53/p21 and p16/Rb pathways, induction of the DNA damage response (DDR) and activation of the NF-κB pathway. Additionally, unbiased mRNA expression analysis shows enrichment of OIS and SASP genes in β-catenin clusters, while SASP gene expression is corroborated by qRT-PCR and ELISA assays. Of translational significance, these results are recapitulated in the β-catenin clusters of human ACP. Furthermore, evidence is presented indicating that the paracrine signals secreted by the β-catenin clusters are involved in non-cell autonomous tumourigenesis through modification of their microenvironment and the recruitment of endothelial progenitors displaying aberrant SOX9 expression. A genetic strategy demonstrated that induction of OIS and the SASP in the clusters is p53-independent, but that p53 is required to prevent a full bias for cell-autonomous tumourigenesis. Finally, a mouse line that also develops β-catenin clusters, albeit with a dampened SASP is described. These clusters do not appear to modify their microenvironment and tumours do not develop. Together, the mouse and human data suggest that senescence and SASP are likely to modify the tumour microenvironment resulting in cell transformation, tumour growth and survival.

ACKNOWLEDGEMENTS

My most sincere gratitude goes to Prof. JP Martinez-Barbera, for accepting to guide me as supervisor more than once and for teaching me what true passion for science and perseverance are about. I am proud for having been part of his lab, and for surviving it. Special thanks go to Dr. Cynthia L. Andoniadou, my third supervisor, who initiated me in the lab and endured the worst of my scientific naivety, but always provided much needed personal guidance and scientific advice.

I do not have words for expressing how grateful I am for beginning and ending this adventure alongside Sara Pozzi and Gabi Carreno, and for being the crazy-but-adorable sisters that I never had. I also thank here my big brother, Dr. Jean-Marie Delalande. I will not forget all that sixty-year-old wisdom of yours, "that's a fact". Thank you all three for all the kindness you have given me and for all the happiness that we have shared together.

I would like to thank current and past members of the JP lab for all their help and for creating a much-needed environment of laughter and dark humour.

I am also grateful to my funding bodies: the Mexican National Council for Science and Technology (CONACYT) and the Bank of Mexico-FIDERH fund.

This work is dedicated to my family: Mario Hugo, María, José Manuel and José Flavio, for being my inspiration to become better every day. I will always be grateful for all the love and support you have given me. Especially my parents, describing all the things they have done to help me get me here would cover another chapter of this thesis. Thank you from the bottom of my heart.

TABLE OF CONTENTS

LIST OF FIGURES

LIST OF TABLES

ABBREVIATIONS

α-Gsu	α-Glycoprotein subunit
ACC	Agenesis of corpus callosum
ACP	Adamantinomatous craniopharyngioma
AP	Anterior pituitary
APH	Anterior pituitary hypoplasia
AVE	Anterior visceral endoderm
AVP	Arginine vasopressin
BB	Basisphenoid bone
BCIP	5-bromo-4-chloro-3-indolyl-phosphate
BMP	Bone morphogenic protein
bp	Base pairs
BrdU	Bromodeoxyuridine
CPHD	Combined pituitary hormone deficiency
CS	Carnegie stage
CSC	Cancer stem cell
DAB	Diaminobenzidine
DAPI	4',6-diamidino-2-phenylindole
DDR	DNA-damage reponse
DIG	Digoxigenin
dpc	Days post coitum
DPEC	Diethylpyrocarbonate
EDTA	Ethylenediaminetetraacetic acid
EdU	5-ethynyl-2'-deoxyuridine
EMCN	Endomucin
EPP	Ectopic posterior pituitary
FCS	Fetal calf serum
FGF	Fibroblast growth factor
FSH	Follicle-stimulating hormone
GFP	Green fluorescent protein
GH	Growth hormone
Hesx1	Homeobox expressed in ES cells 1
HPA	Hypothalamic-pituitary axis
IGHD	Isolated growth hormone deficiency
IL	Intermediate lobe of the pituitary

INF	Infundibulum
LH	Luteinising hormone
mTOR	mechanistic target of rapamycin
NBT	Nitro-blue tetrazolium chloride
NF-κB	Nuclear factor kappa-light-chain-enhancer of activated B cells
OE	Oral ectoderm
OIS	Oncogene-induced senescence
OT	Oxytocin
PBS	Phosphate-buffered saline
PBT	PBS containing Triton-X-100
PCP	Papillary craniopharyngioma
PCR	Polymerase chain reaction
PFA	Paraformaldehyde
POMC	Proopiomelanocortin
PL	Posterior lobe of the pituitary
PRL	Prolactin
RP	Rathke's pouch
SA-β-Gal	Senescence-associated β-galactosidase
SASP	Senescence-associated secretory phenotype
SC	Stem cell
SDF-1	Stromal cell-derived factor 1
SHH	Sonic hedgehog
SIPS	Stress-induced premature senescence
SOD	Septo-optic dysplasia
SOX	Sry-related box
TP53	Tumour suppressor p53
TSH	Thyroid-stimulating hormone
VD	Ventral diencephalon
YFP	Yellow fluorescent protein

1. GENERAL INTRODUCTION

1.1 The pituitary gland

1.1.1 Function and components of the pituitary gland

The pituitary gland, or hypophysis, is a crucial component of the mammalian endocrine system. It relays signals emitted from the hypothalamus, the brain's homeostatic control centre, by secreting various hormones that regulate functions of great importance for the organism such as: growth, metabolism, stress-response, sexual maturation and reproduction (Shlomo Melmed 2011). The hypothalamus is responsible for processing and balancing the demands of these ever-changing biological processes, which lead to the controlled release of hypothalamic factors into the hypophyseal portal blood vessel system. These vessels carry the hypothalamic factors into the pituitary gland where they regulate the release of the pituitary hormones into the systemic circulation. The pituitary hormones can act then either systemically or on specific target organs (adrenals, thyroid gland and gonads), which provide regulatory feedback directly to the pituitary or indirectly into the hypothalamus (Perez-Castro et al. 2012). This complex, yet finely tuned system is called the hypothalamic-pituitary axis (HPA) and is of mayor relevance for medical research as congenital defects or disease affecting any point of the axis will often result in pleiotropic detrimental effects (Denef 2008; Ward et al. 2006).

Anatomically, the pituitary gland is comprised by three distinct structures (Figure 1.1):

1) The anterior lobe (AL) or adenohypophysis, which contains most of the endocrine cells. The pituitary hormones produced in this structure are: growth hormone (GH), prolactin (PRL), adrenocorticotropic hormone (ACTH), thyroid-stimulating hormone (TSH), follicle-stimulating hormone (FSH) and luteinizing hormone (LH) and they are produced by somatotrophs, lactotrophs, corticotrophs, thyrotrophs and gonadotrophs, respectively.

2) The intermediate lobe (IL), which separates the anterior and posterior pituitary lobes. This structure is poorly developed and rudimentary in humans but in mice and other vertebrates it contains a subpopulation of melanotrophs, which produce melanocyte-stimulating hormone (MSH) (Saland 2001).

3) The posterior lobe (PL) or neurohypophysis, which contains axons originated in the hypothalamus that deliver the neurohormones vasopressin (VPN) and oxytocin (OXT) directly into the pituitary circulation (Markakis 2002). The posterior lobe also contains glial cells known as pituicytes.

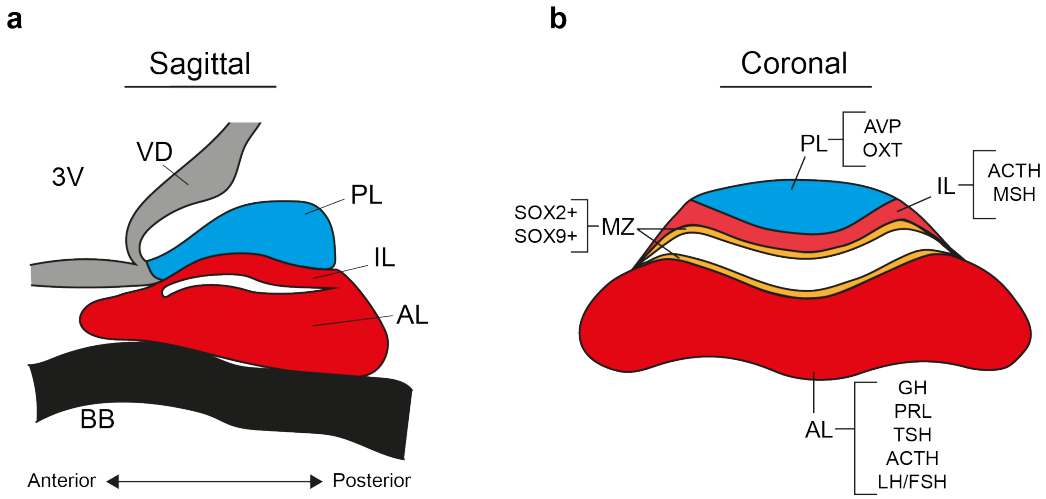

Figure 1.1 Components of the murine pituitary gland.

(a) Representation of the murine pituitary gland and surrounding structures as seen from a sagittal plane (antero-posterior axis). The mature gland lies on top of the basisphenoid bone (BB), below the third ventricle (3V) and the ventral diencephalon (which comprises the hypothalamus). Axons from the hypothalamus directly innervate the posterior lobe (PL). The glandular portion of the pituitary is comprised of the intermediate lobe (IL), which is directly in contact with the PL; and the anterior lobe (AL), which lies on top the BB. **(b)** Coronal representation of the pituitary gland showing the location of different neuroendocrine populations. The PL contains axons derived directly from arginine-vasopressin (AVP) and oxytocin (OXT) producing neurons in the hypothalamus. The IL contains a subpopulation of melanotrophs. The AL contains most of the endocrine cells, namely: somatotrophs, lactotrophs, corticotrophs, thyrotrophs and gonadotrophs. The region of cells lining the lumen of the AL and IL is known as the marginal zone (MZ) and is rich in progenitor cells

expressing stem cell markers such as SOX2 and SOX9. 3V: third ventricle; VD: ventral diencephalon; PL: posterior lobe; IL: intermediate lobe; AL: anterior lobe; BB: basisphenoid bone; AVP: arginine-vasopressin; OXT: oxytocin; ACTH: adrenocorticotropic hormone; MSH: melanocyte-stimulating hormone; GH: growth hormone; PRL: prolactin; TSH: thyroid-stimulating hormone; LH: luteinizing-hormone; FSH: follicle-stimulating hormone; MZ: marginal zone.

1.1.2 Development of the pituitary gland and its components

Morphogenesis of the pituitary gland

Figure 1.2 describes the process of pituitary organogenesis, which begins in mice around 8.5 dpc (days *post coitum*), as a thickened patch of oral ectoderm, which invaginates towards the brain above it, the future ventral diencephalon (VD) (Castinetti et al. 2011). By 10.5 dpc, the pituitary primordium displays a distinctive lumen and is therefore called Rathke's Pouch (RP). In the following days, this structure migrates passively in close contact with a region of the future ventral diencephalon which thickens and forms the PL primordium, known as the infundibulum (IF). By 12.5 dpc, RP has separated completely from the oral ectoderm and its ends have fused creating a closed pouch with clear separation between its dorsal (future IL) and ventral (future AL) regions. The closed lumen is then called the pituitary cleft, and in mice is delimited dorsally by the IL and ventrally by the AL (Hashimoto et al. 1998). For both the IL and the AL, cells directly facing the pituitary lumen are referred to as the marginal zone (MZ) or periluminal region. The MZ contains progenitor cells that will divide continuously in the following days of development, giving rise to committed precursor cells that migrate (ventrally in the case of the AL) and will eventually differentiate between 13.5 and 16.5 dpc into the hormone-producing populations (Garcia-Lavandeira et al. 2009; Florio 2011). Finally,

by 18.5 dpc, the pituitary gland contains all hormone-producing cell types (Bilodeau et al. 2009).

Morphogenic ligands directing pituitary organogenesis

Proper patterning and specification of the pituitary has been shown to depend on signalling cues provided by neighbouring structures such as the VD, the surrounding mesenchyme and the oral ectoderm. These tissues provide crucial factors known as morphogens, which exhibit specific spatio-temporal expression patterns. These factors can then either act directly on the pituitary lineage, by controlling the timely expression of transcription factors responsible for maintaining pools of progenitors/stem cells or controlling their commitment and differentiation into distinct endocrine populations (Kelberman et al. 2009); or they can act indirectly by restricting the expression domains of other morphogenic ligands (Zhu et al. 2007). Examples of these morphogens are Sonic Hedgehog (SHH), Bone Morphogenic Proteins (BMPs), Fibroblast Growth Factors (FGFs) and Wingless-related Integration site proteins (WNTs) (Takuma et al. 1998; Treier et al. 1998; Treier et al. 2001; Potok et al. 2008).

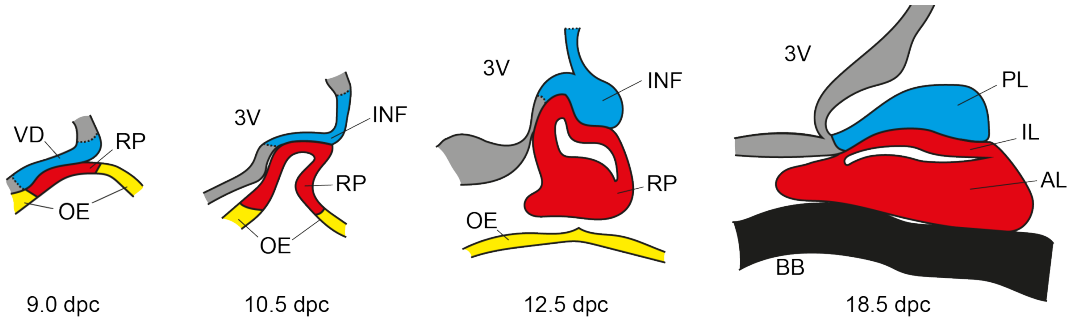

Figure 1.2 Development and components of the pituitary gland.

Sagittal representation of the developing pituitary gland at different embryonic stages. At 9.0 dpc a portion of oral ectoderm (OE) diverges in fate after establishing close contact with the future ventral diencephalon (VD). At 10.5 dpc, the pituitary anlage,

Rathke's Pouch (RP), has begun evaginating from the OE and migrates towards the brain. At the same time, the region of the VD in contact with RP has invaginated in order to form the infundibulum (INF). By 12.5 dpc, the future components of the mature gland can be discerned. RP has separated from the OE and formed a definite pouch displaying a lumen. The dorsal region in contact with the INF will become the IL while the ventral region will become the AL. By 18.5 dpc, the mature components of the pituitary gland have been established. Image adapted from (Kelberman et al., 2009). 3V: third ventricle; VD: ventral diencephalon; RP: Rathke's pouch; OE: oral ectoderm; INF: infundibulum; PL: posterior lobe; IL: intermediate lobe; AL: anterior lobe; BB: basisphenoid bone.

1.1.3 Pituitary embryonic progenitors and stem cells

The pituitary gland is responsible for the maintenance of the organism's endocrine homeostasis as it is challenged by ever-changing physiological demands. Therefore, the mammalian pituitary has evolved mechanisms for outstanding adaptability and plasticity. In the pituitary and other organs, it is now well established that the maintenance of homeostatic cell turnover is highly dependent on a particular cell population with special characteristics, referred to as stem cells.

The most accepted definition for stem cells establishes they are un-differentiated, possess the ability to self-renew (i.e. divide indefinitely) and can give rise to the differentiated cell types of their respective organ or tissue (i.e. they are multipotent). The latter occurs by asymmetric division, which gives rise to one identical stem cell and a progenitor daughter cell with restricted potential (i.e. short or absent self-renewal) but capable of differentiating into committed cell lineages (Vankelecom 2010; Seaberg & Van Der Kooy 2003). Therefore, their multipotentiality and self-renewal characteristics promote replenishment the organ's functional populations according to physiological demands and also allow the maintenance of a tissue's stem cell pool.

Tissue-specific stem cells have been shown to often share the expression of defined transcription factors and markers with the embryonic progenitors that gave rise to the organ during development (Slack 2008). However, if long-term self-renewal has not been demonstrated convincingly, the terms “progenitor” or “progenitor/stem cell” are to be used to define such populations (Vankelecom & Gremeaux 2010).

HESX1+ embryonic progenitors of the pituitary gland

A number of transcription factors have been demonstrated to define the identity of pituitary embryonic progenitor/stem cells (Florio 2011; Vankelecom 2010; Rizzoti 2015). Such is the case of the homeo-box transcription factor *Hesx1* (homeobox expressed in ES cells 1), a gene mostly known for its role in proper forebrain patterning (Andoniadou et al. 2011). However, *HESX1* has been shown to be crucial for proper pituitary development in both mice and humans, where mutations in this gene leads to syndromes characterised by hypopituitarism (Dattani et al. 1998; Kelberman et al. 2006; Jayakody et al. 2012; Sajedi et al. 2013; Gaston-Massuet et al. 2011). Although initially expressed in the anterior-visceral endoderm (AVE) at 6.5 dpc, *Hesx1* is later detected in the anterior neural ectoderm (prospective forebrain) from 7-8.5 dpc, while from 8.5 dpc it is also expressed in the oral ectoderm. Importantly, *Hesx1* is expressed in RP progenitor cells from 8.5 to 13.5 dpc (Thomas et al. 1996; Hermesz et al. 1996). Furthermore, lineage-tracing experiments demonstrated that most cells in the mature pituitary gland (by 18.5 dpc) were derived from the *Hesx1* lineage (Gaston-Massuet et al. 2011; Jayakody et al. 2012). Therefore, *Hesx1* is expressed in embryonic pituitary progenitors, which give rise to all pituitary cells.

SOX2 and SOX9 in pituitary embryonic progenitors and adult stem cells

Other transcription factors of crucial importance for pituitary development are the members of the SOX-family of proteins (SRY-region), specifically members of the SOXB1 group: SOX1, SOX2 and SOX3. SOXB1 factors are known for their importance for the early embryonic development and pluripotency in embryonic stem cells (ESC). Importantly, SOXB1 proteins play important roles during organogenesis by maintaining an undifferentiated phenotype, multipotency and proliferation in progenitor/stem cells in various organs, particularly in the central nervous system (CNS) (K. Liu et al. 2013; Zhang & Cui 2014).

SOX2 is the only SOXB1 member expressed early in pituitary development, and its expression can be observed from 9.5 dpc in pituitary embryonic progenitors (Rizzoti 2015). However, SOX2 is downregulated in differentiating cells that commit to different endocrine lineages. As lineage commitment proceeds, SOX2 expression becomes restricted until the majority of SOX2+ cells become restricted to the periluminal region (or MZ), an expression pattern that is conserved postnatal life. Importantly, absence of SOX2 in *Hesx1*+ embryonic progenitors leads to aberrant pituitary development due to depletion of the pool of progenitor cells (Jayakody et al. 2012).

There is a considerable amount of evidence showing that the adult pituitary gland contains cells that fulfil the definition of stem cells. Although these populations have been isolated and identified by different methods, they share characteristics like the capacity to grow in culture and be passaged multiple times, as well as the ability to differentiate into all or several hormone-producing cell populations (Florio 2011; Vankelecom 2010). Moreover, these pituitary stem cells also share the expression of certain markers, such as SOX2 (Gleiberman et al. 2008; Fauquier et al. 2008; Garcia-Lavandeira et al. 2009; Chen et al. 2009). This SOX2+ population was shown to expand and replenish the organ's cells after pituitary injury (Fu et al. 2012) or in

response to physiological demand (Rizzoti et al. 2013). Additionally, *in vivo* long-term lineage tracing revealed that SOX2+ cells are able to self-renew and differentiate into all hormone-expressing cell populations in the adult pituitary gland (Andoniadou et al. 2013).

Another SOX transcription factor of importance for pituitary development is SOX9, a member of the SOXE group. SOX9 is a transcription factor known to regulate cell fate and differentiation in several organs during embryogenesis, such as the male gonads, the skeleton, cardiac-valves and intestine (Sun et al. 2013; Huang et al. 1999; Ikeda et al. 2004; Hattori et al. 2010; Akiyama et al. 2004; Moniot et al. 2004). SOX9 has been shown to play context-dependent roles within progenitor/stem cell populations (Joa et al. 2012). In the hair-follicle, SOX9 was demonstrated to be indispensable for the formation and maintenance of the follicle's stem cell niche (Adam et al. 2015); and a similar role for SOX9 was found in the maintenance of pancreatic progenitor cells (Seymour et al. 2007). Conversely, in the developing CNS it has been shown that SOX9 regulates neural progenitor cell fate and guides differentiation towards gliogenesis (Stolt et al. 2003; Kang et al. 2012). Additionally, upregulation of SOX9 expression in neural crest (NC) cells after delamination has been revealed to be necessary for their epithelial-mesenchymal transition (EMT) and subsequent migration (Cheung & Briscoe 2003; Theveneau & Mayor 2012).

In the developing pituitary gland, SOX9 is coexpressed with SOX2 from 14.5 dpc. Its expression is thought to coincide with switch from embryonic progenitor cell proliferation towards a more quiescent state (Castinetti et al. 2011). Postnatally, SOX2 expression mostly colocalises with SOX9, including in MZ cells. Additionally, long-term lineage tracing of adult SOX9 cells showed they also differentiate into hormone producing cells throughout life (Rizzoti et al. 2013). Finally, SOX2+/SOX9+ cells have been shown to possess *in vitro* clonogenic potential and the capacity to differentiate into all hormone-producing cell types both *in vivo* and *in vitro* (Fauquier

et al. 2008; Rizzoti et al. 2013; Andoniadou et al. 2013), further suggesting that the SOX2+/SOX9+ population represents *bona fide* adult pituitary stem cells.

1.1.4 Pituitary disease and tumours

Proper pituitary development depends on correct patterning, cell lineage commitment and maintenance of pituitary progenitor/stem cells, all which are determined by interactions between developmental transcription factors (e.g. HESX1, LHX3/4, PITX1/2, PROP1) and signalling pathways (e.g. SHH, WNT, BMP and FGF). Mutations or dysregulation in these genes and/or pathways have been shown to be the cause of pituitary-related conditions of great relevance for paediatric clinical research (described in Table 1), such as: congenital hypopituitarism, septo-optic dysplasia and pituitary tumours (Davis et al. 2009). This knowledge derives in part from expression and sequencing studies in human biopsies or functional experiments in human pituitary cell lines. However, a detailed understanding of the role that these genes and pathways play *in vivo during* pituitary development and the underlying biological mechanisms, could not have been achieved without the use of animal models, particularly genetically engineered mice (Kelberman et al. 2009; Zhu et al. 2007).

The field of pituitary oncology has particularly benefited from the use of genetically modified mouse models. A considerable number of strains has been demonstrated to be useful for the study of pituitary tumours, mostly pituitary adenomas, and this has led to the identification of genes and pathways involved in pituitary adenoma pathogenesis (Cano et al. 2014; Lines et al. 2016), as well as the identification of cancer stem cells (CSCs) in pituitary tumours (Martinez-Barbera & Andoniadou 2016). Table 2 summarises both the syndromic effects of pituitary hormone dysfunction as well as the types of pituitary adenomas arising from each cell type.

Gene	Protein	Murine loss LOF phenotype	Human phenotype	Inheritance murine/human
HESX1	HESX1	Anopthalmia or microopthalmia, Agenesis of corpus callosum (ACC), abscence of septum pellucidum, pituitary dysgenesis or aplasia	Variable. Septo-Optic dysplasia , Combined Pituitary Hormone Deficiency (CPHD), Isoleted Growth Hormone Deficiency (IGHD) with Ectopic Posterior Pituitary (EPP)	Dominant or recessive un humans, recessive in mouse
OTX2	OTX2	Forebrain or midbrain abscence, malformation of optic placode	Anopthalmia, Anterior Pituitary Hypoplasia (APH), EPP, Absent Infundibulum	Heterozygous: haploinsifficiency/dominant negative
SOX2	SOX2	Homozygous null: emyronic lethal Heterozygous or hemizygous: poor growth, reduced fertility, CNS abnormalities, anopthalmia, pituitary hypoplasia with all cell types affected	Hypogonadotrophic Hypogonadism, APH, Abnormal hippocampus, bilateral anophtlamia/micropthalmia, abnormal corpus callosum, learning difficulties, esophageal atresia, hearing loss, hypothalamic hamartoma	*De novo* haploinssuficiency in humans, heterozygous mutation associated with haploinssuficiency in mouse
SOX3	SOX3	Poor growth, craniofacial abnormalities, hypothalamic and infundibular abnormalities	IGHD and mental retardation, hypopituitarism, aph, Infundibular hypoplasia, EPP, midline abnormalities	X-linked recessive in both mice and humans
GLI2	GLI2	Pituitary hypoplasia	Holoprosencephaly, hypopituitarism, craniofacial abnormalities, polydactily, partial ACC	Haploinssuficiency
LHX3	LHX3	Hypoplasia of Rathke´s Pouch	Pituitary hypoplasia with GH, TSH and gonadotropin deficiency. Variable ACTH inssuficiency. Hearing loss. Short, rigid cervical spine.	Recessive in both
LHX4	LHX4	Mild hypoplasia of anterior pituitary lobe	GH, TSH and cortisol deficiency, Persistent cranioharyngeal canal and abnormal cerebellar tonsils, APH, ectopic posterior pituitary, absent infundibulum	Recessive in mouse, dominant in human
PROP1	PROP1	Hypoplasia of anterior pituitary lobe. Affected cell types: GH, PRL, TSH, ACTH, LH and FSH	GH, TSH, PRL, and gonadotropin deficiency. Evolving ACTH deficiency. Enlarged pituitary with later involution	Recessive in both
POU1F1	PIT1	Hypoplasia of anterior pituitary lobe. Affected cell types: GH, PRL, and TSH	Variable posterior pituitary hypoplasia with GH, TSH and PRL deficiency	Recessive in mouse, dominant/recessive in humans

Table 1. Genes involved in pituitary developmental syndromes in mice and humans

Adapted from Kelbermann 2009.

Cell types	Hormone Product	Target		Regulator		Hypopituitarism phenotype	Types of pituitary tumour	Tumour clinical features	Tumour transcription factor expression
		Tissue	Response	Positive	Negative				
Posterior lobe									
Magnocellular	AVP	Kidney	Water reabsorption	Hypovolemia	Hyperosmolarity	Diabetes Insipidus			
Magnocellular	OT	Mammary gland, uterus	Mik-let down, contractions	Suckling	Progesterone	Hypogalactorrhea	-	-	-
Pituicytes (glial cells)	-	-	-	-	-	-	Pituicytomas	Diabetes insipidus, hypopituitarism, visual impairment	-
Intermediate lobe									
Melanotrophs	MSH	Pleiotropic functions	-	-	-	-	Not reported in humans	-	-
Anterior lobe									
Somatotrophs	GH	Liver, kidneys, most tissues	Growth	GHRH	SS	Dwarfism	Somatotropinomas	Acromegaly or gigantism	PIT1
Thyrotrophs	TSH	Thyroid gland	Thyroid hormone (T3, T4)	TRH	Thyroid hormone (T3, T4)	Thyroid hypoplasia, dwarfism, cretisnism, hypothyroidism	Thyrotropinomas	Hyperthyroidism	STF1, GATA2
Lactotrophs	PRL	Mammary gland	Milk production	Oestrogen, TRH	Dopamine	Hypogalactorrhea	Lactotropinomas	Hypogonadism and/or galactorrhea	PIT1
Corticotrophs	ACTH	Adrenal cortex	Glucorticoid production	CRH	Corticosteroids	Adrenal hypoplasia	Corticotropinomas	Cushing disease, hypopituitarism, pituitary hyperplasia	TPIT
Gonadotrophs	LH, FSH	Gonads	Spermatogenesis, ovulation	GnRH	Gonadal steroids	Sexual immaturity, infertility	Gonadotrophic adenomas and null cell adenomas	Silent or pituitary failure	PIT1

Table 2. Pituitary cell types, their biological functions and pathological phenotypes.

Adapted from Watkins-Chow and Camper, 1999 and Melmed 2011.

1.2 Adamantinomatous craniopharyngioma (ACP) and mouse models of ACP

1.2.1 Pathophysiology of human ACP

In addition to pituitary adenomas, there are other two classes of pituitary tumours: Rathke´s cleft cysts and craniopharyngiomas, while the latter can be further divided into papillary and adamantinomatous subtypes. Similar to pituitary adenomas, Adamantinomatous Craniopharyngiomas (ACPs) are non-malignant epithelial tumours, but do not express any pituitary hormones or differentiation markers such as PIT1 and synaptophysin. Despite their low incidence (1.6 cases/million per year for all ages and 2.14 for children), ACPs are the most common non-neuroepithelial intracranial neoplasm in children and represent up to 11.5% of all paediatric CNS tumours (Bunin et al. 1998; Müller 2014). The mean age at diagnosis displays a bimodal distribution, being around 10 years of age for childhood-onset ACP and 74 years for adult-onset ACP (Nielsen et al. 2011). The paediatric and adult manifestations of the disease are not yet considered to differ in terms of treatment of choice, post-treatment survival rates, post-surgical effect on quality of life or recurrence (Nielsen et al. 2011; Dekkers et al. 2006; Zoicas & Schöfl 2012). Despite high survival rates (up to 95% in 5 years), ACPs are considered to be aggressive tumours with high morbidity potential due to the invasion of surrounding brain structures such as the optic tract and hypothalamus (Müller 2013). Additionally, detrimental post-operative effects are frequent and can lead to clinical complications such as onset of hypothalamic obesity (Müller et al. 2004). Therefore, ACP represents a chronic and clinically-challenging disease for which no targeted molecular therapies are currently available (Lughetti & Bruzzi 2011; Müller 2013).

1.2.2 Aetiology and histopathology of human ACP

The aetiology of craniopharyngiomas is an ongoing research subject and the cell-of-origin giving rise to human ACP is currently not known. A longstanding hypothesis is that ACPs are tumours derived from embryonic remnants of Rathke's pouch, a proposition derived from the common expression of certain cytokeratins between the oral epithelium and ACP specimens (Kato et al. 2004; Buslei et al. 2007; Tateyama et al. 2001). The pathogenesis of childhood-onset ACP results particularly interesting as they represent 50% of all ACP cases and scrutiny of clinical data revealed that paediatric ACP patients suffer significantly from height deficit around 12 months of age, well before ACP diagnosis (Müller et al. 2004; Qi et al. 2013). Therefore, childhood-onset ACP is potentially a developmental tumour originating from Rathke's pouch. Further supporting this notion, the occurrence of foetal craniopharyngiomas has been reported in several occasions (Jurkiewicz et al. 2010; Joo et al. 2009; Scagliotti et al. 2015; Kostadinov et al. 2014) and a review of 154 cases of foetal CNS tumours found that 11% were diagnosed as craniopharyngiomas (Isaacs 2009).

ACPs have very distinctive histological features, which differentiate them from other pituitary neoplasms, including the papillary craniopharyngiomas subtype (PCP). ACPs are composed of squamous, epithelial non-differentiated cells that display a variety of histomorphological features: 1) an outer "palisaded epithelium" formed by tightly-packed columnar cells; 2) loosely connected cells in areas with microcystic changes, known as "stellate reticulum"; 3) areas formed by anucleated cell remnants (or "ghost cells") displaying eosinophilic keratinous bodies and occasional calcifications, collectively known as "wet keratin" (Figure 1.3).

The most notable histological feature of human ACP is the presence of nucleo-cytoplasmic β-catenin accumulating cells which form dense nodular structures known as "clusters" (Sekine et al. 2002; Kato et al. 2004; Gaston-Massuet et al. 2011)

(Figure 1.4a). This feature is a hallmark of the disease, as it is not present in PCPs nor in any other type of pituitary tumour and has been observed even in ACPs diagnosed *in utero* (Kostadinov et al. 2014; Scagliotti et al. 2015). Therefore, definitive diagnosis of ACP requires the immunohistochemical observation of nucleo-cytoplasmic accumulation of β-catenin, commonly found as tightly packed "clusters". It must be noted that these cell clusters comprise a very small proportion of the total tumour mass. Importantly, it is now widely accepted that activating mutations in the β-catenin gene (*CTNNB1*) are present in the vast majority of human ACP cases (up to 100% in some cohorts) (Sekine et al. 2002; Kato et al. 2004; Buslei et al. 2005; Brastianos et al. 2014; Oikonomou et al. 2005). These are somatic mutations located in exon 3, resulting in proteosomal degradation resistance that leads to β-catenin accumulation and consequent WNT pathway activation.

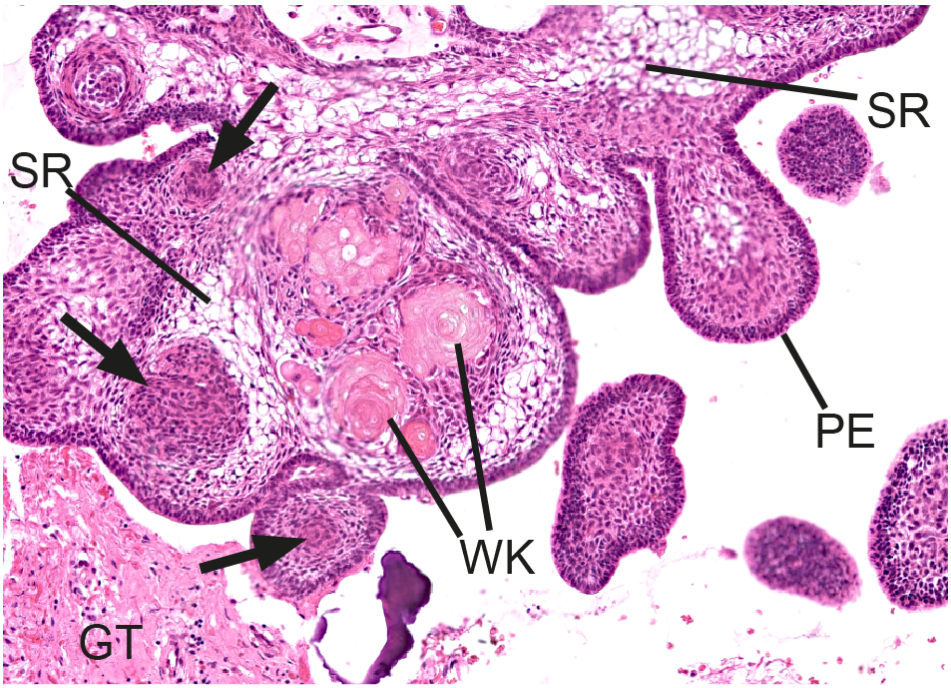

Figure 1.3 Histopathological features of human adamantinomatous craniopharyngioma (ACP).

Haematoxylin & eosin staining in a human ACP section showing distinctive features such as palisaded epithelium (PE) which separates the tumour tissue from the reactive glial tissue (GT) or cystic components. Within the tumour, other features are

observed such as a loosely connected stellate reticulum (SR) and anucleated ghost cells also referred to as wet keratin (WK). The presence of “whorls” or cell clusters (arrows) often close to the invasive front is also a hallmark characteristic of human ACP.

1.2.3 Malignant transformation of human ACP

The malignant transformation of ACP is extremely rare with only 23 cases reported in the literature (Rodriguez et al. 2007; Sofela et al. 2014; Negoto et al. 2015). While the acquisition of the malignant phenotype is based on histopathologic observations, there is a clear difference in the behaviour of these tumours, as median survival after transformation is around 6 months. Non-malignant ACPs are defined as slow growing tumours with a low content of proliferation markers such as Ki67 (Martinez-Barbera 2015; Buslei et al. 2007). Conversely, malignant ACPs display a drastic increase in Ki67 expression (50 to 70% of total cells) (Rodriguez et al. 2007; Sofela et al. 2014), while nucleo-cytoplasmic β-catenin immunoreactivity is observed throughout these tumours instead of being restricted to nodular cell clusters (Rodriguez et al. 2007). Interestingly, malignant ACPs also display increased expression of p53 protein, suggesting the presence of p53 mutations in these tumours (Kristopaitis et al. 2000; Rodriguez et al. 2007; Negoto et al. 2015). On the other side, non-malignant ACPs have been reported to contain a low proportion of p53+ cells while no mutations in the p53 gene (*TP53*) were found in some cohorts (Nozaki et al. 1998; Brastianos et al. 2014). Because it has been suggested that radiotherapy is a factor promoting the malignant transformation of ACP (Kristopaitis et al. 2000; Gao et al. 2011; Aquilina et al. 2010; Negoto et al. 2015), a better understanding of the molecular pathogenesis of ACP will prove crucial in the improvement of current treatment and development of safer therapeutic approaches.

1.2.5 Mouse models for ACP

An embryonic mouse model for ACP: *Hesx1$^{Cre/+}$;Ctnnb1$^{lox(ex3)/+}$* mice

Previously, it was reported that deletion of the exon 3 in the β-catenin gene (*Ctnnb1* in mice) produces a degradation-resistant form of β-catenin (also referred to as oncogenic β-catenin), which is able to accumulate and overactivate the WNT pathway (Harada et al. 1999). This genetic alteration is therefore functionally equivalent to the mutations found in human ACP. Importantly, conditional expression of this degradation-resistant form of β-catenin in pituitary embryonic progenitors (*Hesx1$^{Cre/+}$;Ctnnb1$^{lox(ex3)/+}$* mice) lead to WNT pathway overactivation and the formation of pituitary tumours (Gaston-Massuet et al. 2011). Conversely, expression of oncogenic β-catenin in committed pituitary progenitors or terminally differentiated hormone-producing populations did not lead to tumour formation, supporting a role for pituitary embryonic progenitors in WNT-driven pituitary tumourigenesis.

Hesx1$^{Cre/+}$;Ctnnb1$^{lox(ex3)/+}$ tumours partially resemble human ACP in their histology, as they possessed microcystic changes (stellate reticulum) and nodular, "whorl-like" cell formations. The murine tumour histology differs from their human counterparts in some features as they lack an overall epithelial morphology, the presence of a palisaded epithelium, wet keratin or calcifications. However, molecular characterisation of these tumours concluded that they most closely resemble human ACP, as judged the lack of pituitary hormone expression, presence of β-catenin accumulating clusters and absence of synaptophysin+ cells, a diagnostic marker of neuroepithelial tumours and pituitary adenomas (Gaston-Massuet et al. 2011).

However, the most interesting finding from this study was that *Hesx1$^{Cre/+}$;Ctnnb1$^{lox(ex3)/+}$* pituitaries contain the hallmark feature of ACP: the presence of nucleo-cytoplasmic β-catenin accumulating clusters (Figure 1.4b). These clusters can be observed in RP as early as 9.5 dpc, are present throughout pituitary

development and remain postnatally, before tumour formation. Another interesting finding from this study is that the β-catenin clusters from both *Hesx1*$^{Cre/+}$*;Ctnnb1*$^{lox(ex3)/+}$ pituitaries and human ACP are in a non-proliferative state as indicated by the absence of the proliferation marker Ki67. Additionally, murine clusters show absence of bromo-deoxy-uridine (BrdU) uptake and express cell cycle inhibiting proteins such as p27^{Kip1} and p57^{Kip2} at 18.5 dpc (Gaston-Massuet et al. 2011). This observation, together with the expression of the pituitary stem cell marker SOX2, initially led to the conclusion that the murine β-catenin clusters display a progenitor/stem cell phenotype characterised by a slow-dividing, quiescent state. Similar conclusions were derived from studies in which accumulation of the cell cycle inhibitor p21^{Cip1} was observed in human ACP β-catenin clusters (Buslei et al. 2007; Stache, Hölsken, Fahlbusch, et al. 2014), while Ki67+ cells were only observed in proximity to the clusters (Gaston-Massuet et al. 2011; Stache, Hölsken, Schlaffer, et al. 2014). Again, differences between mouse and humans exist as murine ACP clusters express SOX2, while their human counterparts do not.

Subsequently, microarray expression analysis comparing β-catenin-accumulating cells and non-cluster tissue was conducted after flow-sorting of dissociated *Hesx1*$^{Cre/+}$*;Ctnnb1*$^{lox(ex3)/+}$*;BAT-gal* pituitaries (Andoniadou et al. 2012). In this model, activation of the WNT signalling pathway in cluster cells leads to expression of bacterial β-galactosidase, which can then be detected by the addition of X-gal. Interestingly, the β-catenin cluster fraction showed a significant upregulation of members of several signalling pathways with important roles in carcinogenesis such as WNT, SHH, BMP, FGF and TGFβ (Labeur et al. 2010; Wesche et al. 2011; Yauch et al. 2008). These observations were corroborated by *in situ* hybridisation (ISH) and recapitulated in human ACP samples, suggesting the clusters act as a source of secreted pro-oncogenic factors that feed tumour growth in a paracrine manner. Additionally, this study also reported upregulation of the chemokine receptor

CXCR4 and several chemokines of the CXC- family in the β-catenin clusters (section 1.4).

An inducible model for ACP: *Sox2$^{CreERT2/+}$;Ctnnb1$^{lox(ex3)/+}$* mice

The finding that oncogenic β-catenin leads to cluster formation and consequent induction of pituitary tumours only when expressed in embryonic pituitary progenitors (e.g.not in committed cell types), suggested that cell "stemness" may be involved in the development of WNT-driven pituitary tumours. Tamoxifen-inducible expression of oncogenic β-catenin in SOX2+ stem cells (*Sox2$^{CreERT2/+}$;Ctnnb1$^{lox(ex3)/+}$;R26$^{YFP/+}$* mice) at embryonic and adult stages led to the formation of nucleo-cytoplasmic β-catenin clusters (Figure 1.4c) and the induction of pituitary tumours (Andoniadou et al. 2013). These tumours also resembled human ACP by the lack of pituitary hormone and synaptophysin expression, while the resulting β-catenin clusters were also negative for proliferation markers and overexpressed pro-oncogenic factors belonging to the SHH, WNT, BMP and FGF pathways. Importantly, this study also defined that the cell giving rise to β-catenin clusters in mice is a SOX2+/S100B+ stem cell.

Intriguingly, lineage tracing analysis revealed that the tumours were not derived from oncogenic β-catenin-targeted cells (labelled by YFP expression). While all tumours were negative for the reporter protein (YFP-), β-catenin accumulating clusters that were YFP+ could be observed in their vicinity. This unexpected result was corroborated by PCR analysis of laser-capture microdissected (LCM) tumour tissue, which revealed the absence of recombination in either the reporter (ROSA26) or the *Ctnnb1* loci, demonstrating that *Sox2$^{CreERT2/+}$;Ctnnb1$^{lox(ex3)/+}$;R26$^{YFP/+}$* mice develop tumours that are not derived from the originally mutated cells. Therefore, these tumours develop non-cell autonomously, possibly due to the paracrine activities of the β-catenin clusters. The identity of the cell-of-origin giving rise to tumours in both

the *Hesx1*$^{Cre/+}$;*Ctnnb1*$^{lox(ex3)/+}$ and *Sox2*$^{CreERT2/+}$;*Ctnnb1*$^{lox(ex3)/+}$ models is currently not known.

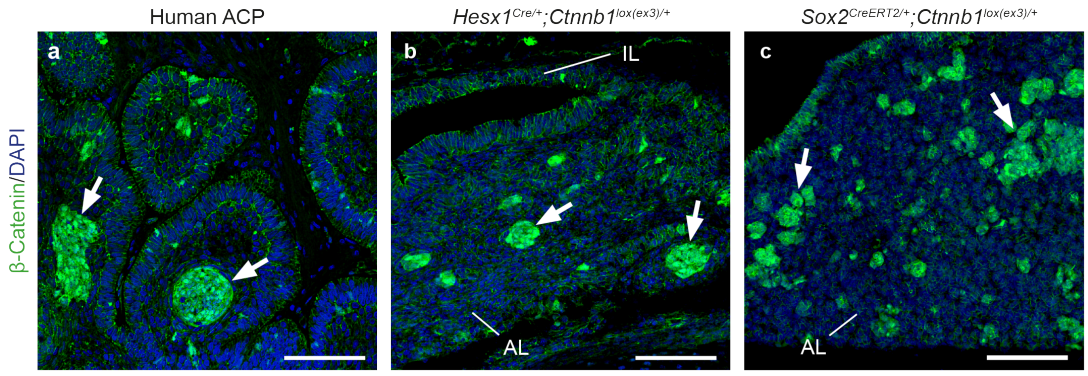

Figure 1.4 Nucleo-cytoplasmic accumulating β-catenin clusters are found in human adamantinomatous craniopharyngioma (ACP) and murine models for ACP.

(a) Immunofluorescence in human ACP showing the nucleo-cytoplasmic accumulation of β-catenin in cell groups known as "clusters" (arrows), a defining characteristic of these tumours. **(b)** Expression of oncogenic β-catenin in embryonic pituitary progenitors also leads to the formation of clusters in *Hesx1*$^{Cre/+}$;*Ctnnb1*$^{lox(ex3)/+}$ pituitaries. An 18.5 dpc specimen is shown. **(c)** Inducible expression of oncogenic β-catenin in adult pituitary stem cells also leads to cluster formation in *Sox2*$^{CreERT2/+}$;*Ctnnb1*$^{lox(ex3)/+}$ pituitaries. 16-week post-tamoxifen induction shown. Scale bars: 100 μm.

1.2.6 Mouse ACP carcinogenesis does not follow the cancer stem cell model

The cancer stem cell (CSC) model

The cancer stem cell (CSC) model establishes that tumours/cancers contain a small group of cells capable of self-renewal and give rise to most of the tumour cells. CSCs recapitulate most characteristics of normal stem cells: they are multipotential and also possess self-renewal capacity (Clarke & Fuller 2006; Nguyen et al. 2012; Beck & Blanpain 2013). Therefore, CSCs divide asymmetrically and give rise to the tumour bulk-mass (Fig 1.5a). These characteristics together with their resistance to chemotherapeutics make CSCs ideal targets in cancer therapy and great effort has been directed to understand their biology, in order to improve their identification and therapeutic targeting. Importantly, a CSC should not be confused with the cell that receives the first oncogenic hit(s), as it may not be directly related to the CSC population giving rise to the tumour mass at a certain point (Visvader et al. 2012; Kreso & Dick 2014).

Lineage tracing studies in mice have been crucial in demonstrating that normal tissue-specific SCs are able to give rise to tumours cell-autonomously when targeted with oncogenic mutations and/or inactivation of tumour-suppressor genes (Schepers et al. 2012; Nakanishi et al. 2013; Zomer et al. 2013). However, this is not always the case and it has been shown that CSCs can arise from committed progenitor cells or differentiated cell types (Clevers 2011; Valent et al. 2012). Still, the cell-autonomous tumour formation from a single originally mutated cell is the predominating mechanism described in the literature and forms the basis for most models of carcinogenesis to date. Importantly, the universal application of this model has recently been challenged by studies showing that cancer cells can arise non-cell

autonomously (i.e. from a cell not carrying the original hit) (Lujambio et al. 2013; Kode et al. 2014; Andoniadou et al. 2013).

A model for the non-cell autonomous origin of mouse ACP tumours

The demonstration of a non-cell autonomous origin for pituitary tumours in *Sox2*$^{CreERT2/+}$;*Ctnnb1*$^{lox(ex3)/+}$ mice is in direct contrast with the established CSC paradigm and suggests that a very different mechanism of tumourigenesis is involved in murine models for ACP.

The model for paracrine tumourigenesis proposed by Andoniadou et al. suggests that SOX2+ cells targeted with oncogenic β-catenin undergo a short burst of proliferation and form nucleo-cytoplasmic β-catenin clusters. The plethora of pro-oncogenic factors secreted by the clusters eventually cause the paracrine transformation of a neighbouring cell, which then propagates and generates a tumour in cell-autonomous fashion (Figure 1.5b).

It has been shown that excessive production of growth factors, such as those produced by the β-catenin clusters, can lead to paracrine cell transformation (Oshima et al. 2014; Martin et al. 2014; Rogelj et al. 1988). These inductive signals can promote the overactivation of oncogenic pathways that induce hyperproliferation and DNA replicative stress, leading to DNA damage and the acquisition of novel mutations which could confer tumourigenic capacity (Zheng et al. 2015; Aaronson 1991; Löbrich & Jeggo 2007; Gaillard et al. 2015). Furthermore, the occurrence of non-cell autonomous tumourigenesis in different contexts is increasingly being supported (Deschene et al. 2014; Nicolas et al. 2003; Arwert et al. 2010; Fomchenko et al. 2011; Lujambio et al. 2013; Kode et al. 2014) (all studies further discussed in the discussion chapter). Therefore, there is considerable evidence supporting the validity of the paracrine model of tumourigenesis proposed by Andoniadou et al. However, the extent of tumour/cancer types that apply to this model remains to be addressed.

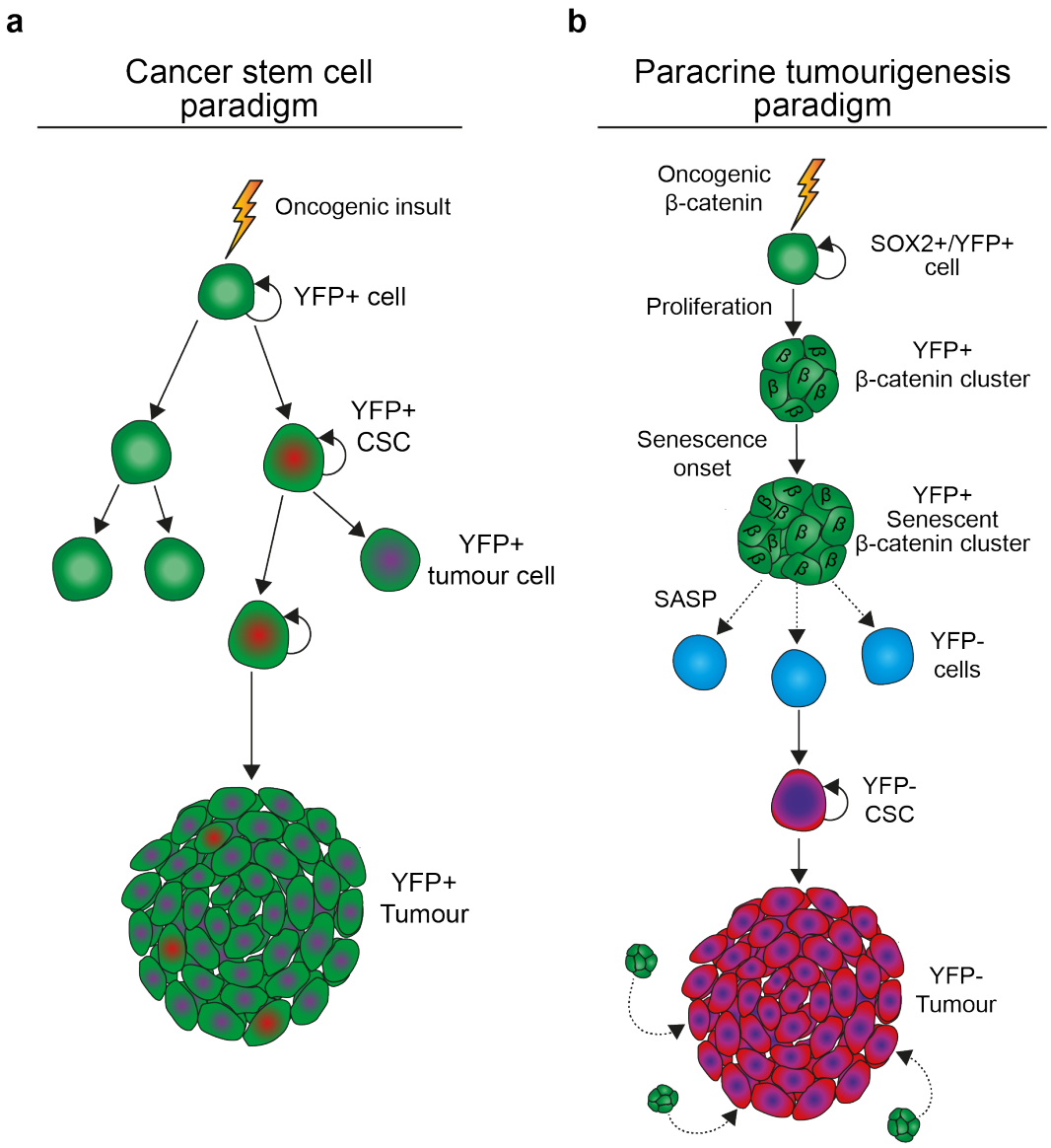

Figure 1.5 Comparison of different models of tumourigenesis.

(a) The cancer stem cell (CSC) model establishes that an original cell, being either a progenitor, committed or differentiated cell type, is initially transformed by an oncogenic stimulus. This cell's lineage can be traced using a genetic reporter strategy (fluorescent YFP labelling in this example, depicted in green). All the descendants from the original cell carry the oncogenic mutation and express YFP. At some point a YFP+ descendant cell acquires a CSC phenotype (green/red cell) which allows it to self-renew and divide asymmetrically giving rise to differentiated tumour cells (green/purple cell), which form the bulk mass of a YFP+ tumour. **(b)** The paracrine model of tumourigenesis proposed by Adoniadou et al. states that expression of oncogenic β-catenin in SOX2+ adult pituitary stem cells leads to non-cell autonomous tumour formation. After a burst of proliferation, targeted cells (also labelled by YFP)

form nucleo-cytoplasmic accumulating β-catenin clusters. These clusters do not proliferate nor form tumours, therefore they must enter a senescent arrest and acquire a Senescence-Associated Secretory Phenotype (SASP) composed of several pro-oncogenic secretory factors. The SASP acts on non-targeted cells (YFP-) and induces the paracrine transformation of the cell-of-origin, which will give rise to a YFP- tumour. Further maintenance or progression of YFP- tumours might also be aided by continuous SASP signalling from the β-catenin clusters.

Therefore, findings derived from both mouse ACP models indicate that overactivation of the WNT pathway in a subset of β-catenin clusters underlies ACP pathogenesis. Intriguingly, these clusters do not proliferate nor form tumours, yet they persist during the early stages of tumourigenesis, suggesting their survival and paracrine actions are of importance for tumour formation/progression. The following sections will introduce three features of the β-catenin clusters' biology of relevance for this thesis: 1) Overactivation of WNT/β-catenin pathway as the initiating oncogenic step; 2) CXCR4/SDF-1 signalling as a candidate pathway promoting β-catenin cluster survival and mediating their interaction with the microenvironment; 3) Cellular senescence and the SASP as biological mechanisms underlying the non-cell autonomous origin of pituitary tumours.

1.3 The β-catenin/WNT signalling pathway

1.3.1 Overview of β-catenin/WNT signalling

WNTs are a group of secreted glycoproteins with crucial roles in embryonic development, stem cell biology, disease and cancer. Since the discovery of the first WNT member, WNT1, 19 different WNT genes have been discovered in humans, with both overlapping and distinct functions depending on the biological context (Mikels & Nusse 2006). WNT genes have been mainly studied for their essential roles in embryonic development, where they act as morphogens (i.e. signalling molecules that act on cell fate determination according to concentration gradients) (Hüsken & Carl 2012); and for their function in regulating stem cells and their niches (Clevers et al. 2014). Moreover, aberrant cell-to cell WNT signalling occurs in disease and cancer. Because WNTs and their overall mechanisms and biological roles have been highly conserved throughout evolution (Klaus & Birchmeier 2008), their study in animal models has proven to be of great value for the understanding and treatment of disease in humans.

WNT signalling can occur through both β-catenin-dependent and independent mechanisms. However, this introduction will focus on signalling mediated by β-catenin, also known as the canonical WNT pathway.

In the absence of WTN ligands, β-catenin is continuously targeted for proteasomal degradation, which prevents its accumulation and translocation to the nucleus. This regulation is achieved by the β-catenin destruction complex, which is composed by a variety of proteins including: glycogen synthase kinase 3 (GSK3β), casein kinase 1 (CK1), adenomatous polyposis coli (APC) and Axin proteins (a constitutively active Axin1 and an induced Axin2 as regulatory feedback). Axins and APC act as scaffold proteins that promote N-terminal phosphorylation of β-catenin by GSK3β and CK1. This phosphorylation allows polyubiquitination of β-catenin by the

E3-ubiquitin ligase βTRCP, which allows proteasomal recognition and degradation. Binding of WNT ligands to a Frizzled receptor (Fzd) and coreceptors Lrp5/6, induces translocation of Dishevelled (Dvl) protein to the plasma membrane. The interaction of Dvl with Fzd and Lpr5/6 then induces sequestration and inactivation of the destruction complex, preventing further degradation of β-catenin protein. When stabilised, β-catenin can translocate to the cell nucleus and displace TLE repressing factors, which normally inhibit TCF/LEF-mediated transcription. β-catenin further promotes transcription by recruiting coactivators such as BCL9 and CBP/p300. The resulting β-catenin-TCF transcription complex ultimately activates genes involved in cell survival, proliferation and differentiation. Importantly, some target genes, such as Axin2, function as a negative-regulatory feedback to the pathway in order to prevent its overactivation (Stamos & Weis 2013).

1.3.2 β-catenin/WNT signalling in cancer

WNT proteins were discovered as a result of a screening for genes activated by viruses that induce mammary tumours in mice (Nusse & Varmus 1982). One such proto-oncogene was named *Int1* (Integration 1) and it was later found that the *Wingless* (Wg) gene in *Drosophila melanogaster* was its homolog. This realization led to the amalgamation of *Wg* and *Int1* into *Wnt* (Klaus & Birchmeier 2008). It took almost a decade in order to establish a link between human cancer and WNT signalling when it was reported that the tumour suppressor APC directly interacted with β-catenin (Rubinfeld et al. 1993; Su et al. 1993).

Mutations in the APC gene had already been associated with familial adenomatous polyposis, which involves the formation of thousands of polyps in the colon and their eventual progression to malignant carcinomas (Bodmer et al. 1987; Leppert et al. 1987). Analysis of APC mutations revealed they were present in up to 85% of sporadic colorectal cancers (Kinzler & Vogelstein 1996), and it was reported

that nuclear accumulation of β-catenin was a defining histological feature of this cancers (Inomata et al. 1996). More recently, whole exome sequencing studies have determined that APC loss-of-function mutations represent driver mutations in colorectal cancers (Wood et al. 2007; The Cancer Genome Atlas Network 2012). Further evidence of their causative nature in human colorectal cancer can be derived from the fact that these tumours display the same frequency of APC mutations independently of their progression stage (early vs. late), and that they have been found even in the earliest lesions (microscopic adenomas) (Fearon 2011).

Both loss-of-function mutations in APC and stabilizing gain-of-function mutations in β-catenin (encoded by the CTNNB1 gene) are known to directly affect the ability of the APC protein to bind β-catenin and facilitate its proteasomal degradation (Korinek et al. 1997; Morin et al. 1997; Rubinfeld et al. 1997). Importantly, mice carrying a truncated form of APC (known as *Min* for Multiple Intestinal Neoplasia) were found to also develop intestinal polyposis (Su et al. 1992). Later, a conditional gain-of-function mutation of β-catenin (exon 3) was shown to lead to intestinal tumourigenesis (Harada et al. 1999). Together, these findings paved the way for further research using genetically engineered mice as models for studying the relationship between aberrant WNT signalling and carcinogenesis. In general, it is now understood that mutations in ACP, β-catenin or other components of the canonical WNT-pathway promote nucleocytoplasmic accumulation of β-catenin which then leads to hyper-activation of target genes involved in cancer cell survival and proliferation (Polaskis 2012).

Despite the existence of a wealth of evidence demonstrating the role of aberrant β-catenin/WNT signalling in the development of colorectal cancer, its role in other types of cancer is less clear. Gain-of-function mutations in CTNNB1 have been reported in a wide number of cancers (Polaskis 2012) and increased levels of nuclear β-catenin are known to often correlate with poor prognosis (Anastas & Moon 2013).

However, the biological relation between CTNNB1 gain-of-function mutations and carcinogenesis has only been addressed in a number of paediatric cancers including: adamantinomatous craniopharyngioma (ACP), WNT-driven medulloblastoma, hepatoblastoma and Wilms' tumours (Gaston-Massuet et al. 2011; Brastianos et al. 2014; Polakis 2007; Austinat et al. 2008; Koesters et al. 1999; Huff 2011). Therefore, the discovery of novel mechanisms of WNT-directed carcinogenesis can provide fresh insight into the pathogenesis of other types of cancer.

1.4 The CXCR4/SDF-1 signalling pathway

1.4.1 Overview of CXCR4/SDF-1 signalling

Chemokines are a family of low-molecular weight secreted proteins whose main function is to direct cell migration (chemotaxis). Chemokines normally act by binding to G-protein Coupled Receptors (GPCRs) present in the cell's membrane, which then activate signal transduction cascades through secondary messengers such as G proteins (Holland et al. 2006). Depending on the distance between their first two cysteine residues, chemokines are grouped as: C-, CC-, CXC- and CX_3C- type chemokines, of which CC- and CXC- families contain the vast majority of known chemokines. Accordingly, chemokine receptors are named after the family of chemokines they bind to (Nomiyama et al. 2013). The most ancient of the CXC-chemokines is SDF-1 (Stromal-Derived Factor 1, also known as CXCL12), being highly conserved in sequence and function throughout evolution and prompting the suggestion that it might represent the original chemokine. Its receptor CXCR4 also appeared earlier in evolution than other chemokine receptors and displays the highest level of conservation among them (Bajoghli 2013; Mithal et al. 2012).

As a chemokine receptor, the main function of CXCR4 in the cell is to direct its migration towards tissues secreting SDF-1. Being a GPCR, it acts mainly through the G-proteins Gαi and the dimer Gβ/Gγ (Massa et al. 2006) which, upon SDF-1 binding, activate multiple signalling pathways including: NF-κB (nuclear factor kappa-light-chain-enhancer of activated B cells), p38/MAPK (Mitogen-activated protein kinases), ERK1/2 and intracellular Ca^{2+} signalling through PLC/IP_3/DAG. The signalling cascades initiated by CXCR4/SDF-1 activation then culminate in the transcription of genes related to cell migration, survival and proliferation (Teicher & Fricker 2010).

1.4.2 CXCR4 in development and homeostasis

The CXCR4/SDF-1 signalling axis has been implicated in the development of the nervous, immune and cardiovascular systems. In the developing nervous system, CXCR4 has been shown to be crucial for the proper migration and arrangement of neuron progenitors of the cortex, hippocampus, cerebellum and spinal cord (Stumm et al. 2003; Lu et al. 2002; Zou et al. 1998; Deaconess et al. 1998; Luo et al. 2005). CXCR4/SDF-1 signalling is also required for the proper migration of cranial neural crest cells involved in the formation of the pharyngeal arches, peripheral ganglia and cardiac structures (Theveneau et al. 2010; Kasemeier-Kulesa et al. 2010; Escot et al. 2013). CXCR4-guided migration of endothelial progenitors has been demonstrated to be crucial during embryonic angiogenesis and blood-vessel patterning in several contexts (Virgintino et al. 2013; Bussmann et al. 2011; Li et al. 2013). During pancreas development, SDF-1 is secreted by the endodermal pancreatic progenitors, which then guides CXCR4-expressing angioblasts in order to form the pancreatic vasculature (Katsumoto & Kume 2011). CXCR4/SDF-1 also plays important roles in homeostasis as it is responsible for the retention and homing of haematopoietic stem cells of the bone marrow and for the migration and maturation of immune cell progenitors (Balabanian et al. 2012; Nie et al. 2004). Additionally, CXCR4 is essential

for the migration of endothelial progenitors to sites of ischemic injury, where it promotes wound repair (Tu et al. 2016).

CXCR4/SDF-1 signalling in pituitary development

Expression of both *Cxcr4* and *Sdf-1* mRNA in the developing pituitary gland has been previously reported (McGrath et al. 1999). Other groups have also observed their expression in normal and tumourigenic pituitary tissue. However, a comprehensive description of both CXCR4 mRNA and protein expression patterns throughout pituitary development has not been reported yet and the question of its function *in vivo* remains to be addressed (Rostène et al. 2011).

1.4.3 CXCR4/SDF-1 signalling in cancer

CXCR4 and SDF-1 have gained considerable attention in the area of cancer research because of their involvement in different aspects of tumour progression and malignancy. Both CXCR4 and SDF-1 are overexpressed in a wide array of human cancers, often correlating positively with tumour malignancy (Burger & Kipps 2006; Fischer et al. 2008; Lippitz 2013). CXCR4 mediates cancer cell metastasis towards sites of high SDF-1 secretion, promotes cancer cell chemoresistance and proliferation, as well as tumour angiogenesis (Liang et al. 2007; Sun et al. 2010; Drury et al. 2011). Importantly, CXCR4/SDF-1 expression can be controlled by signalling pathways like SHH and WNT, often reinforcing proliferative cues and tumour growth (Mo et al. 2013; Sengupta et al. 2012; Singh et al. 2012). Finally, in some tumours/cancers the expression of CXCR4 has been used as a marker to identify and isolate cancer stem cell (CSCs) (Trautmann et al. 2014; Hermann et al. 2007; Würth et al. 2014; Fujita et al. 2015; Jung et al. 2013).

CXCR4/SDF-1 signalling in pituitary adenomas

In the context of pituitary-derived tumours, the study of CXCR4/SDF-1 signalling has been mostly restricted to pituitary adenomas. Overexpression of these genes has been reported mainly in growth hormone-secreting adenoma (GHomas) tissue and GHoma cell lines. Interestingly, the majority of GHomas so far studied overexpressed CXCR4/SDF-1 (Barbieri et al. 2008; Lee et al. 2010; Nomura et al. 2009; Barbieri et al. 2014), while *in vitro* studies found that activation of this pathway induces GHoma cell proliferation and growth hormone production (Kim et al. 2011; Lee et al. 2008; Massa et al. 2006; Yoshida et al. 2010).

Recently, a study reported the identification of CSCs in a large cohort of human pituitary adenomas (Mertens et al. 2015). These CSCs were characterised by the expression of CXCR4, expressed the stem cell markers SOX2 and NESTIN, could be grown and serially passaged in culture and gave rise to hormone expressing cells corresponding to the adenoma type they were isolated from. When the purified CXCR4+ CSCs were injected into SCID mice, they demonstrated increased tumorigenic capacity in comparison to the main population. Importantly, chemical inhibition of CXCR4 lead to a decrease in tumour cell proliferation/viability and a significant reduction in xenograft tumour growth. Therefore, pituitary adenomas contain CXCR4+ CSCs which represent a promising therapeutic target for the treatment of these tumours.

CXCR4/SDF-1 signalling in human and mouse ACP

A possible role for the CXCR4/SDF-1 axis in ACP pathogenesis was previously suggested by Andoniadou et al. Expression analysis of the β-catenin-accumulating clusters from *Hesx1*$^{Cre/+}$*;Ctnnb1*$^{lox(ex3)/+}$ pituitaries showed that *Cxcr4* expression was significantly upregulated in the clusters (2.62-fold change in expression), while its ligand *Sdf-1* was significantly upregulated in the non-cluster fraction (4.91-fold

change in expression). *In situ* hybridisation (ISH) in both *Hesx1*$^{Cre/+}$*;Ctnnb1*$^{lox(ex3)/+}$ pituitaries and human ACP samples demonstrated increased *CXCR4* expression in structures that matched β-catenin cluster location in consecutive histological sections (Andoniadou et al. 2012). Subsequently, a significant correlation was found between poor recurrence-free survival and higher expression of CXCR4 and SDF-1 in patients with paediatric form of ACP (Gong et al. 2014), suggesting this pathway represents a prognostic factor during ACP tumourigenesis.

1.4.4 Other CXC receptors

CXCR7

CXCR7 is the only other receptor known to bind SDF-1. Initially it was considered to act only as a scavenger receptor, as it does not signal through G proteins (Rajagopal et al. 2010). In the developing brain, CXCR7 is necessary for correct CXCR4-mediated cell migration by creating SDF-1 gradients (Wang et al. 2011). However, it has also been shown that it mediates a cell-autonomous regulation of cell migration by forming heterodimers with CXCR4 and thereby affecting receptor sensitisation (Décaillot et al. 2011; Levoye et al. 2009). *In vivo* studies have found CXCR7-mediated regulation of CXCR4 to be crucial for the correct development of the brain, heart and kidney (Sánchez-Alcañiz et al. 2011; Mellado et al. 2007; Haege et al. 2012). Importantly, this complementation of CXCR4 function by CXCR7 has also been found to be involved in a variety of cancers, where CXCR7 can display pro-oncogenic or tumour suppressive functions depending on the context (Grymula et al. 2010; Heckmann et al. 2013; Hernandez et al. 2011).

CXCR2

Angiogenesis and inflammation are well known mechanisms involved in tumour progression (Acosta & Gil 2009). CXCR2 is another receptor that has been shown to

be relevant for regulating CXCR4 function, particularly in inflammation and cancer. It has been investigated mainly for being the receptor for interleukin 8 (IL-8), which is of great importance for neutrophil inflammatory responses in tumours (Wu et al. 2012), including in models were neutrophil invasion has been shown to result pro-tumourigenic (Jamieson et al. 2012). The mechanism by which CXCR2 guides cell migration and invasion often involves antagonising CXCR4 signalling in a cell-autonomous fashion (Eash et al. 2010; Martin et al. 2003). In the mouse, this effect is mainly mediated by the IL-8 analogue chemokines CXCL1, CXCL2 and CXCL3 (Luan et al. 2001). Importantly, the genes encoding these chemokines were overexpressed (2.15, 30 and 29-fold, respectively) by the β-catenin-accumulating cell clusters of the embryonic mouse model for ACP (Andoniadou et al. 2012).

1.5 Cellular Senescence

1.5.1 Definition and role of cellular senescence

Cellular senescence is defined as an irreversible loss of proliferative capacity, while the cell still retains normal metabolic activity and viability. It is now established that senescence occurs as a response to different stress stimuli and reflects abnormalities in the cell's homoeostatic machinery. In contrast, cellular quiescence is also characterised by a long-term cell cycle arrest, but is reversible upon specific mitotic signals. Cellular quiescence occurs normally in some types of differentiated cells (e.g. fibroblasts) and especially in stem cells (Campisi 2013).

The first description of senescence was derived from observing the behaviour of human cells in culture, which showed a gradual decay and eventually permanent arrest in their proliferative capacity, although they remained viable and metabolically active (Hayflick & Moorhead 1961; Hayflick 1965). It is now known that, under normal conditions, cells can only divide a finite number of times (their "Hayflick limit"). This

phenomenon is now known as replicative senescence and it occurs due to gradual telomere erosion (Bodnar et al. 1998).

Further research unveiled other stress-inducing stimuli able to trigger senescence: accumulation of unresolved DNA damage, reactive-oxygen species (ROS), ionizing radiation, cytotoxic chemical agents, the endoplasmic reticulum (ER) stress response or loss of a tumour suppressor such as PTEN (Fitzgerald et al. 2015; Colavitti & Finkel 2005; Le et al. 2010; Liao et al. 2014; Ewald et al. 2010; Matos et al. 2015; Pluquet et al. 2015; Thomas Kuilman et al. 2010; Dörr et al. 2013). Senescence occurring through these mechanisms does not depend on the cell's telomere status and is referred to as Stress-Induced Premature Senescence (SIPS).

A different type of telomere-independent senescence occurs upon the activation of oncogenes such as mutant β-catenin, $HRAS^{V12}$, $BRAF^{V600E}$ and $KRAS^{G12D}$ (Serrano et al. 1997; Gu et al. 2014; Xu et al. 2008; Wajapeyee et al. 2008; Collado et al. 2005; Collado & Serrano 2010) and is referred to as Oncogene-Induced Senescence (OIS). Importantly, OIS has been demonstrated to represent a potent anti-tumourigenic barrier in several contexts by preventing the overproliferation of oncogene-carrying cells. The finding that tumours contain larger numbers of senescent cells in pre-malignant stages compared to malignant ones, lead to the hypothesis that senescence is the rate-limiting step in tumour progression in both mice and humans (Braig et al. 2005; Chen et al. 2005; Collado et al. 2005; Michaloglou et al. 2005).

The Senescence Associated Secretory Phenotype (SASP)

Another feature of senescent cells is that they can promote directly their own clearance and induce tissue repair by means of the Senescence-Associated Secretory Phenotype (SASP). The SASP involves the secretion of a wide variety of soluble and insoluble factors including: interleukins, chemokines, growth factors and

extracellular matrix (ECM) components (Shelton et al. 1999; Coppé et al. 2008; Coppé, Patil, et al. 2010). The SASP signature appears to vary depending on the nature of the senescence-inducing stimuli (Coppé, Patil, et al. 2010; Maciel-Barón et al. 2016). However, some secreted factors appear to be more prevalent among reported SASP signatures. Examples include: the interleukins IL1A, IL1B and IL6; the chemokines IL8 (CXCL1-3 in mice), CCL2, CCL5 and CCL20; growth factors: bFGF, HGF, VEGF and inflammatory cytokines: TGFβ, TNFα and MIF, among others (Coppé, Desprez, et al. 2010; Tchkonia et al. 2013).

In general, the SASP is known to mediate two main effects: 1) the recruitment of the immune system, which then removes senescent cells from the environment (Xue et al. 2007; Kang et al. 2011; Iannello et al. 2013; Chien et al. 2011; Krizhanovsky et al. 2008; Sagiv et al. 2013); and 2) reinforcing the overall senescent response by both autocrine and paracrine signalling (Acosta et al. 2008; Acosta et al. 2013; Hubackova et al. 2012).

Until recently, the prevailing view was that replicative senescence, SIPS and OIS were uniquely beneficial mechanisms preventing the propagation of abnormally stressed cells carrying irreparable damage in their DNA or metabolic machinery (Sharpless & Sherr 2015), while the SASP aided in their immune clearance. However, novel roles have been uncovered for senescent cells, as they are involved in appropriate wound repair and even in tissue remodelling during embryonic development (Krizhanovsky et al. 2008; Demaria et al. 2014; Storer et al. 2013; Muñoz-Espín et al. 2013; Yun et al. 2015). Importantly, these functions also rely greatly on their interaction with the microenvironment and the immune system through the SASP.

1.5.2 Detrimental effects of senescence and the SASP

Senescence and the SASP in ageing

The deleterious consequences of the ineffective clearance of senescent cells and their over-accumulation in tissues have mainly been studied in relation to age-related diseases, which also include an exponential increase in the development of cancer (Krtolica et al. 2001; Campisi 2013). Aged tissues of mice, primates and humans contain larger numbers of senescent cells, particularly in the lungs, skin and spleen (White et al. 2015; Dimri et al. 1995; Herbig et al. 2006; Wang et al. 2009), while the number of senescent cells in the liver and intestine was shown to be an accurate life-span predictor in mice (Jurk et al. 2014). Importantly, genetic or chemical ablation of senescent cells delayed the onset of age-related disorders, leading to increased life-spans and also promoting tissue rejuvenation in late life (Chang et al. 2016; Baker et al. 2011; Baker et al. 2016).

The exact mechanisms connecting senescence and age-related pathologies are still under debate. One hypothesis is that the onset of senescence in stem cells leads to the depletion of a tissue's regenerative potential (Flores et al. 2006; Castilho et al. 2009; Pollina & Brunet 2011). Another emerging possibility is that the accumulation of senescent cells during ageing leads to persistent SASP signalling and the development of chronic inflammation, which leads to overall deterioration of a tissue's homeostatic environment (i.e. "inflammaging") (Franceschi & Campisi 2014; Salminen et al. 2008; Shaw et al. 2010; Hall et al. 2016).

The pro-tumourigenic activities of the SASP

There is increasing evidence indicating that senescence and its SASP can act as a double edged-sword in cancer development. The discovery that SASP factors from senescent fibroblasts are able to promote growth and enhance tumourigenesis

in premalignant epithelial cells, but not normal ones, gave way to research revealing the pro-tumourigenic properties of the SASP (Krtolica et al. 2001; Coppé, Patil, et al. 2010).

Senescent cells and the SASP has been shown to promote carcinogenesis by different mechanisms, which can be categorised as: 1) Direct signalling on pre-malignant or malignant cells; and 2) Indirect signalling by modification of the microenvironment, which then becomes permissive for cancer progression.

The most reported direct effect of the SASP is to induce proliferation in neighbouring non-senescent cells, enhancing their tumourigenic properties (Coppé, Patil, et al. 2010; Laberge et al. 2015; Nakamura et al. 2014; Kuilman et al. 2008; Bavik et al. 2006). Pro-tumourigenic phenotypes characterised by chemoresistance and epithelial-to-mesenchymal transition (EMT) are also enhanced by the SASP (Canino et al. 2012). Importantly, the SASP is also able to induce dedifferentiation and reprogramming of naïve cells, leading to the emergence of CSCs (Parrinello et al. 2005; Cahu et al. 2012; Ohanna et al. 2013).

The SASP has also been shown to promote tumourigenesis indirectly by signalling on the microenvironment. Notably, a large number of proangiogenic factors are known to be secreted by senescent cells, while no angiostatic molecules have been found (Campisi 2013). Indeed, the SASP has been reported to promote tumour-supportive angiogenesis and endothelial cell invasiveness (Yu et al. 2013; Vital et al. 2014; Ancrile et al. 2007). In addition, the SASP displays important modulatory activities on the immune system such as: promoting macrophage polarization towards tumour-promoting phenotypes (Lujambio et al. 2013) and generating immunosuppressive niches permissive for tumour growth or cancer cell metastasis (Ruhland et al. 2016; Luo et al. 2016).

1.5.2 Pathways and mechanisms underlying senescence

Senescent cells have traditionally been identified by the activity of the Senescence-Associated β-Galactosidase (SA-β-Gal). However, the prevailing view is that cellular senescence is a complex state that can only be accurately determined by the use of several molecular markers (Sharpless & Sherr 2015; Campisi 2013; Collado & Serrano 2010). These markers are associated with numerous stress-related biological processes shared by senescent cells such as: loss of proliferative capacity, absence of apoptosis, increased lysosomal activity, acquisition of a DNA-damage-response (DDR) and activation of the SASP.

Cell cycle control and senescence

As previously mentioned, the defining aspect of a senescent cell is that it enters a permanent arrest in the cell cycle. Therefore, a good preliminarily indicator relies on the use of proliferation markers such as the cell-cycle indicator Ki-67, the mitosis marker phosphorylated Histone H3 (Davalos et al. 2010) and the uptake of thymidine analogues (EdU/BrdU) during S-phase DNA synthesis. However, quiescent cells that can resume the cell cycle also lack these markers and this should be taken in consideration.

It is now well established that the senescent cell cycle arrest is mostly mediated by the p53/p21 and the p16/Rb pathways (although some exceptions have been reported). In some cases, either of these pathways is indispensable for senescence onset, while they mostly cooperate and reinforce senescence together (Kamijo et al. 1997; Zhu et al. 2015).

The main effector of the p53/p21 pathway is the tumour suppressor protein p53 (encoded by *TP53* in humans and *Trp53* in mice). p53 is crucial for proper regulation of cell survival. Its function is to mediate the cellular response to multiple stress signals, which include: DNA damage, replicative stress, oncogenic hyper proliferative

signals, hypoxia, oxidative stress and nutrient deprivation (Vousden & Ryan 2009; Bieging et al. 2014). Upon induction, p53 activates multiple responses, mainly through its key effector protein p21 (encoded by *CDKN1A*), including: inducing the cell cycle arrest or slowing cell cycle progression, promotion of DNA repair, senescence, autophagy or apoptosis (Menendez et al. 2009; Meek 2009). Additionally, recent evidence indicates that p53 also has roles in regulating the stem cell phenotype and their differentiation (Spike & Wahl 2011). Importantly, many of these functions are deeply involved in cancer pathogenesis.

It is known that p53 is the gene most frequently found to be mutated in cancer. Around half of all sporadic cancers carry inactivating TP53 mutations (Olivier et al. 2010), while germ-line mutations lead to high predisposition to multiple cancer types, known as Li-Fraumeni syndrome (Nochols et al. 2001). The study of mouse p53 knockout models has provided considerable insight into the mechanisms of p53-mediated tumour suppression and established the unequivocal importance of p53/p21 signalling in preventing cancer development (Donehower 2009). Importantly, many anti-cancer therapies (such as radiotherapy) rely on the induction of DNA-damage, which leads to p53-dependent apoptosis (Norbury & Zhivotovsky 2004).

The role of p53 in the anti-tumourigenic senescent response was initially demonstrated *in vitro* (Sugrue et al. 1997; Fang et al. 1999) and posteriorly *in vivo,* by revealing that premalignant tumours undergo p53-dependent senescence, while full malignant tumours progressed in the absence of p53 and other senescence markers (Dankort et al. 2007; Collado et al. 2005). Furthermore, it has been shown that restoration of p53 function *in vivo* leads to cancer cell senescence and eventual tumour regression (Ventura et al. 2007; Xue et al. 2007; Feldser et al. 2010).

A second pathway responsible for mediating the cell cycle control is the Rb/$p16^{INK4a}$ pathway. Retinoblastoma protein (Rb) is normally associated to E2F transcription factors, preventing the transcription of cell cycle promoting genes.

During the G1 to S transition, the repressing activity of Rb is relieved by the activity of cyclin dependent kinases (CDK4/6). Upon stress stimuli such as DNA damage, there is an increase in the expression of p16 (also known as IKN4A and encoded by the *CDKN2A* locus), which binds and inhibits the activity of CDK4/6, therefore stabilising Rb (Serrano et al. 1993). The activity of p16 has been shown to be crucial for the induction and maintenance of senescence (Dai & Enders 2000; Ohtani & Hara 2013; Baker et al. 2011; Demaria et al. 2014; Burd et al. 2013), including senescence induced by increased WNT signalling (Sato et al. 2015). Therefore, upregulation of p16 has been referred as a reliable functional marker of senescence in different contexts (Salama et al. 2014), even in those where senescence is independent from p53/p21 (Jacobs et al. 2004). Importantly, p16/Rb signalling has also been shown to play a significant role *in vivo* in the context of oncogene-induced senescence (OIS) (Michaloglou et al. 2005; Serrano et al. 1996; Serrano et al. 1997; Sarkisian et al. 2007).

The lysosomal compartment in senescent cells

As previously mentioned, the SA-β-gal assay at pH 6.0 (Dimri et al. 1995; Debacq-Chainiaux et al. 2009) is the gold-standard for the identification of senescent cells and it has been shown that the enzyme's increased activity during senescence reflects an overall expansion of the cell's lysosomal compartment (Kurz et al. 2000; Ivanov et al. 2013). The enzyme responsible for the SA-β-gal activity is encoded by the GLB1 gene (Lee et al. 2006) and it has been shown that its overexpression can be detected using anti-GLB1 antibodies and used as a senescence marker (Wagner et al. 2015). This expansion of the lysosomal compartment is thought to be a consequence of maintaining the highly demanding secretory machinery of senescent cells which leads to endoplasmic reticulum stress, an unfolded-protein response and proteotoxicity (Dörr et al. 2013).

DNA-damage and the DNA-damage response

Compelling evidence indicates that oncogene-induced DNA damage is required in order to establish and perpetuate the OIS phenotype (Bartkova et al. 2006; Mallette et al. 2007). More importantly, DNA damage has been shown to be essential for the activation of the SASP (Rodier et al. 2009; Kang et al. 2015).

The exact mechanisms linking oncogene signalling and DDR induction are complex and not fully understood. However, it has been shown that oncogene expression can force the cell through hyper-replication, leading to sustained DNA replicative stress, which can result in the accumulation of DNA damage (e.g. double strand breaks, DSBs) (Di Micco et al. 2006; Prieur et al. 2011; Halazonetis et al. 2008). Right after DSB formation, proteins recognising DSBs like PARP-1 help the recruitment of kinases like ATM/ATR and DNA-PKcs, which phosphorylate histone H2AX (γH2AX), leading to its rapid accumulation at DSB sites (Weaver & Yang 2013). γH2AX provides a positive feedback loop that amplifies overall protein recruitment, including ATM/ATR, which then initiate a signalling cascade culminating with the activation of DNA-checkpoint pathways, including p53/p21signalling (Gaillard et al. 2015; Bonner et al. 2008). The collection of signalling pathways activated in this manner is known as the DNA-Damage response (DDR).

The mTOR and autophagy pathways

The mechanistic target of rapamycin (mTOR) is a serine/threonine kinase that forms part of a highly-conserved signalling complex (mTORC1), which is crucial for mediating cell growth and proliferation in response to environmental cues such as nutrient availability. The main function of mTOR is to induce the protein synthesis machinery. Upon activation, mTORC1 phosphorylates p70 ribosomal protein S6 kinase 1 (S6K1), which in turn phosphorylates ribosomal protein S6 and activates protein translation; and the eukaryotic initiation factor 4E-binding protein (4E-BP1),

which induces mRNA synthesis, ribosome biogenesis and overall protein translation. Importantly, mTOR signalling has been shown to be involved in the establishment of cellular senescence (Vousden & Ryan 2009; Castilho et al. 2009; Hasty et al. 2013) and activation of the SASP (Laberge et al. 2015; Herranz et al. 2015).

The second function of mTOR is to inhibit autophagy. Autophagy is a process in which cellular components, such as organelles and protein complexes, are sequestrated within vesicles known as autophagosomes, and then degraded within lysosomes (Wirawan et al. 2012). Although the effects of autophagy are many, its main function is to provide the cell with an alternative source of energy upon scarce nutrient availability, which then can be used to maintain the cell's essential anabolic processes. Additionally, autophagy is also involved in the clearance of misfolded proteins, which can result toxic to intracellular homeostasis (Filomeni et al. 2015). The p62/SQTSM protein plays a crucial role during autophagy by functioning as a scavenger able to sequestrate large groups of proteins and facilitate their integration into the autophagosomes (Pankiv et al. 2007). Because p62 is also a target of autophagy, its accumulation can be observed in cells that are autophagy-deficient (Rusten & Stenmark 2010).

The role of autophagy in the induction and maintenance of senescence is controversial as its pro-senescence or anti-senescence activities appear to be context-dependent (White 2012; Kang & Elledge 2016). Some studies have shown that autophagy is required for senescence (Zhang et al. 2014; Young et al. 2009), while others concluded it is necessary to prevent its onset (García-Prat et al. 2016). Additionally, the impairment of autophagic degradation of specific proteins (i.e. selective autophagy) was shown to be required for SASP induction (Kang et al. 2015). In contrast, others have shown that autophagy allows cells to cope with the mass synthesis of proteins required for the SASP (Dörr et al. 2013; Narita et al. 2011).

The Nf-κB pathway

The nuclear factor kappa-light-chain-enhancer of activated B cells (NF-κB) is a conserved complex of transcription factors that are mayor regulators of inflammation and stress signals, with important roles in cancer and disease (Hayden et al. 2006; Lawrence 2009). Stimuli leading to NF-kB activation include: inflammatory signalling through TGF-β, TNFα, and Il1B; oxidative stress through p38MAPK and DNA-damage through PARP-1-mediated activation of NEMO/ATM (Weaver & Yang 2013).

The NF-κB complex is formed by heterodimers of class I (NFKB1 and NFKB2) and class II (RELA, RELB, REL) subfamilies. In the canonical NF-κB pathway, the NF-κB complex is normally held in the cytoplasm by inhibitor proteins belonging to the IκB family. Activation of the pathway initiates when a complex of IκB kinases (IKK) (including the master regulatory kinase NEMO/IKKγ) phosphorylate IκB proteins, leading to their proteasomal degradation and allowing translocation of NF-κB to the cell nucleus where it initiates transcription (Hayden & Ghosh 2012). Target genes of NF-κB include a wide array of cytokines and chemokines, immunoreceptors, stress response genes, growth factors and genes involved in cell survival (Perkins 2007; Lawrence 2009).

Importantly, the process of oncogene-induced senescence culminates with the activation of the SASP by means of the NF-κB pathway. Besides being a requirement for initiating and maintaining the SASP (Crescenzi et al. 2011; Ohanna et al. 2011; Freund et al. 2011; Salminen et al. 2012), NF-κB signalling is also involved in reinforcing senescence in cell-autonomous and non-cell autonomous fashions (Acosta et al. 2008; Rovillain et al. 2011; Chien et al. 2011).

1.6 Rationale and aims of the thesis

Tumours are no longer regarded as simple masses of uncontrolled proliferating cells. They are intricate and continuously-changing entities in which the interactions between the cancer cell and its microenvironment are crucial in determining the outcome of oncogenesis. Therefore, the biological processes guiding their origin must be equally complex. In several cancer models, the role of driver mutations is thought to comply with the CSC paradigm, indicating that the initial hit allows the targeted cell, and its progeny, to gain the advantages required to overcome the organism's anti-cancer mechanisms to eventually form a tumour. In this context, OIS and the SASP were initially proposed to represent one such protective mechanism. However, most of this knowledge has been derived from the study of tumours at later stages of progression. Thus, the study of OIS and the SASP during the earliest steps of tumour formation is imperative if critical advances in cancer prevention are to be achieved.

The work of Andoniadou et al. brought forward outstanding questions regarding tumourigenesis in models of ACP such as:

1) Does this mechanism also apply to tumourigenesis in the embryonic ACP model? Are there similarities with human ACP?

2) Why do β-catenin clusters stop dividing and do not form tumours?

3) What is the mechanism underlying their secretory phenotype?

4) What is the effect of these secreted factors in the microenvironment?

5) What is the actual cell of origin of the tumours?

To answer these questions, the following hypothesis was formulated and forms the core of this work: nucleo-cytoplasmic β-catenin clusters undergo cellular senescence, preventing them from proliferating further, and this endows them with a Senescence-Associated Secretory Phenotype (SASP) capable of signalling to their surroundings and transforming a nearby naïve cell.

.

2. MATERIALS AND METHODS

2.1 Mice

2.1.1 Maintenance of mouse colonies

All animal procedures were performed under compliance of the Animals (Scientific Procedures) Act 1986 and current Home Office legislation. Mice were bred and housed under conditions complying with the Home Office code of practice for the housing and care of animals bred, supplied or used for scientific purposes.

2.1.2 Description of genetic targeting and lineage tracing strategies

Mouse lines expressing Cre recombinase under the control a specific promoter can be bred with lines bearing insertion of *LoxP* sites in genes of interest. The presence of Cre will result in the excision of DNA flanked by *LoxP* in cells in which the chosen promoter is active (Sauer & Henderson 1988). If the flanked sequence is essential for protein function, then a conditional knockout can be achieved in tissues in which the chosen promoter is expressed, as well as of the descendants (i.e. the entire cell lineage). Inducible Cre driver lines have also been developed to allow temporal control in the induction of Cre expression. One such system is the *CreERT2/LoxP* system. This altered form of Cre contains a mutant oestrogen receptor domain, which retains Cre in the cell cytoplasm and is not responsive to endogenous oestrogen. Upon tamoxifen administration, CreER will translocate into the nucleus and excise *LoxP*-flanked DNA (Jaisser 2000; Glaser et al. 2005).

R26$^{YFP/+}$ mice contain the Yellow Fluorescent Protein (*YFP*) gene inserted into the ubiquitously active *ROSA26* locus. Expression of *YFP* is normally inhibited through the presence of an upstream STOP polyadenylation sequence, which is flanked by two *LoxP* sites (Robertson & Soriano 1999). Crossing *R26*$^{YFP/+}$ mice with a Cre driver line will allow the expression of Cre in a specific cell type, leading to

excision of the STOP sequence, and therefore constitutive expression of YFP in the targeted cell and all its descendants. This strategy is known as lineage tracing.

2.1.3 Mouse strains and genetic crosses

The following lines have been previously described and maintained by the host lab for over 50 generations in a C57BL/6 background: *Hesx1*$^{Cre/+}$, *Hesx1*$^{Cre/+}$*R26*$^{YFP/+;}$ *Hesx1*$^{Cre/+}$*;Ctnnb1*$^{lox(ex3)/+}$, *Hesx1*$^{Cre/+}$*;Ctnnb1*$^{lox(ex3)/+}$*;R26*$^{YFP/+}$, *Sox2*$^{CreERT2/+}$*;Ctnnb1*$^{lox(ex3/+)}$*;R26*$^{YFP/+}$ (Andoniadou et al. 2011; Gaston-Massuet et al. 2011; Andoniadou et al. 2013). *Ctnnb1*$^{lox(ex3)/+}$ mice (Harada et al. 1999) contain *LoxP* sites flanking exon 3 of the β-catenin gene. Cre expression leads to exons 2 and 4 connected in frame producing a degradation resistant and transcriptionally functional β-catenin protein.

Cxcr4$^{fl/fl}$ mice (*Cxcr4*^{tm2Yzo}) have been previously described and contain *loxP* sequences flanking exon 2, which represents 98% of the CXCR4 molecule (Nie et al. 2004). *Hesx1*$^{Cre/+}$ and *Cxcr4*$^{fl/fl}$ mice were bred in order to obtain *Hesx1*$^{Cre/+}$*;Cxcr4*$^{fl/+}$ mice, which were then back-crossed with *Cxcr4*$^{fl/fl}$ animals to generate *Hesx1*$^{Cre/+}$*;Cxcr4*$^{fl/+}$ controls and *Hesx1*$^{Cre/+}$*;Cxcr4*$^{fl/fl}$ mutants. Additionally, *Cxcr4*$^{fl/fl}$ and *Ctnnb1*$^{lox(ex3)/lox(ex3)}$ lines were crossed and their progeny was backcrossed order to obtain *Cxcr4*$^{fl/+}$*;Ctnnb1*$^{lox(ex3)/lox(ex3)}$ mice. These were then crossed with *Hesx1*$^{Cre/+}$*;Cxcr4*$^{fl/fl}$ mice in order to obtain *Hesx1*$^{Cre/+;}$ *Ctnnb1*$^{lox(ex3)/+}$*;Cxcr4*$^{fl/+}$ controls and *Hesx1*$^{Cre/+}$*;Ctnnb1*$^{lox(ex3)/+}$*;Cxcr4*$^{fl/fl}$ mutants. CXCR7-GFP embryos were kindly donated by Dr. Ralf Stumm. *Cxcr4*$^{-/-}$ embryos were generated by crossing *Cxcr4*$^{fl/fl}$ with *β-actin*$^{Cre/+}$ mice. *Cxcr7*$^{-/-}$ (*Cxcr7*^{tm1Litt}), and *Cxcl12*$^{-/-}$ (Ara et al. 2003) embryos were kindly donated by Dr. Sarah Ivins and Prof. Peter Scambler.

Trp53$^{fl/fl}$ mice (*Trp53*^{tm1Brn}) have also been previously described (Marino et al. 2000) and contain *LoxP* sequences flanking exons 2 and 10, which effectively produces a null mutation upon Cre expression. *Trp53*$^{fl/fl}$ mice were crossed with

Hesx1$^{Cre/+}$ and *Ctnnb1*$^{lox(ex3)/lox(ex3)}$;*R26*$^{YFP/YFP}$ mice to produce *Hesx1*$^{Cre/+}$;*Trp53*$^{fl/fl}$ and *Trp53*$^{fl/+}$;*Ctnnb1*$^{lox(ex3)/\ lox(ex3)}$;*R26*$^{YFP/YFP}$ mice. These latter strains were bred to obtain *Hesx1*$^{Cre/+}$;*Ctnnb1*$^{lox(ex3)/+}$;*Trp53*$^{fl/+}$;*R26*$^{YFP/+}$ controls and *Hesx1*$^{Cre/+}$;*Ctnnb1*$^{lox(ex3)/+}$;*Trp53*$^{fl/fl}$;*R26*$^{YFP/+}$ mutants.

A similar approach was conducted for generating *Sox2*$^{CreERT2/+}$;*Ctnnb1*$^{lox(ex3)/+}$;*Trp53*$^{fl/+}$;*R26*$^{YFP/+}$ and *Sox2*$^{CreERT2/+}$;*Ctnnb1*$^{lox(ex3)/+}$;*Trp53*$^{fl/fl}$;*R26*$^{YFP/+}$ mice, which were induced once by intraperitoneal injection of 0.15 mg of tamoxifen per gram of weight at 4 to 6 weeks of age.

DNA uptake experiments at different embryonic stages were conducted using 5-ethynyl-2'-deoxyuridine (EdU) according to manufacturer's instructions (Thermo). Pregnant females were injected the day of the desired embryonic stage with a 10mg/ml solution of EdU for a total dose of 100 mg of EdU per kg of weight. After 90 minutes, embryos were dissected and processed as described below.

2.1.4 Sample collection and processing

For embryological studies, female mice were inspected for vaginal plugs the morning after mating set-up. Noon of the day a plug was observed was determined as 0.5 days *post coitum* (dpc) and pregnant females were sacrificed at the appropriate embryological age. For survival studies involving *Hesx1*$^{Cre/+}$;*Ctnnb1*$^{lox(ex3)/+}$;*Cxcr4*$^{fl/fl}$, *Hesx1*$^{Cre/+I}$;*Ctnnb1*$^{lox(ex3)/+}$;*Trp53*$^{fl/fl}$;*R26*$^{YFP/+}$ and *Sox2*$^{CreERT2/+}$;*Ctnnb1*$^{lox(ex3)/+}$;*Trp53*$^{fl/fl}$;*R26*$^{YFP/+}$ mice, the experimental end-point was determined as the onset of health deterioration symptoms such as: hunched posture, intracranial haemorrhage or more than 20% weight-loss, all in line within license established thresholds.

All murine samples including embryos, pituitaries and end-point tumours were collected and further dissected in ice-cold Dulbecco's Modified Eagle's Medium supplemented with 10% Foetal Calf Serum (FCS). Tumours were imaged in

brightfield and under fluorescence for endogenous YFP expression under a stereomicroscope (Leica) using 0.8X magnification and a constant exposure of 3.7 seconds.

Samples to be used for immunohistochemistry or *in situ* hybridisation were washed in phosphate-buffered saline (PBS) and immediately placed in ice-cold freshly made 4% paraformaldehyde (PFA), fixed over-night and posteriorly dehydrated using ethanol (EtOH) gradients. Dehydrated samples were then paraffin-embedded and cut into 6 µm-thick sections using a rotary microtome (Leica) and mounted in Superfrost Plus slides (Thermo). Serial sections were produced in series of 5 for embryos and in series of 8 for tumours and postnatal pituitaries. For embryos, up to 14.5 dpc, sectioning was conducted in a sagittal plane, while for older embryos and postnatal pituitaries sectioning was conducted in the coronal plane.

Samples to be used for RNA extraction were also dissected in ice-cold medium, washed briefly in PBS, placed immediately in 350 µl of buffer RLT and dissociated completely by pipetting to ensure RNA stabilisation. Samples were then stored at -80ºC until further use. Samples for protein extraction were immediately snap-frozen and stored at -80ºC until further use. In the case of embryonic and adult pituitaries the posterior lobe was manually dissected before addition of RLT buffer or snap-freezing.

Unless specified, all experiments performed on mouse embryos and pituitaries were performed with a minimum of three biological replicates at least from 2 different litters.

2.2. Human samples

Use of human samples was either carried out under ethical approval 14 LO 2265 or under the ethical approval of specific tissue banks. Human ACP samples were kindly provided by the GOSH Histopathology Department. For each marker, a

minimum of three independent ACP samples were analysed. Additionally, the expression of each marker was also analysed in tissue microarrays containing a total of 23 different ACP cases and normal brain tissue as a control. Human embryonic samples were provided by the Joint MRC/Wellcome Trust (grant # 099175/Z/12/Z) Human Developmental Biology Resource.

2.3 DNA methods

2.3.1 Genotyping of mice and embryos by PCR of genomic DNA

Genomic DNA was extracted from ear biopsies using DNAreleasy (Anachem) at a 1:5 dilution in a final volume of 25 µl for 30 minutes at 65^{o}C. A negative control without tissue biopsy was included during the extraction step. Polymerase chain reaction (PCR) amplification of target DNA was conducted using 1 µl of sample and reaction conditions optimised for each primer set (Table 1). Depending on the protocol, the reaction used 10X Taq Polymerase Buffer (Bioline) or JD buffer (3x JD Buffer: 60 mM K-glutamate, 24 mM Hepes, 90 mM Tris, 15 mM MgCl2, 6 mM DTT, 180 mM NH4Ac, 3% DMSO, 24% glycerol 3x JD Buffer: 60 mM K-glutamate, 24 mM Hepes, 90 mM Tris, 15 mM MgCl2, 6 mM DTT, 180 mM NH4Ac, 3% DMSO, 24% glycerol). The final components of the reaction mix are described in Table 2. As controls, a positive control of template DNA and a negative control without DNA were included. Initial strand denaturation was performed at 94^{o}C for 2 minutes. Further denaturation steps were conducted at 94^{o}C for 30 seconds followed by a primer-dependent annealing step and polymerization extension at 72^{o}C for 1 minute. The final extension step was conducted at 72^{o}C for 5 minutes.

Component	DNA Mix (µl)		Enzyme Mix (µl)	
	Taq Buffer	JD Buffer	Taq Buffer	JD Buffer
H_20	7.08	1.7	6.4	1.55
Taq Pol Buffer (x10)	1.2	-	0.8	-
$MgCl_2$ (25mM)	0.72	-	0.48	-
JD Buffer (x3)	-	2.5	-	0.83
Primer 1	1 (25 µM)	0.5 (10 µM)	-	-
Primer 2	1 (25 µM)	0.5 (10 µM)	-	-
dNTPs (25mM)	-	0.3	0.16	-
Taq Pol (5U/ul)	-	-	0.16	0.12

Table 3. Reaction mix for PCR genotyping.

Line	Primer sequences	Annealing	Conditions	Products
Hesx1^{Cre}	**OL89:** GGAGACAATTCTTTTGTGAAACCCTG **OL91**: CCAGAGTGTCTGGCTTCTGTC **CreT:** CAGAAGCATTTTCCAGGTATGCTC **OL39:**TCAGCAAAGCTACAAGGTGAACTG	58 for 30 sec 35 cycles	JD	WT: 500 bp MUT: 300 bp
Sox2$^{CreERT2/+}$	Fwd: GATGCAACGAGTGATGAGGTTCGC Rev: ACCCTGATCCTGGCAATTTCGGC	63 for 30 sec 30 cycles	Taq Pol. Buffer	MUT: 500bp
Ctnnb1$^{lox(ex3)/+}$	Fwd: AGAATCACGGTGACCTGGGTTAAA Rev: CATTCATAAAGGACTTGGGAGGTGT	62 for 20 sec 40 cycles	Taq Pol. Buffer	WT: 600 bp MUT: 700bp
Cxcr4$^{fl/fl}$	Fwd: CCACCCAGGACGACAGTGTGACTCTAA Rev: GATGGGATTTCTGTATGAGGATTAGC	65 for 30 sec 30 cycles	Taq Pol. Buffer	WT: 481 bp MUT: 550 bp
Trp53$^{fl/fl}$	Fwd: AAGGGGTATGAGGGACAAGG Rev: GAAGACAGAAAAGGGGAGGG	60 for 30 sec 30 cycles	Taq Pol. Buffer	WT: 270 bp MUT: 390 bp
R26$^{YFP/+}$	R26R1: AAAGTCGCTCTGAGTTGTTAT R26R2: GCGAAGAGTTTGTCCTCAACC R26R3: GGAGCGGGAGAAATGGATATG	60 for 1 min 35 cycles	Taq Pol. Buffer	WT: 250bp MUT: 600bp

Table 4. Primers used for PCR genotyping of mice and embryos.

2.3.2 Cloning of the CXCR2 CDS

In order to produce antisense riboprobes for *in situ* hybridisation, the protein coding DNA sequences (CDS) of the murine and human *CXCR2* genes were first amplified and cloned. Because the CDS in both human and mouse *CXCR2* do not contain any introns, amplification was conducted from genomic DNA. Specific primers were designed and adapted with restriction sites: 5'-XhoI for forward primers and 5'-EcoRI for reverse primers. A 2-3 bp cap was added for improving enzymatic activity (Table 3). PCR amplification was conducted as described earlier using a normal Taq Buffer protocol.

Target	Primer sequences	Insert size
Mouse *Cxcr2*	Fwd: GCCTCGAGTACTGCGTATCCTGCCTCAG	610 bp
	Rev: GCGAATTCTCTGCTAAGAACGTGACCTCT	
Human *Cxcr2*	Fwd: GCCTCGAGATAGTGGCATCCTGCTACTG	633 bp
	Rev: GCGAATTCCTGATCAAGCCATGTATAGC	

Table 5. Primer sequences targeting the CDS of the murine and human *CXCR2* genes.

The PCR products were resolved by electrophoresis in a 1% agarose gel. Bands of the appropriate size were excised under a trans illuminator and purified using a Gel Extraction Kit (Qiagen) according to manufacturer's instructions. The inserts were then digested with XhoI and EcoRI for 3 hours at 37^{o}C, after which enzymes were inactivated by a 10-minute incubation at 65^{o}C and purified using a QIAquick PCR Purification Kit (Qiagen). The PBlueScriptSK vector was linearized also with XhoI and EcoRI for 2 hours at 37^{o}C, incubated with 1 µl of alkaline phosphatase (20 U/µl, Roche) for 1 hour at 37^{o}C to prevent self-ligation and purified in a column kit. Efficient digestion was confirmed by electrophoresis in 1% agarose gels. Ligation of the insert and vector was conducted in a 3:1 insert to vector molar ratio and a total of 50 ng of vector DNA in a 15 µl reaction including

1 µl of T4 DNA ligase, 1.5 µl of 10X T4 reaction buffer (Roche) and incubated for 2 hours at room temperature. A negative control reaction without DNA insert (self-ligated vector only) was included.

The ligation product was then used to transform competent DH5α *E. coli* cells (Thermo) by heat-shock. The cells were plated in agar plates containing ampicillin and grown overnight at 37°C. Resistant colonies were picked and grown in 1.5 ml L-Broth supplemented with ampicillin. DNA was isolated using a QIAprep Miniprep Kit (Qiagen) according to manufacturer's instructions. Positive clones were evaluated for successful insertion by XhoI and EcoRI restriction enzyme digestion and gel electrophoresis. Positive clones were grown further overnight in 100 mL of ampicillin-supplemented L-Broth. Plasmid DNA was extracted using a Qiaprep Maxiprep Kit (Qiagen) according to manufacturer's instructions. DNA quality and quantity were measured using a Nanodrop N-1000 spectrophotometer (NanoDrop Technologies). Verification of the insert was confirmed by Sanger sequencing in Source BioScience (Cambridge).

2.4 RNA methods

2.4.1 RNA isolation, cDNA preparation and quantitative real-time PCR (qRT-PCR)

Total RNA extraction from pituitaries was conducted using the RNeasy microkit (Qiagen), including on-column digestion with DNase I (Qiagen cat. 79254). Quantity and quality of RNA were also measured using a NanoDrop. cDNA transcription was performed on 1 µg of total RNA in a 20µl reaction volume using the iScript™ cDNA synthesis kit and according to manufacturer's instruction. 50ng of cDNA were used for each qRT-PCR reaction. Reactions were performed in triplicates in 96 well-plates on a CFX96 Touch™ Real-Time PCR Detection System using iTaq™ Universal SYBR® Green Supermix (BioRad). Verification of a single product

of the appropriate size was conducted by melting curve analysis and electrophoresis in 1% agarose gels. The expression of Glyceraldehyde 3-phospate dehydrogenase (GAPDH) was used as an expression normaliser. Analysis of expression between mutant and wild type expression was conducted by the comparative C_T (ΔΔCT) method (Livak, 2001). Fold changes were calculated as $2^{-\Delta\Delta Ct}$ for each sample. qRT-PCR experiments presented in Chapter 7 were conducted with the help of Dr. Sara Pozzi.

Gene	Forward (5'-3')	Reverse (5'-3')
Cdkn1a	CAGATCCACAGCGATATCCA	ACGGGACCGAAGAGACAAC
Cdkn2a	CGTGAACATGTTGTTGAGGC	GCAGAAGAGCTGCTACGTGA
Trp53	GCGTAAACGCTTCGAGATGTT	TTTTTATGGCGGGAAGTAGACTG
Il1α	CGCTTGAGTCGGCAAAGAAAT	TGGCAGAACTGTAGTCTTCGT
Il1β	TGCCACCTTTTGACAGTGATG	TGATGTGCTGCTGCGAGATT
Il6	CAAGAAAGACAAAGCCAGAGTC	GAAATTGGGGTAGGAAGGAC
Ccl20	AGCAACTACGACTGTTGCCT	TGACTCTTAGGCTGAGGAGGT
Cxcl1	CTGGGATTCACCTCAAGAACATC	CAGGGTCAAGGCAAGCCTC
Cxcl2	CCAACCACCAGGCTACAGG	GCGTCACACTCAAGCTCTG
Gapdh	ATGACATCAAGAAGGTGGTG	CATACCAGGAAATGAGCTTG

Table 6. List of primers used for quantitative RT-PCR.

2.4.2 RNA *In situ* hybridization (ISH) in paraffin sections

Preparation of antisense riboprobes

Plasmids were digested for linearization using the appropriate enzymes to produce antisense riboprobes (Table 5) and purified using a PCR purification kit (Qiagen). Plasmids were run in agarose gels to confirm complete linearization. For detection of the riboprobe, RNA transcription was conducted using a nucleotide mix containing Digoxigenin-11-2'-deoxy-uridine-5'-triphosphate (DIG-UTP). In this manner, DIG is incorporated into the RNA molecule and can be posteriorly detected

using antibodies. Transcription reactions consisted of: 1µg of linearized plasmid DNA, DIG-RNA labelling mix, 10X transcription buffer, RNase inhibitor, and RNA-polymerase (T3, T7 or SP6). Transcription was conducted for 2 hours at 37^{o}C. 1µl of the reaction product was run on a 1% agarose gel to verify transcription of a product of the appropriate size. Purification of the probe was conducted on CHROMA SPIN 100 columns (Clonetech) according to manufacturer's instructions.

Probe	Enzyme for linearisation	Polymerase
Cxcr4	HindIII	SP6
Cxcr7	SphI	SP6
Cxcl12	SalI	T3
Cxcr2	XhoI	T3
Wnt6	NotI	T3
Bmp4	EcoRI	Sp6
Shh	EcoRI	T7
Axin2	NotI	T3
Lhx3	XhoI	Sp6
CXCR2	XhoI	T3
Fgf8	HindIII	T3

Table 7. List of probes used for ISH.

Cxcr4, Cxcr7, Cxcl12, Wnt6, Bmp4, Shh, Axin2 and *Fgf8* antisense riboprobes were previously validated (Andoniadou et al. 2012; Sánchez-Alcañiz et al. 2011; Andoniadou et al. 2013; Gaston-Massuet et al. 2008).

In situ hybridization in paraffin sections

In situ hybridisation was performed as previously described (Andoniadou et al. 2012). All solutions were treated overnight with 0.1% di-ethyl-pyrocarbonate (DEPC) in double distilled MiliQ water and subsequently autoclaved. Paraffin sections were de-waxed in HistoClear (National Diagnostics) and re-hydrated using ethanol series. Slides were then fixed for 20 minutes in cold 4% PFA, treated with Proteinase K (20ug/ml) for 8 minutes, re-fixed in 4 % PFA and treated with 0.1M triethalolamine and 0.25% acetic anhydride. Slides were then de-hydrated and air-

dried. Antisense riboprobes were diluted 1:100 in 50:50 formamide: 0.3M sodium chloride, 20mM Tris-hydrochloric acid, 5mM EDTA, 10% Dextran sulphate, 1X Denhardt's reagent and RNAse inhibitor. Following overnight incubation at 65ºC, slides were washed in high high-stringency conditions in formamide and saline sodium citrate washes at 65ºC. Slides are then blocked in 0.1M Tris-HCl pH 7.5, 0.15M NaCl solution supplemented with 10% FCS for 1 hour. The detection of DIG-labelled RNA was conducted using a sheep anti-DIG antibody conjugated to alkaline phosphatase at 1:1000 dilution overnight. Subsequently, slides were washed in 0.1M Tris-HCl pH 9.5, 0.15M NaCl, 0.05 $MgCl_2$ buffer. Chromogenic detection of hybridised probes was conducted by adding nitro-blue tetrazolium chloride (NBT, 4.5 µl /ml) and 5-bromo-4-chloro-3-indolyl phosphate (BCIP, 3.5 µl/ml) in 10% polyvinyl alcohol.

2.5 Protein methods

2.5.1 Immunohistochemistry and immunofluorescence on paraffin sections

Immunohistochemical and immunofluorescent stainings were conducted on 6 µm-thick paraffin sections. Sections were dewaxed and rehydrated using ethanol gradients. Epitope unmasking was conducted in an antigen retrieval unit (BioCare Medical Decloaking Chamber NXGEN) for 2 minutes at 95ºC. Optimisation of staining conditions were conducted for each primary antibody by testing different antigen retrieval buffer solutions: 1) 1 M Sodium Citrate pH 6.0, 2) 1mM EDTA pH 8.0 or 3) 20 mM Tris, 0.65 mM EDTA, 0.005% Tween pH 9.0. Subsequently, slides were rinsed and permeabilised for 5 minutes in PBT (PBS, 0.1% Triton-X). Blocking was conducted for 1 hour at room temperature in blocking buffer (PBS, 0.1% Triton-X, 0.15% Glycine, 0.2% Bovine Serum Albumin (BSA)) supplemented with 10% Heat-Inactivated Sheep Serum (HISS). Primary antibodies were then incubated overnight

at 4ºC in blocking buffer supplemented with 1% HISS. Primary antibodies, dilutions and retrieval conditions are shown in Table 6. After incubation, slides were rinsed with PBT and incubated with the appropriate secondary antibodies for 1 hour at room temperature. Except for β-catenin, all primary antibodies were detected using biotin-conjugated secondary antibodies (Dako). For immunofluorescence, the biotinylated secondary was detected by incubation with Streptavidin conjugated to a fluorochrome such as Alexa-Fluor 555 (Thermo) for 1 hour at room temperature. After washing excess antibodies, the slides were subjected to auto fluorescence blocking by incubation in 0.1% Sudan Black (Sigma) in 70% EtOH for 2 minutes at RT in darkness. Excess Sudan Black was then washed with 0.02% Triton-X in PBS. DNA counterstaining was conducted by incubation with 4',6-Diamidino-2-Phenylindole (DAPI, Thermo) for 10 minutes at room temperature. For immunohistochemical stainings, slides were first incubated with an Avidin-Biotinylated Peroxidase Complex (Vector). Chromogenic detection was then conducted by addition of 3,3'-diaminobenzidine (DAB, Vector) for 2-5 minutes and then counterstained with Mayer's haematoxylin (Sigma). Immunolabelling of EdU uptake in paraffin samples was conducted using the EdU Click-It Imaging Kit (Thermo). EdU immunostainings with the help of Dr. Christina Stache. Immunostainings for the NF-κB pathway characterisation were conducted alongside Dr. Grace Kaushal. Triple immunostainings presented in Chapter 7 were conducted with the help of Dr. Alicia Villa-Osaba.

Target	Clonality	Clone	Company	Catalog Number	Dilution	Retrieval Method
4EBP1 (pThr37/46)	Monoclonal	236B4	Cell Signaling	2855	1:200	Tris-EDTA pH9.0
ACTH	Monoclonal	N/A	Fitzgerald	N/A	1:1000	Sodium Citrate pH 6.0
ATM (pSer1981)	Monoclonal	10H11.E 12	NovusBio	NB100-306	1:100	Tris-EDTA pH9.0
CD-31	Polyclonal	N/A	Abcam	ab28364	1:50	Tris-EDTA pH9.0
Cleaved Caspase 3	Polyclonal	Asp175	Cell Signaling	9661	1:300	Tris-EDTA pH9.0
CXCR4	Monoclonal	UMB-2	Abcam	ab124824	1:200	Tris-EDTA pH9.0
Cyclin D2	Polyclonal	M-20	Santa Cruz	sc-593	1:200	Tris-EDTA pH9.0
DNA PKcs (pT2609)	Monoclonal	10B1	Abcam	ab18356	1:200	Tris-EDTA pH9.0
E-cadherin	Monoclonal	36/E-Cadherin	BD Biosciences	610181	1:200	Tris-EDTA pH9.0
Endomucin	Monoclonal	V.5C7	Santa Cruz	SC-53941	1:250	Tris-EDTA pH9.0
FSH	Polyclonal	N/A	DSHB	N/A	1:1000	Sodium Citrate pH 6.0
GFP	Polyclonal	N/A	Abcam	ab13970	1:300	Tris-EDTA pH9.0
GH	Polyclonal	N/A	DSHB	N/A	1:1000	Sodium Citrate pH 6.0
GSU	Polyclonal	N/A	DSHB	N/A	1:500	Sodium Citrate pH 6.0
H2AX (pSer139)	Monoclonal	2F3	Biolegend	613402	1:400-1:800	Sodium Citrate pH 6.0
H2AX (pSer139)	Monoclonal	JBW301	Millipore	05-636	1:800	Sodium Citrate pH 6.0
Histone H3 (pSer10)	Polyclonal	N/A	Millipore	06-570	1:500	Tris-EDTA pH9.0
IκBα (pSer32/36)	Monoclonal	5A5	Cell Signaling	9246	1:100	Tris-EDTA pH9.0
Ki67	Polyclonal	N/A	Leica	NCL-Ki67p	1:100	Tris-EDTA pH9.0
Ki67	Monoclonal	SP6	Abcam	ab16667	1:100	Tris-EDTA pH9.0
LAMP-1	Polyclonal	N/A	Abcam	ab42170	1:200	Tris-EDTA pH9.0
LAMP-2	Monoclonal	H4B4	Abcam	ab25631	1:200	Tris-EDTA pH9.0
LC3	Polyclonal	N/A	AbD Serotec	AHP2167	1:1000	Tris-EDTA pH9.0
LH	Polyclonal	N/A	DSHB	N/A	1:500	Sodium Citrate pH 6.0
Lysozyme	Polyclonal	A009	Dako	A0099	1:200	Tris-EDTA pH9.0
Lyzozomal β-Galactosidase (GLB1)	Polyclonal	N/A	Proteintech	15518-1AP	1:100	Tris-EDTA pH9.0
N-cadherin	Polyclonal	N/A	Abcam	ab76057	1:100	Tris-EDTA pH9.0

P16INK4a	Monoclonal	JC8	Santa Cruz	sc-56330	1:200	Tris-EDTA pH9.0
P21	Polyclonal	M-19	Santa Cruz	sc-471	1:400	Tris-EDTA pH9.0
P53	Polyclonal	CM5	Leica	NCL-p53-CM5p	1:100	Tris-EDTA pH9.0
P62/SQSTM1	N/A	3/P62 LCK LIGAND	BD Biosciences	610833	1:200	Tris-EDTA pH9.0
P65/RELA	Monoclonal	D14E12	Cell Signaling	8242	1:200	Tris-EDTA pH9.0
Pan-Cytokeratin	Monoclonal	AE1/AE3	Santa Cruz	sc-81714	1:100	Tris-EDTA pH9.0
PARP-1	Monoclonal	F-2	Santa Cruz	sc-8007	1:300	Tris-EDTA pH9.0
Pit1	N/A	N/A	DSHB	N/A	1:500	Tris-EDTA pH9.0
PRL	Polyclonal	N/A	DSHB	N/A	1:1000	Sodium Citrate pH 6.0
S6 Ribosomal Protein (pSer240/244)	Monoclonal	D78F8	Cell Signaling	5364	1:200	Tris-EDTA pH9.0
SOX2	Polyclonal	N/A	Millipore	AB5603	1:200	Tris-EDTA pH9.0
SOX9	Polyclonal	N/A	Millipore	AB5535	1:400	Tris-EDTA pH9.0
Synaptophysin	Monoclonal	27G12	Leica	RTU-SYNAP-299	Ready-to-use	Any
TPit	N/A	N/A	Provided by Jacques Drouin	N/A	1:200	Tris-EDTA pH9.0
TSH	Polyclonal	N/A	DSHB	N/A	1:1000	Sodium Citrate pH 6.0
β-Catenin	Monoclonal	6F9	Sigma	C7082	1:300	Tris-EDTA pH9.0
β-Catenin	Polyclonal	N/A	Thermo	RB-9035-P1	1:300	Tris-EDTA pH9.0

Table 8. List of primary antibodies, dilutions and retrieval conditions.

2.5.2 Enzyme-Linked Immunosorbent Assay (ELISA) Arrays

The use of semi-quantitative ELISA cytokine arrays for the detection of SASP factors has been previously described (Coppé et al. 2008; Coppé, Patil, et al. 2010). Mouse C1000 cytokine arrays (AAM-CYT-1000-4, RayBiotech) were used to quantify the expression of SASP factors in protein extracts from whole pituitaries dissected at 18.5 dpc according to manufacturer's instructions. For each experimental sample, total protein was extracted from 4 pituitaries using a cell lysis solution provided by the kit in combination with a TissueRuptor (Qiagen) and passed through a Qiashredder column (Qiagen). Samples were centrifuged for 5 minutes at 10000 x g and supernatants were then transferred for protein quantification. All extraction procedures were conducted on ice. Total protein was then measured using BradfordUltra reagent (Expedeon) 1:1 in double distilled MiliQ water using a spectrophotometer and actual protein concentrations were determined from a standard curve of BSA concentrations. ELISA membranes were blocked for 30 minutes using blocking buffer provided by the manufacturer and then incubated overnight at 4ºC with 70 µg of total protein after a 7.5X dilution to prevent negative effects from detergent present in the cell lysis solution. Membranes were then incubated with biotinylated antibodies and subsequently with HRP-Streptavidin and provided detection reagents, according to manufacturer's instructions. Membranes were developed for 2 minutes prior to imaging.

2.6 Microscopy, Imaging and Statistical Analyses

Whole-mount imaging was conducted in a Leica MZ FLIII stereomicroscope connected to a Leica DC500 camera. Imaging of freshly dissected tumours was conducted at 0.8X magnification. For endogenous fluorescence imaging, the exposure was set to 3.7 seconds. The scale of the image was then calculated from graticule images at the same magnification and Fiji/ImageJ software (Schindelin et al. 2012) was used to measure tumour sizes. Tumour diameters were calculated from averaging the longest side of the tumour and its perpendicular.

Immunofluorescent stainings on paraffin sections were visualized with a Leica DMLM widefield microscope and imaged with a CoolSnap monochrome camera. Visualization of immunohistochemical, ISH and H&E stainings was conducted in a Zeiss Axioplan2 microscope and captured with a Zeiss Axiocam HRc colour camera. Image processing was conducted using Photoshop CC 2015 (Adobe), which included brightness/contrast enhancement and merging of fluorescence channels to produce composite images.

Cell counting from microscope images was conducted manually using Fiji/ImageJ and the cell counter plugin. For tumours, a minimum of 3 histologically distinct regions were counted and in each region a total of 800-1000 cells were counted.

Cell clusters were counted manually for the quantification of colocalisation of senescence markers and clusters. A cluster was defined as group of more than 3 nucleo-cytoplasmic β-catenin accumulating cells. At least 3 sections from each pituitary were counted. Selected sections were considerably apart in distance to prevent counting the same cluster more than once (surrounding structures such as the brain and the basisphenoid bone were used as reference). Colocalisation of the marker was defined as at least 1 cell of the cluster being positive for the marker.

For the quantification of EMCN+ area, appropriately scaled photographs of EMCN stainings were used and regions of 800-1000 cells were randomly selected using Fiji/ImageJ. Using the auto threshold option, a binary image was then created and the total area with positive signal contained within the region was calculated.

Chemiluminescence detection was conducted with a ChemiDoc gel documentation system (BioRad) and imaged using ImageLab Software (Version 5.2.1, BioRad). Different imaging parameters were tested and it was concluded that Chemiluminescence/High Resolution/Intense Bands settings provided best results. Analysis of high resolution images from each membrane was conducted using Fiji/ImageJ and the Protein Microarray Analysis macro (IRB, Barcelona). Overall background was subtracted using a 25-pixel rolling-ball radius. Each ELISA spot was then circumscribed in identically sized circular regions of interest (ROIs). The diameter of the ROI circle was selected to be around 1.5 times larger than the largest signal spot in the membrane. Each ROI was then manually centred around the chemiluminescent spot, avoiding overlap between ROIs. ROI size was maintained consistent to allow comparison between different membranes. The average signal value from negative control and blank spots was subtracted from each target spot signal value. Normalised signal density for each target spot was then calculated according to the following formula: X(NMut) = X(Mut) * P1/P(MUT). Where: P1 is the mean signal density for positive control spots on the reference (wild type) array membrane; P(MUT) is the mean signal density for the positive control spots on the mutant array membrane; X(MUT) is the mean signal density for spot “X” on mutant membrane and X(NMUT) is the normalized signal intensity for spot X in the mutant array. A fold increase in signal intensity for spot X between the mutant and wild type membranes was then calculated as the ratio between X(NMUT) and X(wild type). Statistical analysis was conducted using SPSS Statistics software (IBM). Statistical significance level was set as 0.05.

2.7 Gene-Set Enrichment Analysis (GSEA) and hierarchical clustering

All GSEA analyses were performed using GSEAv. 2.2.0 (Broad Institute) using the pre-ranked tool, weighted enrichment statistic and 1000 permutations and interpreted according to recommendations found in the original GSEA article (Subramanian et al. 2005).

GSEA assesses where genes in a gene set fall within a list of genes that has been ranked according to their expression. It performs statistical analyses to assess whether the ranked gene list is enriched for the genes within the gene set (i.e. they are overrepresented either at the top or bottom of the list than would be expected by chance alone).

For human analyses, Laser Capture Microdissection (LCM), RNA isolation, RNA amplification and RNAseq raw data processing (as well as hierarchical clustering) were conducted by Dr. John Apps. Briefly, RNA-sequencing data was obtained from clusters and palisaded-epithelium tissue isolated by laser capture microdissection (LCM) conducted on two different human ACP samples. A list of 17,779 genes was generated by ranking expression from the most upregulated in clusters to the most upregulated in palisading epithelium (non-clusters) as determined by the DESeq2 method in the bioconductor R package (estimated log2 fold change/standard error of log2 fold change using the Wald statistic)(Love et al. 2014).

For analysis of data obtained from the *Hesx1*$^{Cre/+}$*;Ctnnb1*$^{lox(ex3)/+}$ model, previously published microarray expression analysis data was used (Andoniadou et al. 2012). This microarray data was obtained from dissociated *Hesx1*$^{Cre/+}$*;Ctnnb1*$^{lox(ex3)/+}$*;BAT-gal* pituitaries and flow sorting for the BAT-gal positive and negative populations. This sorting strategy allows to compare the β-catenin cluster population versus non-cluster. Expression data was then ranked by gene

expression from highest fold-change of expression in clusters compared to non-clusters also using the Wald statistic (21891 genes).

Oncogene-Induced Senescence and SASP gene sets were kindly provided by Professor Jesús Gil. The OIS geneset was obtained by RNA-sequencing and the SASP gene sets was derived from proteomics data, both conducted on human IMR90 ER: RAS fibroblasts. These cells express an Esteroid Receptor-KRASV12D chimeric fusion protein that triggers growth arrest, senescence and SASP when induced (Acosta et al. 2013).

For hierarchical clustering analysis, mouse gene symbols were converted to human homologs using BiomaRt (Durinck et al. 2009) and merged with human rLog-scaled read counts obtained from DESeq2. Genes were filtered for differential expression in between human clusters and non-clusters according to a $\log_2$ fold-change larger than 2 and a p-adjusted-value lower than 0.05. Consensus clustering was performed using average clustering algorithms in the BioConductor Consensus Cluster Plus package.

3. INVOLVEMENT OF CELLULAR SENESCENCE AND ITS ASSOCIATED SECRETORY PHENOTYPE IN THE NON-CELL AUTONOMOUS INDUCTION OF PITUITARY TUMOURS

3.1 Introduction

A gain of function mutation in the β-catenin gene (*CTNNB1*) and the consequent accumulation of nucleo-cytoplasmic β-catenin with activation of the Wnt signalling pathway in neoplastic cells is characteristic of many tumours and cancers (Reya & Clevers 2005). However, in mouse ACP models, cells targeted with oncogenic β-catenin stop dividing and remain mostly as cell clusters. Indeed, it has been shown that human ACP clusters are not actively dividing (Buslei et al. 2007; Gaston-Massuet et al. 2011) nor undergo apoptosis (Zhu & You 2015). Why is this small cell population spared and persists during tumour progression? Interestingly, the clusters in both mice and humans are the source of many secreted factors with well-known roles in tumourigenesis and cancer progression, such as: SHH, FGFs, BMPs, WNT ligands and a variety of cytokines and pro-inflammatory factors, suggesting that these cell structures may play an active role in ACP development (Andoniadou et al. 2012).

Previous lineage tracing studies conducted in an inducible mouse model expressing oncogenic β-catenin in adult pituitary stem cells (*Sox2*$^{CreERT2/+}$;*Ctnnb1*$^{lox(ex3)/+}$;*R26*$^{YFP/+}$) unexpectedly revealed the emergence of pituitary tumours in a non-cell-autonomous manner (Andoniadou et al. 2013). In this study, it was proposed that β-catenin clusters undergo cellular senescence, therefore preventing them from further dividing, but also allowing them to acquire a Senescence-Associated Secretory Phenotype (SASP) capable of mediating oncogenesis in a paracrine manner.

In order to test this hypothesis, the *Hesx1*$^{Cre/+}$;*Ctnnb1*$^{lox(ex3)/+}$ model was used to assess if conditional expression of oncogenic β-catenin in embryonic pituitary stem cells could also induce tumours non-cell autonomously. Moreover, it was investigated if this oncogenic process is preceded by the onset of senescence and SASP acquisition in targeted cells. The clinical significance of senescence and the SASP in

human ACP was evaluated in individual human ACP tissue sections and corroborated in tissue microarrays containing 23 different ACP cases and brain tissue as control.

3.2 Lineage tracing of targeted cells during tumour progression in *Hesx1$^{Cre/+}$;Ctnnb1$^{lox(ex3)/+}$;R26$^{YFP/+}$*

Lineage tracing analysis was conducted in *Hesx1$^{Cre/+}$;Ctnnb1$^{lox(ex3)/+}$;R26$^{YFP/+}$* pituitaries at different stages of tumour development, which are described chronologically in this section as: embryonic, early postnatal, intermediate stage tumour and end-stage tumour. At embryonic stage 18.5 dpc, the pituitary parenchyma was mainly composed of YFP+ cells derived from the *Hesx1* lineage (Figure 3.1a), while the pituitary stroma resulted negative. Early postnatal pituitaries contained anaplastic regions of YFP+ cell islands which intermingled with and expanded YFP- stroma. These “pre-tumourigenic” regions were consistently localised ventrally in the pituitary anterior lobe (Figure 3.1b, delimited by dotted line). The same pre-tumourigenic regions could be observed at later postnatal stages with no drastic changes, except for occasional cyst formation (Figure 3.1c, delimited by dotted line). In intermediate stage tumours, the YFP- tissue expanded and rapidly displaced the YFP+ cells, forming a clear boundary between the growing YFP- tumour (Figure 3.1d, asterisk) and the normal pituitary tissue (Figure 3.1d, arrow). Importantly, 64.7% of observed end stage tumours (N=17) were mostly composed of YFP- cells (Figure 3.1e, asterisk), while residual YFP+ tissue could still be observed at the periphery of these tumours (Figure 3.1e, arrow). The analysis conducted for this thesis focused only on YFP negative *Hesx1$^{Cre/+}$;Ctnnb1$^{lox(ex3)/+}$;R26$^{YFP/+}$* tumours.

Double immunostaining for YFP and the proliferation marker Ki67 showed that most of the pituitary YFP+ tissue was proliferative at 18.5 dpc (Figure 3.1f), while at early postnatal stages scarce Ki67+ cells were present in the pituitary, including pre-tumourigenic ventral regions (Figure 3.1g-h, delimited by dotted lines). Finally,

intermediate-stage and end-stage YFP- tumours showed increased Ki67 positivity (Figure 3.1i-j, asterisks), while the residual YFP+ tissue was essentially non-proliferative (Figure 3.1i-j, arrows). These observations indicate that tumour formation occurs after a latency period as a sporadic, rapid wave of proliferation of YFP- cells, rather than being a gradual and continuous process.

Expression analysis of the neuroendocrine marker synaptophysin throughout tumour development showed that the parenchyma (which is YFP+) of the pituitary anterior lobe was mostly synaptophysin positive at embryonic and early postnatal stages (Figure 3.1k-n), while the pituitary stroma was synaptophysin negative (and is also negative for YFP). Notably, the ventral pre-tumourigenic regions contained few synaptophysin positive cells at early postnatal stages (Figure 3.1m-n, delimited by dotted line), suggesting that most of the YFP+ cells present in these regions were also undifferentiated. Intermediate stage tumours showed a marked contrast in synaptophysin expression where the normal pituitary epithelium stained positive (Figure 3.1l, arrow), whereas the growing tumour tissue was negative (Figure 3.1l, asterisk). End-stage tumours were mostly negative for synaptophysin (Figure 3.1o, asterisk), while peripheral regions contained residual positive cells (Figure 3.1o, arrow in inset), delineating these as undifferentiated tumours, as previously reported (Gaston-Massuet et al. 2011). Therefore, the lack of synaptophysin expression discriminates pre-tumourigenic regions and full-grown tumours from normal pituitary tissue, and suggests that end-stage tumours are derived from cells present in these synaptophysin-negative pre-tumourigenic areas.

Previous characterisation of the *Hesx1*$^{Cre/+}$*;Ctnnb1*$^{lox(ex3)/+}$ model revealed that the nucleo-cytoplasmic β-catenin accumulating clusters are present throughout embryonic pituitary development, from 9.5 dpc to 18.5 dpc and after birth at postnatal day 11 (Gaston-Massuet et al. 2011). Analysis of the expression of β-catenin at different stages of tumour development by immunofluorescence revealed that these

clusters were still present at later postnatal stages and that they were mainly localised in the ventral pre-tumourigenic regions (Figure 3.1q-r, arrows). Interestingly, intermediate and end-stage pituitary tumours expressed high levels of β-catenin (Figure 3.1s-t, asterisks), suggesting activation of the Wnt signalling pathway, although it was mostly cytoplasmic accumulation (unlike the nucleo-cytoplasmic pattern found in the original clusters). Importantly, at intermediate tumour stages, the number of β-catenin clusters found in tissue sections was markedly reduced (Figure 3.1s, arrow in inset), while none could be detected in the end-stage tumours. Therefore, the β-catenin clusters are preserved during embryonic and early postnatal stages of tumour formation, until a point where they become dispensable for tumour formation and progression.

In conclusion, pituitary embryonic progenitors bearing the oncogenic β-catenin mutation do not give rise to a proportion of *Hesx1*$^{Cre/+}$*;Ctnnb1*$^{lox(ex3)/+}$*;R26*$^{YFP/+}$ pituitary tumours cell-autonomously, further supporting the paracrine-tumourigenesis model derived from lineage tracing experiments in *Sox2*$^{CreERT2/+}$*;Ctnnb1*$^{lox(ex3)/+}$*;R26*$^{YFP/+}$ mice (Andoniadou et al. 2013). This observation also suggests that both mouse models share a common and age-independent mechanism, where oncogenic β-catenin activation in pituitary stem cells leads first to cell cluster formation, after which pituitary tumours can arise from a non-targeted population.

Hesx1Cre/+;Ctnnb1lox(ex3)/+;R26YFP/+
18.5 dpc
5 wk
15 wk
20 wk
35 wk
pl
il
al
YFP/DAPI
YFP/Ki67/DAPI
Synapt
β-Cat/DAPI

Figure 3.1 *Hesx1*$^{Cre/+}$*;Ctnnb1*$^{lox(ex3)/+}$ pituitary tumours are not derived from targeted embryonic progenitors nor display a differentiated phenotype.

(a-e) Fluorescent immunostaining for YFP in representative specimens at different stages of tumour development, showing that most of the pituitary anterior lobe parenchyma is derived from the *Hesx1* lineage (YFP+) at embryonic (a) and early postnatal stages (b,c), while the stroma is YFP-. Note the presence of anaplastic regions localised ventrally in the anterior lobe of early postnatal stages (delimited from normal pituitary tissue by dotted line). Intermediate (d) and end-stage tumours (e) show a drastic expansion of the YFP- population. **(f-j)** Double immunofluorescence for the proliferation marker Ki67 and YFP at different stages of development, showing that the embryonic pituitary contains YFP+ proliferating cells (f), while the early postnatal stages have low numbers of Ki67+ cells (g,h). Intermediate and end-stage tumours possess large numbers of Ki67+ cells present mostly in YFP- regions (i,j respectively). **(k-o)** Immunohistochemistry for the neuroendocrine marker synaptophysin show positive cells in the anterior lobe parenchyma of embryonic (k) and early postnatal pituitaries (m,n), while their stroma is negative. Note that ventral anaplastic regions contain mostly non-differentiated cells (m,n; delimited by dotted line). Intermediate and end-stage tumours do not contain synaptophysin positive cells (l,o; asterisks) except in residual peripheral regions (l,o; arrows). **(p-t)** Immunofluorescence for β-catenin shows the presence of nucleo-cytoplasmic β-catenin accumulating clusters at 18.5 dpc (p) exclusively in the ventral pre-anaplastic regions of early postnatal pituitaries (q,r; arrows). Cytoplasmic β-catenin accumulation can be observed in growing intermediate and end-stage tumours (s,t; asterisks), while stereotypical clusters could rarely be observed in peripheral regions (s, arrow). al: anterior lobe; il: intermediate lobe; pl: posterior lob; dpc: days *post coitum;* wk: weeks. Scale bars: a, 250 μm; b,c,d, 100 μm.

3.3 Characterisation of the senescent phenotype in *Hesx1$^{Cre/+}$;Ctnnb1$^{lox(ex3)/+}$* and human ACP cell clusters

Cellular senescence is a complex state that cannot be defined by a single molecular marker (Sharpless & Sherr 2015; Campisi 2013; Collado & Serrano 2010). Therefore, the presence of several well-established markers that reflect key biological processes of the senescent phenotype was evaluated *in vivo* with focus on the β-catenin clusters. These include markers of cell proliferation, DNA replication, lysosomal activity, DNA damage and the Senescence-associated Secretory Phenotype (SASP). Analysis of crucial pathways related to, or known to mediate these processes, such as the DNA-Damage Response (DDR), the NF-κB pathway, mTOR signalling and autophagy, was also conducted. Finally, an *in vivo* characterisation of the progression of the senescent phenotype at different stages of embryonic pituitary development was performed to gain a better understanding of the evolution of the senescent phenotype in this context, as current understanding of the development of the senescent phenotype derived mainly from *in vitro* experiments.

3.3.1 *Hesx1$^{Cre/+}$;Ctnnb1$^{lox(ex3)/+}$* clusters contain cells that are viable and non-proliferative

It was previously shown that the clusters of *Hesx1$^{Cre/+}$;Ctnnb1$^{lox(ex3)/+}$* pituitaries at 18.5 dpc do not express the proliferation marker Ki67, suggesting a quiescent state (Gaston-Massuet et al. 2011). To confirm the absence of proliferation at this stage, immunostaining was performed for the mitosis marker phospho-histone H3 (p-HH3) and 5-ethynyl-2'-deoxyuridine (EdU). These experiments showed the general lack of colocalisation of phospho-histone H3 (Figure 3.2a, 2.94% colocalisation, N=34 clusters in 3 embryos) and EdU (Figure 3.2b, 2.5% colocalisation, N=35 clusters in 3 embryos) with the β-catenin clusters at 18.5 dpc. Additionally, colocalisation between β-catenin clusters and the apoptosis marker activated cleaved caspase 3 (CASP3)

could only be observed in single cells in a minority of clusters (Figure 3.2c, 6.98% colocalisation, N=43 clusters in 3 embryos). Therefore, the vast majority of nucleo-cytoplasmic β-catenin accumulating cell clusters in *Hesx1$^{Cre/+}$;Ctnnb1$^{lox(ex3)/+}$* pituitaries do not divide, do not replicate their DNA nor undergo programmed cell death at 18.5 dpc, suggesting a senescent phenotype.

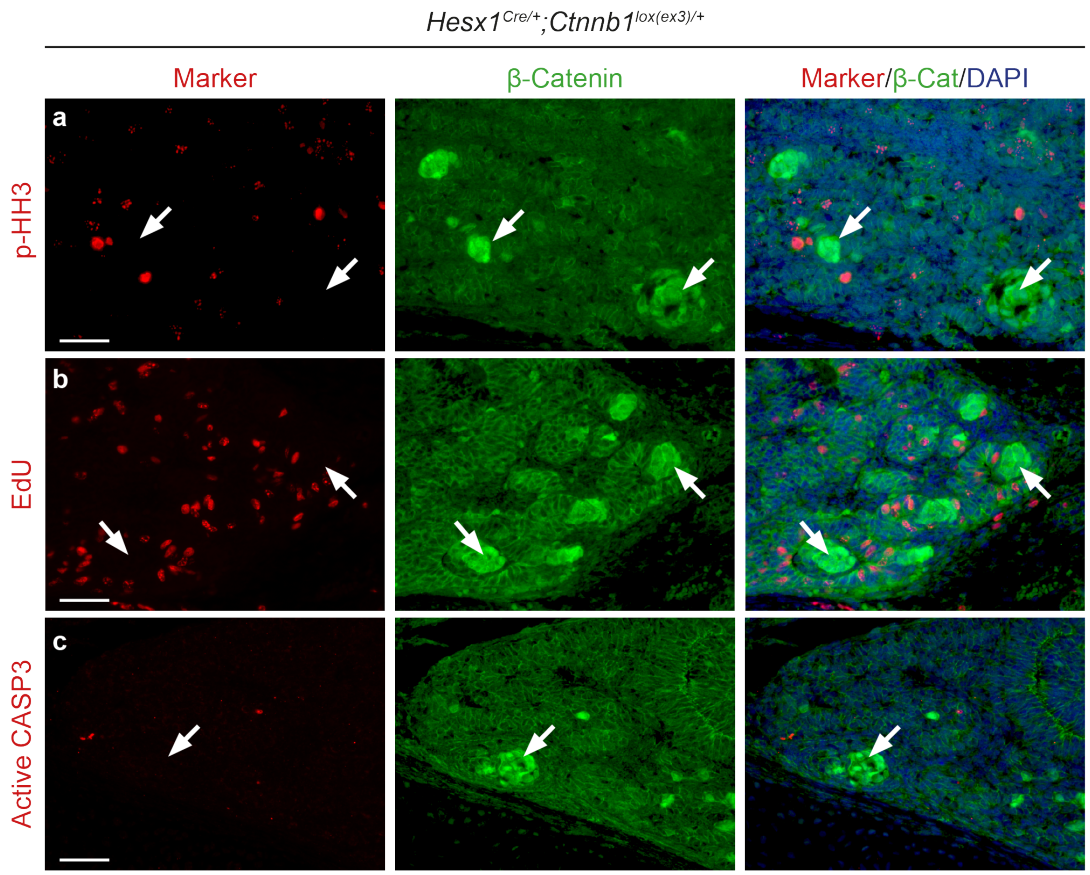

Figure 3.2 *Hesx1$^{Cre/+}$;Ctnnb1$^{lox(ex3)/+}$* embryonic pituitaries at 18.5 dpc contain nucleo-cytoplasmic accumulating β-catenin clusters that are non-proliferating and non-apoptotic.

(a-b) Double immunofluorescence for proliferation markers phosphorylated histone H3 (p-HH3) and EdU showing presence of proliferating cells in the pituitary's anterior lobe but not in β-catenin clusters (arrows). **(c)** Activated caspase 3 staining shows absence of apoptosis in clusters (arrows). Scale bars: 50 μm.

3.3.2 Characterisation of the lysosomal compartment in β-catenin clusters

The most widely used method for identifying senescent cells is the senescence-associated β-galactosidase detection assay (SA-β-Gal) at pH 6.0 (Dimri 2005; Debacq-Chainiaux et al. 2009). This assay produces a blue coloured precipitate in cells containing large amounts of lysosomal β-galactosidase. SA-β-Gal staining of *Hesx1*$^{Cre/+}$*;Ctnnb1*$^{lox(ex3)/+}$ pituitaries at postnatal day 7 revealed a strong positive signal in round cellular formations of the pituitary anterior lobe resembling β-catenin clusters (Figure 3.3a, arrow), whereas in matching wild type pituitaries only the posterior lobe (which contains neuropeptide secreting axons) and the pituitary stroma showed a faint blue signal. In order to better show colocalisation between this senescence marker and the β-catenin clusters, double immunostaining experiments were conducted using an antibody directed against the enzyme responsible for the SA-β-Gal activity (encoded by the *GLB1* gene in mice and humans) (Lee et al. 2006).

Fluorescent immunostaining for GLB1 in 18.5 dpc *Hesx1*$^{Cre/+}$*;Ctnnb1*$^{lox(ex3)/+}$ pituitaries showed that the pituitary parenchyma itself contains GLB1 protein, possibly reflecting the secretory nature of pituitary endocrine cells. However, an evident and strong punctuated signal colocalised with β-catenin clusters in the anterior lobe (Figure 3.3b, arrows, 62% colocalisation, N=60 clusters in 4 embryos). These results were recapitulated in human ACP samples, where positive GLB1 staining localised mostly with the β-catenin clusters (Figure 3.3c, arrows; Figure 3.4a, arrow, 100% colocalisation, N=16 clusters).

Because the accumulation of lysosomal β-galactosidase that characterises senescent cells is a reflection of the overall increase of the lysosomal compartment (Kurz et al. 2000), an assessment of other lysosomal markers was conducted. Double immunofluorescence for β-catenin and lysosomal markers LAMP1 and Lysozyme C also showed their expression in the pituitary parenchyma, although the strongest

signal was localised to the β-catenin clusters (Fig 3.3d, arrows; 82% colocalisation for LAMP1, N=62 clusters in 4 embryos). Moreover, these patterns were also observed in human ACP sections where both LAMP1 and Lysozyme C colocalised with nucleo-cytoplasmic β-catenin clusters (Figure 3.3e, arrows; 100% colocalisation for LAMP1, N=12 clusters; 100% colocalisation for Lysozyme, N=7 clusters). Additionally, the expression of another crucial lysosomal component, LAMP2, was observed to accumulate in human ACP clusters (Figure 3.4 b, arrow; 100% colocalisation, N=21 clusters).

In summary, although the expression of lysosomal markers was observed in different compartments of the *Hesx1*$^{Cre/+}$*;Ctnnb1*$^{lox(ex3)/+}$ pituitary and human ACP, their accumulation could be detected in nucleo-cytoplasmic accumulating β-catenin clusters in an objective manner. This suggests that these cells have an expanded lysosomal compartment, which is a characteristic of metabolically-active senescent cells.

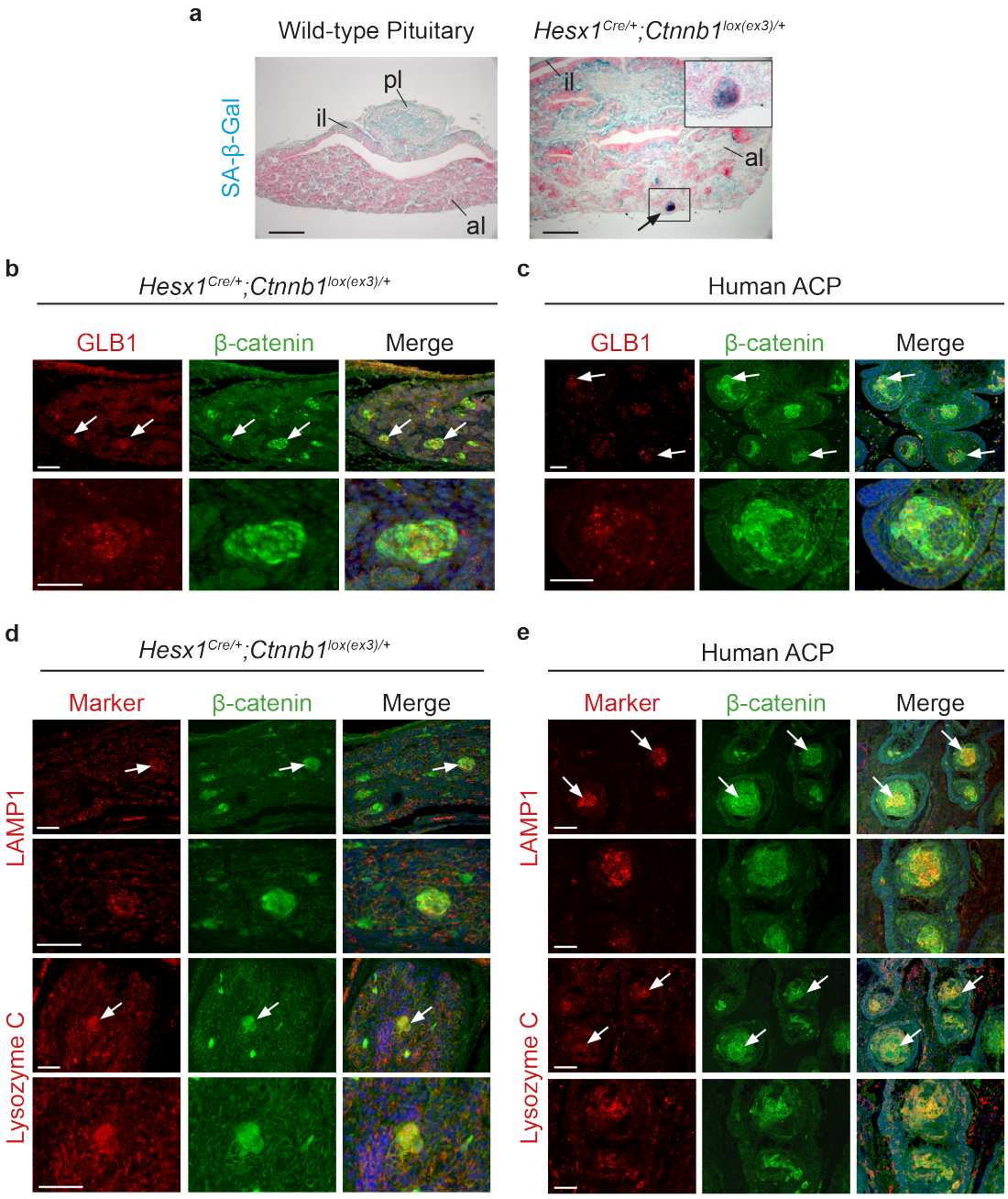

Figure 3.3 β-catenin clusters of the embryonic mouse ACP model possess an expanded lysosomal compartment, a characteristic of senescent cells.

(a) Senescence-Associated β-Galactosidase (SA-β-Gal) staining at pH 6.0 (blue staining, eosin counterstain) in wild-type and mouse ACP postnatal day 7 pituitaries. SA-β-Gal staining faintly labels the posterior lobe and stroma in wild type pituitaries, while it strongly labels round structures resembling β-catenin clusters in mutant pituitaries (arrow, inset). (**b-c**) Double immunofluorescence for β-catenin and lysosomal β-Galactosidase (GLB1) shows accumulation of GLB1 puncta in the nucleocytoplasmic accumulating β-catenin clusters (arrows) of 18.5 dpc mouse ACP

pituitaries (**b**) and human ACP (**c**). (**d-e**) Lysosomal proteins LAMP1 and Lysozyme C also accumulate in the clusters of 18.5 dpc mouse ACP pituitaries (**d**) and human ACP (**e**). Scale bars: a, 200 μm; b, 50 μm (inset: 25 μm); c,d, 50 μm; e, 100 μm . pl: posterior lobe, il: intermediate lobe, al: anterior lobe. Merged figures: DAPI counterstain.

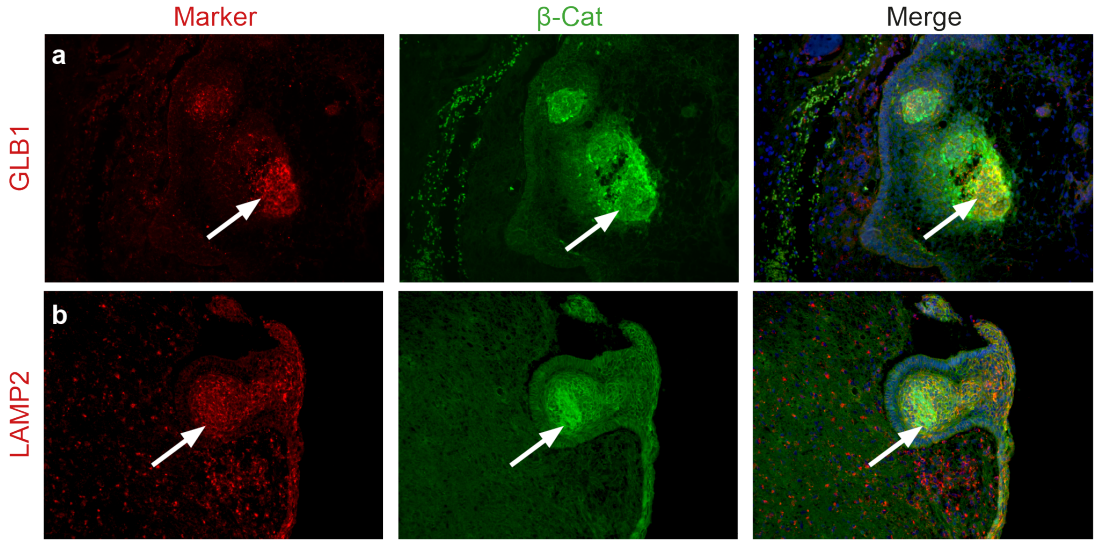

Figure 3.4. Human ACP clusters express LAMP2 an essential lysosome component.

Double immunostaining for β-catenin and lysosomal markers GLB1 and LAMP2 **(a-b)** in human ACP sections shows colocalisation with β-catenin accumulating clusters. Scale bars: 100 μm. Merged figures: DAPI counterstain.

3.3.3 Cell cycle inhibitor expression in β-catenin clusters

The p53/p21 and p16/Rb pathways are main drivers of the senescent cell-cycle arrest (Serrano et al. 1997; Ventura et al. 2007; Sarkisian et al. 2007; Feldser et al. 2010), therefore it was investigated if β-catenin clusters show an increased expression of the cell cycle inhibitors p16, p21 and p53 in both *Hesx1*$^{Cre/+}$*;Ctnnb1*$^{lox(ex3)/+}$ pituitaries at 18.5 dpc and in human ACP. In the mouse, all observed β-catenin clusters contained p16, p21 and p53 positive cells (Figure 3.5a-c, arrows). Quantification of p16 and nucleo-cytoplasmic β-catenin showed that 89% of cluster cells were p16 positive (Spearman correlation coefficient $R=0.929$, $p<0.001$, N= 209 cells), while 77% of cluster cells were p21 positive (Spearman correlation coefficient $R=0.926$, $p<0.001$, N=143 cells).

In human ACP, p16 was detected in mainly in cells of the palisaded epithelium and within β-catenin clusters (Figure 3.5d, arrows; 93% colocalisation, N=29 clusters). Positive staining for p21 was almost exclusively found in cluster cells (Figure 3.5e, arrows; 94% colocalisation, N=32 clusters), while p53 protein was detected in various cells in both glial reactive tissue and the tumour parenchyma, including β-catenin clusters where the staining intensity was strongest (Figure 3.5f, arrows; 100% colocalisation, N= 16 clusters). The co-expression of these crucial cell-cycle inhibiting proteins suggests that a stable senescent phenotype is enforced by the p53/p21 and p16/Rb pathways in both murine and human β-catenin clusters.

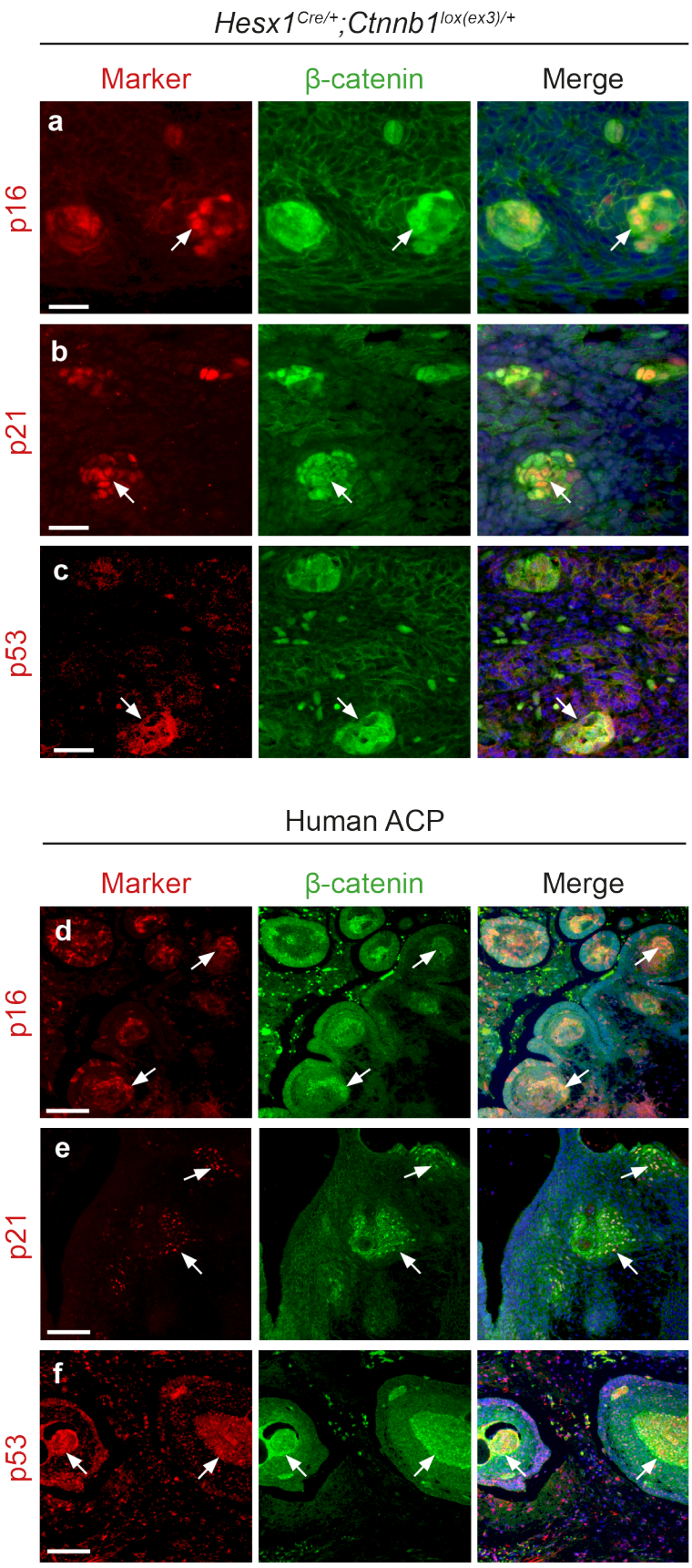

Figure 3.5 β-catenin clusters have elevated expression of cell cycle inhibitors.

(a-c) Double immunofluorescence shows accumulation of p16, p21 and p53 with β-catenin clusters of the embryonic mouse ACP model at 18.5 dpc (arrows). **(d-f)** Results are recapitulated in human ACP clusters (arrows). Scale bars: a-c, 25 μm; d-f, 100 μm. Merged figures: DAPI counterstain.

3.3.4 DNA damage and the DNA damage response (DDR) in β-catenin clusters

The acquisition of DNA damage by the β-catenin clusters was evaluated through the expression of the well-established DNA damage marker γ-H2A.X, which accumulates at double-strand break sites (Bonner et al. 2008). Additionally, the expression of PARP-1 and phospho-DNA-PKcs, two other key DDR effectors, was analysed. Strong positive staining for γ-H2A.X was observed in the *Hesx1*$^{Cre/+}$*;Ctnnb1*$^{lox(ex3)/+}$ clusters at 18.5 dpc (Figure 3.6a, arrow) and in cells dispersed throughout the pituitary anterior lobe. Furthermore, phosphorylated-DNA-PKcs and PARP-1 positive staining was exclusively observed within the murine clusters (Figure 3.6b-c, arrows). These results were recapitulated in human ACP samples where γ-H2A.X, PARP-1 and phospho-DNA-PKcs immunostaining consistently colocalised with nucleo-cytoplasmic β-catenin (Figure 3.6 d,e,f respectively, arrows).

Another factor shown to be crucial for the activation of the DDR is the protein kinase ATM (Aird et al. 2015). Although, the detection of this protein by immunofluorescence was not successful in the mouse tissue, it was possible to label phosphorylated ATM in human ACP tissue, where it was found to colocalise mainly with β-catenin clusters (Figure 3.7b). Collectively, these results indicate that both murine and human β-catenin clusters undergo DNA-damage and activate the DDR, further supporting a senescent phenotype in these cellular structures.

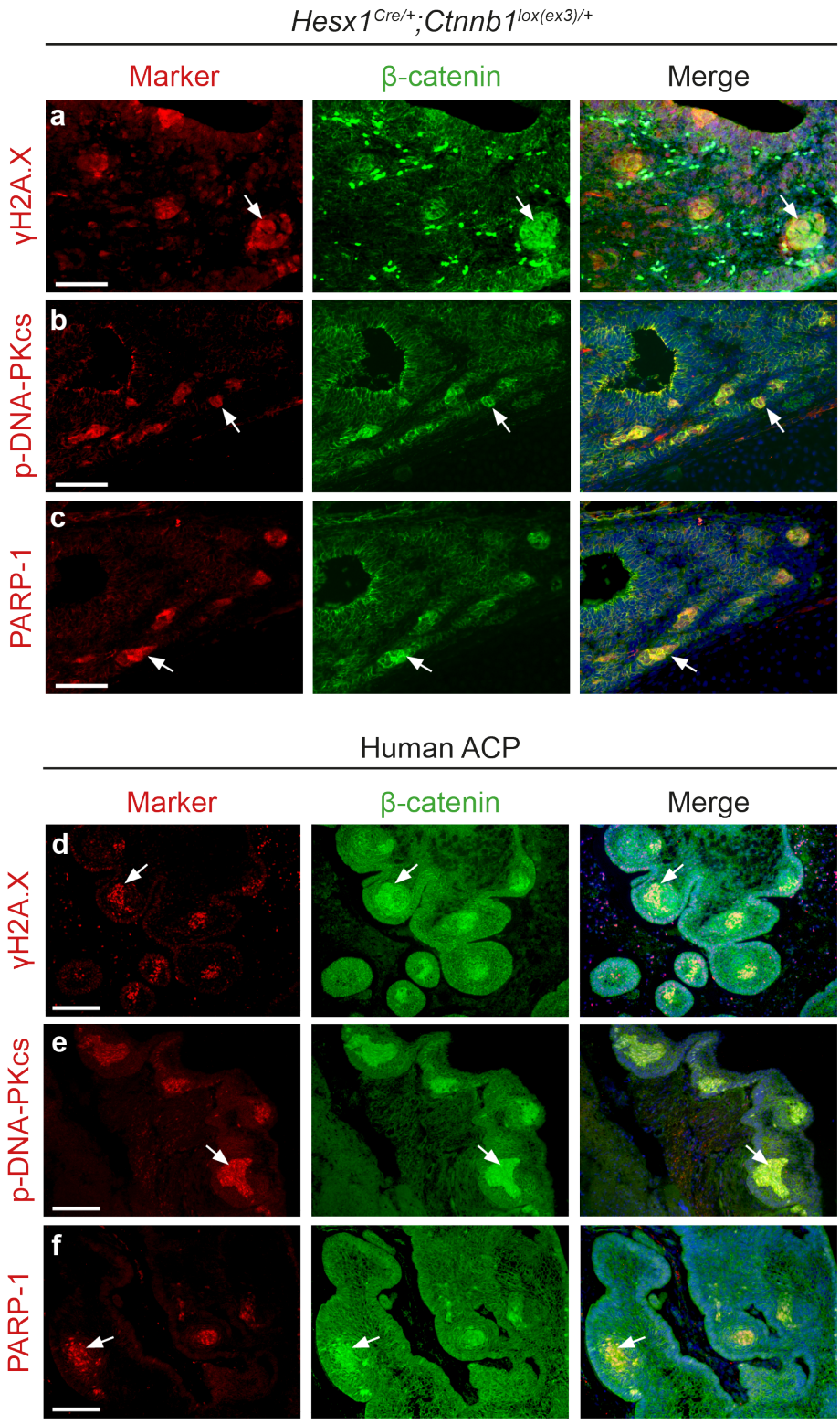

Figure 3.6 β-catenin clusters express markers of DNA damage and the DNA-damage response (DDR).

(a-c) Double immunofluorescence for DNA damage marker γH2A.X and DDR effectors DNA-PKcs and PARP-1 shows colocalisation with nucleo-cytoplasmic accumulating β-catenin clusters in 18.5 dpc mouse ACP pituitaries (arrows). **(d-f)**

Colocalisation of DNA-damage marker expression and β-catenin clusters is recapitulated in human ACP (arrows). Scale bars: a-c, 75 μm; d-f, 125 μm. Merged figures: DAPI counterstain.

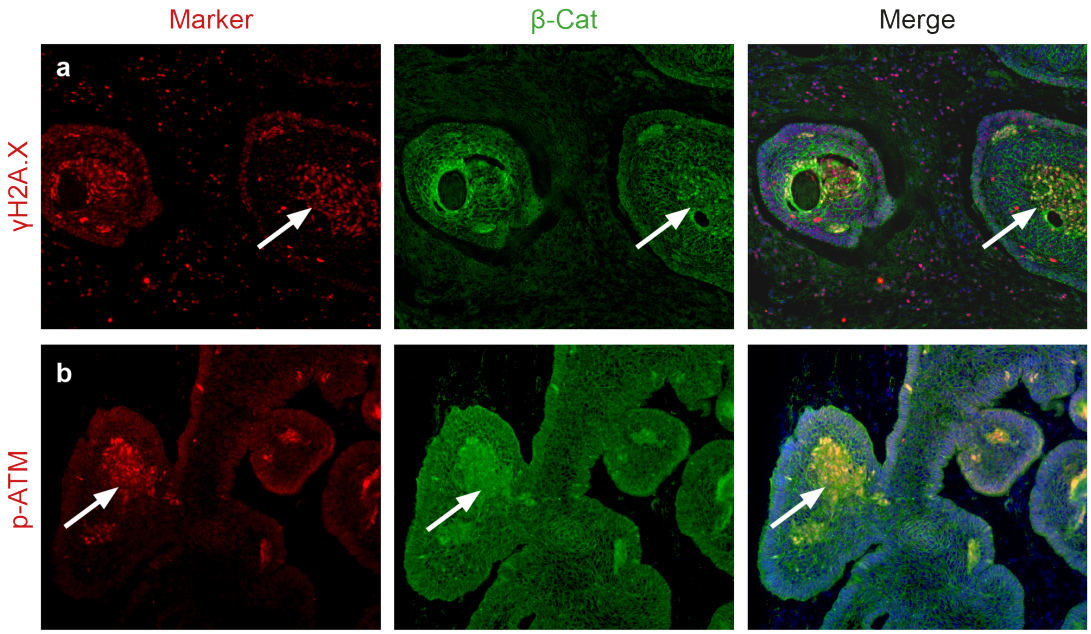

Figure 3.7 Human ACP clusters express the essential DNA-damage response element ATM.

Double immunostaining for β-catenin and DNA-damage indicators γ-H2A.X **(a)** and phosphorylated ATM **(b)** in human ACP sections shows positive staining colocalisation with the β-catenin clusters (arrows). Scale bars: 100 μm. Merged figures: DAPI counterstain.

3.4 Characterisation of the mTOR and autophagy pathways

3.4.1 *Hesx1$^{Cre/+}$;Ctnnb1$^{lox(ex3)/+}$* and human ACP clusters differ in their expression of key mTOR effectors

The mTOR pathway has been shown to be involved in the establishment of cellular senescence (Castilho et al. 2009) and also to mediate the SASP (Laberge et al. 2015; Herranz et al. 2015). The activation of the mTOR pathway can be determined by assessing the presence of phosphorylated ribosomal protein S6 (pS6) and phosphorylated 4E-BP1 (p4E-BP1). In *Hesx1$^{Cre/+}$;Ctnnb1$^{lox(ex3)/+}$* pituitaries, pS6 expression was observed throughout the anterior and intermediate lobes of the pituitary gland, mostly as scattered single cells. Particularly, around 50% of β-catenin clusters were positive for p-S6 (Figure 3.8a, arrows), while the rest did not contain positively labelled cells (Figure 3.8a, arrowheads). On the other hand, p4E-BP1 expression was only observed in rare occasions confined to scattered single cells in the anterior lobe (Figure 3.8b, arrows), while expression in the β-catenin clusters was not observed (Figure 3.8b, arrowheads). However, positive p4E-BP1 cells were observed in the hypothalamic region of the brain, mainly in cells lining the third ventricle (Figure 3.8b, inset), serving as a positive control and showing that p4E-BP1 immunostaining worked properly in mouse tissue.

Analysis of human ACP samples revealed a striking contrast with the mouse model. While pS6 protein expression never colocalised with the β-catenin clusters, it was consistently observed in the palisaded epithelium (Figure 3.8c, arrows), in proximity to the clusters (Figure 3.8c, arrowheads), as well as in reactive tissue. Conversely, the expression pattern of p4E-BP1 was more variable in human samples, where positive signal was observed in a proportion (~50%) of β-catenin clusters (Figure 3.8d, arrows) as well as in the palisaded epithelium.

In summary, the expression pattern of pS6 in murine clusters resembled more that of p4E-BP1 in human ACP, as pS6 is restricted to the palisaded epithelium adjacent to the human ACP clusters. These results suggest that mTOR signalling may play a role in ACP pathogenesis, in both *Hesx1*$^{Cre/+}$;*Ctnnb1*$^{lox(ex3)/+}$ and humans, but through different mechanisms and cellular compartments.

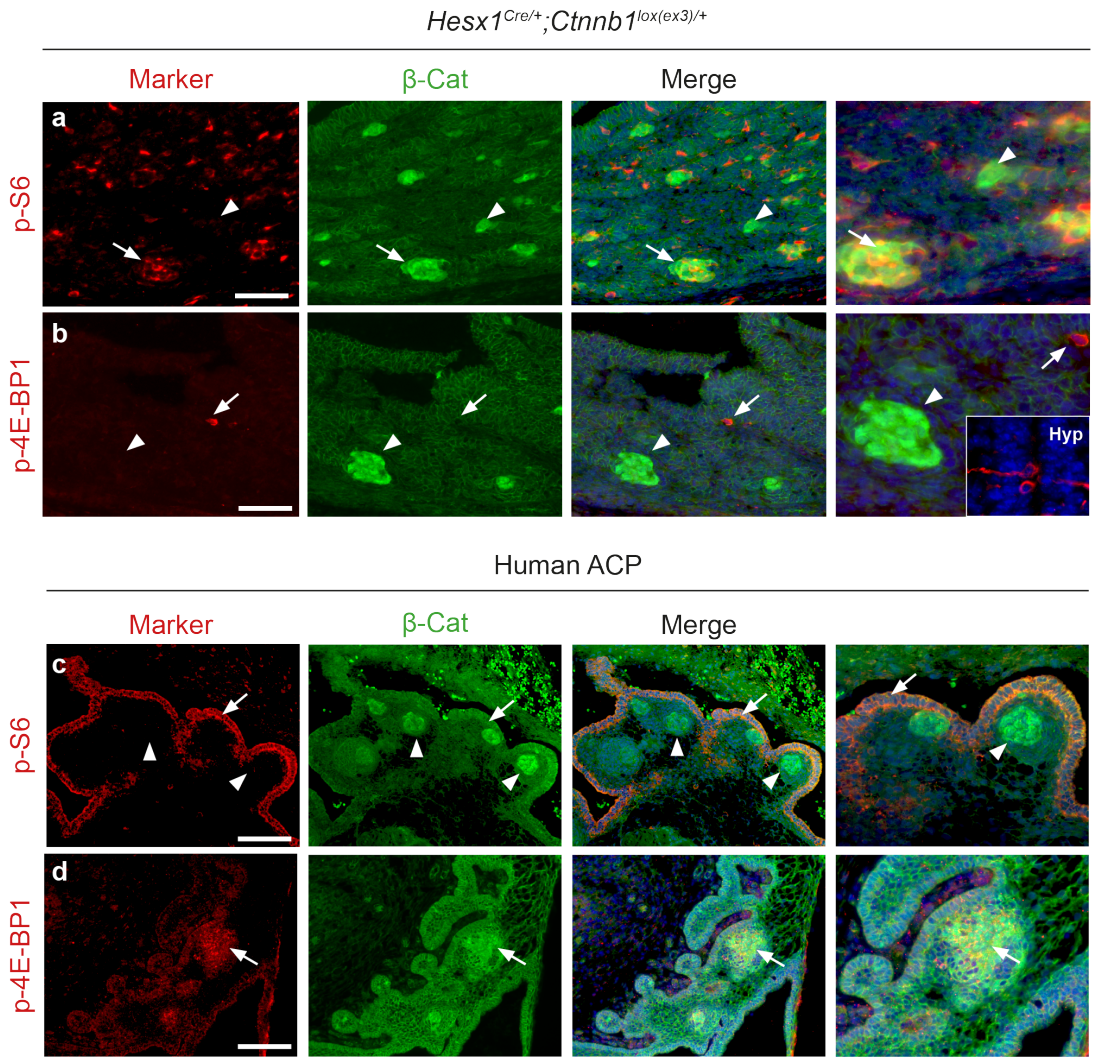

Figure. 3.8 The mTOR signalling pathway is activated in β-catenin clusters of murine and human ACP through different downstream effectors.

(a) Phosphorylated ribosomal protein S6 (pS6) positive staining is observed in scattered cells of the pituitary anterior lobe at 18.5 dpc. A number of β-catenin clusters contain pS6 expressing cells (arrow), while others are negative (arrowhead). **(b)** Phosphorylated 4E-BP1 staining is not observed in most of the anterior lobe tissue, including the clusters (arrowhead), but was observed occasionally in single cells

(arrow) and consistently expressed in neurons of the lining of the third ventricle of the hypothalamus (inset). **(c)** Staining for pS6 in human ACP shows absence of colocalisation with β-catenin clusters (arrowheads), while the palisaded epithelium adjacent to the clusters shows strong positive pS6 staining (arrow). **(d)** Positive staining for phosphorylated 4E-BP1 is found in the clusters of human ACP (arrow). Scale bars: a,b 50 μm; c,d 100 μm. Merged figures: DAPI counterstain.

3.4.2 The autophagy pathway in β-catenin clusters

The autophagy pathway is a main target of mTOR, which has been implicated in the regulation of senescence and the SASP (Dörr et al. 2013; Kang et al. 2015). The status of the autophagic machinery in β-catenin clusters was investigated by immunostaining for key autophagy markers p62/SQSTM1 (a downstream target of the pathway) and LC3 (a crucial component of the autophagosome). Both p62 and LC3 were observed throughout the anterior lobe epithelium of *Hesx1*$^{Cre/+}$*;Ctnnb1*$^{lox(ex3)/+}$ 18.5 dpc pituitaries. However, only P62 appeared to accumulate in the clusters (Figure 3.9a-b, arrows), while LC3 staining was reduced in the β-catenin clusters (Figure 3.9c-d; arrowheads) compared to the surrounding pituitary epithelium, which was strongly positive for this marker. In human ACP, P62 colocalised with β-catenin clusters (Figure 3.9e-f, arrows), as well with the palisaded epithelium. Additionally, LC3 positive staining appeared to colocalise specifically in the β-catenin clusters (Figure 3.9g-h, arrows) within the tumour tissue, as well as in the reactive glial tissue surrounding the tumours. In conclusion, p62 protein expression was found to accumulate in the β-catenin clusters of both mouse and human ACP, while LC3 only accumulated in the human clusters.

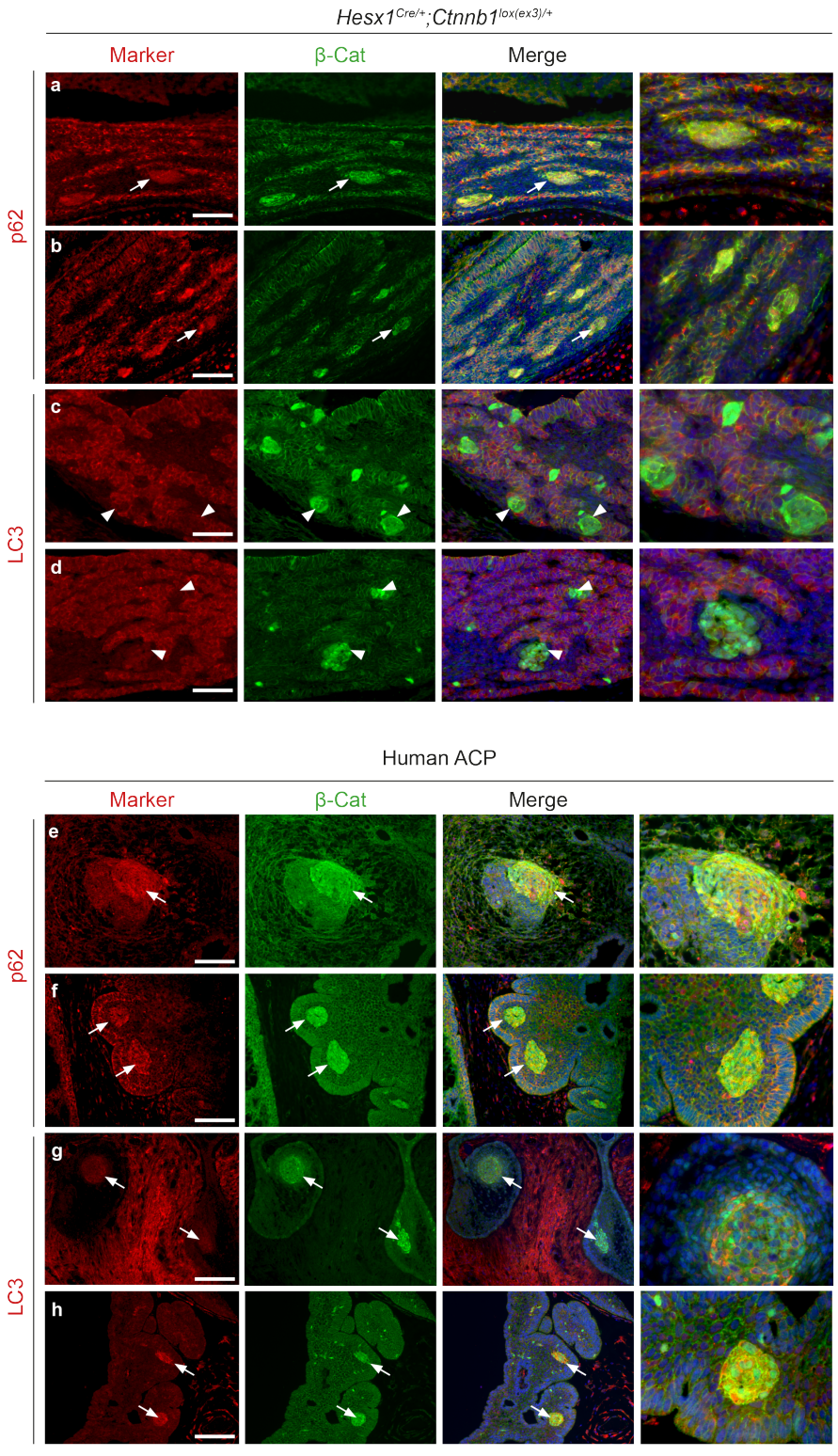

Figure 3.9 The expression of autophagy markers in β-catenin clusters differs between mouse and human ACP.

Double immunofluorescence for components of the autophagy pathway in *Hesx1*$^{Cre/+}$*; Ctnnb1*$^{lox(ex3)/+}$ pituitaries at 18.5 dpc and human ACP (DAPI counterstain in merge). **(a-b)** p62/SQSTM staining is observed throughout the pituitary epithelium, including

the β-catenin clusters (arrows), while the pituitary stroma is mainly negative. **(c-d)** Expression of the essential autophagosome component LC3 in β-catenin clusters (arrowheads) is clearly reduced in comparison to the surrounding pituitary epithelium. **(e-f)** In human ACP, p62/SQSTM1 is expressed in the palisaded epithelium and in the β-catenin accumulating clusters (arrows). **(g-h)** Increased LC3 protein expression was observed in human ACP clusters (arrows) and in surrounding reactive glial tissue. Scale bars: a-f, 50 µm; g-h, 100 µm. Merged figures: DAPI counterstain.

3.5 Characterisation of the NF-κB pathway and the SASP in *Hesx1$^{Cre/+}$;Ctnnb1$^{lox(ex3)/+}$* and human ACP clusters

3.5.1 The NF-κB pathway in β-catenin clusters

Activation of the NF-κB pathway is essential for induction and maintenance of the SASP (Acosta et al. 2008; Ohanna et al. 2011; Chien et al. 2011; Freund et al. 2011). Therefore, the activation of the NF-κB pathway in cluster cells was evaluated by using antibodies against key pathway members such as RelA/p65, phosphorylated IkBα and NEMO/IKKγ. Immunostaining for RELA/P65 revealed that this protein was expressed throughout the pituitary parenchyma and stroma, including in the β-catenin clusters of *Hesx1$^{Cre/+}$;Ctnnb1$^{lox(ex3)/+}$* embryos at 18.5 dpc (Figure 3.10a, arrows). Importantly, phosphorylated IkBα was mainly localised to the β-catenin clusters (Figure 3.10b, arrows), although single positive cells were also observed scattered around the pituitary tissue. Additionally, IKKγ (NEMO) was also detected throughout the pituitary anterior lobe, including the β-catenin accumulating clusters (Figure 3.10c, arrows). Expression analysis in human ACP samples showed that RELA was expressed in various cell compartments of the tumour, such as the palisaded epithelium, but a clear accumulation was observed in β-catenin accumulating clusters (Figure 3.10d, arrows). Moreover, a robust accumulation of phospho-IkBα and NEMO

proteins was observed in the β-catenin clusters of human ACP samples (Figure 3.10d-e, arrows). In summary, oncogenic β-catenin leads to the activation of the NF-κB pathway in senescent β-catenin accumulating clusters in both 18.5 dpc *Hesx1*$^{Cre/+}$;*Ctnnb1*$^{lox(ex3)/+}$ pituitaries and human ACP.

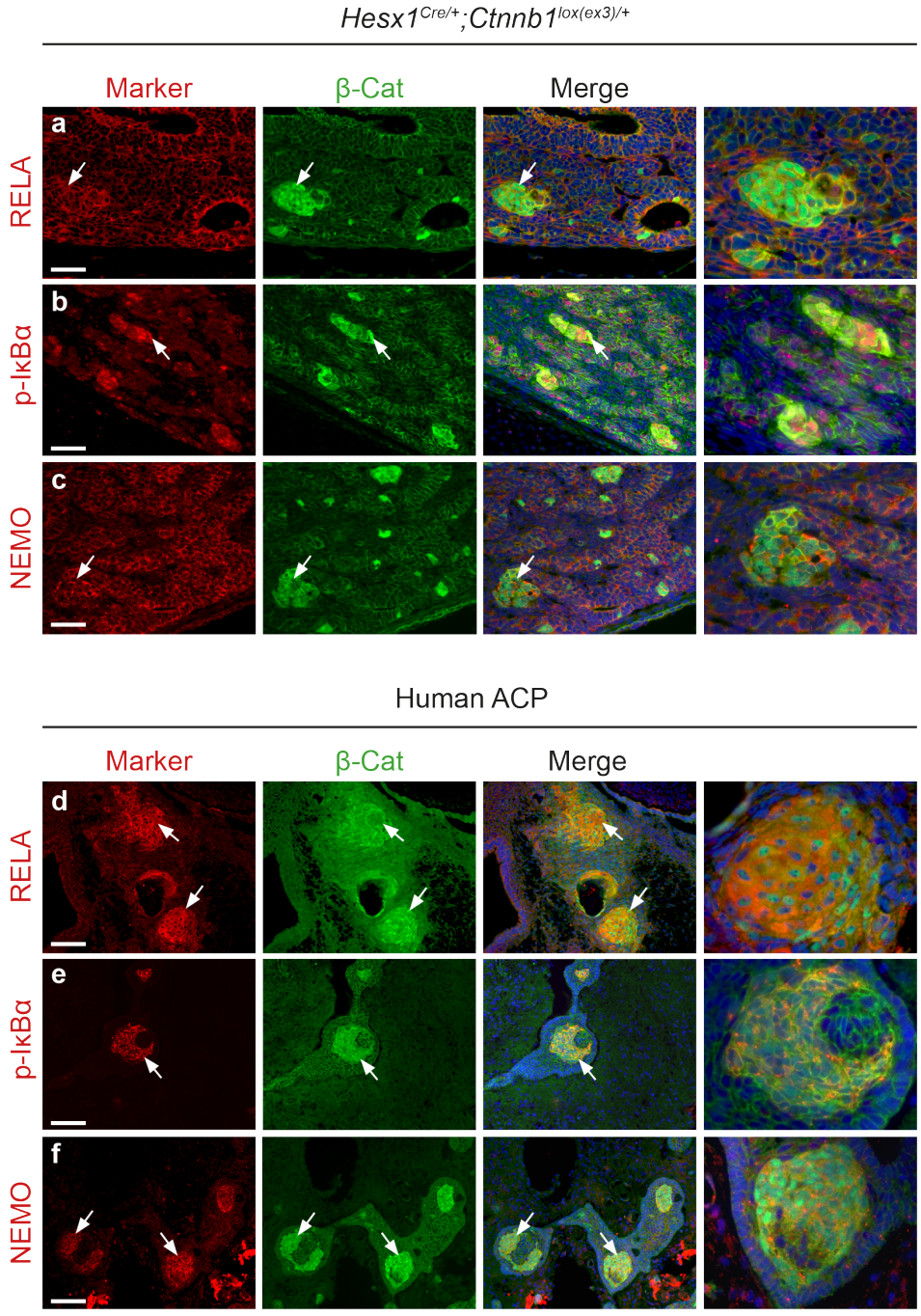

Figure 3.10 Activation of the NF-κB pathway occurs in β-catenin clusters from mouse and human ACP.

Double immunofluorescence for key members of the NF-κB pathway shows they are expressed in β-catenin clusters. **(a)** Staining for RELA/P65, **(b)** phosphorylated IκBα and **(c)** NEMO shows colocalisation with clusters in 18.5 dpc mouse ACP pituitaries (arrows). **(d-f)** The clusters of human ACP also show increased expression of NF-κB pathway effectors (arrows). Scale bars: a,b,c 50 μm; d,e,f 100 μm. Merged figures: DAPI counterstain.

3.5.2 SASP factors are overexpressed in *Hesx1$^{Cre/+}$;Ctnnb1$^{lox(ex3)/+}$* pituitaries and human ACP

The demonstration of a senescent phenotype and the activation of the NF-κB pathway in β-catenin accumulating clusters suggested that they develop a Senescence-Associated Secretory Phenotype (SASP) responsible for driving paracrine tumourigenesis. Previously published data showed that the β-catenin clusters of the *Hesx1$^{Cre/+}$;Ctnnb1$^{lox(ex3)/+}$* (Andoniadou et al. 2012) and S*ox2$^{CreERT2/+}$;Ctnnb1$^{lox(ex3)/+}$* (Andoniadou et al. 2013) models are the source of a wide variety of secreted factors able to promote inflammation and oncogenesis, some of which are well recognised SASP members. Detection of the SASP factors in the β-catenin clusters was unsuccessfully attempted by immunohistochemistry and *in situ* hybridisation. However, an unbiased analysis for senescence and SASP gene expression was conducted using previously published expression microarray data (Andoniadou et al., 2012; Accession E-MEXP-3492). Microarray data was derived from dissociated 18.5 dpc *Hesx1$^{Cre/+}$;Ctnnb1$^{lox(ex3)/+}$;BAT-gal* pituitaries, which were then flow-sorted for the BAT-gal positive and negative populations. The BAT-gal mouse is a reporter of Wnt/β-catenin pathway activation that expresses *E,coli* β-galactosidase under the control of a tandem repeat of LEF1/TCFs consensus binding sites (Maretto et al. 2003). This sorting strategy allowed to produce RNA expression data comparing the β-catenin cluster population (BAT-gal+ve) versus non-cluster cells (BAT-gal –ve).

Gene Set Enrichment Analysis (GSEA) showed that genes associated with oncogene-induced senescence (OIS) and the SASP were significantly enriched in the mouse β-catenin clusters (Figure 3.11a) (see Materials and Methods for details of the reference data sets). Validation of key SASP members *IL1a, Il1b, IL6, Cxcl1, CCL20* and *Tgfb1* by qRT-PCR confirmed that their expression was significantly upregulated in *Hesx1*$^{Cre/+}$*;Ctnnb1*$^{lox(ex3)/+}$ pituitaries at 18.5 dpc when compared to wild types (p<0.05, Student's t test) (Figure 3.11b). Additionally, the expression of 96 different inflammatory cytokines and chemokines in whole pituitary extracts was quantified using ELISA microarrays (Figure 3.11c). Comparison between *Hesx1*$^{Cre/+}$*;Ctnnb1*$^{lox(ex3)/+}$ 18.5 dpc pituitaries and wild-type littermates showed upregulation (up to 8-Log_2 fold change) of 17 factors previously recognised as hallmark SASP factors (Coppé, Desprez, et al. 2010).

A similar analysis was conducted in human ACP samples by performing RNA-sequencing of laser-microdissected (LCM) β-catenin clusters (using surrounding palisaded epithelium as non-cluster comparison) from two ACP cases. LCM and RNAseq data processing, as well as hierarchical clustering were conducted by John Apps. GSEA using ranked gene lists was conducted by the candidate. GSEA of the human cluster *vs.* non-cluster data revealed that the OIS and SASP gene sets were also significantly enriched in the β-catenin cluster fraction (Figure 3.11d). Importantly, when human and mouse gene expression profiles were compared by hierarchical clustering, it was observed that murine and human clusters grouped together, whereas the mouse non-cluster signature grouped with human non-cluster tissue (Figure 3.11e). This analysis indicates that mouse and human clusters share overall similar gene expression profiles, including an enrichment for OIS and SASP genes, which further supports the relevance of the embryonic mouse ACP model.

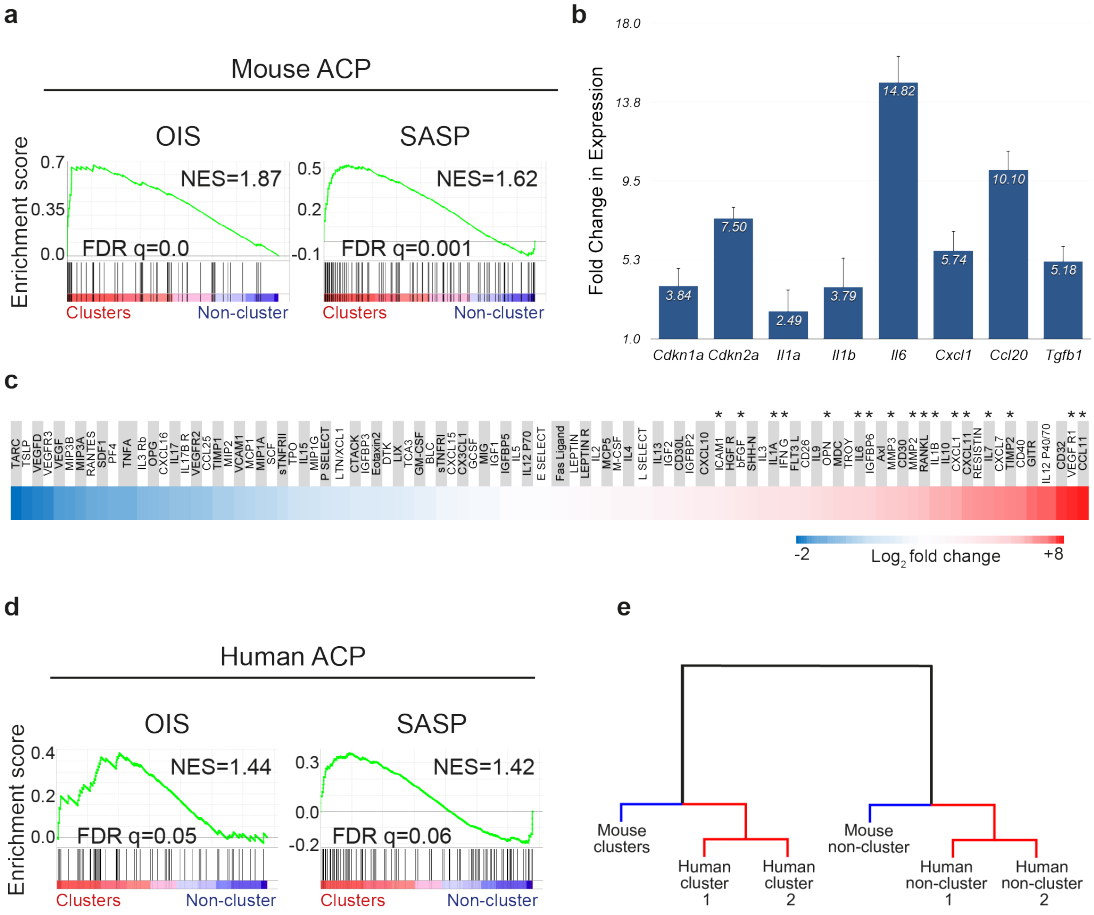

Figure 3.11 Mouse and human ACP clusters are similar structures with enriched gene expression for oncogene-induced senescence (OIS) and the Senescence Associated Secretory Phenotype (SASP) signatures.

(**a**) Gene Set Enrichment Analysis (GSEA) of differentially upregulated genes in β-catenin clusters of 18.5 dpc mouse APC pituitaries shows enrichment for the OIS and SASP gene sets produced in human senescent fibroblasts. (**b**) qRT-PCR for cell cycle inhibitors *Cdkn1a* (p21) and *Cdkn2a* (p16) as well as key SASP factors *Il1a, Il1b, Il6 Cxcl1, Ccl20* and *Tgfb1* shows their upregulation in 18.5 dpc mouse ACP pituitaries compared to wild type pituitaries (n=3). **(c)** Heat map showing $\log_2$-fold changes in protein content of 95 inflammatory cytokines and soluble factors between *Hesx1*$^{Cre/+}$;*Ctnnb1*$^{lox(ex3)/+}$ and wild type pituitaries at 18.5 dpc (n=2). Asterisks indicate upregulated factors previously recognised as part of the SASP. (**d**) Genes upregulated in human ACP laser capture micro-dissected β-catenin clusters also show enrichment for the OIS and SASP signatures. (**e**) Hierarchical clustering analysis shows that the clusters of mouse and human ACP group together and vice versa for non-cluster tissues. NES: Normalized Enrichment Score; FDR: False

Discovery Rate; OIS: Oncogene-Induced Senescence; SASP: Senescence-Associated Secretory Phenotype.

3.6 Dynamics of cellular senescence during pituitary oncogenesis

3.6.1 *Hesx1$^{Cre/+}$;Ctnnb1$^{lox(ex3)/+}$* clusters stop dividing and replicating their DNA early in pituitary development

To gain a better understanding of the *in vivo* senescence process in murine β-catenin clusters, an analysis of the senescent phenotype was conducted at different stages of pituitary embryonic development. DNA replication was assessed by EdU uptake 90 minutes after injection at the specified stage. As previously shown (Figure 3.2b), mutant pituitaries did not contain clusters with EdU positive cells at 18.5 dpc. However, EdU staining colocalised with β-catenin accumulating cells at 10.5, 12.5, 14.5 and 16.5 dpc, indicating that β-catenin clusters contain few cells that replicate their DNA before 18.5 dpc (Figure 3.12a, arrows). Quantification of total EdU+ cluster cells showed that at 10.5 dpc 33% of cluster cells were EdU+, in comparison with 6.45% at 14.5 dpc and 2.5% at 18.5 dpc. Ki67 immunostaining revealed that most clusters had exited the cell cycle by 12.5 dpc (Figure 3.12b), as Ki67 and nucleo-cytoplasmic β-catenin were found to colocalise evidently only at 10.5 dpc (Figure 3.12b, arrowhead). Quantification of Ki67+ cluster cells showed that 12% of cluster cells were positive at 10.5 dpc., while at 14.5 and 18.5 dpc., this proportion was reduced to 2.6% and 2%, respectively.

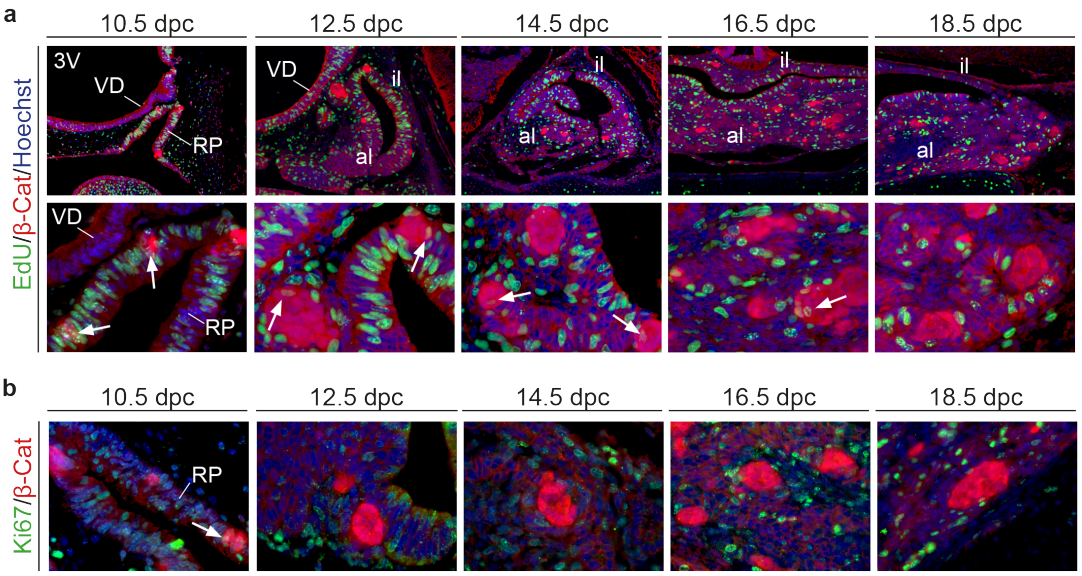

Figure 3.12 The expression of proliferation markers in β-catenin clusters has a dynamic profile during pituitary embryonic development.

(**a**) Double immunofluorescence for EdU (indicative of DNA replication) and β-catenin shows colocalisation in the clusters at 10.5, 12.5 and 16.5 dpc (arrows) but not at 18.5 dpc. (**b**) Ki67+ staining (indicative of cell cycle progression) is only observed to colocalise with clusters at 10.5 dpc and not at later stages (DAPI counterstain). RP= Rathke's Pouch, VD= Ventral Diencephalon, 3V=Third ventricle, il= intermediate lobe of the pituitary, al= anterior lobe of the pituitary.

3.6.2 Cell cycle inhibiting pathways are active in clusters throughout pituitary development

The absence of Ki67 in the clusters after 12.5 dpc suggested that the activation of cell cycle inhibiting pathways occurs early in pituitary development. This hypothesis was investigated by immunofluorescence for the crucial effectors p16 and p21 at different stages of development. Expression of both p21 and p16 in β-catenin clusters was observed at all analysed stages (Figure 3.13a), suggesting that cell cycle inhibitor expression is an acute response of the activation of the β-catenin oncogene. Quantification of p21 expression in cluster cells showed that the proportion of p21+ cluster cells was 73.3% at 10.5 dpc, 75% at 14.5 dpc and 76% at 18.5 dpc.

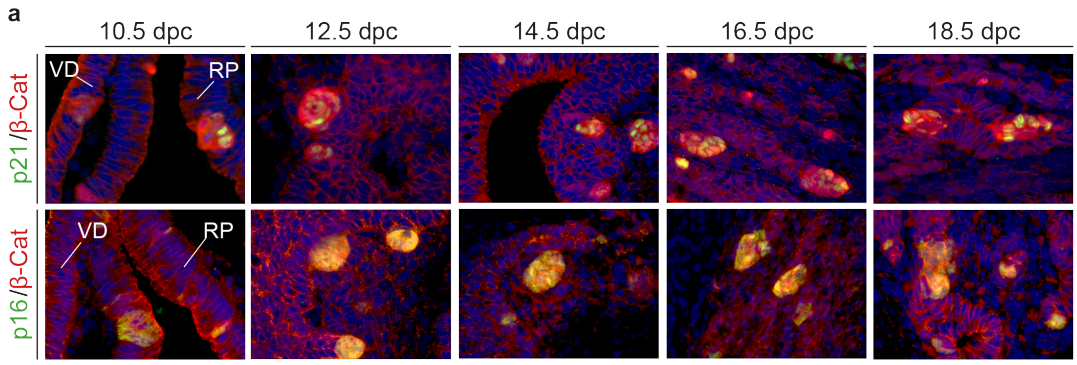

Figure 3.13 The cell cycle inhibitors p21 and p16 are expressed in β-catenin clusters throughout embryonic pituitary development.

Double immunostaining for main cell cycle inhibitors and β-catenin at different stages of development in *Hesx1*$^{Cre/+}$;*Ctnnb1*$^{lox(ex3)/+}$ pituitaries. **(a)** p21 positive staining colocalises with nucleo-cytoplasmic β-catenin accumulating cells at all analysed stages (10.5, 12.5, 14.5 16.5 and 18.5 dpc). **(b)** p16 expression is observed exclusively in β-catenin clusters at all stages analysed. VD= Ventral diencephalon, RP= Rathke's Pouch. DAPI counterstain.

3.6.3 Other senescence-associated markers have a dynamic expression profile in β-catenin clusters during pituitary development

An analysis of additional important cellular senescence markers (shown in this chapter to be expressed at the 18.5 dpc stage) was conducted at different developmental stages. Interestingly, the expression of GLB1 (SA-β-Gal) was not observed until 16.5 dpc, indicating that there is a progressive accumulation of lysosomal β-galactosidase within the β-catenin clusters in the mouse (Figure 3.14a). Importantly, elevated expression of GLB1 protein was detected in the form of puncta in cells of the mesonephric tubules in 14.5 dpc embryos (Figure 3.15), a pattern that coincides with increased levels of SA-β-Gal expression in these structures as previously reported (Storer et al. 2013), validating the absence of GLB1 accumulation in the β-catenin clusters at this stage. Additionally, expression of the DNA-damage

response marker DNA-PKcs, was observed at all analysed stages with no clear change in staining intensity (Figure 3.14b). Similar results were obtained for phosphorylated IkBα, which colocalised with all β-catenin clusters at each stage analysed (Figure 3.14c). The results presented in this section suggest that while the expression of some markers of the senescent phenotype might be a direct response to the activation of the β-catenin oncogene (DNA-damage, cell cycle inhibitor expression and NF-κB activation), others, such as the lysosomal compartment and DNA replication, show a dynamic progression during pituitary development.

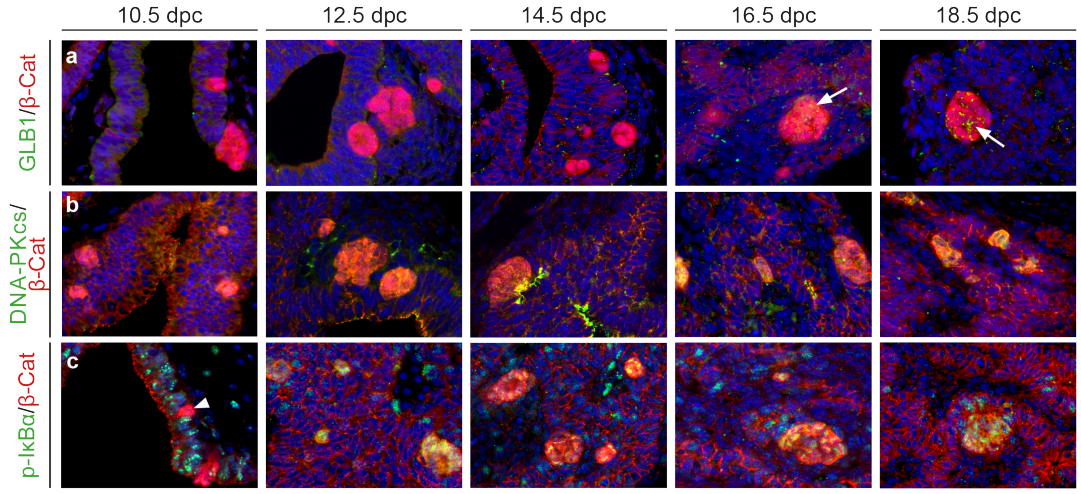

Figure 3.14 There is a dynamic behaviour in the expression of senescence-associated markers in the β-catenin clusters throughout embryonic pituitary development.

Double immunostaining for markers of senescence and β-catenin at different stages of development in *Hesx1*$^{Cre/+}$*;Ctnnb1*$^{lox(ex3)/+}$ pituitaries. **(a)** An accumulation of GLB1 staining is observed only at the 16.5 and 18.5 dpc stages (arrows). **(b)** Positive staining for the DNA-Damage Response marker DNA-PKcs is observed at all observed stages. **(c)** Activation of the NF-κB pathway in clusters is observed by accumulation of phospho-IkB staining at 12.5, 14.5, 16.5 and 18.5 dpc stages. Negative clusters can be observed at the 10.5 dpc stage (arrowhead). DAPI counterstain.

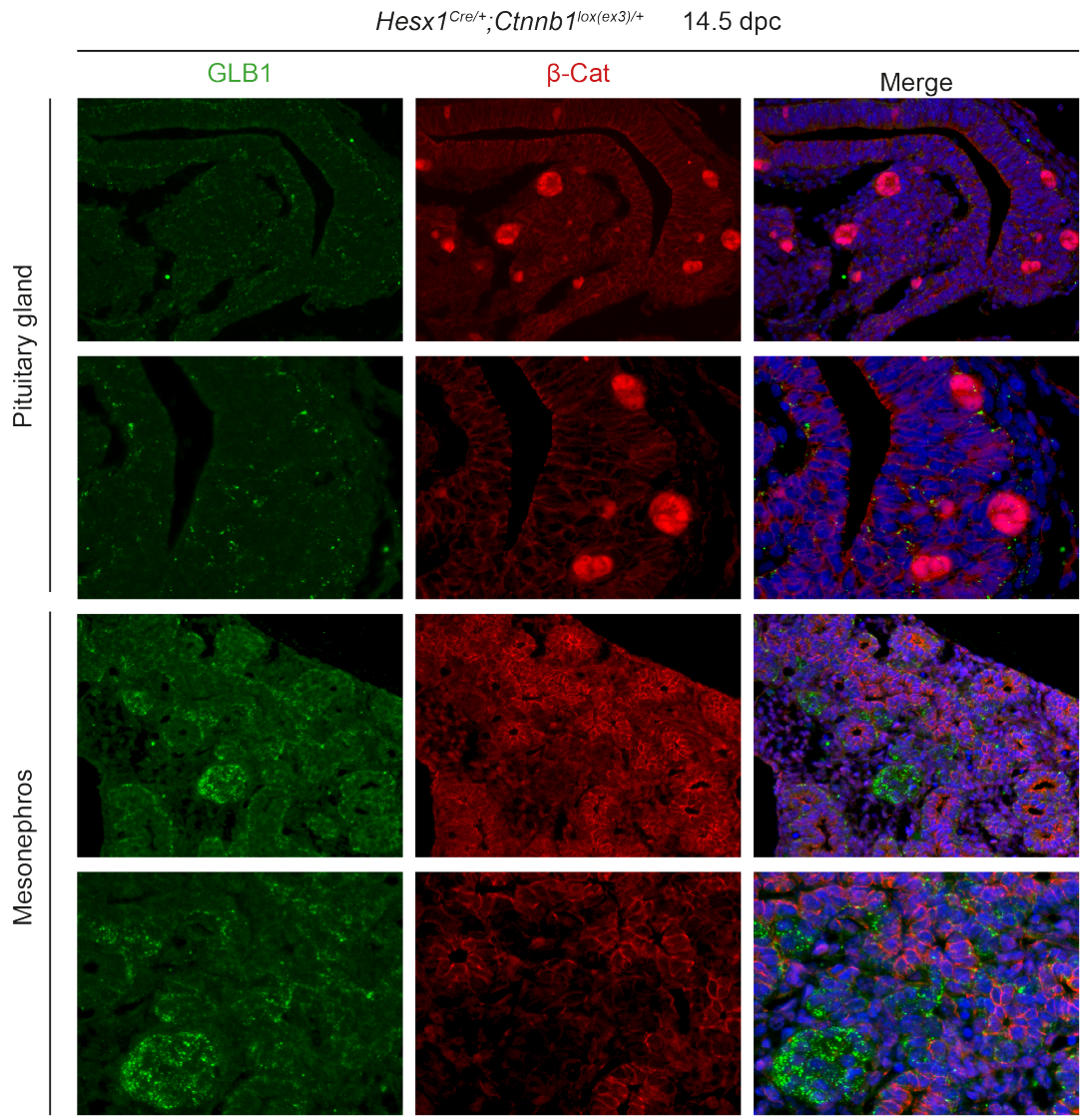

Figure 3.15 Specific detection of GLB1 protein at embryonic stage 14.5 dpc.

Double immunostaining for GLB1 in different regions of a *Hesx1*$^{Cre/+}$;*Ctnnb1*$^{lox(ex3)/+}$ embryo at 14.5 dpc. Note the absence of GLB1 accumulation in the β-catenin clusters at this stage in the pituitary gland, while the mesonephric tubules still show protein accumulation. Merged figures: DAPI counterstain.

3.7 The effect of SASP paracrine signalling on the tumourigenic microenvironment

3.7.1 A population of endothelial-like cells expands in the stroma during early pituitary tumourigenesis

The demonstration of a non-cell autonomous induction of pituitary tumours in the murine ACP model suggested that β-catenin clusters modify their microenvironment by means of the SASP. Because increased angiogenesis and the recruitment of different pro-oncogenic cell types into the tumour stroma are a characteristic effect of the SASP (Coppé et al. 2010), an analysis of the vascular and stromal compartment of *Hesx1*$^{Cre/+}$*;Ctnnb1*$^{lox(ex3)/+}$ pituitaries was conducted.

To assess the state of the pituitary vasculature, immunostaining was conducted for Endomucin (EMCN), a O-sialoglycoprotein routinely used as a marker of endothelial cells (Samulowitz et al. 2002; Kinoshita et al. 2001)). Additionally, the expression of fibronectin and laminin were analysed to explore the stromal compartment.

In 18.5 dpc wild type pituitaries EMCN expression was restricted to cells with a thin and elongated morphology surrounding the lumen of blood vessels in the anterior lobe (Figure 3.16a,c). Interestingly, 18.5 dpc *Hesx1*$^{Cre/+}$*;Ctnnb1*$^{lox(ex3)/+}$ pituitaries displayed a drastic expansion of the EMCN+ population, which formed large and dense groups of cells without the presence of a lumen throughout the pituitary anterior lobe (hereafter also referred as “swarms”) (Figure 3.16b,d).

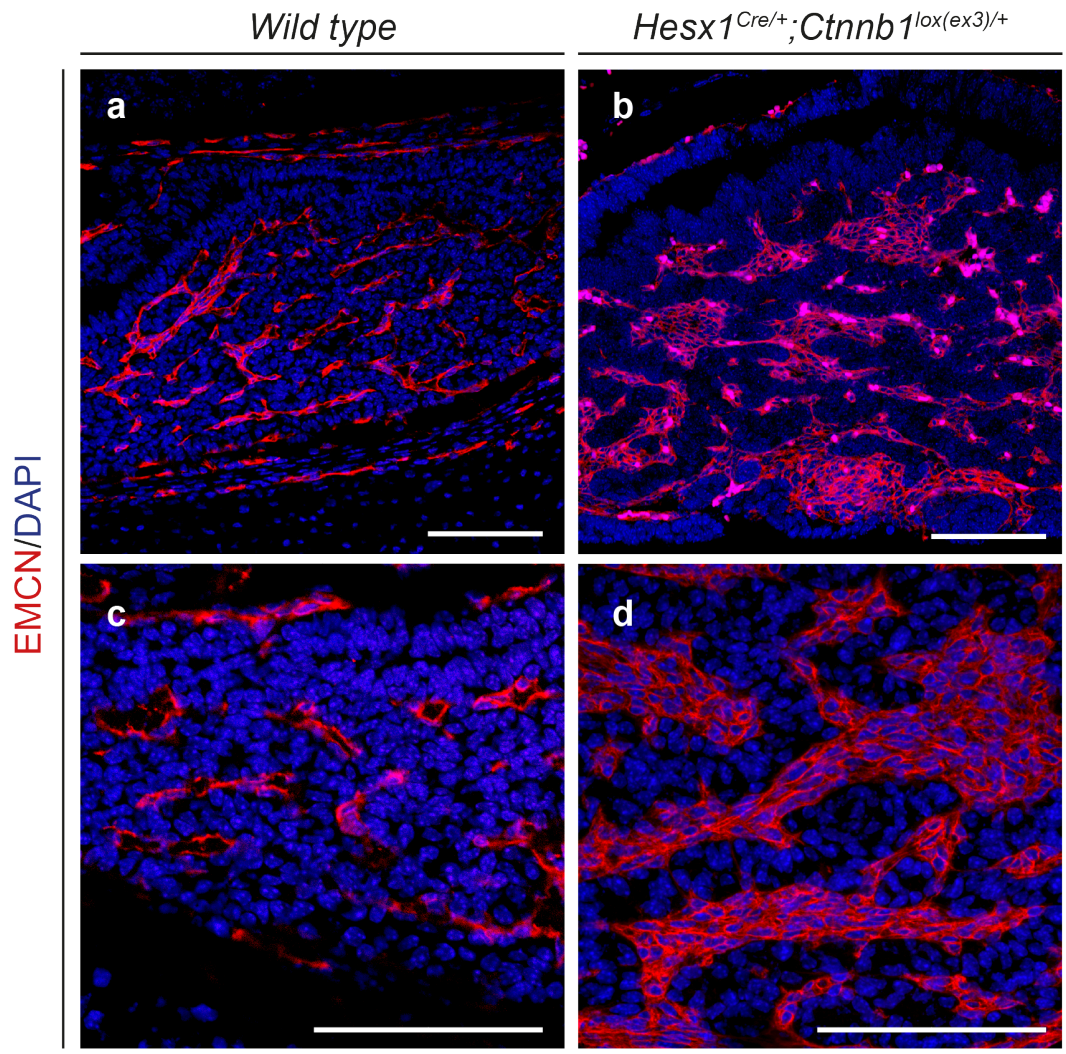

Figure 3.16 Cells expressing the endothelial marker endomucin (EMCN) are present in larger numbers in *Hesx1$^{Cre/+}$;Ctnnb1$^{lox(ex3)+/}$* pituitaries.

Fluorescent immunostaining for EMCN at 18.5 dpc **(a)** The vasculature of the wild type pituitary anterior lobe contains EMCN+ cells with an elongated thin/elongated morphology. **(b)** *Hesx1$^{Cre/+}$;Ctnnb1$^{lox(ex3)/+}$* pituitaries contain larger numbers of EMCN+ cells throughout the anterior lobe. **(c)** EMCN+ cells of the wild type pituitary often surround the lumen of blood vessels (note empty spaces within positive signal strands). **(d)** In mutant pituitaries, the EMCN+ population forms large, tightly-packed, cell groups which do not form a lumen. Scale bars: 100 µm

To investigate the origin of this peculiar EMCN+ population, concomitant lineage tracing of the pituitary lineage was conducted in *Hesx1*$^{Cre/+}$*;Ctnnb1*$^{lox(ex3)/}$*;R26*$^{YFP/+}$ at 18.5 dpc. Double immunostaining against YFP and EMCN showed a clear absence of colocalisation between both markers in mutant pituitary glands and showed that EMCN+ cells occupied YFP- areas in their entirety (Fig 3.17a). Interestingly, EMCN cells frequently formed ring-like structures by surrounding islands of YFP+ epithelial tissue, which resembled the β-catenin clusters in size and shape (arrows, Figure 3.17a).

This extensive YFP- expression domain suggested that EMCN+ cells formed most of the pituitary stroma in *Hesx1*$^{Cre/+}$*;Ctnnb1*$^{lox(ex3)/+}$ mice. In fact, EMCN staining widely colocalised with the extra-cellular matrix (ECM) component fibronectin throughout the pituitary stroma (Figure 3.17b), suggesting active secretion of ECM-modifying factors by EMCN+ cells. Moreover, laminin immunostaining showed that the basal lamina clearly separated EMCN+ cells from the pituitary epithelium (Figure 3.17c), which appeared to be displaced by EMCN+ cell groups branching-off from larger EMCN+ cell masses (arrows, Figure 3.17c). Therefore, EMCN+ cells occupy most of the *Hesx1*$^{Cre/+}$*;Ctnnb1*$^{lox(ex3)/+}$ pituitary stroma at 18.5 dpc, possibly by actively migrating and displacing the *Hesx1*-derived pituitary epithelium.

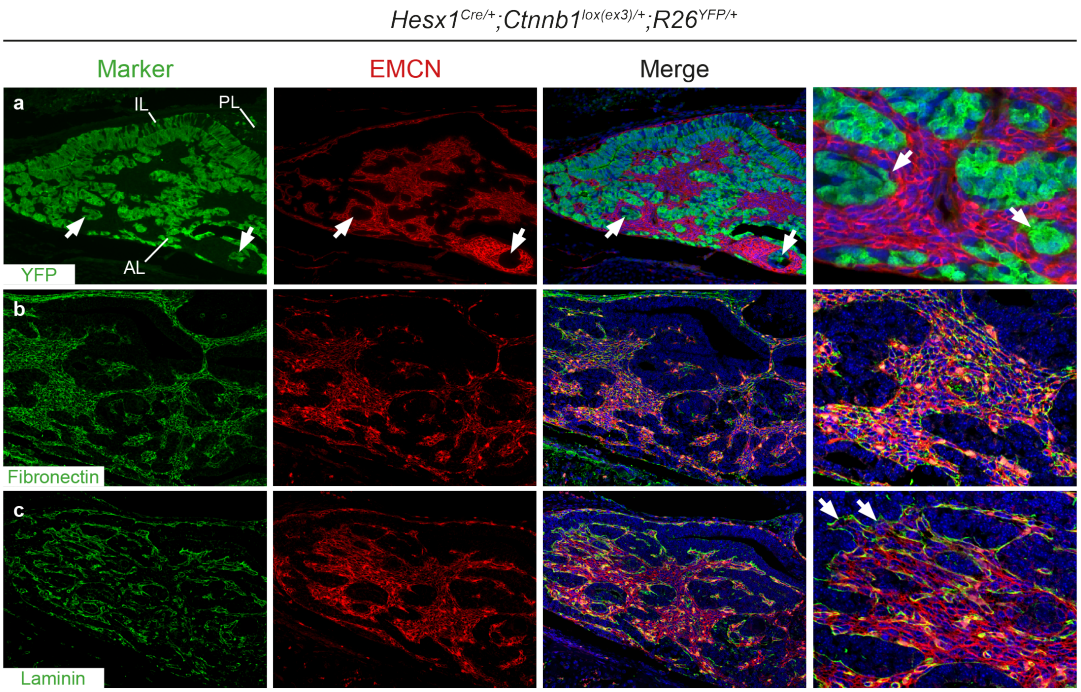

Figure 3.17 EMCN+ endothelial-like cells occupy most of the stroma in *Hesx1$^{Cre/+}$;Ctnnb1$^{lox(ex3)/+}$;R26$^{YFP/+}$* pituitaries.

(a) Double immunofluorescence for YFP and EMCN at 18.5 dpc shows that EMCN+ cells are present throughout the YFP- stroma of the tumourigenic pituitary gland in the form of large groups. Arrows: EMCN+ cells form “rings” that surround YFP+ epithelia. **(b)** The expression of the extracellular matrix (ECM) component fibronectin colocalises with EMCN+ cells throughout the pituitary anterior lobe. **(c)** Laminin immunostaining shows that EMCN+ cells are separated from the pituitary parenchyma by a basal lamina. Note that EMCN+ cells protrude from main cell groups and displace the pituitary epithelium (arrows). DAPI counterstain.

3.7.2 EMCN+ cells have an aberrant phenotype and interact closely with β-catenin clusters

To better understand the identity of the EMCN+ cells, immunostaining was conducted against another common endothelial marker: PECAM (CD31). In wild type 18.5 dpc pituitaries, EMCN and PECAM colocalised in endothelial cells showing the thin and elongated morphology that is characteristic of normal pituitary blood vessels (Figure 3.18a,b,e,f). Surprisingly, this pattern was not recapitulated in *Hesx1*$^{Cre/+;}$*Ctnnb1*$^{lox(ex3)/+}$ pituitaries, as PECAM+ cells retained a wild type vascular morphology and did not form large cell swarms, unlike EMCN+ cells (Figure 3.18d). Moreover, double immunostaining for EMCN and PECAM showed that scarce, single PECAM+ cells could be found both within and outside the EMCN+ cell groups (arrows, Figure 3.18g,h). These results suggest that the EMCN+ cells from *Hesx1*$^{Cre/+;}$*Ctnnb1*$^{lox(ex3)/+}$ pituitaries have a different phenotype from those found in the normal pituitary vasculature. Additionally, immunostaining for the mesenchymal marker vimentin suggested that in both the wild type and oncogenic contexts, EMCN+ cells possess a mesenchymal phenotype (Figure 3.18i-p).

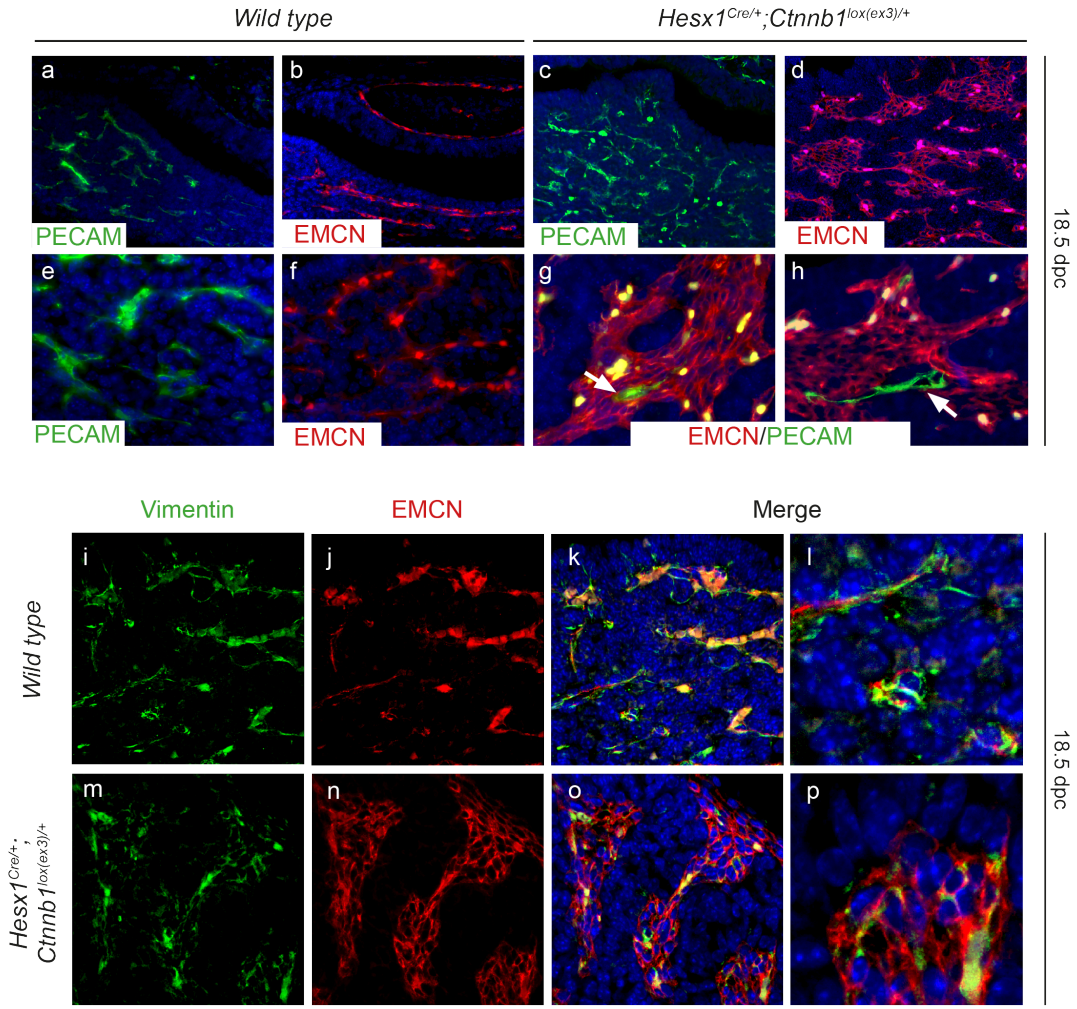

Figure 3.18 Phenotypic characterisation of EMCN+ cells in wild type and *Hesx1*$^{Cre/+;}$*Ctnnb1*$^{lox(ex3)/+}$ pituitaries.

(a-b) 18.5 dpc wild-type pituitaries contain elongated blood vessels that express PECAM and EMCN. **(c)** PECAM staining in *Hesx1*$^{Cre/+;}$*Ctnnb1*$^{lox(ex3)/+}$ pituitaries shows a similar expression profile restricted to blood vessels. **(d)** EMCN+ cells form large cell groups that do not resemble PECAM+ vessels. **(e,f)** High magnification image of a wild type anterior lobe with PECAM+ and EMCN+ pituitary vessels. **(g-h)** Double immunostaining for PECAM and EMCN shows absence of colocalisation in *Hesx1*$^{Cre/+;}$*Ctnnb1*$^{lox(ex3)/+}$ pituitaries. **(i-l)** Staining for the mesenchymal marker Vimentin shows colocalisation with EMCN+ endothelium in wild types. **(m-p)** Vimentin is also expressed in EMCN+ cell swarms from *Hesx1*$^{Cre/+;}$*Ctnnb1*$^{lox(ex3)/+}$ pituitaries. DAPI counterstain.

Because β-catenin clusters are known to express a plethora of chemokines, it was hypothesized that cluster signalling may be responsible for attracting EMCN+ cells into the tumourigenic microenvironment. Double immunostaining for β-catenin and EMCN at 18.5 dpc showed that the clusters are in close contact with the EMCN+ cell swarms, which formed “ring” structures surrounding the clusters and separated them from the rest of the pituitary epithelium (arrows, Figure 3.19a-d).

It has been previously reported that the clusters are often found surrounded by large numbers of SOX9+ cells (Gaston-Massuet et al. 2011) and therefore it was assessed if these were positive for EMCN. In 18.5 dpc wild type pituitaries, SOX9 expression was mainly found restricted to scattered epithelial cells of the anterior lobe and in those lining the MZ (Figure 3.19e), but rarely in EMCN+ cells. Surprisingly, strong SOX9 expression was found in large EMCN+ ring formations of mutant pituitaries (arrows, Figure 3.19f-g). Increased SOX9 staining intensity (SOX9+^{high}) was also present in large patches of EMCN+ cells and was not restricted only to those directly in contact with the epithelium (arrows, Figure 3.19h). Moreover, triple immunostaining for SOX9, β-catenin and EMCN confirmed that the SOX9+^{high}/EMCN+ ring formations closely interacted with β-catenin clusters (Figure 3.19i-l). Therefore, the secretory phenotype of the β-catenin clusters is possibly involved in attracting and inducing abnormal levels of SOX9 expression in endothelial-like EMCN+ cells during embryonic pituitary development.

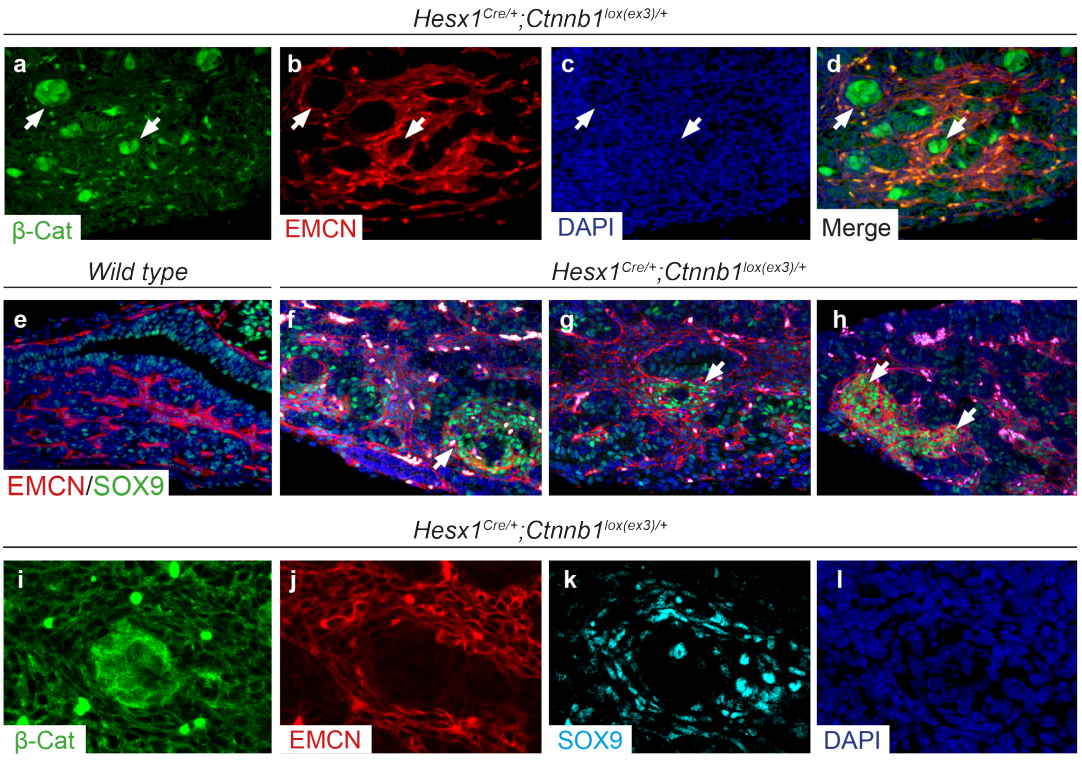

Figure 3.19 EMCN+ cells are attracted to the β-catenin clusters and express SOX9 in an aberrant manner.

(a-d) Double fluorescent immunostaining against β-catenin and EMCN shows EMCN+ cell swarms forming ring structures around β-catenin clusters (arrows) of the *Hesx1*$^{Cre/+}$;*Ctnnb1*$^{lox(ex3)/+}$ pituitary. **(e)** Double immunostaining for EMCN and SOX9 in an 18.5 dpc wild type pituitary shows the presence of few SOX9+/EMCN+ cells in the anterior lobe. **(f-g)** Mutant pituitaries contain large numbers of SOX9+^{high}/EMCN+ cells (arrows) that form ring structures around pituitary epithelial islands. **(h)** Extensive patches of SOX9+^{high}/EMCN+ are also found in mutant pituitaries. **(i-l)** Triple immunostaining for β-catenin, EMCN and SOX9 shows SOX9+^{high}/EMCN+ cells closely interacting with a β-catenin cluster. Note stronger SOX9 expression in EMCN+ closer to the cluster. DAPI counterstain: e-h.

3.7.3 EMCN+ cells initiate contact with the β-catenin clusters early in development but cease EMCN expression after birth

A broader characterisation of the EMCN+ population and its relationship with the β-catenin clusters was conducted throughout pituitary embryonic development. Characterisation of the EMCN+/SOX9+ population in wild type embryos showed that double-positive cells were present as a layer surrounding Rathke's Pouch as early as 10.5 dpc (Figure 3.20a) and through 12.5 dpc (Figure 3.20b). At 14.5 dpc, a wave of EMCN+/SOX9+ cells invaded the pituitary parenchyma of the future anterior lobe (arrow, Figure 3.20c). However, 16.5 dpc wild type pituitaries did not contain a similar population of EMCN+/SOX9+ cells within the anterior lobe. Instead, most EMCN+ cells lacked SOX9 expression and displayed an endothelial-like phenotype restricted to the lining of developing blood vessels (Figure 3.20d). This suggests that in wild type developing pituitaries the EMCN+/SOX9+ population differentiates after invading the anterior lobe parenchyma, to form part of the normal pituitary vasculature.

A similar analysis conducted in *Hesx1*$^{Cre/+}$*;Ctnnb1*$^{lox(ex3)/+}$ embryos showed that few EMCN and SOX9+ cells interacted with the β-catenin clusters at 10.5 dpc (Figure 3.20e), while at 12.5 dpc, double positive cells could be found in their vicinity (arrow, Figure 3.20f). Interestingly, a drastic increase in the number of double-positive cells was evident in mutant embryos at 14.5 dpc (Figure 3.20g) and importantly this expanded population was maintained through 16.5 dpc, where the EMCN+/SOX9+ cells already formed swarms surrounding the β-catenin clusters (arrows, Figure 3.20h). These observations suggest that the clusters act upon a population of EMCN+/SOX9+ vascular precursors by affecting their differentiation and proliferation early in pituitary development.

The postnatal expression of EMCN was then analysed to explore the possibility that the expanded EMCN+/SOX9+ population was involved in the non-cell autonomous formation of pituitary tumours. Unexpectedly, the number of EMCN+

cells was not evidently increased in adult *Hesx1*$^{Cre/+}$;*Ctnnb1*$^{lox(ex3)/+}$ pituitaries in comparison to wild types (Figure 3.20j). Instead, abnormally scarce numbers of EMCN+ cells were found in the ventral pre-neoplastic regions (asterisk, Figure 3.20l), suggesting that the expanded EMCN+/SOX9+ population differentiated postnatally, downregulated EMCN expression and became part of the YFP- pre-neoplastic regions.

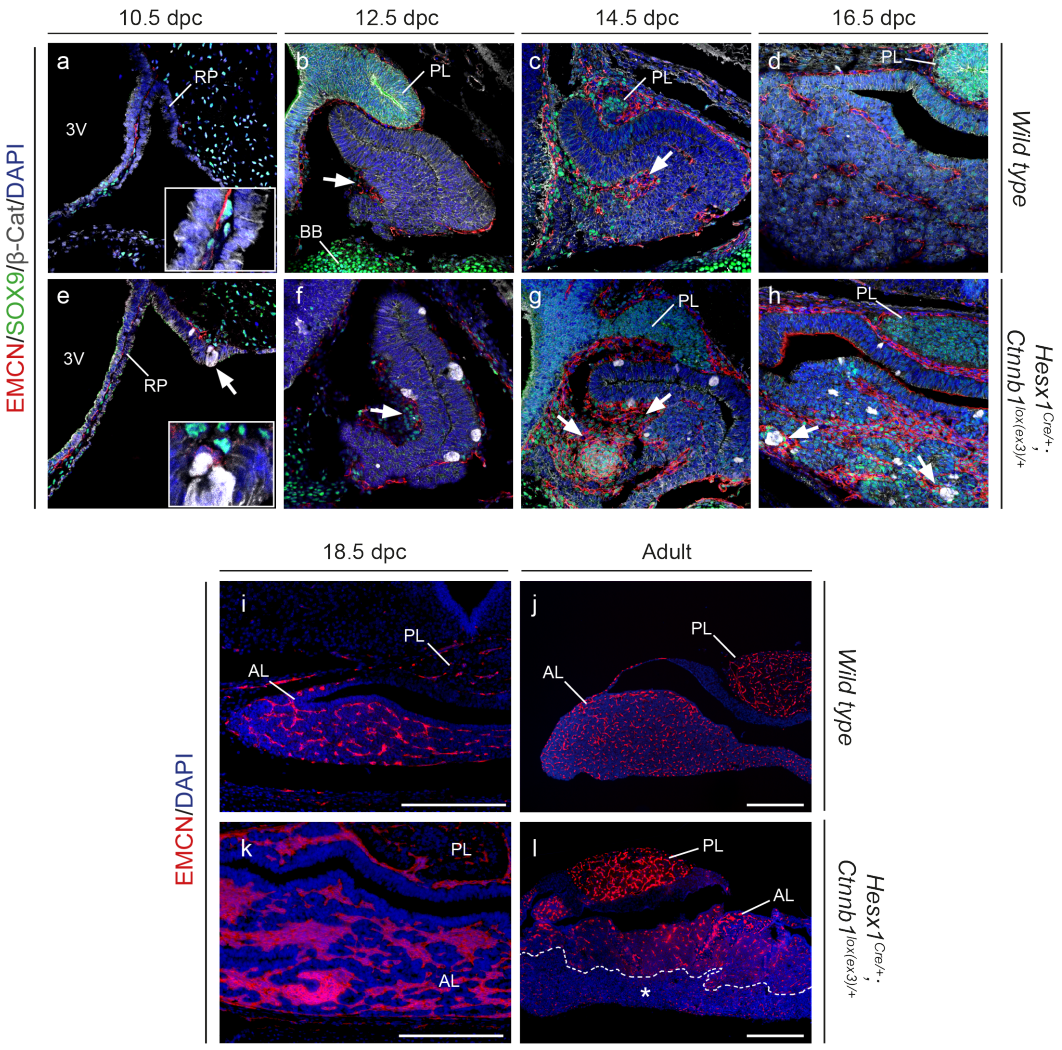

Figure 3.20 EMCN+/SOX9+ cells interact with β-catenin clusters early in pituitary development.

Triple immunostaining for EMCN, SOX9 and β-catenin at different stages of pituitary development. **(a)** At 10.5 dpc, a layer of EMCN+/SOX9+ cells surrounds the wild type Rathke's Pouch (RP). **(b)** At 12.5 dpc, the pouch is still surrounded by a layer of EMCN+/SOX9+ cells (arrow). A small population of EMCN+/SOX9+ cells can be

observed outside the ventral region of the anterior lobe (AL) (arrow). At this stage, the developing posterior lobe (PL) and basisphenoid bone (BB) also express high levels of SOX9. **(c)** At 14.5 dpc, a wave of EMCN+/SOX9+ cells has invaded the epithelium of developing AL (arrow). **(d)** By 16.5 dpc, EMCN expression is restricted to the lining of blood vessels that mostly do not express SOX9. **(e)** The 10.5 dpc RP of *Hesx1*$^{Cre/+}$*;Ctnnb1*$^{lox(ex3)/+}$ embryos contains β-catenin clusters that interact with both SOX9+ and EMCN+ cells. **(f)** At 12.5 dpc, EMCN+/SOX9+ cells interact closely with clusters at the RP surface. **(g)** The number of EMCN+/SOX9+ cells has increased at 14.5 dpc (arrows). **(h)** At 16.5 dpc, the mutant anterior lobe contains an expanded EMCN+/SOX9+ compartment that maintains close contact with the β-catenin clusters (arrows). **(i-j)** EMCN staining in wild type pituitaries at 18.5 dpc and 3 months of age adult shows that positive cells are restricted to normal vasculature of the anterior and posterior lobes. **(k)** Mutant pituitaries at 18.5 dpc contain an expanded EMCN+ compartment. **(i)** Adult mutant pituitaries lack an expansion of the EMCN compartment compared to wild types. While the AL appears to have normal vascularisation, ventral pre-neoplastic regions (delimited by dotted line) contain decreased numbers of EMCN+ vessels (asterisk). Scale bars: i,k: 500 μm. RP: Rathke's Pouch; 3V: Third Ventricle; PL: Posterior Lobe; AL: Anterior Lobe; BB: Basisphenoid Bone.

3.7.2 Large groups of EMCN+ endothelial-like cells are also present in human ACP

To determine if an expanded EMCN+ cell population also exists in human ACP, double immunostaining for β-catenin and EMCN was conducted in ACP paraffin sections (including a tissue microarray containing 23 different cases). This revealed that all samples contained EMCN+ cells, albeit with a variety of phenotypes. EMCN+ cells were rarely observed within the tumour parenchyma but were found in the lining of blood vessels of most tumours (arrowheads Figure 3.21a,c,g). Besides blood vessel-associated cells, EMCN+ staining was observed in non-vascular EMCN+ populations present both outside the tumour parenchyma (Figure 3.21b) and within tumour microcysts (arrow, Figure 3.21c). Interestingly, a number of tumours

contained large numbers of non-vascular EMCN+ cells that occupied most of the extra-tumoural tissue (Figure 3.21d,e,f). Closer inspection showed that in low-EMCN+ content tumours, positive cells within microcysts were either found as large cell agglomerates (arrow, Figure 3.21g) or single round-shaped cells (Figure 3.21h). Conversely, in tumours with high-EMCN+ content, positively-labelled cells had a distinctive mesenchymal phenotype with an elongated morphology and formed large cell-groups that intermingled with the tumour epithelium (Figure 3.21i-l). This last phenotype resembled, rather strikingly, the EMCN+ cell-swarms found in *Hesx1*$^{Cre/+;}$*Ctnnb1*$^{lox(ex3)/+}$ embryonic pituitaries during early stages of tumourigenesis.

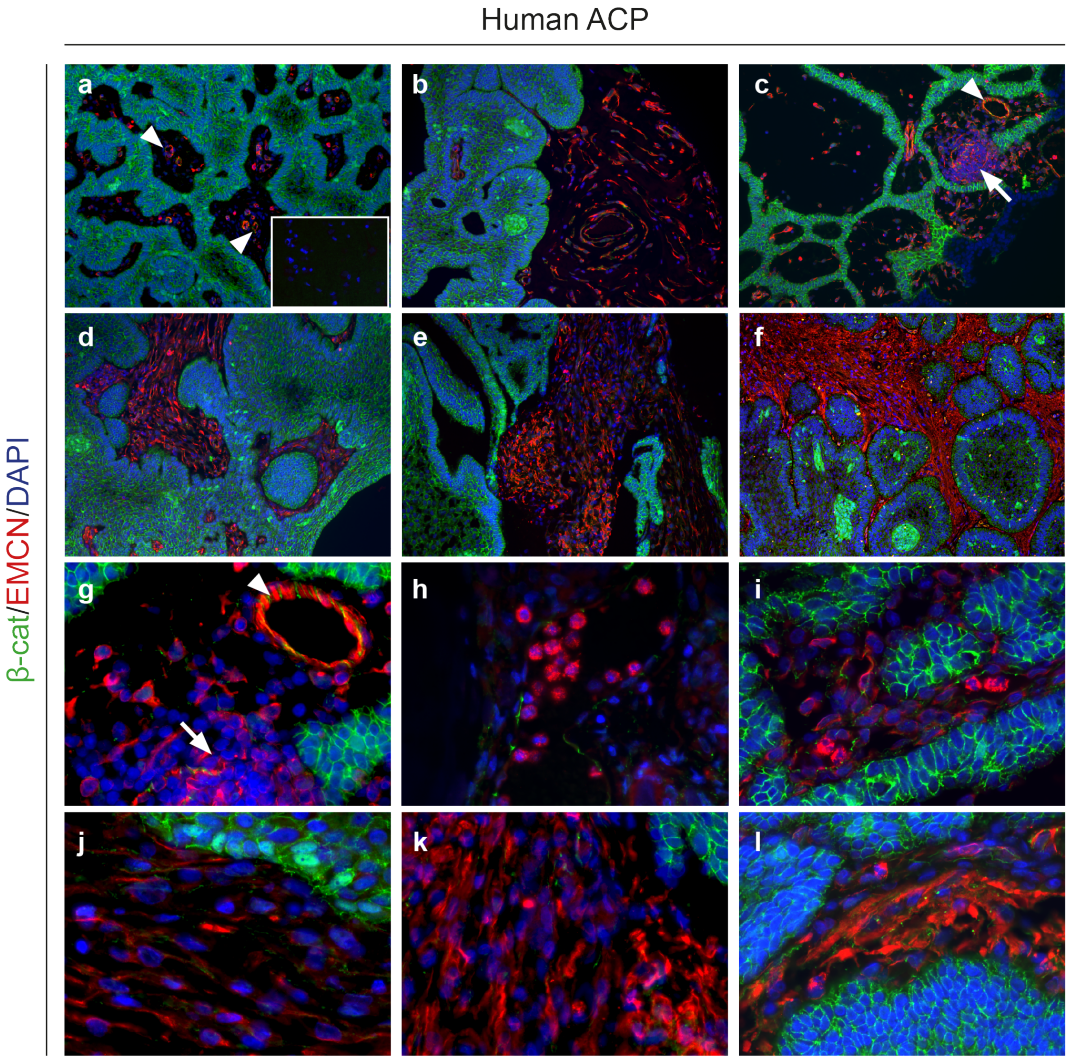

Figure 3.21 EMCN+ cells display different phenotypes in human ACP.

Double immunostaining for EMCN and β-catenin showing representative examples of different phenotypes found in human ACP. **(a)** EMCN+ staining is often detected in vascular cells present within microcysts (arrowheads). Inset: control staining in normal brain. **(b)** A different ACP case shows EMCN+ cells with a different elongated phenotype present outside the tumour parenchyma. **(c)** Large non-vascular EMCN+ cell groups are found within microcysts (arrow). Note positive staining in a large blood vessel (arrowhead). **(d-f)** Representative examples of tumours with high content of EMCN+ cells which are present throughout the extra-tumoural tissue. **(g)** High magnification photograph from (c) shows vascular (arrowhead) and non-vascular (arrow) EMCN+ phenotypes. **(h)** Single round-shaped EMCN+ phenotype found occasionally found within cysts and vessels. **(i-l)** High magnification images from high-EMCN+ content tumours showing the mesenchymal, elongated phenotype of EMCN+ cells that occupy the extra-tumoural space.

3.7 Chapter 3 conclusions

In summary, the results presented in this chapter show that pituitary tumours can develop non-cell autonomously in an embryonic mouse model for ACP. Additionally, analysis of a wide array of markers for key senescence pathways demonstrates that the β-catenin clusters of mouse and human ACP become senescent and activate the SASP. Unbiased transcriptomic analyses provided further support for the validity of mouse models of ACP by demonstrating that human and mouse clusters are similar biological structures. Further experiments are required to clarify the role of pathways such as mTOR and autophagy in mouse in human clusters.

Finally, evidence is presented of the effects the SASP may have on the tumourigenic microenvironment in mice and humans. In mice, it is possible that the SASP is directly involved in the recruitment and transformation of the cell-of-origin, while in humans it might have a role in remodelling of the microenvironment or to provide growth signals to dividing cells.

4. THE ROLE OF THE CXCR4/SDF-1 SIGNALLING AXIS IN NORMAL PITUITARY DEVELOPMENT AND ONCOGENESIS

4.1 Introduction

In the previous chapter, a mechanism was described by which the β-catenin accumulating clusters of murine ACP models provide signals to their environment and possibly induce the changes necessary for non-cell autonomous tumourigenesis to occur. Although these clusters secrete a wide number of signalling factors, the role that some of these cytokines play during oncogenesis is better understood than others, at least in the context of senescence and the SASP. Chemokine signalling is such an example, as increasing evidence has shown how SASP chemokines are able to recruit and/or alter the phenotype of various cell types of the microenvironment (e.g. leukocytes, fibroblasts, vasculature and other supportive cells) during both homeostatic and pathologic processes (Tasdemir et al. 2016; Lujambio et al. 2013; Storer et al. 2013; Muñoz-Espín et al. 2013). Therefore, this chapter aims to shed insight into the role of chemokine-mediated paracrine signalling during normal pituitary development and oncogenesis, with focus on the CXCR4/SDF-1 signalling axis.

The importance of the CXCR4/SDF-1 signalling axis in cancer and stem cell biology has been widely described (Teicher & Fricker 2010), making it an attractive candidate for studying chemotaxis and paracrine signalling, as SDF-1 is the only known ligand for CXCR4; a rather non-promiscuous interaction considering that most chemokine receptors bind various different ligands (Busillo & Benovic 2007). Importantly, its role during normal pituitary development and pituitary oncogenesis *in vivo* has not been investigated in detail (Barbieri et al. 2007), especially in adamantinomatous craniopharyngiomas (ACP).

4.2 The role of the CXCR4/SDF-1 axis in normal pituitary development

The expression of both *Cxcr4* and *Sdf-1* mRNA in the developing pituitary gland has been previously reported (McGrath et al. 1999). However, a comprehensive description of both CXCR4 mRNA and protein expression patterns throughout pituitary development has yet to be reported, and the question of its function *in vivo* remains to be addressed (Rostène et al. 2011).

The expression pattern of *Cxcr4* during normal pituitary development was analysed as part of a masters' project (Gonzalez-Meljem 2012) and it was shown that CXCR4 protein and mRNA expression are mainly restricted to the prospective pituitary intermediate lobe throughout development. For this chapter, a more detailed analysis was conducted and novel data is presented, while making emphasis on aspects not explored or discussed in the masters' thesis.

4.2.1 The expression pattern of CXCR4, CXCR7 and SDF-1 during normal pituitary development

CXCR4 is expressed early in Rathke's Pouch and is mainly restricted to the intermediate lobe during development

The expression pattern *of Cxcr4* during normal pituitary development was determined by *in situ* hybridisation (ISH) (Gonzalez-Meljem 2012; section 3.2) and immunostaining at different stages of pituitary development. CXCR4 protein expression was observed at all stages of pituitary development (10.5 to 18.5 dpc) and localised mainly to the dorso-medial region of Rathke's Pouch, which is the prospective intermediate lobe (IL) (Figure 4.1a). Positive staining was also observed in regions where the IL and the posterior lobe (PL) are physically in contact (inset, Figure 4.1b) as well in cells lying between the IL and PL (arrowhead in inset, Figure

4.1b). At 18.5 dpc and postnatal stages, CXCR4 expression was restricted mostly to cells of the intermediate lobe (Figure 4.1c,d). Interestingly, CXCR4 protein was also observed occasionally in cells of the anterior lobe (AL) that resembled endothelial cells (inset, Figure 4.1c). This observation was corroborated using the endothelial marker endomucin (EMCN), which colocalised with CXCR4+ cells at 15.5 and 18.5 dpc stages (Figure 4.1e,f).

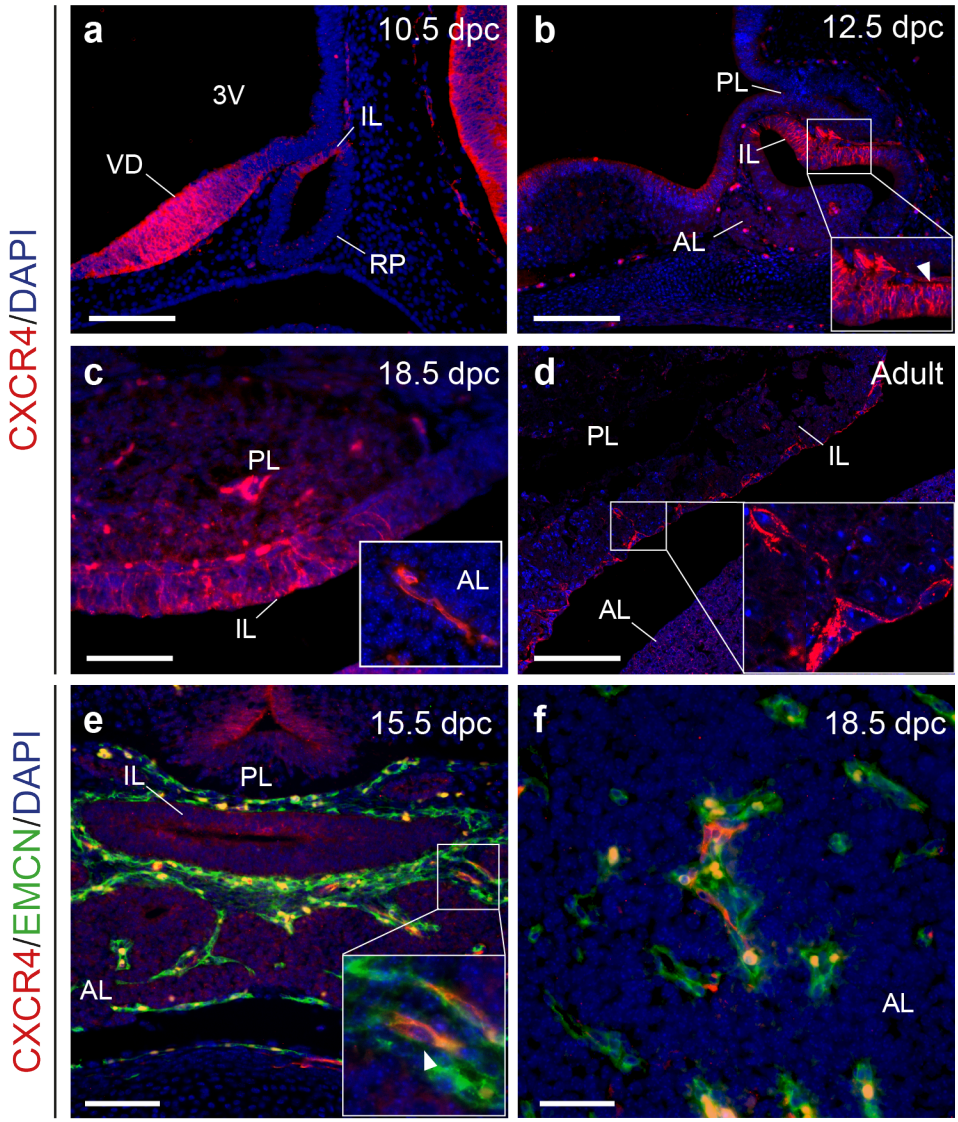

Figure 4.1 Expression pattern of CXCR4 at different stages of murine pituitary development.

Fluorescent immunostaining showing CXCR4 expression in mouse pituitaries at different stages of development. **(a)** At 10.5 dpc CXCR4 expression is observed in the ventral diencephalon (VD) and the prospective intermediate lobe (IL) of Rathke's

Pouch (RP). **(b)** At 12.5 dpc, CXCR4+ cells are observed throughout the IL, including in regions directly in contact with the posterior lobe (PL) and in cells lying between both structures (arrowhead). **(c)** The IL of the 18.5 pituitary also contains CXCR4+ cells, while positive staining can also be observed in the PL. Inset: CXCR4+ cells with endothelial morphology are observed in the anterior lobe. **(d)** Adult pituitaries contain CXCR4+ cells mainly localised in the IL lining of the pituitary lumen. **(e-f)** Double immunostaining for the endothelial marker endomucin (EMCN) and CXCR4 shows double positive cells are present among the developing pituitary vasculature at 15.5 and 18.5 dpc. Scale bars: a,b: 200 μm; c,d,e: 100 μm; e: 50 μm. 3V: Third ventricle; VD: Ventral diencephalon; IL; Intermediate lobe; RP: Rathke's Pouch; AL: Anterior Lobe; PL: Posterior Lobe.

The alternative SDF-1 receptor, CXCR7, is expressed in a domain that is complementary to CXCR4

Expression analysis of the SDF-1 alternative receptor, CXCR7, was conducted by immunostaining and ISH. Interestingly, CXCR7 displayed an expression pattern complementary to that of CXCR4. *Cxcr7* mRNA expression was observed in the oral epithelium and the ventral region of Rathke's Pouch as early as 10.5 dpc (arrows, Figure 4.2a). At 12.5 dpc and 15.5 dpc, its expression was observed in the PL and AL (arrows, Figure 4.2b,c), while low or absent expression levels were observed in the IL. By 18.5 dpc, *Cxcr7* was expressed in cells lining the pituitary cleft in the AL, commonly known as the periluminal area or marginal zone (MZ) (arrows, Figure 4.2d). Interestingly, *Cxcr7* was not expressed in the PL at this later stage, while *Cxcr4* expression was maintained in this structure. The mRNA expression pattern was recapitulated by immunostaining of CXCR7-GFP pituitaries at 12.5 dpc (Figure 4.2i), while double immunostaining with CXCR4 antibody confirmed mutual exclusivity between CXCR4 and CXCR7 expression domains (Figure 4.2j).

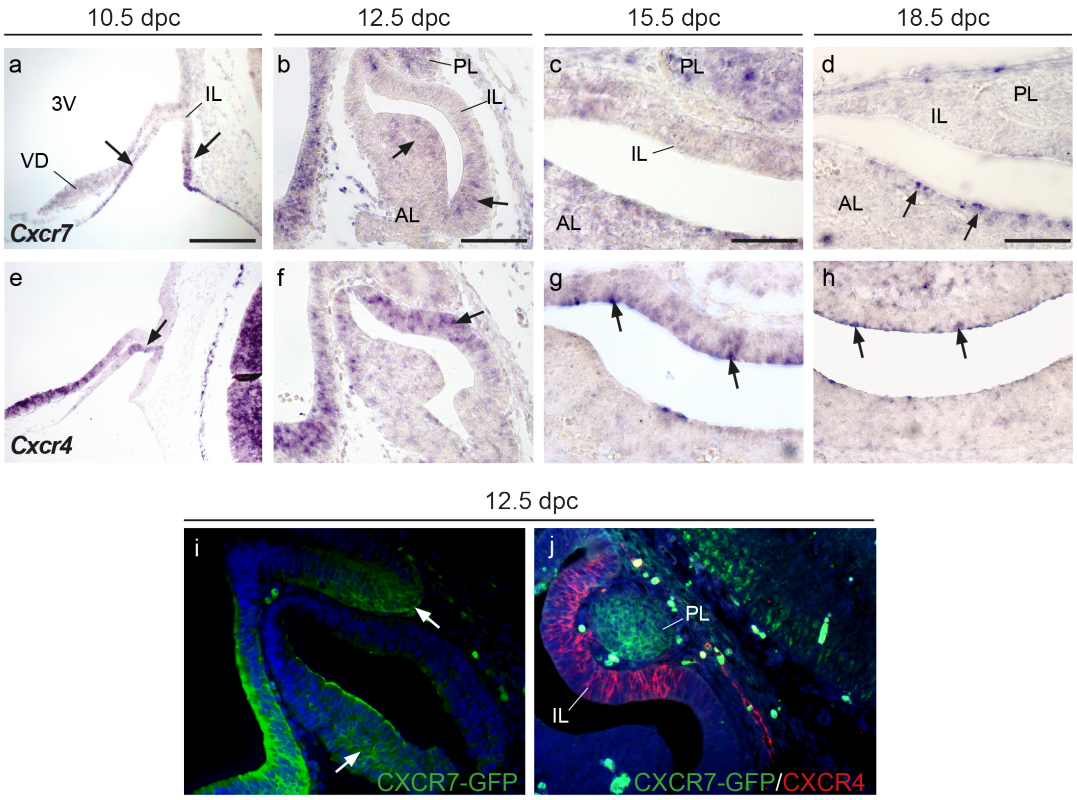

Figure 4.2 Expression pattern of CXCR7 during pituitary development.

(a-d) ISH showing *Cxcr7* expression during normal pituitary development is restricted mainly to the AL (arrows) and the PL. Note reduced mRNA levels in the IL. **(e-h)** ISH for *Cxcr4* at each stage and matched histological regions shows strong expression confined to the IL, opposite to that of *Cxcr7*. **(i)** Immunofluorescence for GFP in CXCR7-GFP pituitaries at 12.5 dpc showing expression in both AL and PL. **(j)** Double immunostaining for GFP and CXCR4 in 12.5 dpc *Cxcr7*$^{GFP/+}$ embryos shows opposite expression patterns of both proteins. DAPI counterstain: i-j. Scale bars: 200 μm. 3V: Third Ventricle; VD: Ventral diencephalon; IL; Intermediate lobe; RP: Rathke's Pouch; AL: Anterior Lobe; PL: Posterior Lobe.

The CXCR4 ligand, SDF-1, is mainly expressed by the mesenchyme surrounding Rathke's Pouch and in cells of the anterior lobe

The expression of *Sdf-1* was characterised by ISH and was observed to mainly localise in mesenchymal cells surrounding the pituitary gland throughout its development (arrows, Figure 4.3a,b). Additionally, it was also observed at later stages in cells of the anterior lobe and in the MZ (arrowheads, Figure 4.3b).

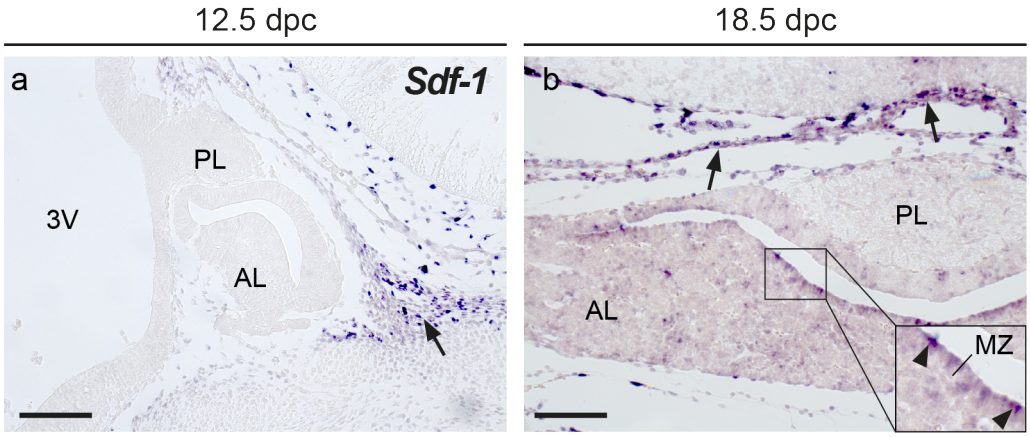

Figure 4.3 *In situ* hybridisation showing the expression of *Sdf-1* during normal pituitary development.

(a) At 12.5 dpc, expression is mainly observed in mesenchymal tissue surrounding the developing pituitary gland (arrow). **(b)** At 18.5 dpc, the supportive mesenchyme still expresses *Sdf-1* (arrows), although *Sdf-1*+ cells can also be observed in the anterior lobe and the periluminal region (arrowheads). Scale bars: a,b: 200 μm. 3V: Third Ventricle; AL: Anterior Lobe; PL: Posterior Lobe; MZ: Marginal Zone.

4.2.2 The expression pattern of CXCR4 during human pituitary development

The expression pattern of CXCR4 was also analysed in foetal human pituitaries at stages CS18 and CS20 by immunostaining. At both stages, CXCR4 expression resembled that of the mouse embryonic pituitary, localising mainly to the prospective intermediate lobe and posteriorly to the pouch's cleft (Figure 4.4a-f). Interestingly, a group of cells with high CXCR4 expression were identified in proximity to the

developing pituitary gland at these stages (arrowheads, Figure 4.4b,c,e,f). These cells displayed filopodial processes and formed luminal structures, suggesting these might be endothelial progenitors involved in the formation of the pituitary vasculature at later stages. Therefore, the expression pattern of CXCR4 during pituitary development is strikingly similar between mice and humans, suggesting a conserved function between species.

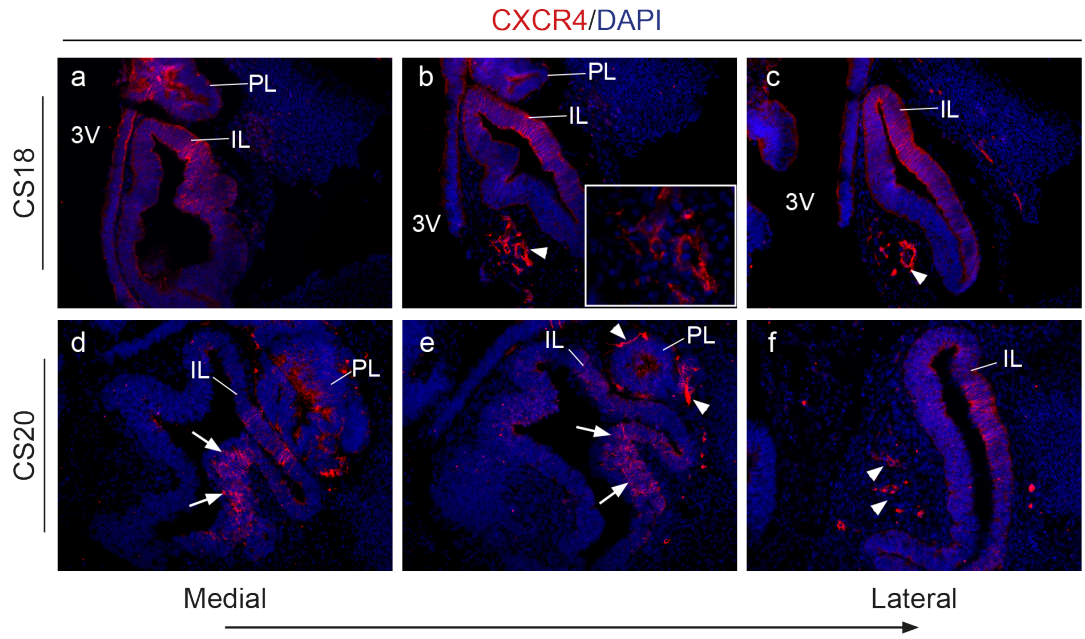

Figure 4.4 Immunofluorescence for CXCR4 at different stages of human embryonic pituitary development.

(a-c) CXCR4 positive cells are found throughout the dorsomedial region of Rathke's Pouch (prospective intermediate lobe) at the CS18 stage. Positive staining is also observed in the developing infundibulum (prospective posterior lobe). Strong positive signal is observed in endothelial cells located near the future anterior lobe and were only observed in more lateral regions of RP (arrowheads). **(d-f)** A similar expression pattern is observed at CS20, with strong CXCR4 expression in the postero-dorsal region of RP (arrows) and in developing blood vessels in lateral regions (arrowheads). IL; Intermediate lobe; PL: Posterior Lobe

4.2.3 Conditional knockout of CXCR4 in the developing pituitary gland

Mice with null mutations in members of the CXCR4/SDF-1 pathway are characterised by embryonic and perinatal lethality mainly due to vascular defects (Cavallero et al. 2015; Ivins et al. 2015). Therefore, specific ablation of CXCR4 in the pituitary gland was conducted using the *Cre-loxP* system to study this signalling pathway in the absence of potentially confounding systemic effects. The *Hesx1*$^{Cre/+}$ line was used to drive Cre recombinase expression as most of the mature pituitary gland is formed by the descendants of *Hesx1*-expressing cells (Jayakody et al. 2012).

Conditional ablation of CXCR4 in *Hesx1*$^{Cre/+}$;*Cxcr4*$^{fl/fl}$ mice does not affect normal pituitary development

Successful and specific removal of *Cxcr4* mRNA and protein in *Hesx1*$^{Cre/+}$;*Cxcr4*$^{fl/fl}$ embryos was evaluated by ISH and IHC and previously reported (Gonzalez-Meljem, 2012; section 3.2). A representative immunostaining at 15.5 dpc is shown in Figure 4.5. Although CXCR4 protein was clearly removed from the IL of *Hesx1*$^{Cre/+}$;*Cxcr4*$^{fl/fl}$ pituitaries, positive cells could still be observed in the boundary between the IL and PL (arrowheads, Figure 4.5a,b). Additionally, cells with endothelial morphology where also located in the AL stroma of *Hesx1*$^{Cre/+}$;*Cxcr4*$^{fl/fl}$ pituitaries (arrowhead, Figure 4.5b). This indicated that CXCR4+ cell populations present in between the IL and PL, as well as in the AL stroma are not derived from the *Hesx1* lineage.

A phenotypic characterisation of *Hesx1*$^{Cre/+}$;*Cxcr4*$^{fl/fl}$ mice was also previously reported (Gonzalez-Meljem, 2012; results section 3). Litters derived from crossing *Hesx1*$^{Cre/+}$;*Cxcr4*$^{fl/+}$ and *Cxcr4*$^{fl/fl}$ mice displayed normal mendelian ratios (N=59 for embryos, N=69 for postnatal mice, Chi-square test ($P>0.05$)), indicating that removal of CXCR4 in the developing pituitary does not cause embryonic or postnatal lethality.

Mutant pituitaries were morphologically normal and all pituitary endocrine cell populations reached normal terminal differentiation as determined by IHC. Born mice were healthy and fertile until late adulthood while measurement of pituitary hormone content suggested normal function of the adult gland. Finally, the effect of CXCR4 knockout in the pituitary stem/progenitor cell population was assayed by an *in vitro* assay of colony formation, which showed no difference between mutant and control pituitaries (Gonzalez-Meljem, 2012, section 3.1).

The expression domain of *Cxcr7* was characterised by ISH in *Hesx1*$^{Cre/+}$*;Cxcr4*$^{fl/fl}$ pituitaries at 12.5 dpc (Figure 4.5e,f) to assess a possible compensation for the lack of CXCR4 function. However, the pattern of *Cxcr7* expression in *Cxcr4* mutants was not different from wild type littermates. Additionally, no change was observed in the expression domain of genes required for proper pituitary development, such as *Fgf10* (Figure 4.5g,h) and *Lhx3* (Figure 4.5i,j). Altogether, these results suggest that the lack of CXCR4 expression in pituitary gland progenitors does not affect its normal development or overall function, and that this is not due to a compensation mechanism occurring through the canonical CXCR4/SDF-1 pathway.

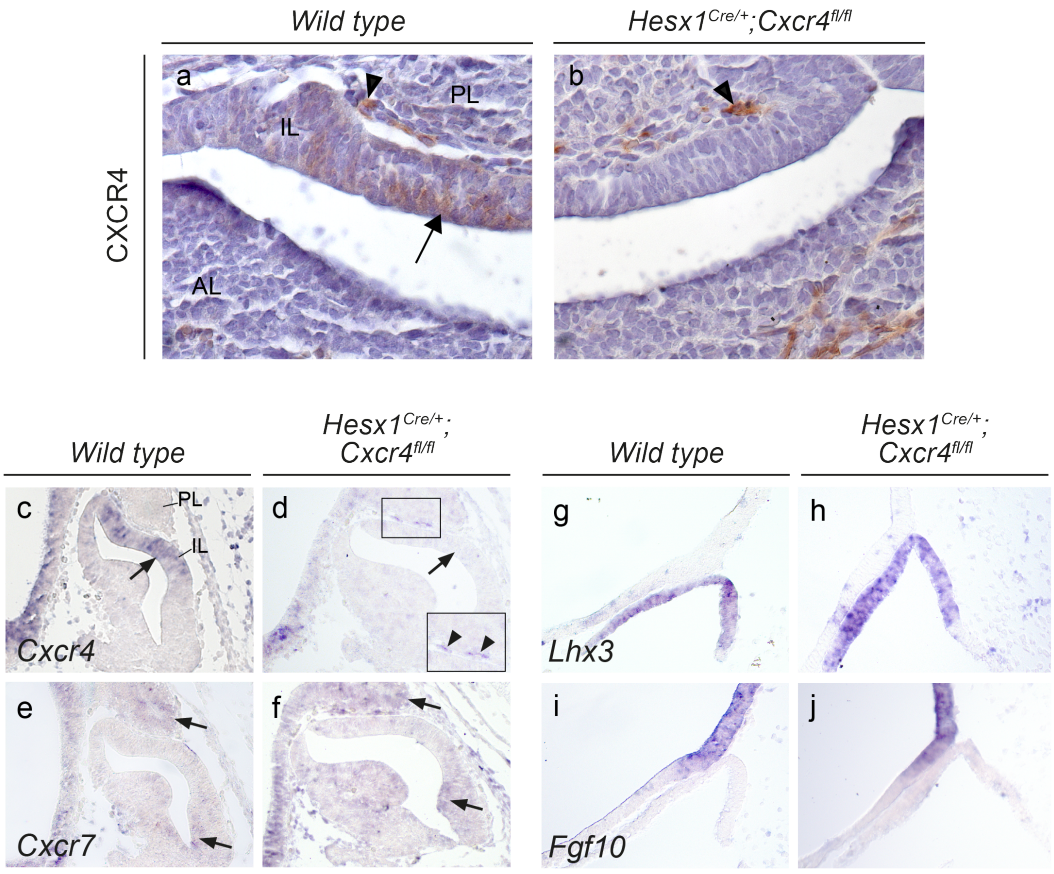

Figure 4.5 Characterisation of *Hesx1*$^{Cre/+}$*;Cxcr4*$^{fl/fl}$ pituitaries.

(a) Immunohistochemistry against CXCR4 in a 15.5 dpc wild type pituitary shows stereotypical expression pattern in cells of the intermediate lobe (arrow) as well as in cells lying in the boundary between the intermediate and posterior lobes (arrowhead). **(b)**. CXCR4 protein is effectively removed from the intermediate lobe in *Hesx1*$^{Cre/+}$*;Cxcr4*$^{fl/fl}$ pituitaries. Note that CXCR4+ cells resembling blood vessels are still observed in the anterior lobe and also in the boundary between the intermediate and posterior lobes (arrowheads). **(c-d)** *In situ* hybridisation of *Cxcr4* mRNA at 12.5 dpc shows absence of expression in the intermediate lobe of *Hesx1*$^{Cre/+}$*;Cxcr4*$^{fl/fl}$ pituitaries. Note the presence of positive signal in cells lying in the boundary between the intermediate and posterior lobes (arrowheads in inset). **(e-f)** The expression pattern of *Cxcr7* is not affected in mutant pituitaries at 12.5 dpc. **(g-h)** The expression of the transcription factor *Lhx3,* essential for pituitary development, is not affected in mutant pituitaries. **(i-j)** The expression domain of *Fgf10* in the ventral diencephalon is also not affected in mutants. IL; Intermediate lobe; PL: Posterior Lobe.

4.2.4 Phenotypic characterisation of *Cxcr4*$^{-/-}$, *Cxcr7*$^{-/-}$ and *Sdf-1*$^{-/-}$ pituitaries

Only *Sdf-1*$^{-/-}$ mutants show abnormalities in pituitary development

The lack of a phenotypic alteration in *Hesx1*$^{Cre/+}$;*Cxcr4*$^{fl/fl}$ mice led to the hypothesis that CXCR4/SDF-1 signalling could play a role by acting on cells not derived from pituitary progenitors (e.g. vasculature, pericytes, fibroblasts), as CXCR4+ cells were still observed in these embryos. Therefore, an analysis of the pituitary phenotype was conducted on *Cxcr4* $^{-/-}$, *Cxcr7*$^{-/-}$ and *Sdf-1*$^{-/-}$ embryos.

Cxcr4 $^{-/-}$ and *Cxcr7* $^{-/-}$ embryos displayed normal pituitary glands at all observed stages (Figure 4.6c,d,g,h,k,l). Additionally, immunostaining for markers of normal pituitary development like Pit1 and TPit, as well for most pituitary hormones, did not reveal any differences when compared to wild type littermates at 18.5 dpc (data not shown).

Surprisingly, *Sdf-1* $^{-/-}$ pituitaries had an aberrant morphology at 16.5 and 18.5 dpc (Figure 4.6f,j). This phenotype consisted of abnormal involutions of the intermediate lobe, which were observed fusing with the anterior lobe in some histological sections (not shown); as well as structural abnormalities of the basisphenoid bone (BB, Figure 4.6f) and presence of ectopic blood vessels (arrows, Figure 4.6f,j). However, no evident dysmorphic phenotype was found at 11.5 dpc (Figure 4.6b), indicating that the appearance of pituitary phenotype occurs after this stage.

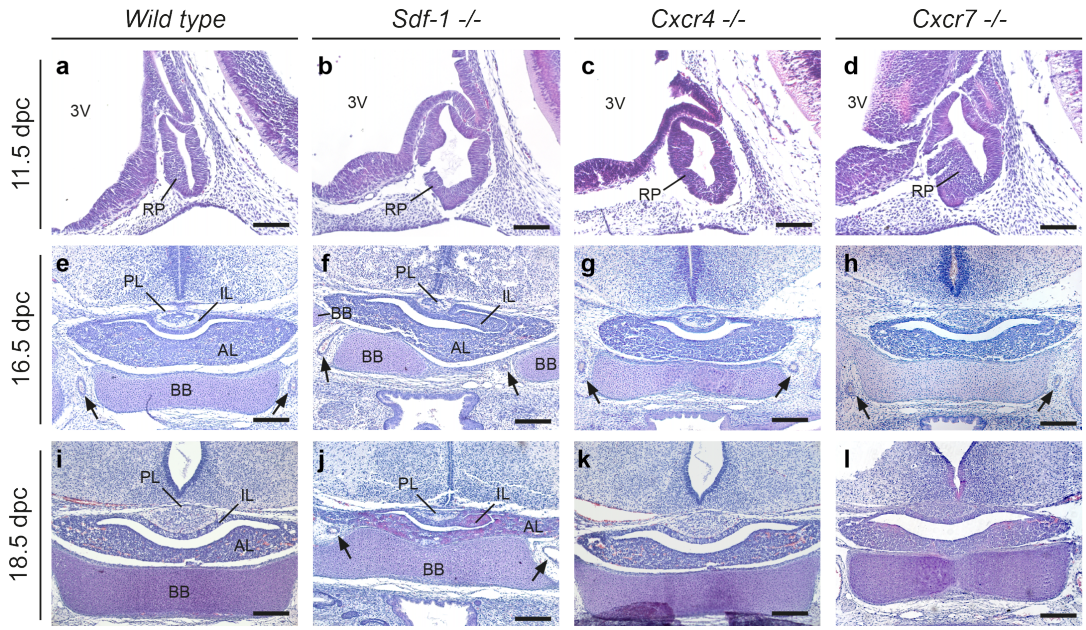

Figure 4.6 Haematoxylin/Eosin (H&E) staining in wild type, *Sdf-1*$^{-/-}$, *Cxcr4*$^{-/-}$, *Cxcr7*$^{-/-}$ pituitaries at different developmental stages.

(a-d) At 11.5 dpc, the RP from *Sdf-1*$^{-/-}$, *Cxcr4*$^{-/-}$ and *Cxcr7*$^{-/-}$ embryos is not affected. **(e)** At 16.5 dpc the wild type developing pituitary sits on top of the basisphenoid bone (BB), which is flanked by large blood vessels (arrows). **(f)** *Sdf-1*$^{-/-}$ pituitaries at this stage have an abnormal shape, invaginations of the intermediate lobe (IL) and a deformed BB. Note ectopic blood vessels intermingling in between the BB (arrows). **(g-h)** *Cxcr4*$^{-/-}$ and *Cxcr7*$^{-/-}$ pituitaries resemble wild types at 16.5 dpc. **(i-j)** The *Sdf-1*$^{-/-}$ pituitary phenotype at 18.5 dpc also presents an invaginated IL and deformed BB with ectopic blood vessels (arrows). **(k-l)** *Cxcr4*$^{-/-}$ and *Cxcr7*$^{-/-}$ pituitaries are morphologically normal at 18.5 dpc. Scale bars: a-d: 100 µm; i-l: 200 µm. RP: Rathke's Pouch; 3V: Third Ventricle; PL: Posterior Lobe; AL: Anterior Lobe; IL: Intermediate Lobe; BB: Basisphenoid Bone.

Normal patterning and terminal differentiation occurs in *Sdf-1*$^{-/-}$ pituitaries

Proper development of the pituitary gland is highly dependent on factors secreted by the ventral diencephalon (VD), all which have specific expression domains. Therefore, proper patterning of the *Sdf-1*$^{-/-}$ VD was evaluated by ISH at 11.5 dpc, which showed no abnormalities in the expression patterns of *Cxcr4*, *Bmp4*, *Fgf10* and *Shh* (Figure 4.7a-h). Furthermore, ISH for oxytocin and vasopressin revealed proper specification of the hypothalamic nuclei in *Sdf-1* mutants (data not shown). Finally, expression of *Lhx3* was not affected in *Sdf-1*$^{-/-}$ embryos (Figure 4.7i,j), indicating a proper specification of the pituitary lineage in early development.

An assessment of the terminal differentiation of different pituitary endocrine lineages was conducted by immunofluorescence in 18.5 dpc pituitaries and showed no differences between *Sdf-1*$^{-/-}$ pituitaries and wild types (Figure 4.7k-r). Finally, a possible vascular phenotype in *Sdf-1*$^{-/-}$ pituitaries was investigated as CXCR4+ cells were previously observed closely associated to endothelial cells in the pituitary (Figure 4.1e,f). However, immunostaining against the endothelial marker endomucin (EMCN) showed no obvious defects in the architecture of the mutant pituitary microvasculature (Figure 4.7s,t).

Overall, these results suggest that the *Sdf-1*$^{-/-}$ pituitary phenotype is mostly morphological in nature and that it might depend on a complex interaction between different tissues and structures not related to the pituitary itself, such as the surrounding mesenchyme (basisphenoid bone and cranial blood vessels).

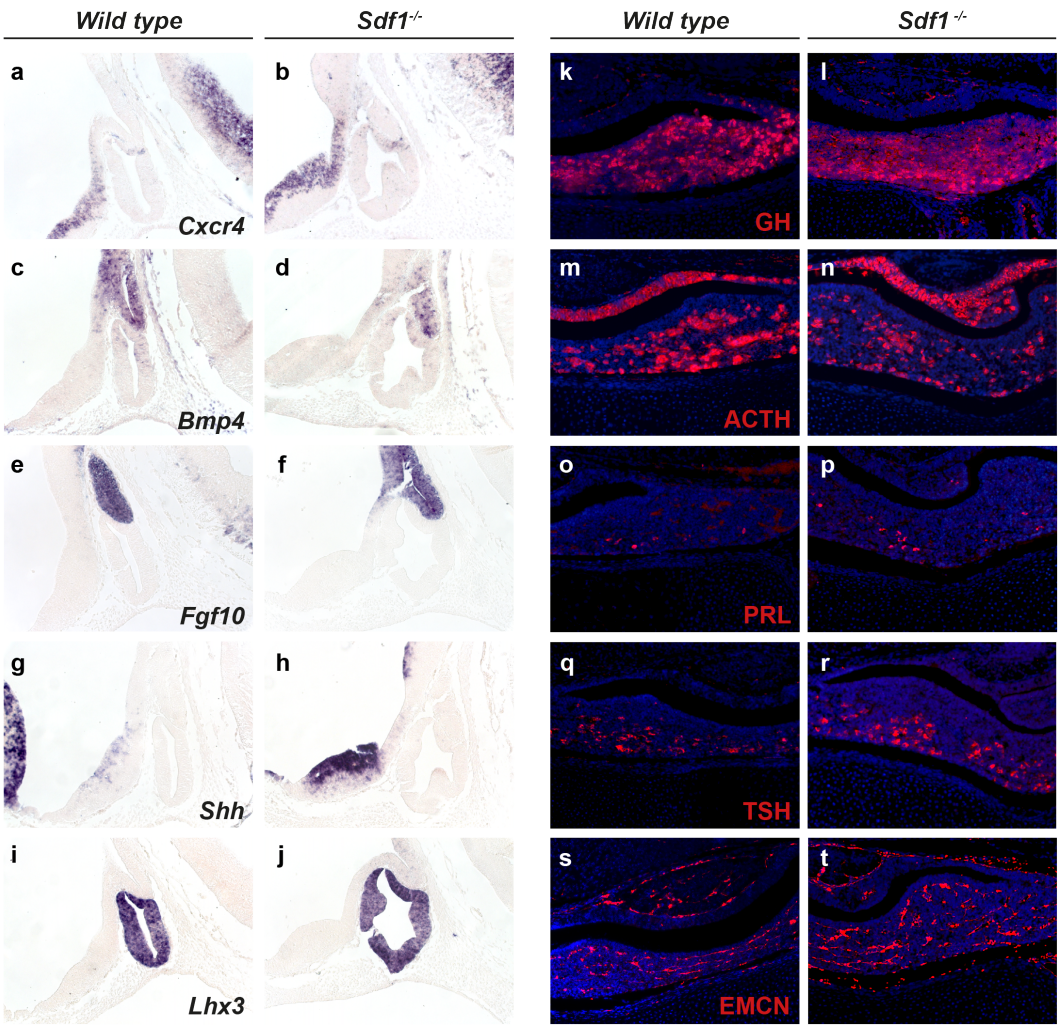

Figure 4.7 Molecular characterisation of *Sdf1*$^{-/-}$ mutants.

(a-b) *In situ* hybridisation in 11.5 dpc embryos shows that *Cxcr4* expression is not significantly altered in *Sdf1*$^{-/-}$ mutants. **(c-h)** No differences are found in the expression domains of hypothalamic factors crucial for proper pituitary specification and patterning such as *Bmp4*, *Fgf10* and *Shh*. **(i-j)** The expression of the transcription factor *Lhx3* (necessary for normal pituitary development) is not altered in *Sdf1*$^{-/-}$ mutants. **(k-r)** Fluorescent immunostaining against different pituitary hormones at 18.5 dpc shows proper terminal differentiation of the pituitary endocrine lineages in *Sdf1*$^{-/-}$ mutants. **(s-t)** Endomucin (EMCN) staining shows a normal pattern of vascularization in mutant pituitaries. DAPI counterstain: k-t. GH: Growth Hormone; ACTH: Adeno-Corticotropic Hormone; TSH: Thyroid Stimulating Hormone

4.3 The Role of CXCR4/SDF-1 in Pituitary Oncogenesis

It has been reported that high expression of CXCR4 and SDF-1 predicted tumour recurrence in human ACP (Gong et al. 2014). Additionally, overexpression of *CXCR4* was reported to localise in the β-catenin clusters of both human ACP and *Hesx1*$^{Cre/+}$*;Ctnnb1*$^{lox(ex3)/+}$ pituitaries (Andoniadou et al. 2012), while *Sdf-1* was overexpressed in the non-cluster fraction. This suggested a crosstalk between the stroma and the clusters through this axis, which could be potentially targeted to prevent or delay tumour growth. Therefore, a detailed expression analysis was conducted in order to better understand the relation of CXCR4+ cells with the β-catenin-accumulating clusters in both the *Hesx1*$^{Cre/+}$*;Ctnnb1*$^{lox(ex3)/+}$ model and human ACP.

4.3.1 The expression pattern of CXCR4 in the craniopharyngioma mouse model.

CXCR4 is expressed in cells inside and outside β-catenin cell clusters

Double immunostaining experiments demonstrated that most clusters in *Hesx1*$^{Cre/+}$*;Ctnnb1*$^{lox(ex3)/+}$ pituitaries contain CXCR4+ cells at 18.5 dpc (arrows, Figure 4.8a-f). The number of CXCR4+ cells varied among the clusters. However, most CXCR4-expressing cells were found outside the clusters and interestingly, were often closely associated to them (arrowheads, Figure 4.8a-f). This pattern was reproduced in a second ACP mouse model (*Sox2*$^{CreERT2/+}$*;Ctnnb1*$^{lox(ex3)/+}$ mice) in which oncogenic β-catenin expression was only induced in SOX2+ adult stem cells (Figure 4.8g-i). Therefore, CXCR4 is widely expressed in the β-catenin clusters of two different mouse models of ACP, as well as in other non β-catenin-accumulating cells that closely interact with the clusters.

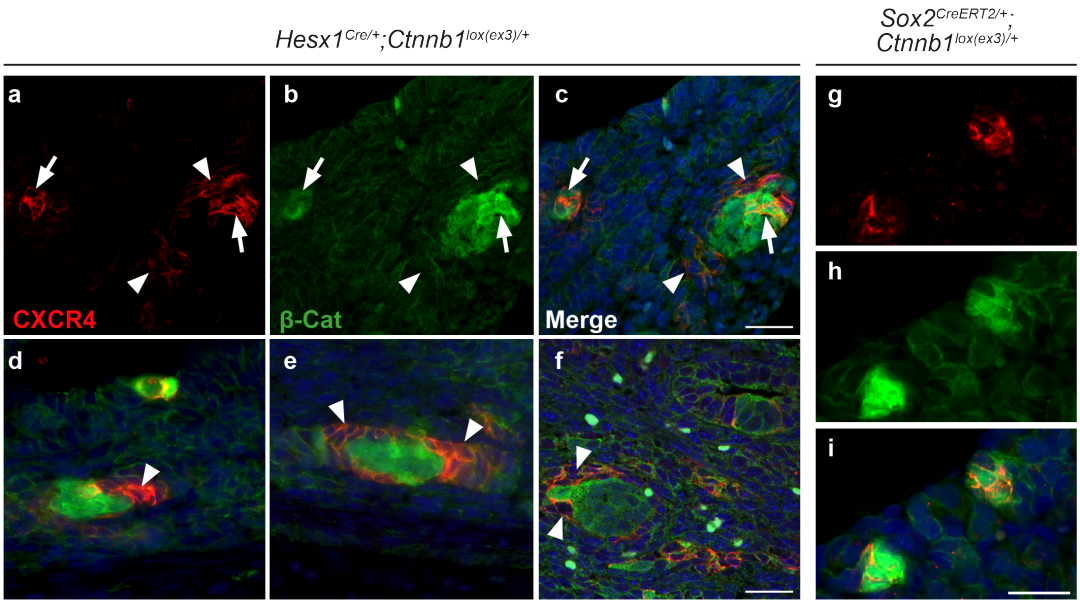

Figure 4.8 Double immunofluorescence for CXCR4 and β-catenin in two mouse models of adamantinomatous craniopharyngioma.

(a-b) Most nucleo-cytoplasmic β-catenin accumulating clusters in *Hesx1*$^{Cre/+}$;*Ctnnb1*$^{lox(ex3)/+}$ pituitaries contain CXCR4+ cells at 18.5 dpc (arrows). However, groups of CXCR4+ cells are often located in the vicinity of some clusters (arrowheads). **(d-f)** Further histological examples showing the close interaction between the clusters and the CXCR4+ cells (arrowheads). **(g-h)** The β-catenin clusters of adult pituitaries in the inducible *Sox2*$^{CreERT2/+}$;*Ctnnb1*$^{lox(ex3)/+}$ model also contain CXCR4+ cells. DAPI counterstain. Scale bars: 25 μm

4.3.2 The expression pattern of *Sdf-1*, *Cxcr7* and *Cxcr2* in mouse ACP

The increased expression of *Cxcr4* in cells of both the pituitary and stroma in *Hesx1*$^{Cre/+}$*;Ctnnb1*$^{lox(ex3)/+}$ pituitaries (including the β-catenin clusters) suggested activation of the pathway by ligand binding and therefore, the presence of a nearby source of SDF-1 secretion. It was previously reported a 4.92-fold up regulation in *Sdf-1* expression in non-cluster cells at 18.5 dpc (Andoniadou et al. 2012) and that *Sdf-1* mRNA expression was not present in cluster formations (Reddy 2011). However, this last study failed to report any *in situ* expression of *Sdf-1* that could reconcile the rather drastic 4.92-fold up regulation detected by microarray analysis. Therefore, a more detailed analysis of *Sdf-1 in situ* expression was conducted.

A similar analysis was conducted for *Cxcr7*, which is often involved in regulating CXCR4 signalling. Finally, the expression of *Cxcr2* was investigated as this receptor is known to antagonise CXCR4 signalling cell-autonomously (Eash et al. 2010), and also because microarray data revealed the overexpression of the three main *Cxcr2* ligands (*Cxcl1, Cxcl2* and *Cxcl3)* in the β-catenin clusters (Andoniadou et al. 2012).

Hesx1$^{Cre/+}$*;Ctnnb1*$^{lox(ex3)/+}$ pituitaries and tumours are invaded by *Sdf-1* and *Cxcr2* expressing cells

Unlike wild type pituitaries, where the strongest *Sdf-1* expression was found in the supportive mesenchymal tissue (arrows, Figure 4.9a), *Hesx1*$^{Cre/+}$*;Ctnnb1*$^{lox(ex3)/+}$ pituitaries showed strong *Sdf-1* staining in large cell masses within the anterior lobe (arrowheads, Figure 4.9b,c). Several of these cell groups were found per pituitary and commonly located in the ventral-most region. Interestingly, these cell groups were also observed clearly invading the pituitary anterior lobe and remaining continuous with the exterior of the organ, suggesting that high *Sdf-1*+ cells also invade the pituitary gland from an external compartment (inset, Figure 4.9c).

Conversely, the expression pattern of *Cxcr7* was not different between mutant and wild type pituitaries, where mRNA expression was strongest in the lining of the third ventricle (arrows, Fig 4.9d,e,f), surrounding mesenchyme and some cells of the MZ.

While no clear expression of *Cxcr2* could be observed in 18.5 dpc wild type pituitaries (Figure 4.9g), strong *Cxcr2*+ staining was observed throughout mutant pituitaries (arrows, Figure 4.9h), suggesting that secretion of CXCR2 ligands by the clusters is involved in crosstalk with other cell types during embryonic stages. Interestingly, end-stage tumours also contained large numbers of *Cxcr2*+ cells that accumulated mainly in regions surrounding cysts within the tumours (arrows, Figure 4.9i). Therefore, in late stage tumours, there is possibly a different source of ligands contributing to CXCR2 signalling and reinforcing cell recruitment into the microenvironment of these tumours when they have become independent from signals secreted by the clusters.

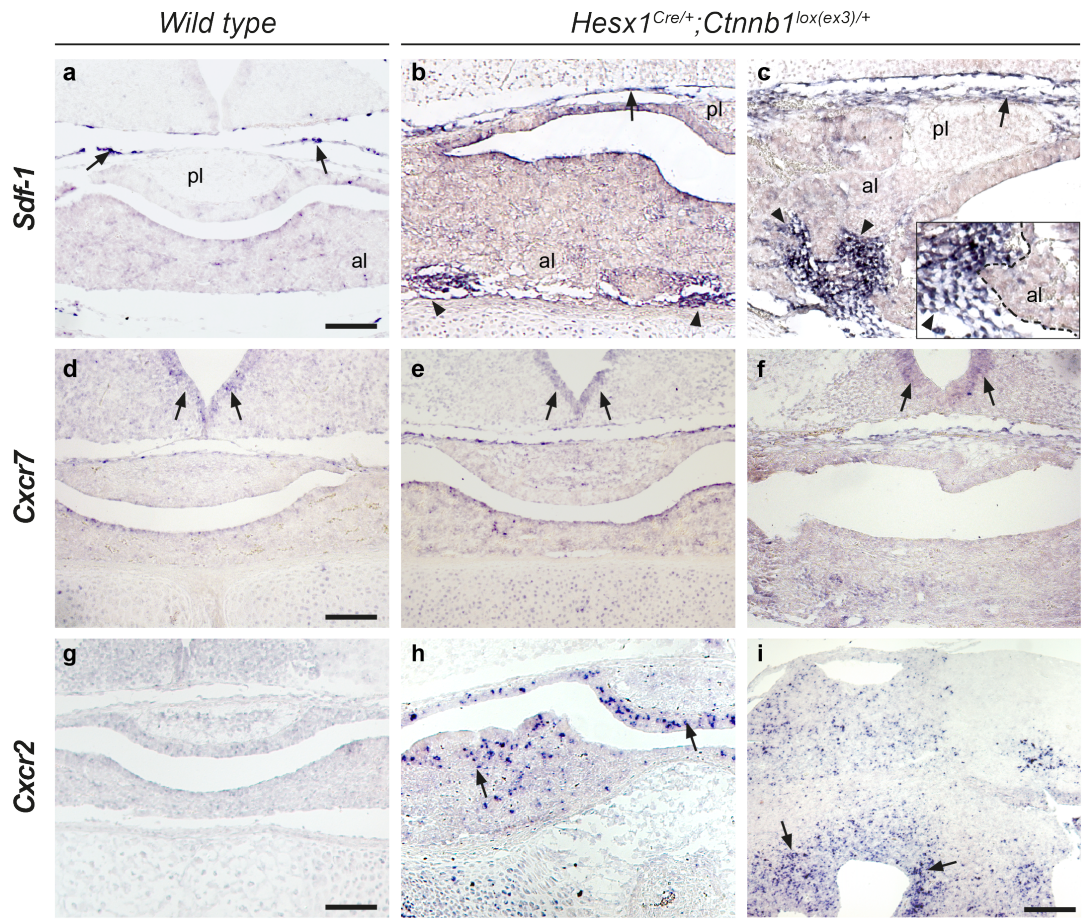

Figure 4.9 Expression of other members of the CXCR4/SDF-1 signalling axis in *Hesx1$^{Cre/+}$;Ctnnb1$^{lox(ex3)/+}$* pituitaries.

(a) *Sdf-1* is strongly expressed in the mesenchymal supportive tissue surrounding the wild type pituitary gland at 18.5 (arrows). Lower levels of expression can be observed in cells of the anterior lobe. **(b)** *Hesx1$^{Cre/+}$;Ctnnb1$^{lox(ex3)/+}$* pituitaries also show strong *Sdf-1* expression in ventrally located cell groups (arrowheads). **(c)** High-*Sdf-1* cells invade the mutant pituitary gland ventrally (arrowheads). Inset: *Sdf-1* cells (arrowhead) embedded within the anterior lobe epithelium (dotted line) are continuous with the exterior of the pituitary. **(d-f)** The expression pattern of *Cxcr7* is not altered in mutants, but is still observed in the lining of the third ventricle (arrows). **(g)** *Cxcr2* is not expressed in wild type pituitaries at 18.5 dpc. **(h)** Strong expression of *Cxcr2* is evident in cell groups present throughout mutant pituitaries (arrows). **(i)** Large numbers of *Cxcr2*-positive cells are observed in end-stage tumours, mostly surrounding cystic areas (arrows). Scale bars: a-h: 100 µm; i: 200 100 µm. PL: Posterior Lobe; AL: Anterior Lobe

4.3.3 The expression pattern of CXCR4 in human ACP

The CXCR4 and SDF-1 genes are highly conserved between mice and humans, as is their role in cancer (Teicher & Fricker 2010). The expression pattern of CXCR4 was studied in four independent human adamantinomatous craniopharyngioma (ACP) samples, as well in a tissue microarray containing 23 different ACP samples and normal brain control tissue. Surprisingly, CXCR4+ cells mostly did not colocalise with β-catenin clusters, in contrast with the two murine ACP models where CXCR4+ cells were frequently seen inside the clusters (Figure 4.8). However, CXCR4+ cells and the β-catenin clusters were consistently found in close association with each other in human ACP, in part recapitulating previous observations from the mouse models (arrowheads, Figure 4.10a-f). This expression pattern of mutual exclusivity, yet invariable proximity, was observed in a clear majority of human clusters and suggests an active cross-talk between both cell populations.

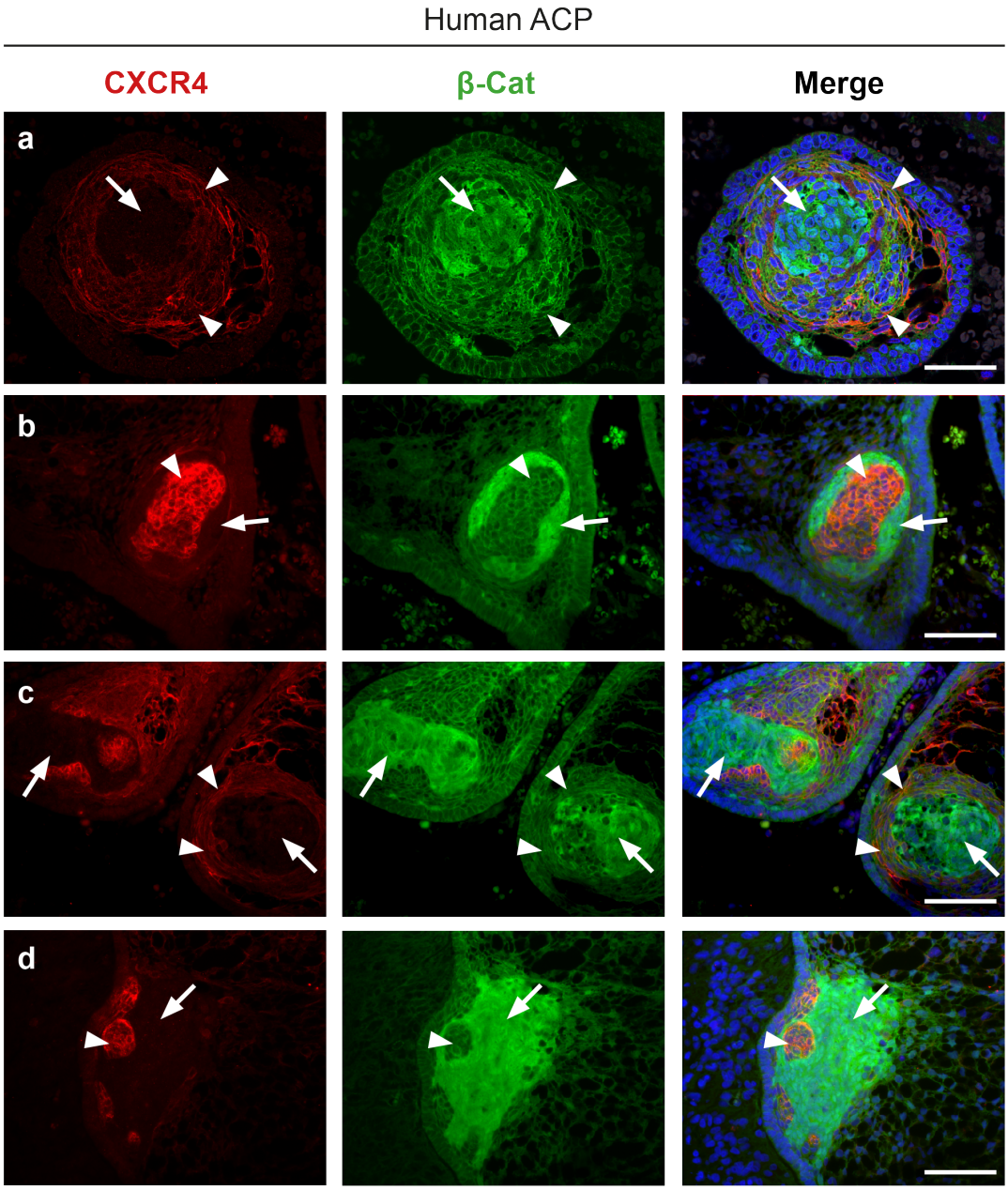

Figure 4.10 Double immunofluorescence for CXCR4 and β-catenin in human adamantinomatous craniopharyngioma.

(a) CXCR4-positive cells (arrowheads) are seen commonly in close contact with β-catenin clusters (arrow) but appear to be mutually exclusive. **(b-d)** Further examples of β-catenin clusters interacting with CXCR4+ cells within human ACP samples. DAPI counterstain. Scale bars: a: 50 μm; b,c,d: 100 μm

4.3.4 The expression of *SDF-1, CXCR7*, and *CXCR2* in human ACP

ISH was conducted in ACP samples to determine the expression pattern of other CXCR4 pathway signalling members. *SDF-1* mRNA expression was observed in discreet areas within the tumours (arrows, Figure 4.11a-c) and did not correlate to cluster/whorl-like formations. Furthermore, *CXCR2* expression was observed throughout the tumour, including the palisaded epithelium and whorl-like cell structures (Figure 4.11d-f), suggesting *CXCR2* activation occurs throughout ACP tumours by binding IL-8 (or its analogues CXCL1, CXCL2 and CXCL3) possibly secreted by the clusters. Clear *CXCR7* expression could not be observed in tumours (not shown). Therefore, the expression of CXCR4 signalling members appears to be restricted to specific and different compartments within the tumour parenchyma.

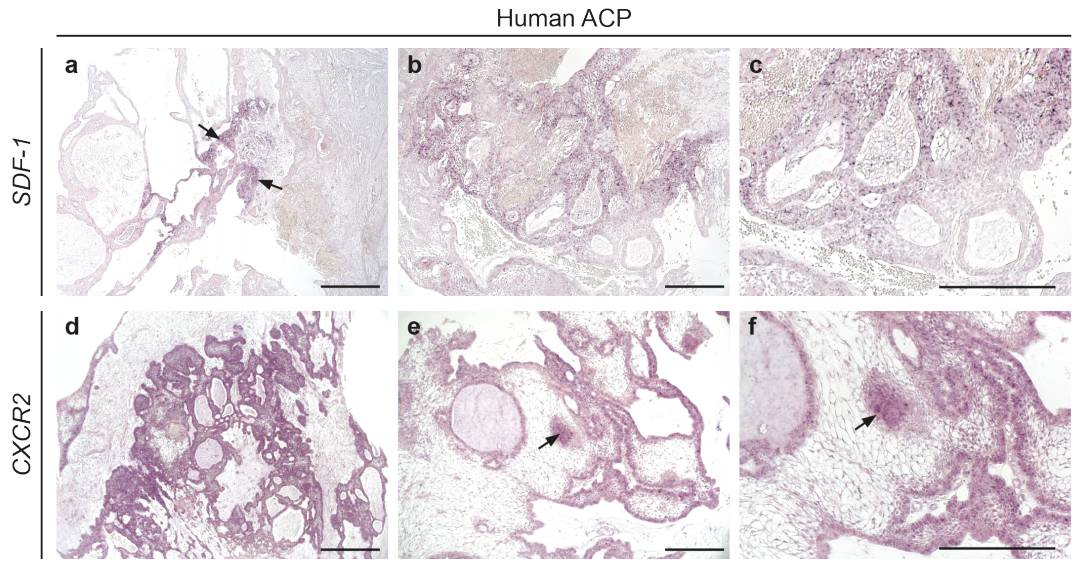

Figure 4.11 *In situ* hybridisation for *SDF-1* and *CXCR2* in human ACP.

(a) *SDF-1* expression can only be observed in restricted regions of human ACP. **(b-c)** Higher magnification photographs of another region (same tumour). **(d)** *CXCR2* is widely expressed in the tumour parenchyma. **(e-f)** *CXCR2* expression is mainly localised to the palisaded epithelium and whorl-like cell structures (arrow), while the stellate-reticulum appears to be *CXCR2*-negative. Scale bars: 250 μm.

4.3.5 Conditional knockout of CXCR4 in the murine ACP background

The notable specificity of CXCR4 co-expression within nucleocytoplasmic accumulating β-catenin in the murine clusters, as well as the absence of a detrimental phenotype in *Hesx1*$^{Cre/+}$*;Cxcr4*$^{fl/fl}$ mice, suggested that CXCR4-knockout in the developing pituitary gland could potentially restrict the clusters from an important growth/survival factor and therefore abrogate tumour progression in the mouse ACP model. Additionally, other CXCR4+ cells were found to interact closely with the clusters in both murine and human ACP, suggesting a supportive/trophic role for these cells.

In order to study the role CXCR4 signalling within the β-catenin clusters and tumour progression, knockout of CXCR4 expression was conditionally targeted to pituitary embryonic progenitors in the context of mouse ACP resulting in mice carrying the genotype *Hesx1*$^{Cre/+}$*;Ctnnb1*$^{lox(ex3)/+}$*;Cxcr4*$^{fl/fl}$ (hereafter also referred as *Cxcr4* triple mutants).

CXCR4 is successfully removed in *Hesx1*$^{Cre/+}$*;Ctnnb1*$^{lox(ex3)/+}$*;Cxcr4*$^{fl/fl}$ clusters

Double immunostaining for CXCR4 and β-catenin showed successful ablation of CXCR4 expression in all the nucleocytoplasmic accumulating β-catenin clusters of *Hesx1*$^{Cre/+}$*;Ctnnb1*$^{lox(ex3)/+}$*;Cxcr4*$^{fl/fl}$ pituitaries at 18.5 dpc (Figure 4.12; 45.95% colocalisation in heterozygous control, N=37 clusters in 3 embryos; 0% colocalisation in homozygous mutant, N=41 clusters counted in 3 embryos). No evident differences were observed in the number or size of the β-catenin clusters between *Hesx1*$^{Cre/+}$*;Ctnnb1*$^{lox(ex3)/+}$*;Cxcr4*$^{fl/fl}$ and *Hesx1*$^{Cre/+}$*;Ctnnb1*$^{lox(ex3)/+}$*;Cxcr4*$^{fl/+}$ genotypes. Interestingly, *Cxcr4*$^{fl/fl}$ pituitaries still contained considerable numbers of CXCR4+ cells present outside the clusters (arrowheads, Figure 4.12), a similar observation to that made during the analysis of *Hesx1*$^{Cre/+}$*;Cxcr4*$^{fl/fl}$ pituitaries at the same stage (See

Figure 4.5b). This indicates that CXCR4+ cells in the β-catenin clusters are derived from the *Hesx1* lineage and that the non-cluster/CXCR4+ population is not derived from *Hesx1* progenitors at this stage.

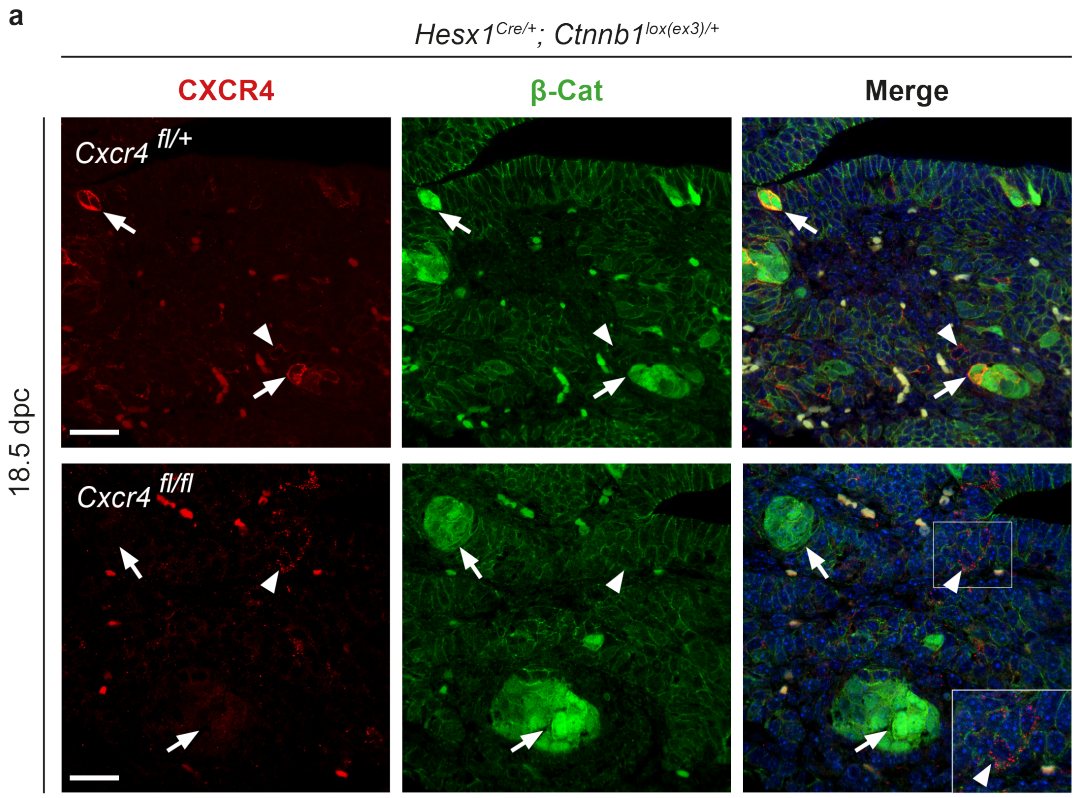

Figure 4.12 The expression of CXCR4 in *Hesx1*$^{Cre/+}$;*Ctnnb1*$^{lox(ex3)/+}$;*Cxcr4*$^{fl/fl}$ pituitaries and controls.

(a) Double immunofluorescence for CXCR4 and β-catenin in mutant pituitaries where CXCR4 has been conditionally ablated in the *Hesx1*$^{Cre/+}$;*Ctnnb1*$^{lox(ex3)/+}$ background. The β-catenin clusters of control *Cxcr4*$^{fl/+}$ pituitaries contain CXCR4+ cells (arrows) but several CXCR4+ cells also present outside of them (arrowhead). The β-catenin clusters of *Cxcr4*$^{fl/fl}$ pituitaries lack CXCR4 expression (arrows), although individual CXCR4+ cells remain outside the clusters (arrowhead). DAPI counterstain. Scale bars: 25 μm.

Removal of CXCR4 does not alter the embryonic pituitary phenotype in the *Hesx1$^{Cre/+}$;Ctnnb1$^{lox(ex3)/+}$* background

It was previously reported that *Hesx1$^{Cre/+;}$Ctnnb1$^{lox(ex3)/+}$* embryonic pituitaries are hyperplastic and characterised by reduced differentiation of Pit1-dependent endocrine lineages, leading to hypopituitarism in adult mice (Gaston-Massuet et al. 2011). In order to assess the impact of removing CXCR4 in the *Hesx1$^{Cre/+;}$Ctnnb1$^{lox(ex3)/+}$* background, the pituitary phenotype of *Hesx1$^{Cre/+}$;Ctnnb1$^{lox(ex3)/+}$;Cxcr4$^{fl/fl}$* embryos was analysed at 18.5 dpc by H&E staining and immunohistochemistry against pituitary hormones.

Triple mutant pituitaries were also hypertrophic and with morphological aberrations that resembled that of *Hesx1$^{Cre/+;}$Ctnnb1$^{lox(ex3)/+}$* controls such as multiple involutions of the intermediate lobe which altered the otherwise stereotypic appearance of the wild type pituitary lumen (Figure 4.13a-d). A common feature observed in *Hesx1$^{Cre/+;}$Ctnnb1$^{lox(ex3)/+}$* embryos is an abnormal closure of the basisphenoid bone, which is filled by remnants of the growing Rathke's Pouch and leads to an open canal in the bone that is also present postnatally. This altered closure of the basisphenoid bone appeared to be more pronounced in *Hesx1$^{Cre/+;}$Ctnnb1$^{lox(ex3)/+}$;Cxcr4$^{fl/fl}$* embryos at the 18.5 dpc stage with ectopic pituitary tissue present in between the bone (arrows, Figure 4.13d).

Immunohistochemical characterisation of pituitary endocrine lineages revealed an impaired terminal differentiation of the somatotroph and thyrotroph lineages in both *Hesx1$^{Cre/+;}$Ctnnb1$^{lox(ex3)/+}$* and *Hesx1$^{Cre/+;}$Ctnnb1$^{lox(ex3)/+}$;Cxcr4$^{fl/fl}$* pituitaries when compared to wild types (Figure 4.13e-j), whereas differentiation of the corticotroph lineage was not affected (Figure 4.13k-m). Therefore, ablation of CXCR4 did not rescue defects in endocrine lineage commitment that occur in the context of oncogenic β-catenin.

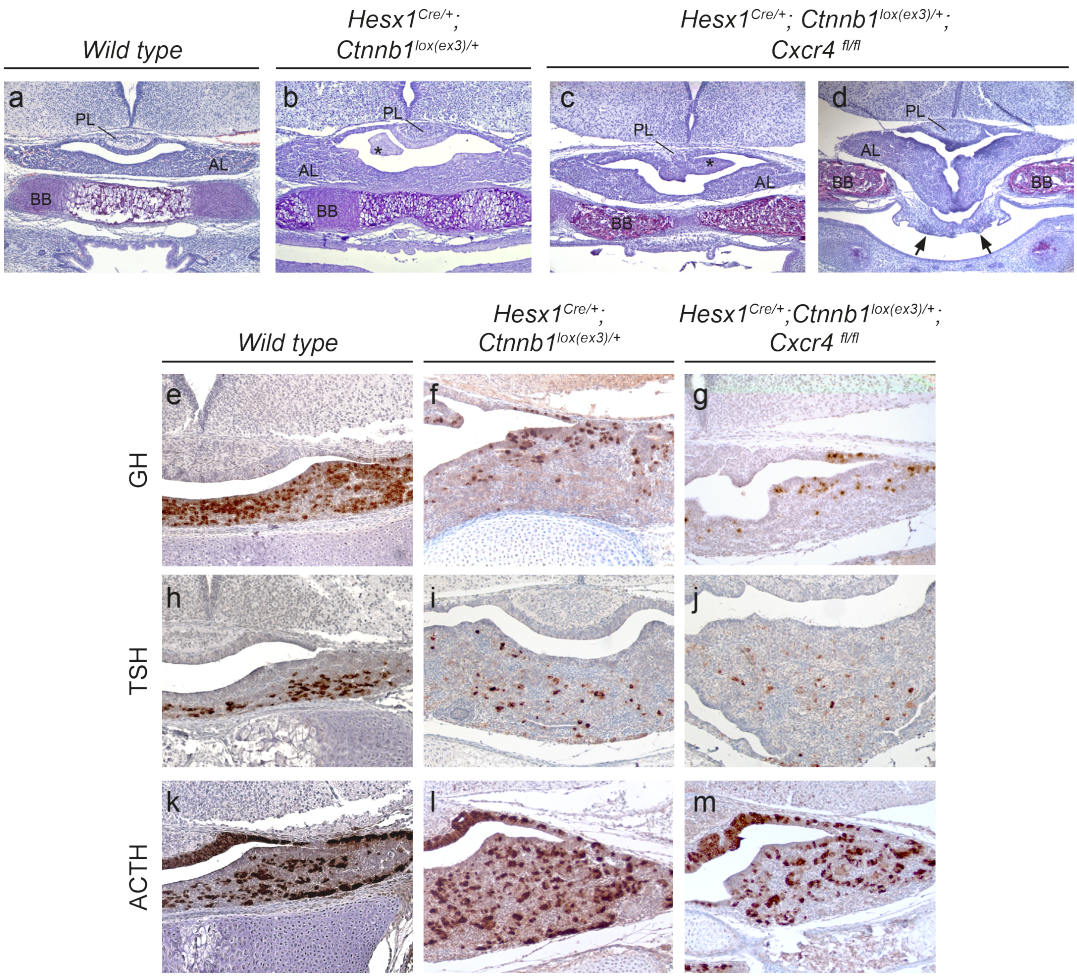

Figure 4.13 Characterisation of *Hesx1$^{Cre/+}$;Ctnnb1$^{lox(ex3)/+}$;CXCR4$^{fl/fl}$* pituitaries.

(a) H&E staining of a wild type pituitary at 18.5 dpc shows the normal appearance of the different pituitary compartments with a stereotypical lumen separating the intermediate and anterior lobes. Note proper fusion of the basisphenoid bone. **(b)** *Hesx1$^{Cre/+}$;Ctnnb1$^{lox(ex3)/+}$* pituitary at the same stage shows an hyperplastic anterior lobe and ectopic intermediate lobe involutions (asterisk). **(c-d)** *Hesx1$^{Cre/+}$;Ctnnb1$^{lox(ex3)/+}$;Cxcr4$^{fl/fl}$* pituitaries are also hyperplastic with intermediate lobe involutions (asterisk). Basisphenoid bone fusion is occasionally prevented by ectopic growth of the pituitary (arrows). **(e-g)** IHC against GH shows that somatotroph differentiation is affected in both *Hesx1$^{Cre/+}$;Ctnnb1$^{lox(ex3)/+}$* and *Cxcr4* triple mutant pituitaries. **(h-j)** The thyrotroph lineage is also affected in both mutants. **(k-m)** Corticotroph differentiation is not affected in either Hesx*1$^{Cre/+}$;Ctnnb1$^{lox(ex3)/+}$* and *Cxcr4* triple mutants. GH: Growth Hormone; ACTH: Adeno-Corticotropic Hormone; TSH: Thyroid Stimulating Hormone; PL: Posterior Lobe; AL: Anterior Lobe; BB: Basisphenoid Bone.

Removal of CXCR4 does not affect the molecular nor secretory phenotype of the embryonic β-catenin clusters

A molecular characterisation was conducted by immunofluorescence in order to determine the effect of CXCR4 ablation in the β-catenin clusters of the *Hesx1*$^{Cre/+;}$*Ctnnb1*$^{lox(ex3)/+}$ background. It was previously shown that the majority of the clusters express the stem cell factor SOX2, but rarely express SOX9 and lack the proliferation marker Ki67 (Gaston-Massuet et al. 2011). Double immunostaining experiments showed no difference in the expression of SOX2 in the clusters of *Hesx1*$^{Cre/+}$*;Ctnnb1*$^{lox(ex3)/+}$*;Cxcr4*$^{fl/fl}$ pituitaries and controls (Figure 4.14a,b). Conversely, SOX9 expression was extremely rare within the clusters of both *Hesx1*$^{Cre/+;}$*Ctnnb1*$^{lox(ex3)/+}$ and *Hesx1*$^{Cre/+;}$*Ctnnb1*$^{lox(ex3)/+}$*;Cxcr4*$^{fl/fl}$ pituitaries, whereas it was strongly expressed in cells directly surrounding the clusters of both genotypes (arrowheads, Figure 4.14c,d). Finally, Ki67 staining did not reveal any differences in the proliferation of the β-catenin clusters (Figure 4.14e,f), suggesting the senescent phenotype is also not altered in the absence of CXCR4.

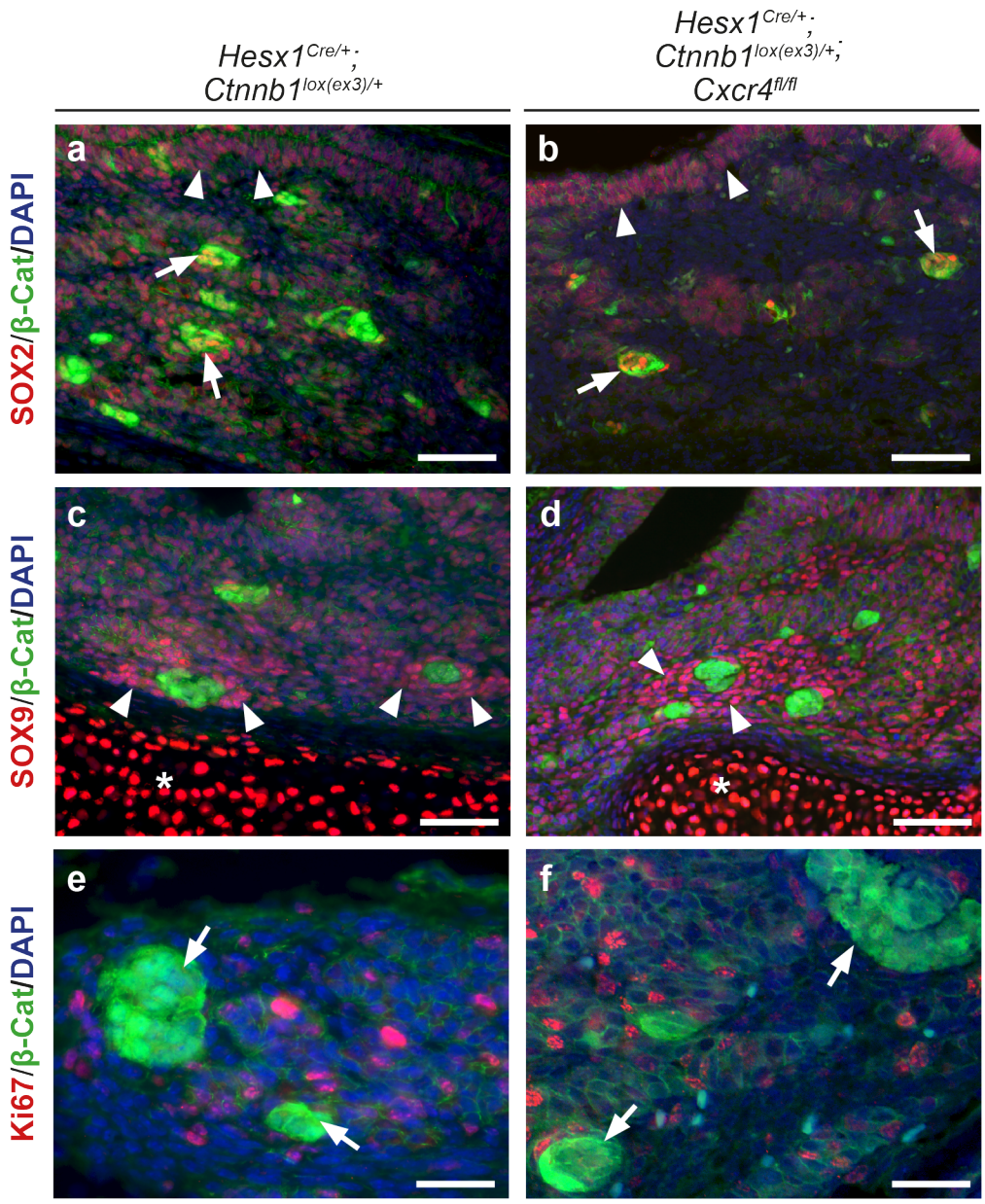

Figure 4.14 Molecular analysis of the β-catenin clusters after CXCR4 ablation.

(a-b) Double immunofluorescence for SOX2 and β-catenin shows positive staining in progenitor areas of the marginal zone (arrowheads) and in β-catenin clusters of *Hesx1*$^{Cre/+}$;*Ctnnb1*$^{lox(ex3)/+}$ and *Hesx1*$^{Cre/+}$;*Ctnnb1*$^{lox(ex3)/}$;*Cxcr4*$^{fl/fl}$ pituitaries at 18.5 dpc (arrows). **(c-d)** SOX9 is rarely expressed within the clusters but SOX9+ cell groups surround the β-catenin clusters in both genotypes (arrowheads). Asterisk indicates osteogenic cells of the basisphenoid bone, which normally express high levels of SOX9. **(e-f)** CXCR4 ablation in the clusters does not have an impact on proliferation of these structures as indicated by the absence of Ki67 positive staining. Scale bars: a,b,c,d: 50 μm; e,f: 25 μm

CXCR4/SDF-1 signalling has been shown to crosstalk and promote the expression of members of the SHH, WNT, BMP and FGF families (Sengupta et al. 2012; Holland et al. 2013; Singh et al. 2012; C. Liu et al. 2013). An ISH analysis of factors known to be overexpressed by *Hesx1*$^{Cre/+}$;*Ctnnb1*$^{lox(ex3)/+}$ clusters (Andoniadou et al. 2012) was conducted but showed no differences between *Hesx1*$^{Cre/+;}$*Ctnnb1*$^{lox(ex3)/+}$ and *Hesx1*$^{Cre/+;}$*Ctnnb1*$^{lox(ex3)/+}$;*Cxcr4*$^{fl/fl}$ pituitaries at 18.5 dpc (Figure 4.15). These results suggest that CXCR4 signalling is not required for inducing nor maintaining the molecular and secretory phenotype of the β-catenin clusters at embryonic stages.

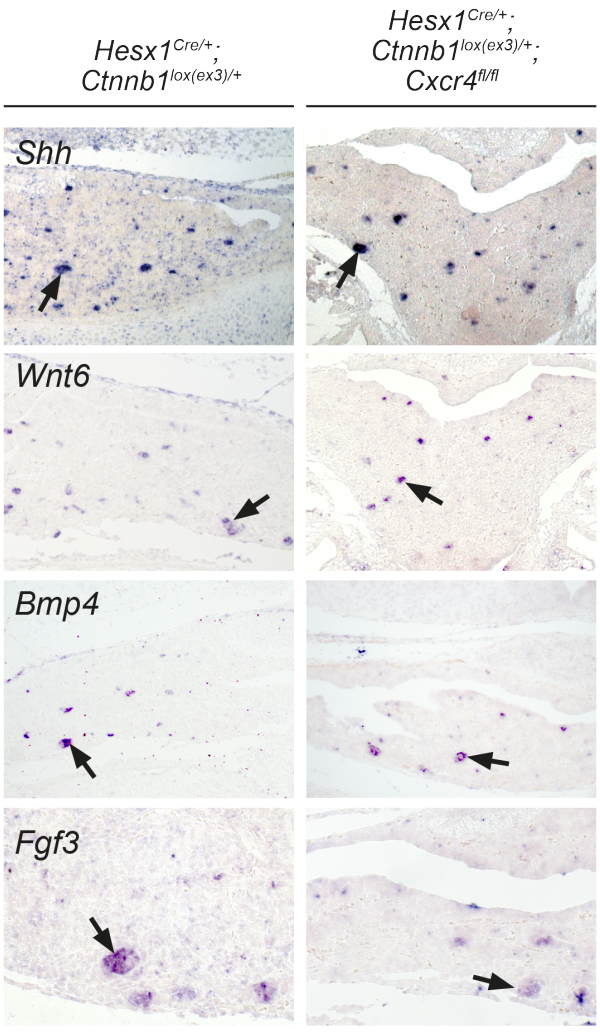

Figure 4.15 Characterisation of the secretory phenotype in β-catenin clusters after CXCR4 ablation.

In situ hybridisation shows the clusters of both *Hesx1*$^{Cre/+;}$*Ctnnb1*$^{lox(ex3)/+}$ and *Hesx1*$^{Cre/+;}$*Ctnnb1*$^{lox(ex3)/+}$*;Cxcr4*$^{fl/fl}$ pituitaries at 18.5 dpc overexpress *Shh*, *Wnt6*, *Bmp4*, and *Fgf3* (arrows).

Removal of CXCR4 in pituitary cells does not have a beneficial effect on tumour progression

In the previous chapter it was shown that after birth, *Hesx1*$^{Cre/+;}$*Ctnnb1*$^{lox(ex3)/+}$ pituitaries undergo a period of latency during which the β-catenin clusters persist in pre-neoplastic regions until tumours eventually develop (see Figure 3.1), suggesting a role for the β-catenin clusters in postnatal stages of tumour progression. In order to assess the importance of CXCR4 signalling in postnatal tumour development, an analysis of tumourigenic pituitaries and end-stage tumours was conducted in *Hesx1*$^{Cre/+;}$*Ctnnb1*$^{lox(ex3)/+}$*;Cxcr4*$^{fl/fl}$ mice and *Hesx1*$^{Cre/+;}$*Ctnnb1*$^{lox(ex3)/+}$*;Cxcr4*$^{fl/+}$ controls.

Mendelian ratios at weaning showed no significant difference between possible genotypes obtained from crossing *Ctnnb1*$^{lox(ex3)/lox(ex3)}$*;Cxcr4*$^{fl/+}$ and *Hesx1*$^{Cre/+}$*;Cxcr4*$^{fl/fl}$ mice (Figure 4.16a), indicating that removal of CXCR4 in the *Hesx1*$^{Cre/+;}$*Ctnnb1*$^{lox(ex3)/+}$ background does not result in perinatal lethality. At 30 days of age there was no obvious difference between *Hesx1*$^{Cre/+;}$*Ctnnb1*$^{lox(ex3)/+}$*;Cxcr4*$^{fl/fl}$ and *Hesx1*$^{Cre/+;}$*Ctnnb1*$^{lox(ex3)/+}$*;Cxcr4*$^{fl/+}$ pituitaries, as in both genotypes these were characterised by dysmorphic anterior lobes (Figure 4.16b) due to the presence of ventrally located pre-neoplastic regions containing β-catenin clusters (Figure 4.16c). End-stage tumours did not show any obvious histological differences between triple mutants and their controls (Figure 4.16d). Finally, a survival analysis between *Hesx1*$^{Cre/+;}$*Ctnnb1*$^{lox(ex3)/+}$*;Cxcr4*$^{fl/fl}$ and *Hesx1*$^{Cre/+;}$*Ctnnb1*$^{lox(ex3)/+}$*;Cxcr4*$^{fl/+}$ mice indicated that CXCR4 knockout did not have a beneficial effect on tumour development and growth (Figure 4.16e). In fact, by the end of this experiment 20% of *Cxcr4* heterozygous mice died from tumour burden compared to 60% of *Cxcr4*

homozygotes. Although the resulting survival curve suggested that CXCR4 removal could have a negative effect on survival rate, this difference was not statistically significant (p=0.191, Log-Rank Mantel-Cox Test, n=5 for *Hesx1*$^{Cre/+;}$*Ctnnb1*$^{lox(ex3)/+}$*;Cxcr4*$^{fl/+}$ and n=13 for *Hesx1*$^{Cre/+;}$*Ctnnb1*$^{lox(ex3)/+}$*;Cxcr4*$^{fl/fl}$). Overall, these results indicate that the absence of CXCR4 in cells from the *Hesx1* lineage does not impair early development and progression of the murine tumours derived from oncogenic β-catenin activation.

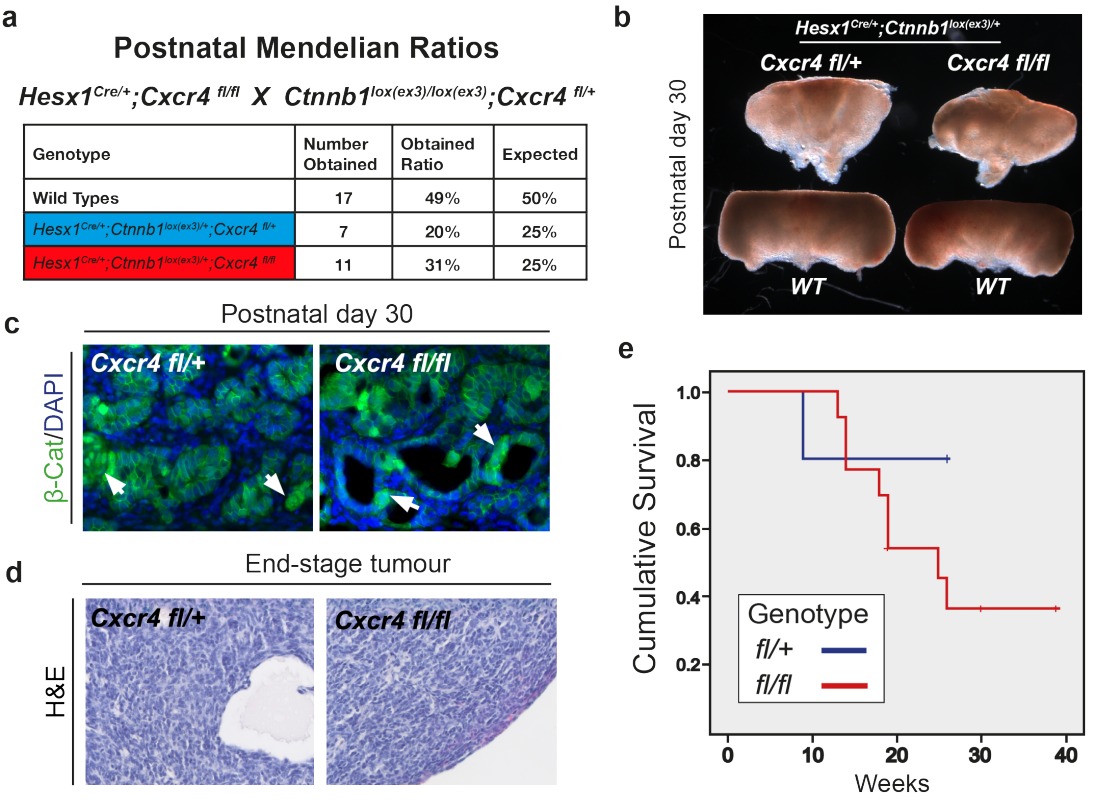

Figure 4.16 Postnatal characterisation of *Hesx1*$^{Cre/+;}$*Ctnnb1*$^{lox(ex3)/+;}$*Cxcr4*$^{fl/fl}$ mice and tumours.

(a) Normal mendelian ratios are observed after weaning litters derived from *Ctnnb1*$^{lox(ex3)/lox(ex3)}$*;Cxcr4*$^{fl/fl}$ and *Hesx1*$^{Cre/+}$*;Cxcr4*$^{fl/fl}$ crosses (Chi Square test, p=0.62). **(b)** A dysmorphic anterior lobe phenotype is observed in freshly dissected pituitaries from both *Hesx1*$^{Cre/+;}$*Ctnnb1*$^{lox(ex3)/+}$*;Cxcr4*$^{fl/fl}$ and controls. **(c)** Immunostaining for β-catenin at the same stage shows the presence of β-catenin clusters in the anterior lobe pre-neoplastic regions of both genotypes. **(d)** H&E staining in end-stage tumours

shows a common histological landscape between *Hesx1*$^{Cre/+;}$*Ctnnb1*$^{lox(ex3)/+}$*;Cxcr4*$^{fl/fl}$ and controls. **(e)** A postnatal survival analysis indicates that absence of CXCR4 does not alter tumour progression beneficially (p=0.191, Log-Rank Mantel-Cox Test, N=18).

4.3.6 CXCR4+ cells invade the murine ACP pituitary

CXCR4-expressing cells are present in *Hesx1*$^{Cre/+}$*;Ctnnb1*$^{lox(ex3)/+}$*;Cxcr4*$^{fl/fl}$ pituitaries and tumours

In section 4.2 it was shown that CXCR4+ cells are present in the stroma of the embryonic pituitary gland, even when CXCR4 expression is removed from the *Hesx1* lineage, and that they are closely associated to the developing pituitary vasculature. It was also shown that CXCR4+ cells invade the pre-neoplastic regions postnatally and later form extensive vascular networks in end-stage tumours from *Hesx1*$^{Cre/+}$*; Ctnnb1*$^{lox(ex3)/+}$ mice. Because removal of CXCR4 in the *Hesx1* lineage did not affect the β-catenin clusters' phenotype nor impair the development of pituitary tumours, a possible role of CXCR4 signalling in mediating angiogenesis during tumour development was investigated.

Immunostaining for CXCR4 at 16.5 dpc revealed that both *Hesx1*$^{Cre/+}$*; Ctnnb1*$^{lox(ex3)/+}$*;Cxcr4*$^{fl/+}$ and *Hesx1*$^{Cre/+}$*;Ctnnb1*$^{lox(ex3)/+}$*;Cxcr4*$^{fl/fl}$ pituitaries contain CXCR4+ endothelial-like cells (Figure 4.17a,b), recapitulating observations made in *Hesx1*$^{Cre/+}$*;Cxcr4*$^{fl/fl}$ pituitaries. Additionally, strong positive staining was found in tip cells displaying filopodial processes (arrows, Figure 4.17a), suggesting a role for CXCR4-mediated chemotaxis in these cells. Furthermore, all end-stage tumours from both genotypes contained profuse CXCR4+ vascular structures (14 weeks, Figure 4.17c,d). In both tumour types CXCR4+ cells were also found in larger, tightly packed groups (insets). Therefore, CXCR4 signalling potentially drives angiogenesis throughout the tumourigenic process in *Hesx1*$^{Cre/+}$*;Ctnnb1*$^{lox(ex3)/+}$ mice.

CXCR4+ cells exist within invading EMCN+ swarms

In section 3.7 it was shown that mutant pituitaries are invaded by large numbers of EMCN+ cells, suggesting an active migration process in this population. Double immunostaining for CXCR4 and EMCN was conducted in 16.5 dpc pituitaries and showed the presence of CXCR4+ cells within the EMCN+ population (Figure 4.17e), suggesting active migration occurs in a proportion of EMCN+/CXCR4+ cells at this stage.

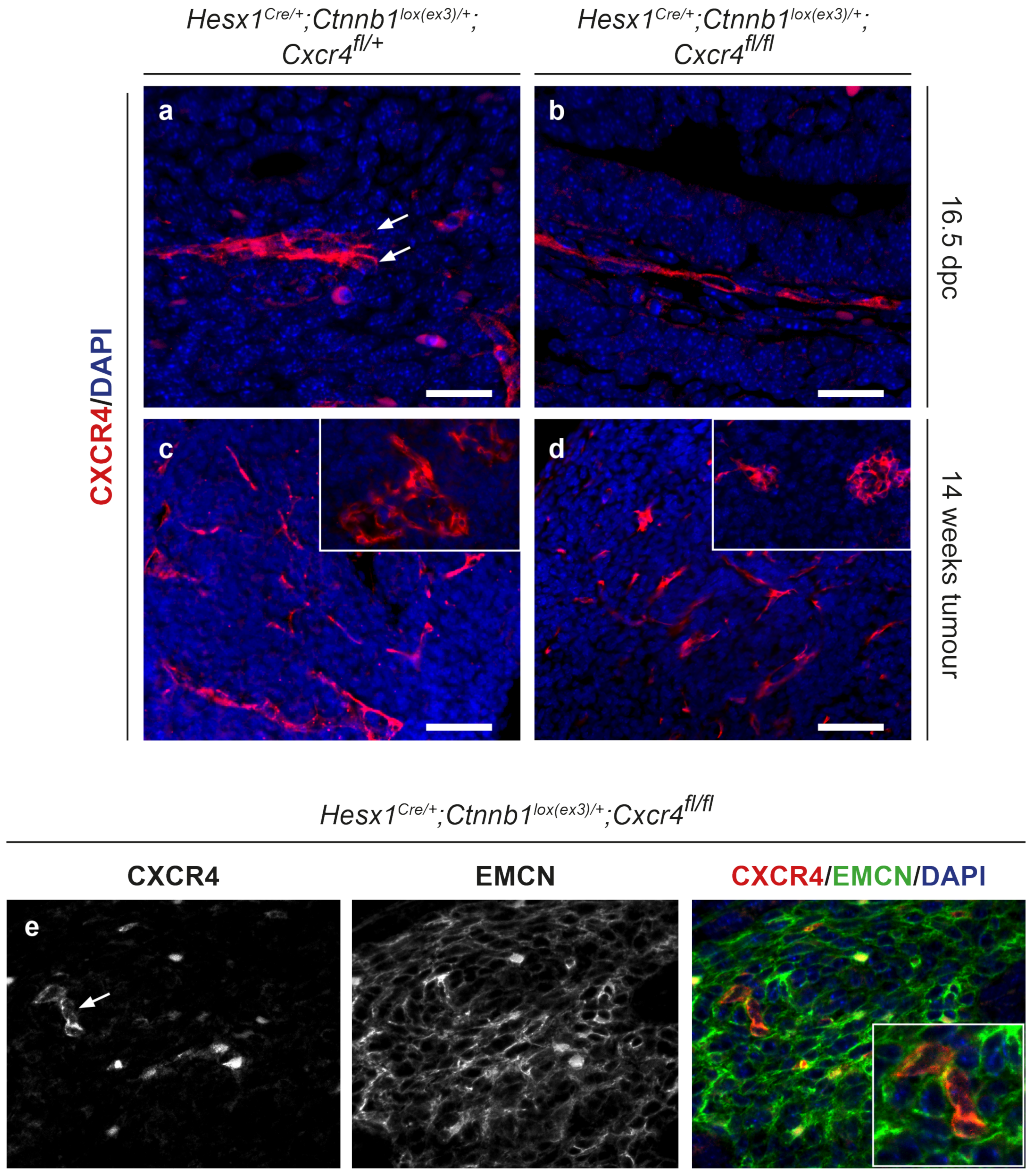

Figure 4.17 CXCR4 expression in endothelial-like cells of *Hesx1$^{Cre/+}$;Ctnnb1$^{lox(ex3)/+}$;Cxcr4$^{fl/fl}$* pituitaries and tumours.

(a-b) Immunofluorescence for CXCR4 shows positive staining in cells with endothelial morphology that are present even after CXCR4 ablation in pituitary progenitors and their lineage. Note the presence of filopodia in leading tip cells (arrows). **(c-d)** CXCR4+ cells are also present in blood vessels of end-stage tumours and in larger groups forming anastomoses (insets). **(e)** Double immunostaining for CXCR4 and the endothelial marker endomucin (EMCN) reveals CXCR4+/EMCN+ cells are present within a much larger population of EMCN+ cells. Scale bars: a,b: 20 μm.

The number of CXCR4+ cells increases with tumour progression

As described in the previous chapter, postnatal *Hesx1*$^{Cre/+}$*;Ctnnb1*$^{lox(ex3)/+}$ pituitaries contained pre-neoplastic regions largely formed by cells not derived from the *Hesx1* lineage nor targeted with oncogenic β-catenin but that eventually progressed to full-grown tumours. Because these regions contained low numbers of proliferating cells (see Figure 3.1), CXCR4-mediated cell migration could explain in part the initial growth of these lesions. The presence of CXCR4+ cells was analysed in detail during tumour progression by CXCR4 immunostaining in combination with lineage-tracing in *Hesx1*$^{Cre/+}$*;Ctnnb1*$^{lox(ex3)/+}$*;R26*$^{YFP/+}$ pituitaries at different postnatal stages of tumour progression.

In early postnatal pituitaries (around 4 weeks), increased expression of CXCR4 was observed in epithelial cells of the anterior lobe and colocalised with YFP expression (arrows, Figure 4.18a,b). This high expression of CXCR4 was absent in adult wild type pituitaries, where clear membranous CXCR4 protein expression was only observed in the intermediate lobe (see Figure 4.1d), suggesting that increased CXCR4 expression in *Hesx1*-derived cells is an outcome of oncogenic β-catenin expression and increased WNT signalling. Interestingly, the stroma of the pre-neoplastic regions also contained mesenchymal CXCR4+/YFP- cells (arrowheads, Figure 4.18b), which could also be observed in later stage pituitaries (arrows, Figure 4.18c,d). The expression pattern of CXCR4 in end-stage tumours was region-

dependent, where it could be observed in large patches of mesenchymal YFP- cells (Figure 4.18e,f).

Besides the epithelial/YFP+/CXCR4+ and mesenchymal/YFP-/CXCR4+ cells already described, other types of CXCR4+ cells were identified during this analysis. A number intermediate stage specimens (2/5, around 10 weeks of age,) contained large numbers of mesenchymal CXCR4+ cells possessing filopodial processes, which were only found in restricted regions of pre-neoplastic tissue (Figure 4.18g). Finally, all end-stage tumours contained large numbers of CXCR4+ blood vessels (Figure 4.18i), where CXCR4 expression appeared stronger in vascular branches and tip cells (arrows, Figure 4.18j).

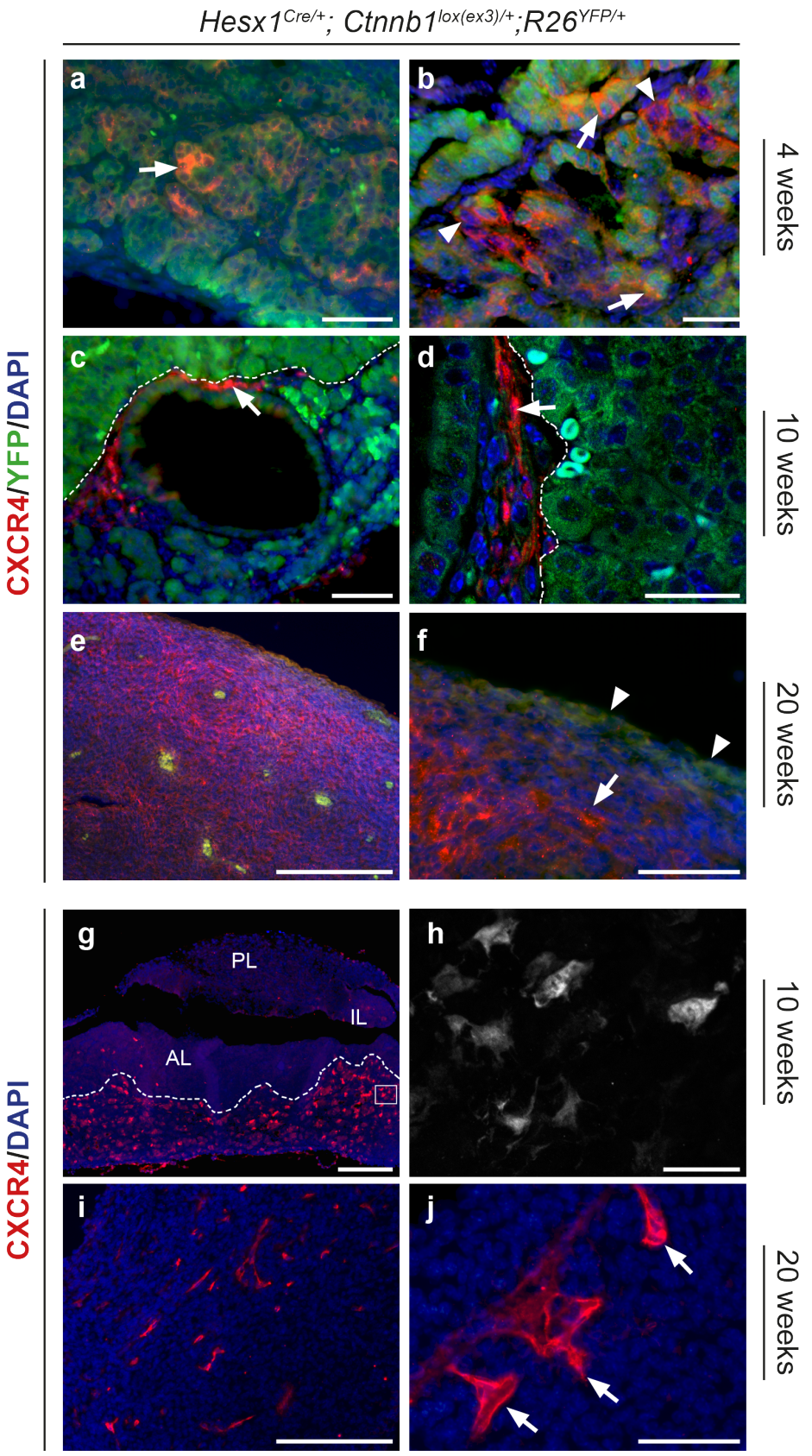

Figure 4.18 Characterisation of CXCR4 expression during mouse ACP progression.

(a) Double immunofluorescence for YFP and CXCR4 in *Hesx1*$^{Cre/+}$; *Ctnnb1*$^{lox(ex3)/+}$;*R26*$^{YFP/+}$ pituitaries in a 4-week old specimen shows that pre-neoplastic areas are formed of YFP+ epithelium and a YFP- stroma. Most CXCR4+ cells are found in the YFP+ fraction (arrow). **(b)** Closer inspection of one of such regions shows that some CXCR4+/YFP- cells are present in the stroma (arrowheads) which intermingles with the epithelium containing CXCR4+/YFP+ cells (arrows). **(c-d)** Later stage specimens (10 weeks of age example) show an expanded pre-neoplastic region (delimited by dotted line) containing CXCR4+ cells with a clear mesenchymal phenotype. These cells were often observed forming elongated vessel-like structures (arrows). **(e-f)** End-stage tumours contain regions with high numbers of CXCR4+/YFP- cells. Note how the YFP+ pituitary tissue has been displaced to the tumour periphery (arrowhead). **(g-h)** CXCR4+ cells with a distinctive mesenchymal morphology were found in large numbers in the pre-neoplastic regions in 3 out of 5 specimens around 10 weeks of age. **(i-j)** All end-stage tumours (20 weeks of age specimen shown) contained profuse CXCR4+ vasculature. Note a stronger staining intensity in cells branching off from a main vessel (arrows). Scale bars: b,d,h: 25 μm; a,c,j: 50 μm; f,j: 100 μm; e,g,i: 200 μm. PL: Posterior Lobe; IL: Intermediate Lobe; AL; Anterior Lobe.

4.4 Chapter 4 conclusions

In summary, this chapter provides evidence suggesting that CXCR4/SDF-1 signalling is not essential in cells derived from pituitary embryonic progenitors during development and adulthood, but might play a role in the proper formation of supportive tissues of the pituitary gland during development, such as the vascular system. Additionally, it is shown that CXCR4 is not necessary for the survival of the *Hesx1*$^{Cre/+}$;*Ctnnb1*$^{lox(ex3)/+}$ β-catenin clusters and that its ablation does not disrupt the cluster's paracrine signalling and non-cell autonomous tumourigenesis. However, the data here presented suggests that CXCR4/SDF-1 signalling could be involved in pro tumourigenic cell recruitment to the microenvironment in mouse and human ACP, as CXCR4+ cells are observed closely interacting with the clusters.

5. CHALLENGING SENESCENCE IN EMBRYONIC AND INDUCIBLE MODELS OF PITUITARY TUMOURIGENESIS

5.1 Introduction

In the previous chapter, it was shown that restricting the clusters from a well-known pro-oncogenic growth factor (CXCR4) did not lead to their ablation nor impede tumour growth. Importantly, the clusters remained in a non-proliferative state and still induced changes in their microenvironment early in development. Therefore, it was hypothesized that preventing the clusters from becoming senescent and consequently activating the SASP could abrogate tumour formation or growth.

There is a growing body of evidence demonstrating a crucial role for the tumour suppressor p53 (encoded by the *Trp53* gene in mice) in the induction and maintenance of cellular senescence (Campisi 2013; Sharpless & Sherr 2015). Indeed, p53 activation is a convergence point for many senescence-activating stimuli such as DNA-damage and oncogenic signalling (Muñoz-Espín & Serrano 2014). Therefore, conditional knockout of p53 in pituitary embryonic precursors was conducted by crossing $Hesx1^{Cre/+};Trp53^{fl/fl}$ and $Ctnnb1^{lox(ex3)/\,lox(ex3)};Trp53^{fl/+};R26^{YFP/YFP}$ genotypes, in order to obtain $Hesx1^{Cre/+};Ctnnb1^{lox(ex3)/+};Trp53^{fl/fl};R26^{YFP/+}$ mice (hereafter also referred as $Trp53^{fl/fl}$ mutants).

5.2 Analysis of the $Hesx1^{Cre/+};Ctnnb1^{lox(ex3)/+};Trp53^{fl/fl}$ embryonic phenotype

5.2.1 Demonstration of p53 knockout in β-catenin clusters from $Hesx1^{Cre/+};Ctnnb1^{lox(ex3)/+};Trp53^{fl/fl}$ mutants

To assess efficient knockout of p53 protein in the β-catenin clusters from the $Hesx1^{Cre/+};\ Ctnnb1^{lox(ex3)/+}$ background, double immunostaining for p53 and β-catenin was conducted in 18.5 dpc pituitaries. While p53 protein accumulation was observed in clusters from $Hesx1^{Cre/+};\ Ctnnb1^{lox(ex3)/+}$ and $Hesx1^{Cre/+};\ Ctnnb1^{lox(ex3)/+};Trp53^{fl/+}$

control pituitaries (Figure 5.1a,b), the β-catenin clusters from *Trp53*$^{fl/fl}$ mutant pituitaries did not show positive staining (Figure 5.1c,d). However, residual p53 signal could be observed in these pituitaries, mainly in the intermediate lobe, an area known to be populated by cells that are not derived from the *Hesx1* cell lineage and therefore, where *Hesx1*-mediated recombination is less efficient (Jayakody et al. 2012) (asterisk, Figure 5.1d). Therefore, p53 knockout was efficiently achieved in the nucleo-cytoplasmic β-catenin accumulating clusters of the *Hesx1*$^{Cre/+}$*; Ctnnb1*$^{lox(ex3)/+}$ model.

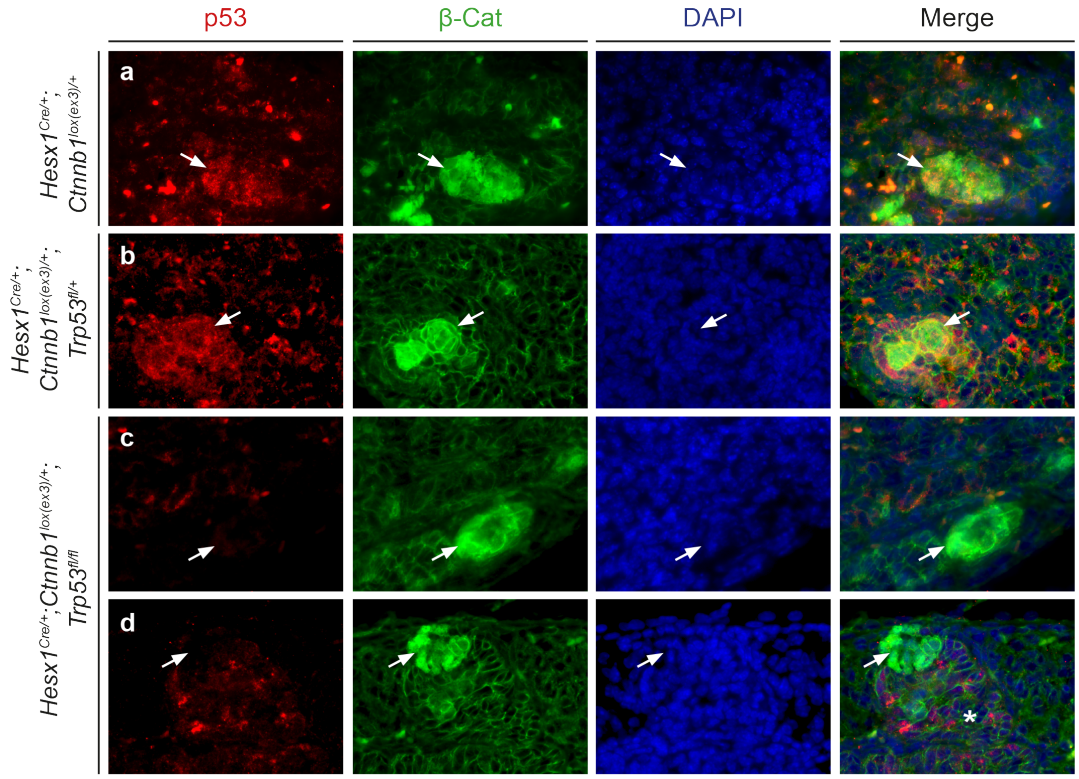

Figure 5.1 Double immunostaining for p53 and β-catenin in control and *Hesx1*$^{Cre/+}$*;Ctnnb1*$^{lox(ex3)/+}$*;Trp53*$^{fl/fl}$ pituitaries at 18.5 dpc.

(a) *Hesx1*$^{Cre/+}$*; Ctnnb1*$^{lox(ex3)/+}$ pituitaries contain β-catenin clusters that accumulate p53 protein (arrow). **(b)** The clusters from *Hesx1*$^{Cre/+}$*; Ctnnb1*$^{lox(ex3)/+}$;*Trp53*$^{fl/+}$ also contain p53- β-catenin accumulating clusters (arrow). **(c)** The β-catenin clusters from *Hesx1*$^{Cre/+}$*; Ctnnb1*$^{lox(ex3)/+}$;*Trp53*$^{fl/fl}$ pituitaries are negative for p53 (arrow). **(d)** Example from a different *Trp53*$^{fl/fl}$ mutant embryo where a cluster negative for p53

(arrow) is observed next to positively-stained cells of the pituitary intermediate lobe (asterisk).

5.2.2 Analysis of the senescent phenotype in *Hesx1$^{Cre/+}$;Ctnnb1$^{lox(ex3)/+}$;Trp53$^{fl/fl}$* embryonic clusters

In the third chapter, it was shown that the murine β-catenin clusters display a full senescent phenotype at 18.5 dpc. Therefore, a similar analysis was conducted at this stage for markers of proliferation, apoptosis, cell-cycle inhibition and DNA-damage. Finally, the impact of p53 knockout on the expression of SASP factors by the β-catenin clusters and their effect on the pituitary microenvironment were also evaluated.

Knockout of p53 in the β-catenin clusters does not prevent proliferative arrest nor induce apoptosis

Double immunostaining for Ki67 and β-catenin showed that the clusters present in control *Hesx1$^{Cre/+}$; Ctnnb1$^{lox(ex3)/+}$* and *Hesx1$^{Cre/+}$; Ctnnb1$^{lox(ex3)/+}$;Trp53$^{fl/+}$* pituitaries do not proliferate at this stage (Figure 5.2a,b). Unexpectedly, all clusters in *Hesx1$^{Cre/+}$; Ctnnb1$^{lox(ex3)/+}$;Trp53$^{fl/fl}$* pituitaries also lacked Ki67 expression (Figure 5.2c,d). This suggested that p53 is not necessary to prevent or maintain the proliferative arrest in these structures up to 18.5 dpc. Additionally, immunostaining for cleaved Caspase 3 showed that absence of p53 did not promote apoptosis in *Trp53$^{fl/fl}$* mutant β-catenin clusters (Figure 5.3).

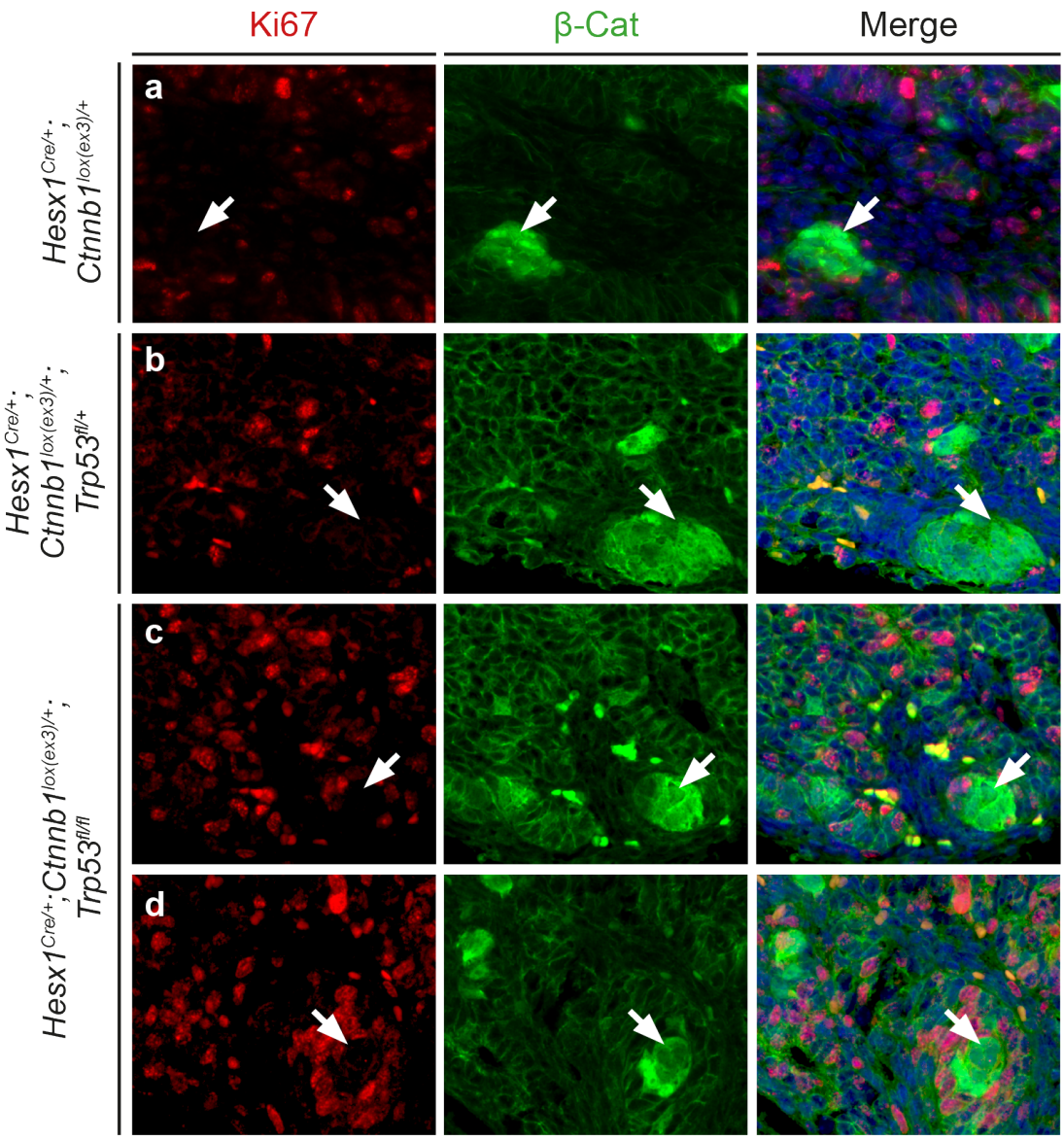

Figure 5.2 Double immunostaining for the proliferation marker Ki67 and β-catenin in *Hesx1$^{Cre/+}$;Ctnnb1$^{lox(ex3)/+}$;Trp53$^{fl/fl}$* pituitaries and controls at 18.5 dpc.

(a) *Hesx1$^{Cre/+}$; Ctnnb1$^{lox(ex3)/+}$* β-catenin clusters do not express Ki67, whereas cells surrounding them are positively stained. **(b)** The clusters from control *Hesx1$^{Cre/+}$; Ctnnb1$^{lox(ex3)/+}$;Trp53$^{fl/+}$* embryos are also negative for Ki67. **(c-d)** *Hesx1$^{Cre/+}$; Ctnnb1$^{lox(ex3)/+}$;Trp53$^{fl/fl}$* β-catenin clusters are also Ki67-negative.

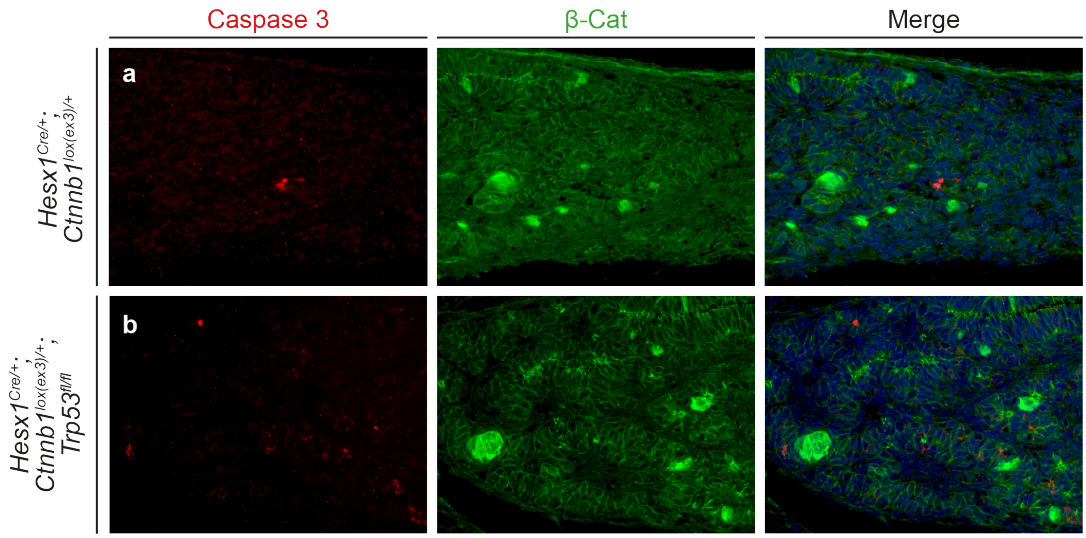

Figure 5.3 Double immunostaining for cleaved Caspase 3 and β-catenin in *Hesx1$^{Cre/+}$;Ctnnb1$^{lox(ex3)/+}$;Trp53$^{fl/fl}$* pituitaries and controls at 18.5 dpc.

(a) Positive staining for Caspase 3 is only observed sporadically in isolated cells of the anterior lobe, but not in clusters. **(b)** *Hesx1$^{Cre/+}$;Ctnnb1$^{lox(ex3)/+}$;Trp53$^{fl/fl}$* pituitaries show a similar pattern of cleaved Caspase 3 expression.

Knockout of p53 does not alter the activation of cell cycle-inhibiting pathways or the DNA-damage response

Activation of p53 during the senescent response is known to lead to the activation of its transcriptional target p21 (*Cdkn1a*), which is a strong inducer of cell cycle arrest (Gire & Dulic 2015). Additionally, the senescent cell cycle arrest has also shown to be strongly dependent on the p16/Rb pathway, either independently or by reinforcing the activity of the p53/p21 pathway (Beauséjour et al. 2003).

The effect of p53 inactivation in the β-catenin clusters was analysed at 18.5 dpc by double immunostaining, which showed no difference in the expression of p21 (Figure 5.4a,b) and p16 proteins (Figure 5.4c,d) between *Trp53$^{fl/fl}$* mutants and *Hesx1$^{Cre/+}$; Ctnnb1$^{lox(ex3)/+}$* controls, consistent with the absence of proliferation markers previously shown.

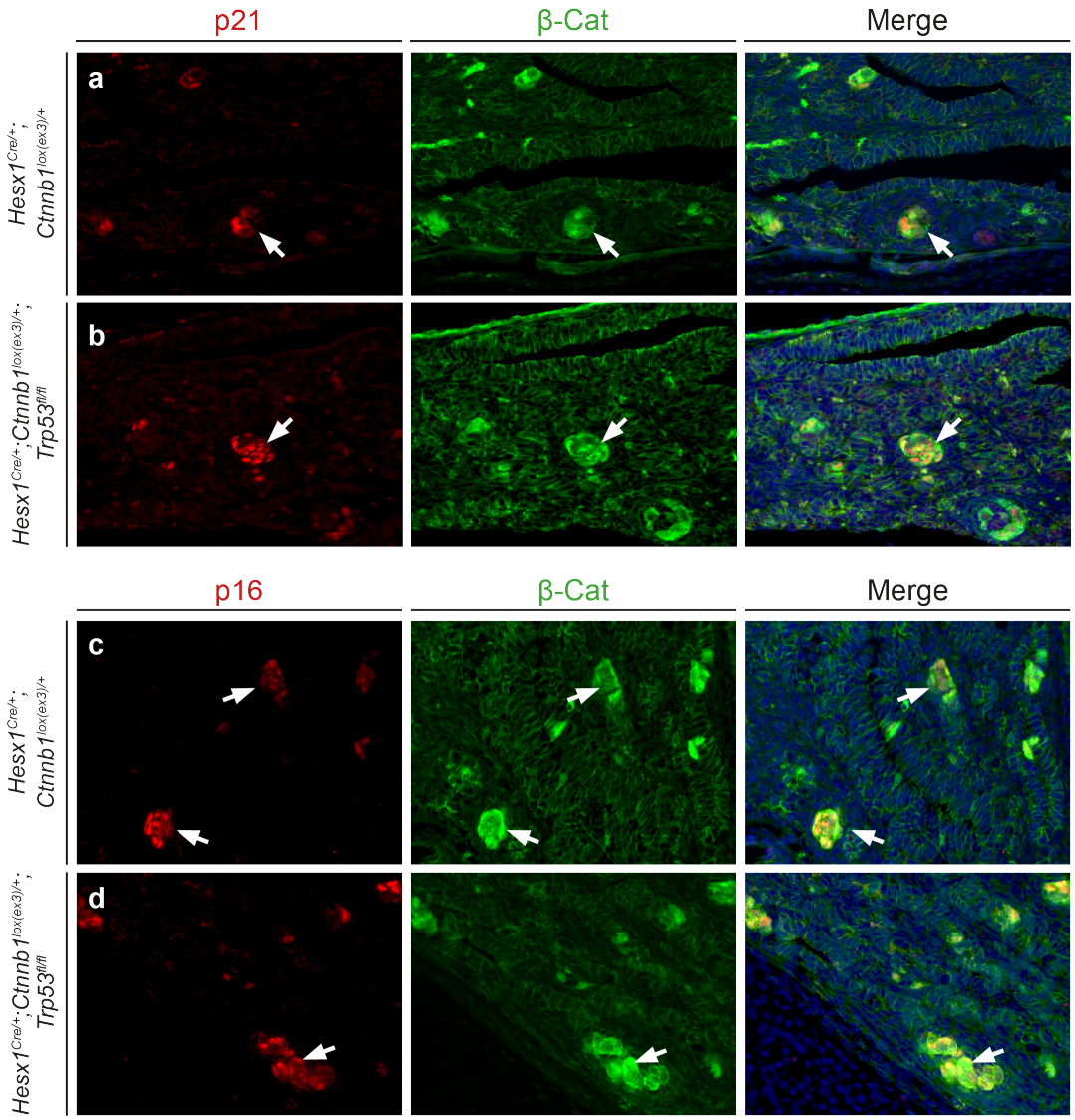

Figure 5.4 The expression of markers of cell cycle inhibition in β-catenin clusters of *Hesx1$^{Cre/+}$;Ctnnb1$^{lox(ex3)/+}$;Trp53$^{fl/fl}$* 18.5 dpc pituitaries and controls

(a) p21 protein is highly expressed in *Hesx1$^{Cre/+}$Ctnnb1$^{lox(ex3)/+}$* clusters (arrows). **(b)** Knockout of p53 does not prevent the accumulation of p21 in clusters from *Hesx1$^{Cre/+}$Ctnnb1$^{lox(ex3)/+}$;Trp53$^{fl/fl}$* embryos. **(c)** p16 protein also accumulates in *Hesx1$^{Cre/+}$Ctnnb1$^{lox(ex3)/+}$* clusters. **(d)** The expression of p16 is not altered upon p53 knockout in the β-catenin clusters of *Trp53$^{fl/fl}$* mutants.

The effect of p53 knockout on the activation of the DNA-damage response (DDR) was also evaluated, as p53 is known to mediate this process in senescent cells (Williams, 2016). However, immunostaining against phospho-DNA-PKcs (Figure 5.5a,b) and PARP-1 (Figure 5.5d,c) revealed that these markers were highly expressed in all the clusters found within control and *Trp53*$^{fl/fl}$ mutant pituitaries. Together, these results indicate that absence of p53 expression does not result in senescence bypass in the β-catenin clusters during embryonic stages.

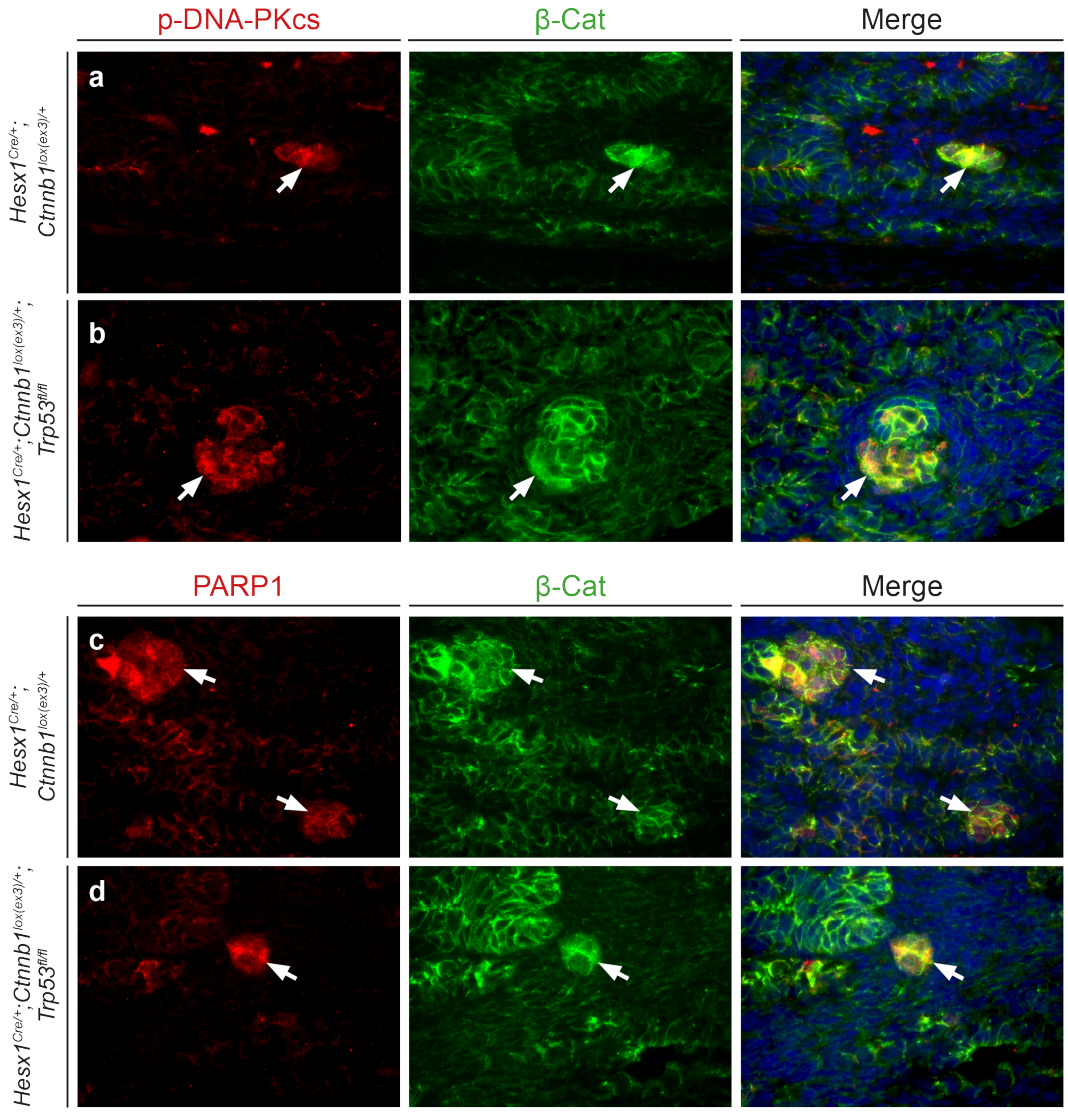

Figure 5.5 Characterisation of DDR marker expression in clusters from 18.5 dpc *Hesx1*$^{Cre/+}$*Ctnnb1*$^{lox(ex3)/+}$ and *Hesx1*$^{Cre/+}$*;Ctnnb1*$^{lox(ex3)/+}$*;Trp53*$^{fl/fl}$ pituitaries.

(a) Double immunostaining against phosphorylated DNA-PKcs and β-catenin shows colocalisation in a β-catenin accumulating cluster from a *Hesx1*$^{Cre/+}$*Ctnnb1*$^{lox(ex3)/+}$ pituitary. **(b)** This expression pattern is not altered in *Trp53*$^{fl/fl}$ mutant clusters. **(c)** PARP-1 accumulation is observed in control β-catenin clusters. **(d)** The clusters from p53 *Trp53*$^{fl/fl}$ mutants also accumulate PARP-1 protein.

5.2.3 The SASP is maintained in embryonic β-catenin clusters after p53 knockout

The induction of cellular senescence by p53-independent pathways has been previously reported, including cases where p21-mediated cell cycle arrest also occurred in the absence of p53 (Prieur et al. 2011; Chan et al. 2011; Cipriano et al. 2011; Aliouat-Denis et al. 2005; Phalke et al. 2012) and under the expression of oncogenic β-catenin (Xu et al. 2008). However, it has been reported that inactivation of p53 in senescent cells leads to exacerbation of the SASP and its promalignant activities (Coppé et al. 2008). In order to explore this possibility, an analysis of the expression of secretory factors expressed by the clusters was conducted in *Hesx1*$^{Cre/+}$*;Ctnnb1*$^{lox(ex3)/+}$*;Trp53*$^{fl/fl}$ pituitaries at 18.5 dpc.

Knockout of p53 does not alter the expression of SASP factors

In situ hybridization (ISH) analysis showed that the β–catenin clusters (observed by *Axin2* overexpression, Figure 5.6 a,b) from both *Hesx1*$^{Cre/+}$*Ctnnb1*$^{lox(ex3)/+}$ and *Hesx1*$^{Cre/+}$*Ctnnb1*$^{lox(ex3)/+}$*;Trp53*$^{fl/fl}$ pituitaries overexpressed the secretory factors *Shh, Bmp4, Ffg3* and *Wnt6* (arrows, Figure 5.6c,e,g,i). Moreover, qRT-PCR analysis in control and *Trp53*$^{fl/fl}$ mutant pituitaries showed no statistically significant differences in the expression of hallmark senescence and SASP factors (Figure 5.7), further indicating that p53 knockout did not alter the secretory phenotype of the β-catenin clusters.

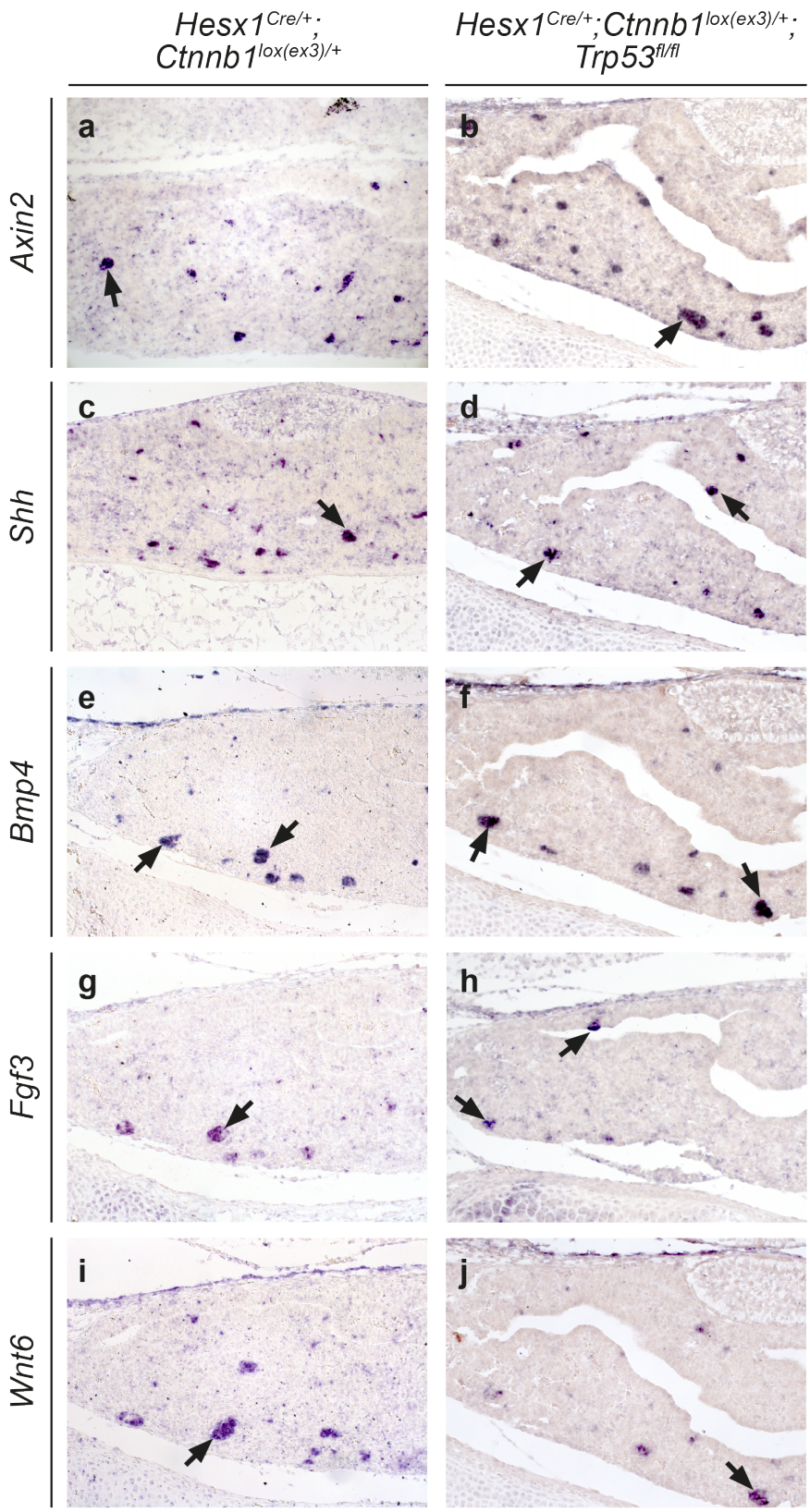

Figure 5.6 *In situ* hybridisation (ISH) analysis of the secretory phenotype in β-catenin clusters after p53 ablation.

(a-b) *Axin2* overexpression is used as control for the presence of clusters in both *Hesx1*$^{Cre/+}$*;Ctnnb1*$^{lox(ex3)/+}$ and *Hesx1*$^{Cre/+}$*;Ctnnb1*$^{lox(ex3)/+}$*;Trp53*$^{fl/fl}$ pituitaries. ISH in consecutive sections shows increased mRNA expression of the secretory factors: *Shh* **(c-d)**, *Bmp4* **(e-f)**, *Fgf3* **(g-h)** and Wnt6 **(i-j)** in cluster formations of both controls and *Trp53*$^{fl/fl}$ mutants**.**

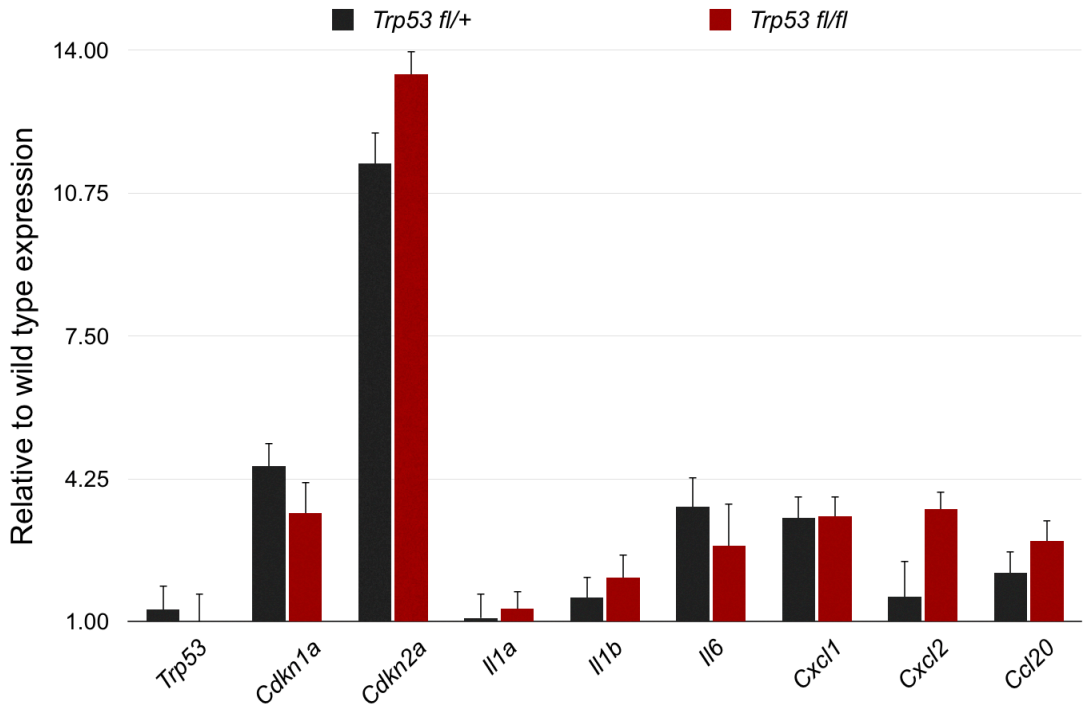

Figure 5.7 Quantitative expression analysis of hallmark senescence and SASP factors in *Hesx1*$^{Cre/+}$*;Ctnnb1*$^{lox(ex3)/+}$*;Trp53*$^{fl/fl}$ pituitaries at 18.5 dpc.

qRT-PCR for markers of senescence: *Trp53, Cdkn1a* (p21) and *Cdkn2a* (p16), as well as the SASP: *Il1a, Il1b, Il6, Cxcl1, Cxcl2* and *Ccl20*. Bars represent mean expression± SEM relative to wild type littermates of target genes in individual *Hesx1*$^{Cre/+}$*;Ctnnb1*$^{lox(ex3)/+}$*;Trp53*$^{fl/+}$ (blue) and *Hesx1*$^{Cre/+}$*;Ctnnb1*$^{lox(ex3)/+}$*;Trp53*$^{fl/fl}$ (red) pituitaries (p>0.05, Student's t-test, n=3).

P53 knockout does not prevent remodelling of the microenvironment by the clusters

The persistence of the SASP after p53 ablation suggested that the clusters also maintained their capacity to affect the tumourigenic microenvironment. In the third chapter it was shown that a population of EMCN+ endothelial-like cells expanded early in development, interacted closely with the clusters and maintained an aberrant expression of SOX9 up to 18.5 dpc.

Double immunostaining for EMCN and YFP in 18.5 dpc pituitaries revealed that a non-*Hesx1*-derived EMCN+ population also expanded drastically in *Hesx1*$^{Cre/+}$;*Ctnnb1*$^{lox(ex3)/+}$;*Trp53*$^{fl/fl}$;*R26*$^{YFP/+}$ embryos (Figure 5.8a,b). Similarly to *Hesx1*$^{Cre/+}$;*Ctnnb1*$^{lox(ex3)/+}$ controls, *Trp53*$^{fl/fl}$ mutants also contained swarms of EMCN+/SOX9^{high} cells that formed “rings” around islands of epithelial tissue resembling the β-catenin clusters (arrows, Figure 5.8c,d).

Altogether, these results indicate that p53 is not required at embryonic stages for the onset and maintenance of senescence in the β-catenin clusters, as well for SASP induction and the non-cell autonomous modification of the tumourigenic microenvironment.

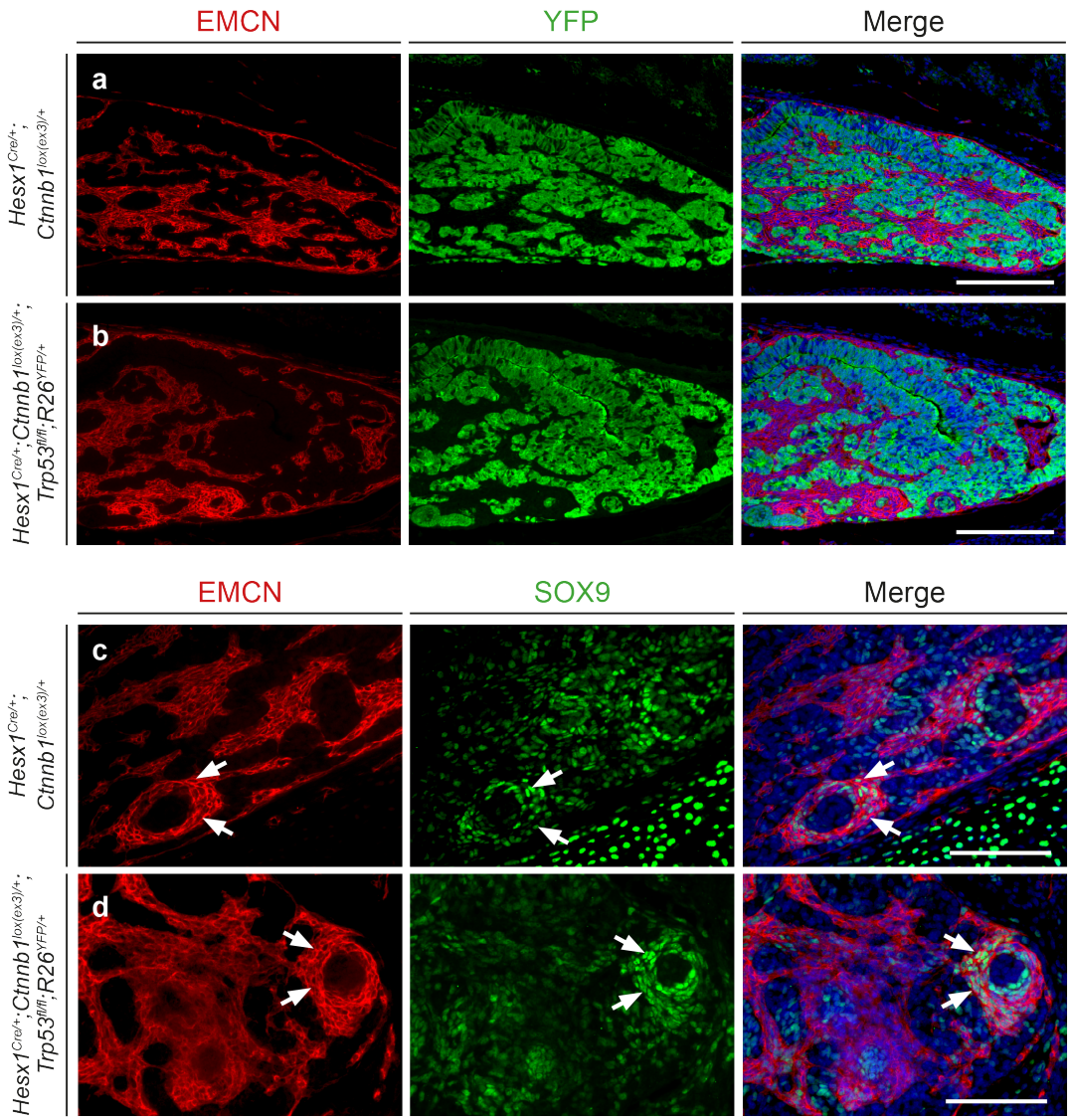

Figure 5.8 Characterisation of the effect of p53 knockout on the embryonic pituitary microenvironment.

(a) Double immunostaining for the endothelial marker Endomucin (EMCN) and YFP shows *Hesx1*$^{Cre/+}$*;Ctnnb1*$^{lox(ex3)/+}$ 18.5 dpc pituitaries contain an expanded EMCN+/YFP- population that occupies the totality of the stromal compartment. **(b)** *Hesx1*$^{Cre/+}$*;Ctnnb1*$^{lox(ex3)/+}$*;Trp53*$^{fl/fl}$ pituitaries contain a similar expanded EMCN+/YFP- population. **(c)** Nests of EMCN+/SOX9^{high} cells are observed surrounding islands of pituitary epithelium in *Hesx1*$^{Cre/+}$*;Ctnnb1*$^{lox(ex3)/+}$ pituitaries (arrows). **(d)** EMCN+/SOX9^{high} ring structures are also found in *Hesx1*$^{Cre/+}$*;Ctnnb1*$^{lox(ex3)/+}$*;Trp53*$^{fl/fl}$ pituitaries (arrows). Scale bars: a,b: 200 μm; c,d: 100 μm.

5.3 Analysis of the *Hesx1$^{Cre/+}$;Ctnnb1$^{lox(ex3)/+}$;Trp53$^{fl/fl}$* postnatal phenotype

It has been previously shown (see Figure 3.1) that the postnatal development of pituitary tumours in *Hesx1$^{Cre/+}$;Ctnnb1$^{lox(ex3)/+}$* mice displays a latency period. During this latency-period, non-proliferative pre-neoplastic regions exist in the pituitary anterior lobe, in which a sudden proliferative burst eventually initiates in non-*Hesx1* lineage cells, leading to tumour formation. Because these pre-neoplastic regions also contain β-catenin clusters, the possibility that p53 knockout affected tumour development or progression during postnatal stages was investigated in *Hesx1$^{Cre/+}$;Ctnnb1$^{lox(ex3)/+}$;Trp53$^{fl/fl}$;R26$^{YFP/+}$* mice.

5.3.1 Survival analysis and lineage tracing in tumours derived from *Hesx1$^{Cre/+}$;Ctnnb1$^{lox(ex3)/+}$;Trp53$^{fl/fl}$* mice

p53 knockout in the *Hesx1$^{Cre/+}$;Ctnnb1$^{lox(ex3)/+}$* background leads to decreased survival rates and an increase in pituitary tumour size

A survival analysis of *Hesx1$^{Cre/+}$;Ctnnb1$^{lox(ex3)/+}$;Trp53$^{fl/fl}$;R26$^{YFP/+}$* mice was conducted alongside with *Hesx1$^{Cre/+}$;Ctnnb1$^{lox(ex3)/+}$;Trp53$^{fl/+}$;R26$^{YFP/+}$* littermates (also referred to as *Trp53$^{fl/+}$*) and *Hesx1$^{Cre/+}$;Trp53$^{fl/fl}$;R26$^{YFP/+}$* controls (Figure 5.9a).

Hesx1$^{Cre/+}$;Trp53$^{fl/fl}$;R26$^{YFP/+}$ control mice were viable and sexually reproductive; and no mice from this genotype died during the course of the survival experiment. Additionally, they did not display pituitary tumours (a maximum of 24 months follow up) when sacrificed and dissected (n=4), suggesting that absence of p53 by itself is not sufficient to induce pituitary tumours when expressed in embryonic progenitors.

Interestingly, a significant difference was found in the cumulative survival rate between *Trp53$^{fl/fl}$* and *Trp53$^{fl/+}$* mice (p=0.02, Log-rank Mantel-Cox test). While

Trp53$^{fl/fl}$ mice displayed a mean survival time of 272 days (95% confidence interval, 207-338 days, n=33), the mean for *Trp53*$^{fl/+}$ mice was 422 days (95% confidence interval, 323-520 days, n=25). Additionally, measurement of average tumour diameter upon dissection revealed a significant increase (p=0.01, ANOVA, Figure 5.9b) in mean tumour size in *Trp53*$^{fl/fl}$ (5.73±0.346 mm) compared to those from *Trp53*$^{fl/+}$ (4.2±0.39 mm). Therefore, knockout of p53 has a detrimental effect in survival rate and leads to a significant increase in pituitary tumour size.

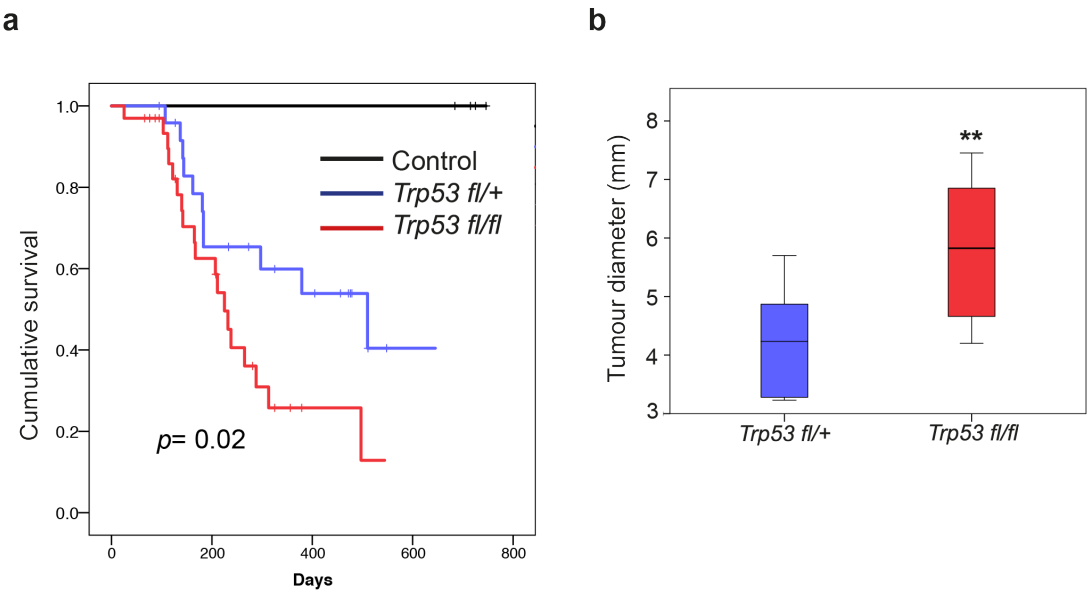

Figure 5.9 Survival and tumour size analysis of *Hesx1*$^{Cre/+}$*;Ctnnb1*$^{lox(ex3)/+}$*;Trp53*$^{fl/fl}$ mice.

(a) Kaplan-Meier survival curve for *Hesx1*$^{Cre/+}$*;Ctnnb1*$^{lox(ex3)/+}$*;Trp53*$^{fl/fl}$*;R26*$^{YFP/+}$ mice (red line), *Hesx1*$^{Cre/+}$*;Ctnnb1*$^{lox(ex3)/+}$*;Trp53*$^{fl/+}$*;R26*$^{YFP/+}$ (blue line) and *Hesx1*$^{Cre/+}$*;Trp53*$^{fl/fl}$*;R26*$^{YFP/+}$ mice (black line). Comparison between *Trp53*$^{fl/fl}$ (n=33) and *Trp53*$^{fl/+}$ (n=25) genotypes was conducted by log-rank test (p=0.02). **(b)** Box plot representation of mean tumour diameters (p=0.01, single variable ANOVA, N=18).

P53 knockout promotes the cell-autonomous formation of pituitary tumours

To assess the effect of p53 knockout on the non-cell autonomous origin of the pituitary tumours, lineage tracing of the *Hesx1* lineage was conducted in *Hesx1*$^{Cre/+}$;*Ctnnb1*$^{lox(ex3)/+}$;*Trp53*$^{fl/fl}$;*R26*$^{YFP/+}$ tumours. YFP positivity was assessed upon fresh dissection and corroborated by YFP immunostaining in paraffin sections. YFP+ tumours developed in both *Trp53*$^{fl/fl}$ and *Trp53*$^{fl/+}$ backgrounds, albeit with different frequencies (Figure5.10a-h). While YFP immunostaining in the non-fluorescent *Hesx1*$^{Cre/+}$;*Ctnnb1*$^{lox(ex3)/+}$;*R26*$^{YFP/+}$ and *Trp53*$^{fl/+}$ tumours showed the presence of residual YFP+ cells at the periphery of the tumour mass (arrows, Figure 5.10i-j), immunostaining in sections from *Trp53*$^{fl/fl}$ tumours confirmed that the tumour bulk mass was composed of YFP+ cells (Figure 5.10k). Staining for p53 protein in non-fluorescent *Hesx1*$^{Cre/+}$;*Ctnnb1*$^{lox(ex3)/+}$ tumours showed strong nuclear p53 signal (Figure 5.10l). Non-fluorescent *Trp53*$^{fl/+}$ tumours were also positive for p53 (Figure 5.10m). Conversely, no signal was observed in *Trp53*$^{fl/fl}$ tumours (Figure 5.10n).

While 35.3% of tumours obtained from control *Hesx1*$^{Cre/+}$;*Ctnnb1*$^{lox(ex3)/+}$;*R26*$^{YFP/+}$ mice were YFP- (n=17), 44.4% of *Trp53*$^{fl/+}$ (n=10) and 100% of *Trp53*$^{fl/fl}$ tumours (n=12) were YFP+ (p=0.006, Fisher's exact test, Figure 5.10o). The difference between *Hesx1*$^{Cre/+}$;*Ctnnb1*$^{lox(ex3)/+}$;*R26*$^{YFP/+}$ and *Trp53*$^{fl/+}$ tumours is not significant. Therefore, complete p53 inactivation generates a bias for fully penetrant cell-autonomously derived tumours.

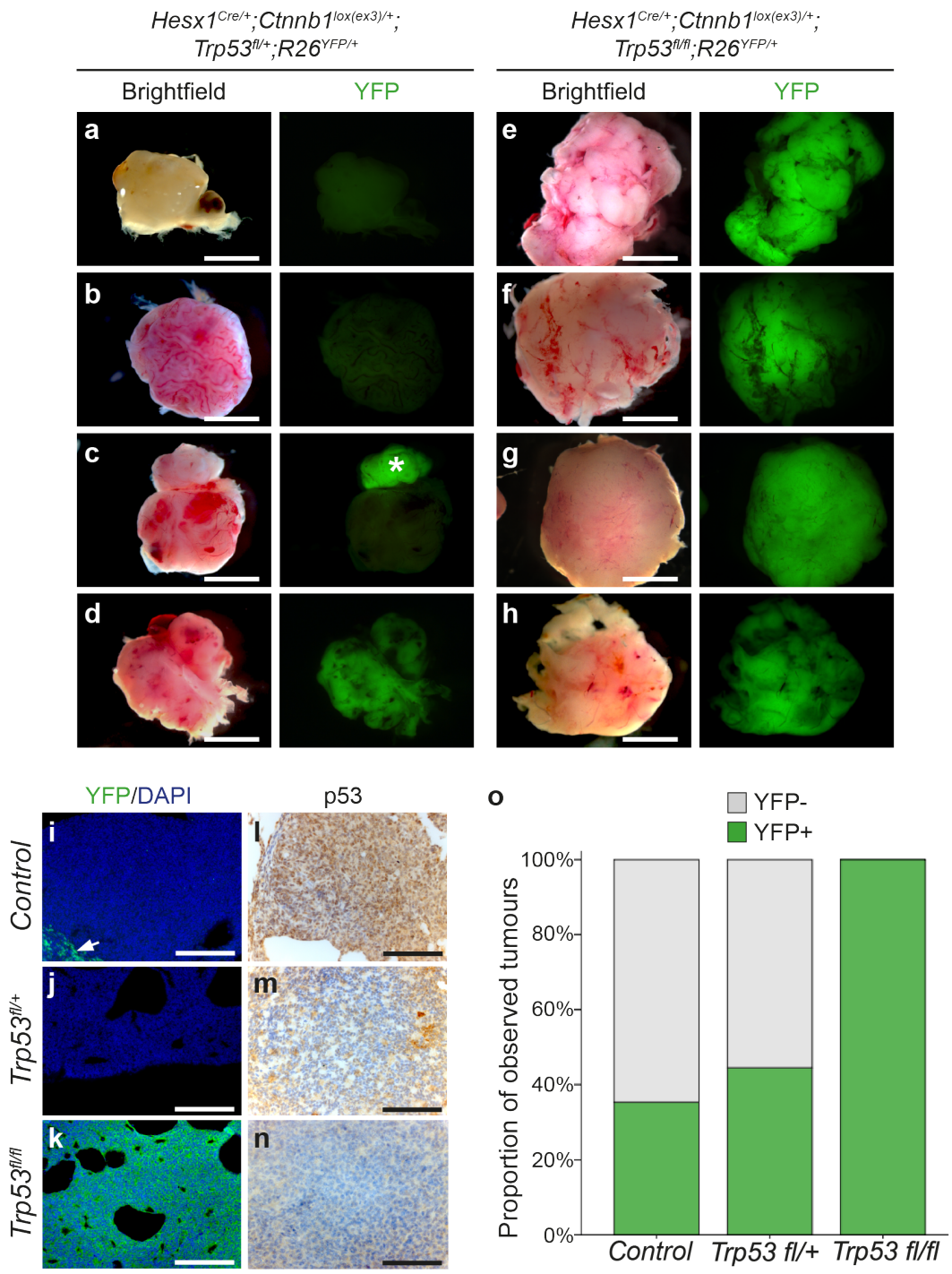

Figure 5.10 Lineage tracing in *Hesx1*$^{Cre/+}$;*Ctnnb1*$^{lox(ex3)/+}$;*Trp53*$^{fl/fl}$;*R26*$^{YFP/+}$ tumours and controls.

(a-d) Representative end-point tumours from *Trp53*$^{fl/+}$ mice at fresh dissection. Shown examples: (a,b) tumours fully negative for endogenous YFP fluorescence, (c) a YFP- tumour displaying peripheral pituitary remnants (asterisk), (d) a *Trp53*$^{fl/+}$ YFP+ tumour. **(e-h)** Representative examples of *Trp53*$^{fl/fl}$ tumours which display strong endogenous YFP fluorescence. **(i)** Immunostaining in a

Hesx1$^{Cre/+}$*;Ctnnb1*$^{lox(ex3)/+}$*;R26*$^{YFP/+}$ tumour shows absence of YFP positive signal except in residual cells displaced to the tumour periphery (arrow). **(j)** Immunostaining in a section from *Trp53*$^{fl/+}$ tumour shown in (c). Note presence of YFP+ pituitary cells in the periphery of the tumour mass (arrow). **(k)** Immunostaining against YFP in a section from *Trp53*$^{fl/fl}$ tumour shown in (f). **(l-n)** p53 immunostaining for tumours shown in (i-k). **(o)** Bar chart showing significant increase in the proportion of YFP+ tumours observed in *Trp53*$^{fl/fl}$ tumours (p=0.006, Fisher's exact test). *"Control"* denotes *Hesx1*$^{Cre/+}$*;Ctnnb1*$^{lox(ex3)/+}$*;R26*$^{YFP/+}$ tumours. Scale bars: a, b, c, d, e, f, g, h: 2.5 mm; i,j,k: 200 μm; l,m,n: 100 μm.

5.3.2 Histological characterisation and proliferation analysis of *Hesx1*$^{Cre/+}$*;Ctnnb1*$^{lox(ex3)/+}$*;Trp53*$^{fl/fl}$ tumours

The detrimental effect of p53 knockout on survival and tumour size, together with the finding that tumours formed cell-autonomously suggested they also displayed different histopathologic and molecular characteristics compared to the non-cell autonomously-derived tumours found in *Hesx1*$^{Cre/+}$*;Ctnnb1*$^{lox(ex3)/+}$ mice. It must be noted that for this thesis, all phenotypic comparisons were made between YFP+ *Hesx1*$^{Cre/+}$*;Ctnnb1*$^{lox(ex3)/+}$*;Trp53*$^{fl/fl}$*;R26*$^{YFP/+}$ and YFP- *Hesx1*$^{Cre/+}$*;Ctnnb1*$^{lox(ex3)/+}$*;R26*$^{YFP/+}$ and *Hesx1*$^{Cre/+}$*;Ctnnb1*$^{lox(ex3)/+}$*;Trp53*$^{fl/+}$*;R26*$^{YFP/+}$ tumours.

Hesx1$^{Cre/+}$*;Ctnnb1*$^{lox(ex3)/+}$*;Trp53*$^{fl/fl}$ tumours display histological features indicative of higher malignancy

Histological analysis of *Hesx1*$^{Cre/+}$*;Ctnnb1*$^{lox(ex3)/+}$ tumours has been previously reported (Gaston-Massuet et al. 2011). These tumours showed a consistent histology characterised by the presence of large cysts and were formed mostly by non-epithelial undifferentiated cells that often formed "whorl-like" arrangements (Figure 5.11a,e). The majority of *Hesx1*$^{Cre/+}$*;Ctnnb1*$^{lox(ex3)/+}$*;Trp53*$^{fl/fl}$ tumours had less cystic content (i.e. displayed a larger solid content) but also displayed non-epithelial histology (Figure 5.11b,c). However, these tumours contained high numbers of mitotic

bodies (arrows, Figure 5.11f), suggesting increased proliferation, as well the presence of cell debris resembling “dirty necrosis” (Figure 5.11g), a feature of invasive colorectal carcinomas. Interestingly, two *Hesx1*$^{Cre/+}$;*Ctnnb1*$^{lox(ex3)/+}$;*Trp53*$^{fl/fl}$ tumours displayed a very distinct histology with features not previously observed or reported (Figure 5.11d). These tumours were characterised by an overall serrated morphology and closer inspection revealed they were mostly composed of compact sheets of folded epithelial tissue separated by microcysts (Figure 5.11h). These findings were corroborated with expert histopathologist, Dr. Tom Jacques, and it was concluded that in general, the histopathological features observed in *Hesx1*$^{Cre/+}$;*Ctnnb1*$^{lox(ex3)/+}$;*Trp53*$^{fl/fl}$ tumours indicate a higher level of malignancy.

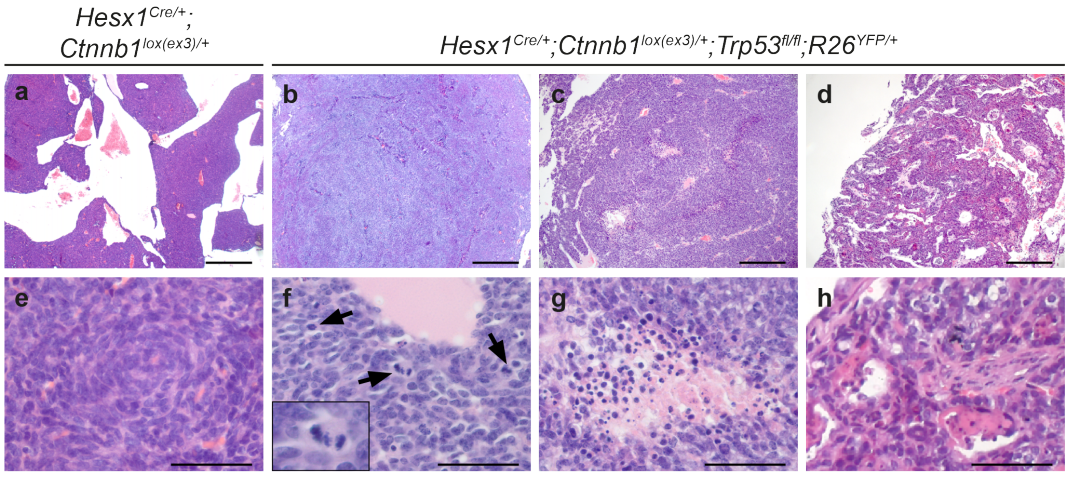

Figure 5.11 Histological characterisation of *Hesx1*$^{Cre/+}$;*Ctnnb1*$^{lox(ex3)/+}$;*Trp53*$^{fl/fl}$;*R26*$^{YFP/+}$ tumours.

Haematoxylin/eosin (H&E) staining of representative specimens. **(a)** *Hesx1*$^{Cre/+}$;*Ctnnb1*$^{lox(ex3)/+}$ tumours are characterised by the presence of large cysts within a mass of non-epithelial tumour cells. **(b-c)** Histological sections from *Hesx1*$^{Cre/+}$;*Ctnnb1*$^{lox(ex3)/+}$;*Trp53*$^{fl/fl}$ tumours shown in Figure 5.10 f and g, respectively. Note higher solid tumour content. **(d)** Example of *Hesx1*$^{Cre/+}$;*Ctnnb1*$^{lox(ex3)/+}$;*Trp53*$^{fl/fl}$ tumour (shown in Figure 5.10e) displaying a distinct histologic phenotype characterised by a “serrated” tissue morphology in contrast to the “smooth” morphology from other specimens. **(e)** High magnification photograph of (a) shows a compact “whorl-like” arrangement of non-epithelial cells in *Hesx1*$^{Cre/+}$;*Ctnnb1*$^{lox(ex3)/+}$

tumours. **(f)** High magnification image from (b) shows presence of multiple mitotic bodies in *Trp53*$^{fl/fl}$ tumours. **(g)** High magnification of (c) showing presence of "dirty necrosis". **(h)** High magnification image of (d) showing compact epithelial sheets and presence of microcysts. Scale bars: a, b, c, d: 500 μm; e, f, g, h: 50 μm.

Hesx1$^{Cre/+}$*;Ctnnb1*$^{lox(ex3)/+}$*;Trp53*$^{fl/fl}$ tumours display higher proliferation rates

The significant increase in tumour size and number of mitotic bodies suggested that p53 knockout lead to an increase in proliferation in *Hesx1*$^{Cre/+}$*;Ctnnb1*$^{lox(ex3)/+}$ tumours. Therefore, double immunostaining for proliferation markers Ki67 and phosphorylated Histone H3 (pHH3), in conjunction with YFP, was conducted in *Hesx1*$^{Cre/+}$*;Ctnnb1*$^{lox(ex3)/+}$*;Trp53*$^{fl/fl}$*;R26*$^{YFP/+}$ tumour sections and compared with *Hesx1*$^{Cre/+}$*;Ctnnb1*$^{lox(ex3)/+}$*;Trp53*$^{fl/+}$*;R26*$^{YFP/+}$ tumours shown to have low or absent YFP+ expression. While *Trp53*$^{fl/+}$ tumours displayed low levels of Ki67 and pHH3 positivity (Figure 5.12a,b), *Trp53*$^{fl/fl}$ tumours displayed an evident increase in the expression of both markers (Figure 5.12c,d). Quantification of the proportion of Ki67+ cells (Figure 5.12e) showed a significant difference between *Trp53*$^{fl/+}$ (15.7±8.5%) and *Trp53*$^{fl/fl}$ (64±9.8%) tumours (p=0.01, single variable ANOVA, N=7), suggesting further that p53 knockout promotes a higher malignancy phenotype in oncogenic β-catenin-driven tumours.

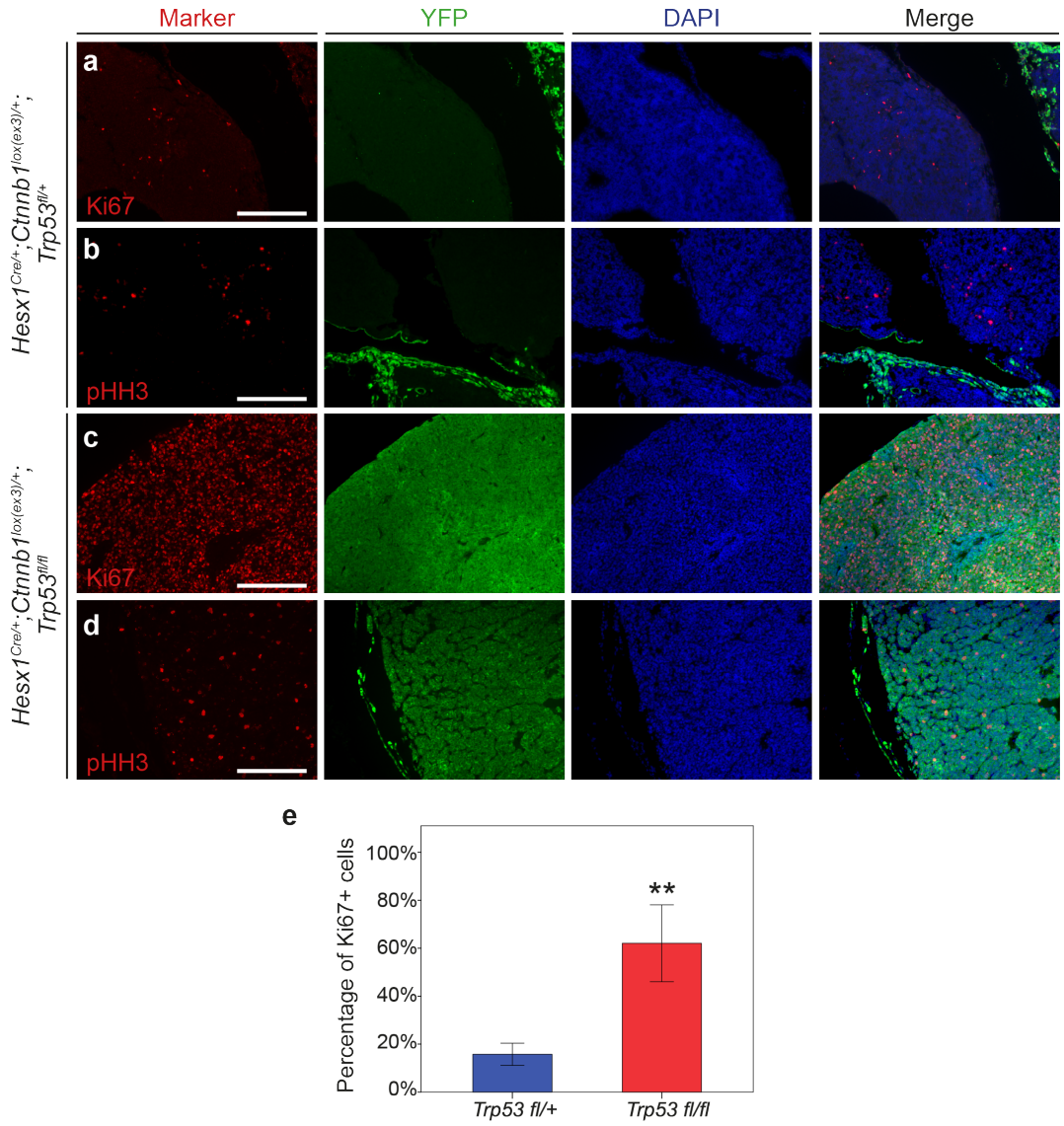

Figure 5.12 Proliferation analysis of *Hesx1$^{Cre/+}$;Ctnnb1$^{lox(ex3)/+}$;Trp53$^{fl/fl}$;R26$^{YFP/+}$* tumours.

(a) Double fluorescent immunostaining for the proliferation marker Ki67 and YFP in a representative example of a mostly YFP- *Hesx1$^{Cre/+}$;Ctnnb1$^{lox(ex3)/+}$;Trp53$^{fl/+}$;R26$^{YFP/+}$* tumour, showing the presence of scarce Ki67+ cells. **(b)** Double immunostaining for phosphorylated-histone H3 (pHH3) and YFP also reveals a small proportion pHH3+ cells are present in *Trp53$^{fl/+}$* tumours. **(c)** Double fluorescent immunostaining for Ki67 and YFP in *Hesx1$^{Cre/+}$;Ctnnb1$^{lox(ex3)/+}$;Trp53$^{fl/fl}$;R26$^{YFP/+}$* tumour shows a drastic increase in the number of Ki67+ cells. **(d)** The proportion of pHH3+ cells is also higher in *Hesx1$^{Cre/+}$;Ctnnb1$^{lox(ex3)/+}$;Trp53$^{fl/fl}$;R26$^{YFP/+}$* tumours. **(e)** Bar chart showing the mean percentage of Ki67+ cells found in *Trp53$^{fl/+}$* (15.7±8.5%, n=4) and *Trp53$^{fl/fl}$* tumours (64±9.8%, n=3). Bars in (e) represent mean±SEM; ** p=0.01, ANOVA. Scale bars: 200 μm.

5.3.3 Molecular characterisation of tumours after p53 ablation

Previous characterisation of *Hesx1*$^{Cre/+}$;*Ctnnb1*$^{lox(ex3)/+}$ tumours determined they were mainly composed by undifferentiated cells, as determined by the lack of expression of pituitary hormones, cytokeratins, pituitary-specific transcription factors PIT1 and TPIT; as well as synaptophysin, a neuroendocrine phenotype marker (Gaston-Massuet et al. 2011). Therefore, a similar analysis was conducted to evaluate the effect in tumour cell differentiation after p53 ablation in the *Hesx1*$^{Cre/+}$;*Ctnnb1*$^{lox(ex3)/+}$ background.

Hesx1$^{Cre/+}$;*Ctnnb1*$^{lox(ex3)/+}$;*Trp53*$^{fl/fl}$ tumours retain a non-differentiated phenotype

Immunostainings were conducted in *Trp53*$^{fl/fl}$ mutant tumours and controls for synaptophysin, a cocktail of pituitary hormones (GH, PRL, TSH, ACTH, LH, FSH), PIT1 and TPIT (only synaptophysin and pan-cytokeratin shown). While clear synaptophysin-positive staining was only observed in peripheral pituitary remnants of control tumours (arrow Figure 5.13a), the tumours themselves did not contain positive cells (asterisk, Figure 5.13a). Similarly, *Hesx1*$^{Cre/+}$;*Ctnnb1*$^{lox(ex3)/+}$;*Trp53*$^{fl/fl}$ tumours did not contain synaptophysin-positive cells (Figure 5.13b). A similar pattern was observed for a pan-cytokeratin antibody, which revealed positive signal only in remnants of the anterior lobe in control tumours and not in the tumour mass (Figure 5.13c). *Trp53*$^{fl/fl}$ mutant tumours also did not contain pan-cytokeratin-positive cells (Figure 5.13d). These results were recapitulated for pan-hormonal, PIT1 and TPIT stainings. Together, these results suggest that although *Hesx1*$^{Cre/+}$;*Ctnnb1*$^{lox(ex3)/+}$;*Trp53*$^{fl/fl}$ tumours are derived from a different cell of origin than *Hesx1*$^{Cre/+}$;*Ctnnb1*$^{lox(ex3)/+}$ tumours, they are also composed of non-differentiated cells, at least in terms of pituitary-related markers.

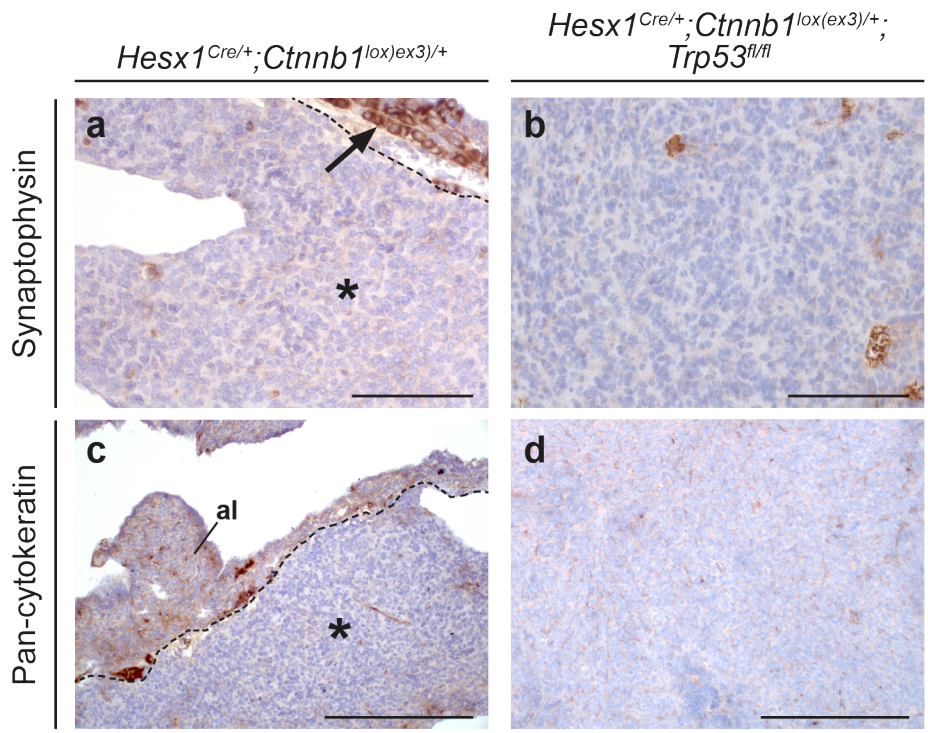

Figure 5.13 Analysis of the expression of pituitary differentiation markers in *Hesx1$^{Cre/+}$;Ctnnb1$^{lox(ex3)/+}$;Trp53$^{fl/fl}$* tumours.

(a) Immunohistochemical staining against the neuroendocrine marker synaptophysin in a *Hesx1$^{Cre/+}$;Ctnnb1$^{lox(ex3)/+}$* tumour. Remnants of the pituitary anterior lobe (al) are positively stained (arrow) while the tumour mass does not contain positive cells (asterisk). **(b)** *Hesx1$^{Cre/+}$;Ctnnb1$^{lox(ex3)/+}$;Trp53$^{fl/fl}$* tumours do not contain synaptophysin-positive cells. **(c)** Pan-cytokeratin immunostaining labels cells are present in remnants of the pituitary anterior lobe while the tumour is mostly negative. **(d)** *Hesx1$^{Cre/+}$;Ctnnb1$^{lox(ex3)/+}$;Trp53$^{fl/fl}$* tumours are also negative for pan-cytokeratin staining. Haematoxylin counterstain. Scale bars: 100 μm a,b; 250 μm, c,d.

Hesx1$^{Cre/+}$*;Ctnnb1*$^{lox(ex3)/+}$*;Trp53*$^{fl/fl}$ tumours differ in their expression of E/N-cadherin

It has been shown that the expression patterns of N- and E-cadherin change dynamically throughout pituitary development and postnatal maturation. Because early postnatal *Hesx1*$^{Cre/+}$*;Ctnnb1*$^{lox(ex3)/+}$ pituitaries already contain pre-neoplastic regions from which tumours eventually arise, possible alterations in cadherin expression were investigated in early postnatal stages and end-point tumours.

During most of embryonic development, E-cadherin is expressed throughout Rathke's Pouch, while N-cadherin expression is only observed from 15.5 dpc in regions of the anterior lobe containing differentiated or committed cell types. After birth, E-cadherin expression is drastically downregulated in most of the pituitary gland parenchyma and eventually is restricted to the marginal zone (MZ), a region known to contain high numbers of pituitary stem cells, while N-cadherin is expressed throughout most of the pituitary parenchyma (Kikuchi et al. 2007; Chauvet et al. 2009).

Consistent with previous reports, wild type pituitaries only displayed E-cadherin expression in cells lining the MZ, while N-cadherin was expressed throughout cells of the anterior lobe (Figure 5.14a). Intriguingly, the epithelial cells present in *Hesx1*$^{Cre/+}$*;Ctnnb1*$^{lox(ex3)/+}$ pre-neoplastic regions also expressed E-cadherin (Figure 5.14b), suggesting that these regions are remnants of the embryonic pituitary. This abnormal E-cadherin expression was maintained at later stages of tumourigenesis (Figure 5.14c). Conversely, non-epithelial cells of the pre-neoplastic tissue (which were shown previously to be negative for YFP) were negative for both cadherin types.

Interestingly, growing *Hesx1*$^{Cre/+}$*;Ctnnb1*$^{lox(ex3)/+}$ tumours displayed low or absent N/E-cadherin expression (Figure 5.14d), suggesting the absence of cadherin expression in YFP- tumour-forming cells is maintained in early growing tumours. Earlier analysis of E-cadherin expression at 18.5 dpc showed its expression in β-

catenin clusters (Figure 5.14e-h). End-point tumours displayed different levels of diffuse and cytoplasmic N-cadherin expression, (Figure 5.14i-l), while E-cadherin expression was only observed sporadically in the tumour periphery or in the lining of cysts. Conversely, analysis of *Hesx1*$^{Cre/+}$;*Ctnnb1*$^{lox(ex3)/+}$;*Trp53*$^{fl/f}$;*R26*$^{YFP/+}$ tumours revealed they contained higher expression of both N- and E-cadherin. While some tumours only displayed N-cadherin expression (Figure 5.14m), others solely expressed E-cadherin (Figure 5.14n). Additionally, some tumours were also found to contain increased expression of both N- and E-cadherin, which occupied non-overlapping domains (Figure 5.14o-p). Interestingly, tumours previously observed to display a novel epithelial histology (shown in Figure 5.11d,h) possessed clear membranous E-cadherin expression in most cells, while membranous N-cadherin (i.e. non-diffuse or cytoplasmic) expression was also observed throughout the tumours (Figure 5.14q-t).

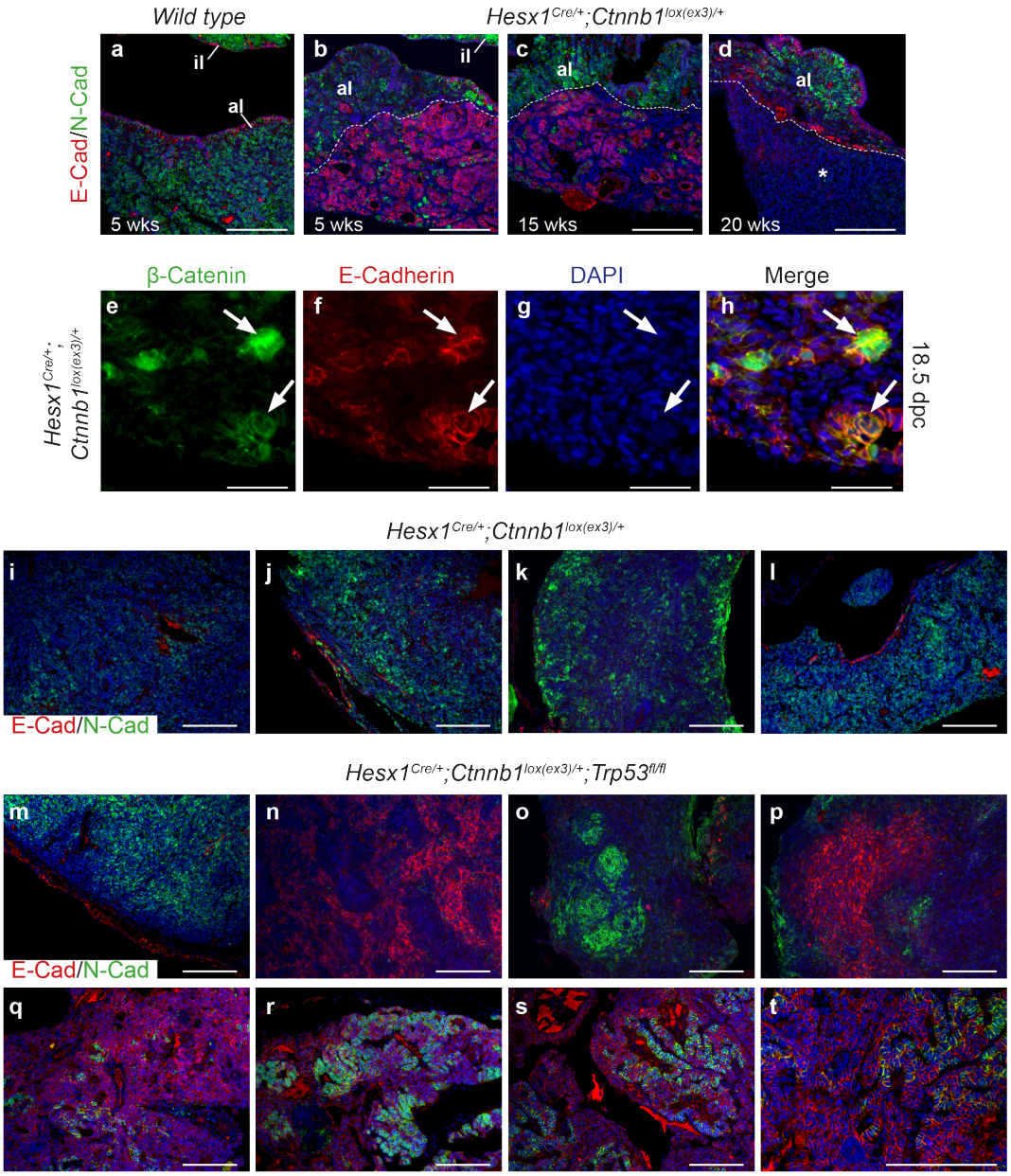

Figure 5.14 The expression of N- and E-cadherin in *Hesx1$^{Cre/+}$;Ctnnb1$^{lox(ex3)/+}$* and *Hesx1$^{Cre/+}$;Ctnnb1$^{lox(ex3)/+}$;Trp53$^{fl/fl}$* tumours.

(a) Double immunostaining for N- and E-cadherin in a 5-week-old wild type pituitary showing that E-cadherin expression is mainly restricted to cells of the marginal zone (MZ) lining the pituitary lumen, while N-cadherin is expressed throughout the anterior lobe. **(b)** A *Hesx1$^{Cre/+}$;Ctnnb1$^{lox(ex3)/+}$* pituitary at the same stage shows accumulation of E-cadherin expression in the ventral pre-neoplastic regions (delineated by dotted line), while N-cadherin expression remains in normal anterior lobe regions. **(c)** A 15-week-old *Hesx1$^{Cre/+}$;Ctnnb1$^{lox(ex3)/+}$* specimen recapitulates this expression pattern. **(d)** A 20-week-old specimen in which non-cell autonomous tumour growth has initiated (growing tumour indicated by asterisk). Note the absence of expression of either N-

and E-cadherin in the early stage tumour. **(e-h)** Double immunostaining for β–catenin and E-cadherin in a 18.5 dpc *Hesx1*$^{Cre/+}$*;Ctnnb1*$^{lox(ex3)/+}$ pituitary showing the co-expression of E-cadherin in β–catenin accumulating clusters and also in contiguous epithelial cells. Note the lack of E-cadherin expression in other cells surrounding the clusters. **(i-l)** Examples of different *Hesx1*$^{Cre/+}$*;Ctnnb1*$^{lox(ex3)/+}$ end-point tumours where diffuse N-cadherin expression can be found throughout the tumour tissue, while E-cadherin expression is restricted to peripheral remnants or cysts linings. **(m)** A *Hesx1*$^{Cre/+}$*;Ctnnb1*$^{lox(ex3)/+}$*;Trp53*$^{fl/fl}$ tumour showing a similar cadherin expression pattern (diffuse N-cadherin in tumour cells and peripheral E-cadherin). **(n)** Example of a *Trp53*$^{fl/fl}$ tumour showing predominant E-cadherin expression. **(o)** *Trp53*$^{fl/fl}$ tumour displaying patches of cells with strong membranous E-cadherin expression. **(p)** A different region in same tumour as in (k) showing a large patch of membranous E-cadherin expressing cells. **(q-t)** Examples from different regions in an epithelial *Trp53*$^{fl/fl}$ tumour. E-cadherin is expressed in most epithelial tumour cells, while N-cadherin is also expressed in large patches of epithelial cells throughout the tumour. **(t)** High magnification of (s) showing the tumour is composed of sheets of folded epithelium mostly positive for membranous E-cadherin, while some membrane N-cadherin+ cells are also observed. al: anterior lobe; il: intermediate lobe. Scale bars: a-d;m-t:150 μm, e-h: 75 μm .

5.4 Absence of p53 also leads to the cell-autonomous formation of pituitary tumours in an inducible mouse model for ACP

5.4.1 p53 knockout demonstration and lineage tracing of targeted cells in *Sox2$^{CreERT2/+}$;Ctnnb1$^{lox(ex3)/+}$;Trp53$^{fl/fl}$;R26$^{YFP/+}$* pituitaries

It was previously reported that inducible activation of oncogenic β-catenin in *Sox2$^{CreERT2/+}$;Ctnnb1$^{lox(ex3)/+}$;R26$^{YFP/+}$* mice also lead to the non-cell autonomous development of pituitary tumours, as indicated by lineage tracing of targeted cells (Andoniadou et al. 2013). Importantly, preliminary RNA-sequencing data from the host lab has shown that the β-catenin clusters present in *Sox2$^{ERT2/+}$;Ctnnb1$^{lox(ex3)/+}$* pituitaries also undergo senescence and possess a SASP (Scott Haston, unpublished data). Therefore, *Sox2$^{CreERT2/+}$;Ctnnb1$^{lox(ex3)/+}$;Trp53$^{fl/fl}$;R26$^{YFP/+}$* mice were bred, induced and analysed postnatally in order to evaluate if p53 knockout could also lead to the cell-autonomous development of pituitary tumours in this inducible model.

Knockout of p53 in the *Sox2$^{CreERT2/+}$;Ctnnb1$^{lox(ex3)/+}$* β-catenin clusters

The expression of p53 protein in β-catenin clusters was evaluated by double immunostaining in *Sox2$^{CreERT2/+}$;Ctnnb1$^{lox(ex3)/+}$;Trp53$^{fl/fl}$;R26$^{YFP/+}$* (also referred to as *Trp53$^{fl/fl}$*) and *Sox2$^{CreERT2/+}$;Ctnnb1$^{lox(ex3)/+}$;Trp53$^{fl/+}$;R26$^{YFP/+}$* pituitaries at 16 weeks post-tamoxifen induction. While *Trp53$^{fl/+}$* pituitaries showed p53 expression in β-catenin clusters (arrows, Figure 5.15a), no positive staining was found in *Trp53$^{fl/fl}$* clusters (Figure 5.15b), indicating successful removal of p53 in the *Sox2$^{CreERT2/+}$;Ctnnb1$^{lox(ex3)/+}$* β-catenin clusters.

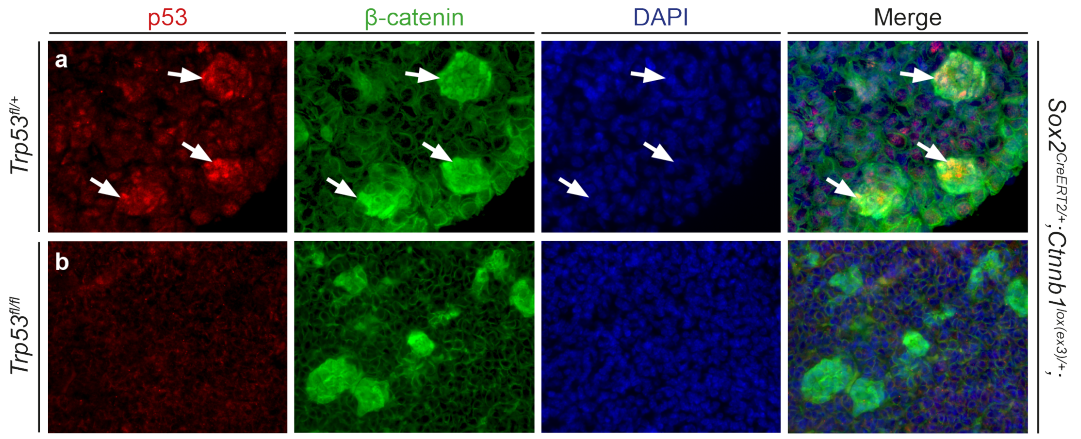

Figure 5.15 Double immunostaining for p53 and β-catenin in *Sox2$^{CreERT2/+}$;Ctnnb1$^{lox(ex3)/+}$;Trp53$^{fl/fl}$;R26$^{YFP/+}$* pituitaries and controls.

(a) p53 protein accumulates in β-catenin clusters in a 16-week post-induction *Sox2$^{CreERT2/+}$;Ctnnb1$^{lox(ex3)/+}$;Trp53$^{fl/+}$;R26$^{YFP/+}$* pituitary (arrows). **(b)** Successful knockout of p53 in the β-catenin clusters of a *Sox2$^{CreERT2/+}$;Ctnnb1$^{lox(ex3)/+}$;Trp53$^{fl/fl}$;R26$^{YFP/+}$* pituitary at the same stage.

Sox2$^{CreERT2/+}$;Ctnnb1$^{lox(ex3)/+}$;Trp53$^{fl/fl}$;R26$^{YFP/+}$ pituitaries develop neoplastic lesions in both cell-autonomous and non-cell autonomous fashions

To analyse the effect of p53 in the origin of pituitary tumours in the inducible model, pituitaries were collected at time of death and analysed for endogenous YFP expression as well as by immunostaining in paraffin sections. Notably, both *Trp53$^{fl/+}$* and *Trp53$^{fl/fl}$* genotypes contained YFP+ and YFP- lesions (Figure 5.16a-d), suggesting once again that p53 is not required for senescence and SASP induction, but that it is necessary to prevent cell-autonomous tumour formation.

The analysis of full-grown tumours was precluded as most mice died prematurely due to severe gastrointestinal complications between 11 to 13 weeks post-induction. These consisted of hypertrophy and neoplastic growth of the pyloric region which caused irreversible physical blockage. Consequently, the animals developed extreme swelling throughout the intestinal canal. Histologic analysis of pyloric lesions (n=2) showed that they were mostly composed of nucleocytoplasmic

β-catenin accumulating cells, of which only a small proportion where YFP+ (data not shown.)

Therefore, only 3 pituitaries (one *Trp53*$^{fl/+}$ control and two *Trp53*$^{fl/fl}$ mutants) were found displaying full-grown tumours (over 500 μm across). Interestingly, the *Trp53*$^{fl/+}$ tumour was mostly YFP- (Figure 5.16e), while both *Trp53*$^{fl/fl}$ tumours were mostly YFP+ (Figure 5.16b,d,f). Quantification of the number of lesions in all obtained pituitaries did not reveal any statistically significant differences in the number of YFP+ lesions between the *Trp53*$^{fl/+}$ and *Trp53*$^{fl/fl}$ genotypes (Means: 2±0.67 and 2.87±0.65 YFP+ lesions, respectively; p=0.421, ANOVA, N=11). Additionally, no differences were found in the number of YFP- lesions between the *Trp53*$^{fl/+}$ and *Trp53*$^{fl/fl}$ pituitaries (Means: 0.4±0.5 and 0.87±0.484 YFP- lesions, respectively; p=0.225; ANOVA, N=11). Also, no significant differences were found when both genotype and the age of death post-induction were considered together in the statistical analysis (p=0.466 for YFP+ lesions and p=0.568 for YFP- lesions, ANOVA).

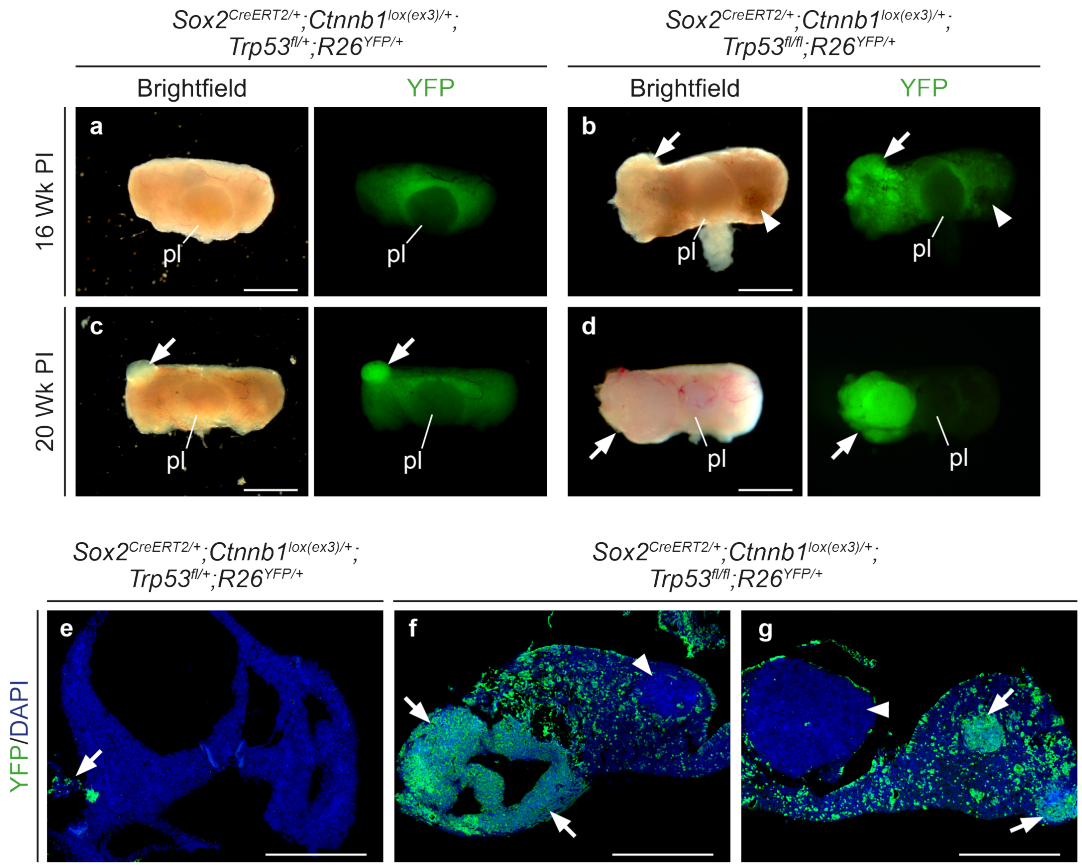

Figure 5.16 Lineage tracing analysis of *Sox2*+ cells in *Sox2*$^{CreERT2/+}$;*Ctnnb1*$^{lox(ex3)/+}$;*Trp53*$^{fl/fl}$;*R26*$^{YFP/+}$ and control pituitaries.

(a) Fresh-dissected 16-week post-induction (PI) *Trp53*$^{fl/+}$ pituitary showing endogenous YFP fluorescence in the *Sox2*+ lineage present throughout the pituitary anterior and intermediate lobes. **(b)** Example of a 16-wk. PI *Trp53*$^{fl/fl}$ pituitary displaying a large YFP+ tumour (arrow) and a smaller YFP- lesion. **(c)** Example of a 20-wk. PI *Trp53*$^{fl/+}$ pituitary with a YFP+ lesion (arrow). **(d)** Example of a 20-wk. PI *Trp53*$^{fl/fl}$ pituitary with YFP+ tumour (arrow). **(e)** Fluorescent immunostaining for YFP in an end-point *Trp53*$^{fl/+}$ tumour shows that most of the tumour is YFP-, while YFP+ signal is observed in peripheral cells. **(f-g)** Immunofluorescence for YFP in sections from pituitary shown in (b) exhibiting a large YFP+ tumour (arrows, f) next to a YFP negative lesion (arrowhead, f). A larger YFP- lesion is observed in a different non-consecutive section (contralateral) next to other YFP+ lesions (g, arrows). Scale bars: 1 mm a,b,c,d; 500 μm e,f,g.

5.5 Chapter 5 conclusions

Altogether, chapter 5 presents evidence indicating that p53 is not necessary to induce senescence and the SASP in β-catenin-accumulating clusters. In addition, the SASP from these clusters was no different from that found in the *Hesx1*$^{Cre/+}$;*Ctnnb1*$^{lox(ex3)/+}$ background, which was reflected in the presence of an altered microenvironment (e.g. SOX9+/EMCN+ cell swarms interacting with the clusters). Importantly, complete p53 inactivation generated a bias towards cell-autonomous pituitary tumours with increased malignancy phenotypes. This could possible be due to senescence escape from a cluster cell or any other target cell bypassing senescence. Despite the objective of ablating p53 being to prevent senescence and SASP activation, this result still falls in line with the paracrine model of tumourigenesis, as it suggests that a period of latency before tumour formation might involve the competition between cell-autonomous and non-cell autonomous populations competing. This phenomenon could be visualised in *Sox2*$^{CreERT2/+}$;*Ctnnb1*$^{lox(ex3)/+}$;*Trp53*$^{fl/fl}$;*R26*$^{YFP/+}$ pituitaries in which both types of tumours could be observed growing in the same organ. In this regard, it is interesting to consider the possibility that the SASP might be necessary for both types of tumourigenesis.

6. GENERAL DISCUSSION

In this thesis, the role of senescence and the SASP during ACP pathogenesis were studied under a model of paracrine tumourigenesis. In Chapter 3, an embryonic mouse model of ACP was validated for the study of non-cell autonomous tumour formation. Additionally, the senescent phenotype and the SASP of the β-catenin clusters were characterised in murine and human ACP. Finally, changes in the tumourigenic microenvironment mediated by the SASP were investigated. Chapters 4 and 5 described attempts to ablate the β-catenin clusters and the SASP in order to abrogate paracrine tumourigenesis. In Chapter 4, the CXCR4/SDF-1 chemokine pathway was targeted to restrict pro-survival signalling in the clusters. In Chapter 5, an attempt to challenge senescence was conducted by ablation of the tumour suppressor p53 and a potential role for p53 in preventing cell-autonomous tumourigenesis was revealed. Additionally, an appendix chapter was included in chapter 7, which describes preliminary data of great importance for this discussion chapter.

6.1 A proportion of mouse ACP tumours are not derived from embryonic pituitary progenitors

Lineage tracing studies previously revealed the intriguing non-cell autonomous origin of pituitary tumours derived upon activation of oncogenic β-catenin in adult SOX2+ pituitary stem cells (Andoniadou et al. 2013). This was surprising as it does not fit with the established cancer stem cell paradigm. Similar lineage-tracing studies have elegantly demonstrated the cell-autonomous origin of tumours in different contexts such as in the intestine, mammary gland, skin and prostate (Schepers et al. 2012; Nakanishi et al. 2013; Zomer et al. 2013). This evidence helped to reinforce the notion that tumours are commonly formed from descendants of those cells carrying the initial oncogenic hit.

In chapter 3, the origin of pituitary tumours was addressed in an embryonic mouse model for human ACP (*Hesx1*$^{Cre/+}$*;Ctnnb1*$^{lox(ex3)/+}$*;R26*$^{YFP/+}$ mice), in which the

vast majority of the pituitary progenitor cells would be targeted with oncogenic β-catenin (instead of only a subset of SOX2+ cells). Tracing of the *Hesx1*-lineage at different time points of tumour formation showed: first, that most of the pituitary parenchyma is derived from *Hesx1* progenitors at embryonic and postnatal stages; and second, that around 65% of pituitary tumours are not derived from the *Hesx1*-lineage and are therefore induced non-cell autonomously (Figure. 3.1). Further evidence supporting these findings is currently being generated using *Hesx1*$^{Cre/+}$;*Ctnnb1*$^{lox(ex3)/+}$;*R26*$^{mTmG/+}$ mice in which targeted cells (pituitary cells) express membrane-EGFP, while tumours only express membrane-Tomato and are therefore derived from cells that have not undergone recombination. In conclusion, the expression of oncogenic β-catenin either in pituitary embryonic progenitors or adult pituitary stem cells leads to WNT-pathway overactivation in β-catenin cluster-forming cells and the non-cell autonomous formation of pituitary tumours.

Interestingly, all *Hesx1*$^{Cre/+}$;*Ctnnb1*$^{lox(ex3)/+}$;*R26*$^{YFP/+}$ postnatal pituitaries contained dysplastic regions in their ventral sides. These “pre-neoplastic” regions were formed by YFP+ epithelium (which contained nucleo-cytoplasmic β-catenin accumulating clusters) and an expanded YFP- stroma. These pre-neoplastic regions remained in a non-proliferative state after birth and throughout early postnatal life, until a sudden burst of proliferation occurred in YFP- cells leading to their expansion until they formed full-grown YFP- tumours (Fig. 3.1). The absence of proliferation, followed by a drastic neoplastic growth suggests the existence of a latency period necessary for the tumour cell-of-origin to undergo a transformation process, during which the continuous paracrine activity of the clusters might also be involved.

There is increasing evidence showing that tumours can also arise non-cell autonomously, which falls in line with findings here reported and also with those published in a different mouse model for ACP (Andoniadou et al. 2013). For example, cells carrying mutations in Notch1 or β-catenin in mouse epidermis and hair follicle

respectively, were shown to induce overactivation of the WNT pathway in neighbouring cells and non-cell autonomous tumour formation (Deschene et al. 2014; Nicolas et al. 2003). One notable example showed that expression of oncogenic β-catenin specifically in osteoblasts resulted in the development of transformed hematopoietic stem cells (HSCs), which carried a different set of genetic alterations and could give rise to acute myeloid leukaemia (AML). Furthermore, after wild-type HSCs were transplanted into lethally irradiated mice expressing oncogenic β-catenin in osteoblasts, it was demonstrated that the HSCs became proper CSCs able to give rise to AML, even when transplanted back into wild type hosts (Kode et al. 2014). Therefore, it is proposed that *Hesx1*$^{Cre/+}$*;Ctnnb1*$^{lox(ex3)/+}$ mice represent a valid model for the study of paracrine tumourigenesis.

6.2 β-catenin accumulating clusters of mouse and human ACP undergo senescence and activate the SASP

Nucleo-cytoplasmic β-catenin accumulating clusters are a defining feature of human ACP. However, their role in the development and progression of ACP is not yet fully understood. This thesis provides further evidence supporting a model of a paracrine tumourigenesis mechanism orchestrated by the clusters in mice and humans. Specifically, it is demonstrated that the clusters undergo cellular senescence and it is proposed that this enables them to secrete pro-tumourigenic factors that potentially drive ACP development.

6.2.1 Mouse and human ACP β-catenin clusters express markers of senescence

It was previously suggested that the absence of proliferation markers in the β-catenin clusters from both murine and human ACP indicated that they undergo a quiescent state (Buslei et al. 2007; Gaston-Massuet et al. 2011). This, together with the expression of different stem cell markers led to the initial hypothesis that the clusters possessed a stem cell-like nature (Gaston-Massuet et al. 2011; Garcia-Lavandeira et al. 2011; Hölsken et al. 2013). However, the discovery that murine ACP tumours are not derived from cluster cells challenges this notion and would make difficult to explain the persistence of such as small, non-dividing, cell population throughout tumour development, besides being spared by the immune system or not being out-competed by growing tumour cells. In this thesis, cellular senescence was investigated as a potential mechanism able to explain both the clusters' proliferative inactivity and their paracrine contribution to the tumourigenic microenvironment.

Here it was confirmed that embryonic *Hesx1*$^{Cre/+}$*;Ctnnb1*$^{lox(ex3)/+}$ clusters lack the expression of proliferation markers and do not undergo apoptosis at 18.5 dpc (Fig. 3.2), which indicates a permanent but viable cell-cycle arrest in accordance with a

senescent phenotype *in vivo* (Michaloglou et al. 2005; Xue et al. 2007). Human ACP clusters have previously been described to not be proliferative nor apoptotic (Buslei et al. 2007; Gaston-Massuet et al. 2011; Zhu & You 2015).

Because cellular senescence cannot be determined accurately using a single marker, an extensive characterisation was conducted for the expression of markers involved in pathways and biological mechanisms shown to be crucial for the induction and maintenance of senescence: the lysosomal compartment, cell cycle inhibition and the DNA-damage response (DDR).

First it was shown that *Hesx1*$^{Cre/+}$*;Ctnnb1*$^{lox(ex3)/+}$ β-catenin clusters accumulate SA-β-Gal, the most widely used marker for senescence (Fig. 3.3a). Additionally, an antibody against the SA-β-Gal enzyme, GLB1, was used to accurately determine the accumulation of this protein in the β-catenin clusters in both mouse and human ACP (Fig. 3.3b,c). Finally, *Hesx1*$^{Cre/+}$*;Ctnnb1*$^{lox(ex3)/+}$ clusters and human ACP also accumulated lysosomal proteins such as Lysozyme C, LAMP1 and LAMP2 (Figs. 3.3d,e and 3.4). Together, this indicates that the β-catenin clusters possess an expanded lysosomal compartment, in agreement with a senescent phenotype, as senescent cells display increased metabolic requirements in order to maintain their highly active secretory machinery (Kurz et al. 2000; Dörr et al. 2013).

The p53/p21 and Rb/p16^{INK4a} pathways are known to be crucial for oncogene-induced senescence (OIS) *in vivo* (Serrano et al. 1997; Ventura et al. 2007; Sarkisian et al. 2007; Feldser et al. 2010), including senescence induced by WNT pathway overactivation (Sato et al. 2015; Debies et al. 2008). Here it was shown that human and murine β-catenin clusters are mostly composed of p53+, p21+ and p16+ cells (Fig. 3.5), further supporting their senescent phenotype and suggesting that the induction and maintenance of senescence could be mediated by at least one of these pathways in clusters. Studies in human ACP have focused on showing a correlation between the expression of the tumour suppressors p53 and p16 in histological

sections with clinico-pathological data, such as tumour recurrence, in hopes of finding better molecular prognostic markers. Although this approach has been successful for other types of tumours (Collado et al. 2005; Junttila et al. 2010), immunohistochemical analysis for p53 in human ACP has reported conflicting results (Momota et al. 2003; Lefranc et al. 2003; Tena-Suck et al. 2006), while p16 expression was reported to be variable between samples (Rodriguez et al. 2007). Additionally, mutations in *TP53* have not been found in human ACP (Nozaki et al. 1998; Janzer et al. 2000). Because the analysis of single sections or the sequencing of whole tumour samples makes it difficult or impossible to take into account restricted cell populations, these results help explain previous confounding data by suggesting that cell cycle-inhibiting pathways play an important role in the onset and maintenance of senescence mainly in β-catenin clusters rather than throughout the tumour tissue.

DNA damage induced by oncogene signalling and the resulting DDR are essential for onset of senescence and the SASP (Bartkova et al. 2006; Mallette et al. 2007; Fumagalli et al. 2014; Rodier et al. 2009; Kang et al. 2015). Here it is shown that both murine and human clusters express the DNA damage marker γH2AX, as well as key DDR effectors PARP-1 and phosphorylated-DNA-PKcs (Figs. 3.6 and 3.7), in agreement with findings showing that β-catenin/WNT pathway overactivation mediates senescence and DNA-damage *in vitro* and *in vivo* (Gu et al. 2014; Zhang et al. 2011; Xu et al. 2008).

6.2.2 Differences in senescence-related pathways between mouse and human ACP

There is strong evidence supporting the role of mTOR signalling for senescence and SASP induction (Herranz et al. 2015; Laberge et al. 2015). In this thesis, analysis of the mTOR and autophagy pathways in murine and human clusters revealed

inconclusive results. While ~50% of murine clusters displayed activation of downstream mTOR signalling by phosphorylation of ribosomal protein S6 and none by phosphorylation of 4E-BP1, phosphorylated S6 was absolutely absent from human ACP clusters and ~50% displayed 4E-BP1 phosphorylation (Fig. 3.8). These discrepancies might be related to the presence of distinctly phosphorylated species of S6 and 4E-BP1, which might not be detectable with the antibodies used in this study. However, it must also be taken in consideration that the p70 S6K and 4E-BP1 downstream responses are not necessarily redundant and could play context-dependent or even species-dependent roles. In the developing murine cerebellum, it has been shown that these two mTOR signalling branches have very distinct functions in the proliferation of neural precursors: while S6K activity lead to cell cycle arrest, eIF4E is required for their proliferation (Mainwaring & Kenney 2011). Interestingly, these differential responses were shown to depend on SHH signalling, a factor known to be highly expressed by the clusters. Additionally, it has also been shown that the effect of the mTOR inhibitor rapamycin can have distinct effects on S6K and 4E-BP1 (Choo et al. 2008).

Activation of mTOR signalling is known to lead to the inhibition of autophagy (Sarkar 2013), which can be assessed by the accumulation of autophagy effector proteins p62/SQSTM and LC3 (Tanida et al. 2010). While p62/SQSTM protein clearly accumulated in clusters from both mouse and human ACP, suggesting impairment of autophagy, clear LC3 accumulation could only be observed in human ACP clusters. Overall, these results are difficult to reconcile using only immunostaining data, and despite p62 and LC3 accumulation determined by immunostaining can serve as reliable markers in some contexts, caution should be taken as their accumulation can also be context-dependent (He & Klionsky 2009). Therefore, further experiments are needed to appropriately determine the status of the autophagic machinery in mouse and human ACP. Particularly, the conversion of LC3I to its lipidated form, LC3II, is

considered a robust marker for autophagy and should be evaluated by western blotting (Klionsky et al. 2016).

Although further experiments are needed to clarify the results here presented, these observations suggest that mTOR signalling could be involved in the onset of senescence and the SASP through distinct downstream mechanisms in the β-catenin clusters of mice and humans. Importantly, mTOR inhibition by rapamycin treatment has also been shown to abrogate the translation of SASP factors and their pro-tumourigenic effects (Herranz et al. 2015; Laberge et al. 2015). Therefore, further insight into the role of mTOR and autophagy in ACP pathogenesis could validate the use of mTOR inhibitors as therapeutic options for the treatment of ACP.

6.2.3 Mouse and human ACP β-catenin clusters activate the NF-κB pathway and the SASP

It was previously shown that the β-catenin clusters of human ACP, as well as those from two different mouse ACP models (*Hesx1*$^{Cre/+}$*;Ctnnb1*$^{lox(ex3)/+}$ and Sox*2;Ctnnb*$^{1lox(ex3)/+}$ mice), express a wide array of secretory mitogenic and inflammatory signalling molecules, some of which are recognised as commonly expressed SASP factors (Andoniadou et al. 2012; Andoniadou et al. 2013).

The activation of the SASP has been shown to depend on the NF-κB pathway (Acosta et al. 2008; Ohanna et al. 2011; Freund et al. 2011). Therefore, the expression of key markers of NF-κB pathway activation (RelA/p65, NEMO, and phosphorylated IκBα) was analysed in the β-catenin clusters, showing a robust activation of the pathway in both the *Hesx1*$^{Cre/+}$*;Ctnnb1*$^{lox(ex3)/+}$ and human ACP clusters (Fig. 3.10). This suggests that onset of senescence and NF-κB pathway activation enables the clusters to become the source of a broad number of previously validated mitogenic factors like SHH, FGFs, BMPs and WNTs (Andoniadou et al. 2012). In fact, these pathways have been shown to be activated by NF-κB

(Kasperczyk et al. 2009; Salminen et al. 2012; Park et al. 2016; Du & Geller 2010). Importantly, an unbiased transcriptomic analysis revealed a significant enrichment for oncogene-induced senescence (OIS) and SASP genes in *Hesx1*$^{Cre/+}$*;Ctnnb1*$^{lox(ex3)/+}$ and human ACP β-catenin clusters in comparison to non-cluster tissue (Fig. 3.11a,d). Interestingly, murine and human ACP cluster gene expression signatures group together (Fig. 3.11e), indicating these are analogous biological entities. In the mouse, the overexpression of key SASP factors in mutant pituitaries was validated at mRNA and protein levels (Fig. 3.11b,c). Additionally, a similar analysis has been conducted in FACS-sorted β-catenin cluster cells from *Sox2*$^{CreERT2/+}$*;Ctnnb1*$^{lox(ex3)/+}$*;R26*$^{YFP/+}$ pituitaries, which also displayed enrichment for the expression of OIS and SASP genes (Scott Haston, unpublished results).

6.3 Remodelling of the tumourigenic microenvironment by the SASP precedes non-cell autonomous tumourigenesis

The non-cell autonomous origin pituitary tumours in *Hesx1*$^{Cre/+}$*;Ctnnb1*$^{lox(ex3)/+}$ and *Sox2*$^{CreERT2/+}$*;Ctnnb1*$^{lox(ex3)/+}$ mice, together with the demonstration of a senescent phenotype in the β-catenin clusters suggests the SASP is responsible for generating a pro-tumourigenic microenvironment that will promote the recruitment and/or transformation of an unknown cell of origin. As mentioned in the introduction, the SASP can achieve this in part by mediating angiogenesis (Davalos et al. 2010) and remodelling of the extracellular matrix (ECM) (Krizhanovsky et al. 2008; Coppé et al. 2008).

6.3.1 A population of EMCN+/SOX9+ endothelial progenitors responds to β-catenin cluster signalling

Here, the effects of the SASP on the vascular compartment and the ECM were investigated in *Hesx1*$^{Cre/+}$*;Ctnnb1*$^{lox(ex3)/+}$ embryonic pituitaries, well before the onset of tumour growth. Surprisingly, an aberrant population of EMCN+ cells was discovered in mutant embryonic pituitaries, existing in much larger numbers than their wild type counterparts (Fig. 3.16). These cells were not derived from pituitary embryonic progenitors (as determined by lineage tracing). In addition, they occupied the totality of the pituitary stroma and were associated with ECM components (Fig. 3.17). Initial characterisation of the *Hesx1*$^{Cre/+}$*;Ctnnb1*$^{lox(ex3)/+}$ EMCN+ population showed they did not form part of the normal pituitary vasculature, as they did not colocalise with PECAM nor form normal tubular vessels (forming instead large cell "swarms") and expressed the mesenchymal progenitor marker vimentin (Fig. 3.18). Interestingly, EMCN+ swarms expressing high levels of SOX9 (EMCN/SOX9^{high}) interacted closely with the β-catenin clusters (Fig. 3.19). The EMCN+/SOX9+ population was also present during wild type pituitary development and it was observed to invade the pituitary parenchyma around 14.5 dpc., consistent with observations describing the formation of the pituitary stroma (Hashimoto et al. 1998). However, in 16.5 dpc wild type embryos SOX9 expression was already downregulated in EMCN+ cells, which formed part of the normal pituitary vasculature by that stage (Fig. 3.20a-d). Conversely, in *Hesx1*$^{Cre/+}$*;Ctnnb1*$^{lox(ex3)/+}$ pituitaries EMCN+/SOX9+ cells interacted with the clusters as early as 12.5 dpc and this close association was maintained throughout embryonic development (Figure 3.20e-h). Because EMCN+ cells maintained their large numbers and SOX9 expression was not downregulated in the presence of β-catenin clusters, these results suggest that the paracrine signals produced by the clusters are involved in the recruitment and maintenance of a EMCN+/SOX9+ population of endothelial progenitors. Furthermore,

EMCN+/SOX9+ swarms were also found in *Hesx1*$^{Cre/+}$;*Ctnnb1*$^{lox(ex3)/+}$;*Cxcr4*$^{fl/fl}$ (Figs. 4.14 and 4.17) and *Hesx1*$^{Cre/+}$;*Ctnnb1*$^{lox(ex3)/+}$;*Trp53*$^{fl/fl}$ pituitaries (Fig. 5.8). Here, the expression of secretory factors in embryonic β-catenin clusters appears to remain unaltered, while it was previously shown that *Sox2*$^{CreERT2/+}$;*Ctnnb1*$^{lox(ex3)/+}$ β-catenin clusters also interact closely with EMCN+ blood vessels (Andoniadou et al. 2013).

6.3.2 Remodelling of the microenvironment and non-cell autonomous tumourigenesis does not occur in the presence of a dampened secretory phenotype

The expansion of an EMCN+/SOX9+ population that closely interacts with the β-catenin clusters suggests this is a phenomenon mediated by the SASP. In order to further interrogate the role of senescence and the SASP in pituitary tumourigenesis, these were investigated in *Hesx1*$^{Cre/+}$;*Apc*$^{fl/fl}$ mice, in which overactivation of the WNT pathway in embryonic pituitary progenitors occurs in the context of wild-type β-catenin. An overview of ongoing results is presented as an appendix (Chapter 7). Importantly, *Hesx1*$^{Cre/+}$;*Apc*$^{fl/fl}$ pituitaries also contained nucleo-cytoplasmic β-catenin accumulating clusters similar to those from *Hesx1*$^{Cre/+}$;*Ctnnb1*$^{lox(ex3)/+}$ embryos (Fig. 7.1a,b and 7.2a). *Hesx1*$^{Cre/+}$;*Apc*$^{fl/fl}$ clusters display a senescent phenotype, as they are also non-proliferative, express p16 and p21, activate a DDR, and the NF-κB pathway (Fig. 7.2b). However, analysis of the expression of SASP factors by qRT-PCR and ISH revealed these clusters display a dampened SASP signature (Fig. 7.2c,d). Notably, an expanded EMCN+/SOX9+ population was not observed *Hesx1*$^{Cre/+}$;*Apc*$^{fl/fl}$ embryonic pituitaries, while the EMCN+ vasculature resembled more that of wild type pituitaries and did not appear to interact with the clusters (Fig. 7.2e,f). Analysis of postnatal *Hesx1*$^{Cre/+}$;*Apc*$^{fl/fl}$ pituitaries revealed they did not contain β-catenin clusters nor pre-neoplastic regions and, crucially, *Hesx1*$^{Cre/+}$;*Apc*$^{fl/fl}$ adult mice did not develop pituitary tumours at any point, even after several generations. Preliminary data obtained in *Sox2*$^{CreERT2/+}$;*Ctnnb1*$^{lox(ex3)/+}$ mice induced at advanced

age indicates that they also do not develop pituitary tumours and that their β-catenin clusters also possess a dampened SASP signature (Scott Haston, unpublished results).

These observations provide strong evidence supporting the role of senescence and the SASP in the induction of non-cell autonomous tumourigenesis in mouse models for ACP. However, it is not possible to dissect the role of WNT signalling from senescence and the SASP using the models and tools here presented. Further experiments aiming to ablate the clusters should be conducted, either through genetic strategies or chemically, by using drugs that selectively target senescent cells (senolytics). One promising candidate is ABT263, an inhibitor of BCL-2 and BCL-xL, which was recently shown to specifically induce apoptosis in bone marrow senescent cells (Chang et al. 2016). Therefore, selective targeting of senescent cluster cells in mouse ACP models will provide conclusive evidence demonstrating the role of these structures in pituitary tumourigenesis and support their use in the treatment of human ACP.

6.3.3 The EMCN+/SOX9+ cell as candidate cell-of-origin of non-cell autonomous pituitary tumourigenesis in mice

During the writing process of this thesis, the host lab began a thorough analysis of 15 *Hesx1*$^{Cre/+}$*;Ctnnb1*$^{lox(ex3)/+}$ tumours by exome sequencing. Preliminary results identified 130 different mutations of which 5 were found to be recurrent, which indicates that these are indeed neoplastic entities and further supports the idea that the SASP might be involved in the transformation of a cell-of-origin. Additionally, the host lab is currently analysing transcriptomic data of *Hesx1*$^{Cre/+}$*;Ctnnb1*$^{lox(ex3)/+}$ tumours at different time points. Further interrogation of expression data from these tumours could potentially provide clues leading to the identity of the cell of origin.

However, an interesting possibility arising from the results here presented is that a EMCN+/SOX9+ cell could be the cell-of-origin giving rise to *Hesx1*$^{Cre/+}$*;Ctnnb1*$^{lox(ex3)/+}$ tumours. As previously described, this population interacts very closely with the clusters throughout pituitary development and suggests these cells respond to their signalling. The aberrant expression of SOX9 in these cells also suggests alterations in their genetic programme. SOX9 is a transcription factor involved in the multipotential capacity of progenitor cells in many tissues and also in cancer stem cells (Jo et al. 2014). SOX9 was shown to promote the cancer stem cell phenotype and self-renewal in basal cell carcinoma (BCC) (Larsimont et al. 2015). Additionally, SOX9+ was found to promote self-renewal in hepatocellular carcinoma (HCC) CSCs *in vitro* (Liu et al. 2016), while SOX9+ was specifically expressed in HCC cells with CSC potential as determined by xenotransplantation experiments (Kawai et al. 2016). Importantly, SOX9 is thought to lie downstream of SHH, one of the most upregulated factors secreted by the β-catenin clusters. In the developing neural tube, SOX9 has been shown to mediate SHH-dependent maintenance of neural progenitors (Scott et al. 2010), while it was shown that the dependence of different types of medulloblastoma for SHH signalling was mediated by SOX9 (Swartling et al. 2012). Intriguingly, EMCN/SOX9 cells could not be observed postnatally, whereas in the embryonic pituitary they occupy vast regions of the pituitary stroma. This suggests further phenotypic/molecular changes occurring in these cells and that they may eventually become part of the non-epithelial/YFP-component of *Hesx1*$^{Cre/+}$*;Ctnnb1*$^{lox(ex3)/+}$ pre-neoplastic regions from which tumours are hypothesised to eventually arise (Fig. 3.1). Further evidence suggesting that the pre-neoplastic regions are remnants of the embryonic pituitary is provided in figure 5.14a-d, where the pre-neoplastic epithelia (which contain the remaining β-catenin clusters) maintained the expression of E-cadherin, whereas it is known that E-cadherin expression in the wild type pituitary is downregulated postnatally and restricted only to progenitors of the marginal zone (MZ) (Chauvet et al. 2009; Kikuchi

et al. 2007). Therefore, the hypothesis of an EMCN+/SOX9+ cell as candidate cell-of-origin is supported by the possibility that these cells represent the (non-*Hesx1* derived*)* population that maintains closest contact with the clusters for an extensive period that encompasses embryonic development and postnatal life.

To demonstrate the connection between EMCN/SOX9+ cells with the YFP- pre-neoplastic regions and YFP- tumours, chimeric experiments using a SOX9-lineage reporter should be conducted. However, identification of the tumour-cell-of origin might require a more extensive approach involving similar chimeric experiments with reporter lines for distinct candidate lineages. Although EMCN is a well-established endothelial marker, the exact origin of the components of the pituitary vasculature has not been extensively investigated in mice and humans. A candidate lineage of origin for the pituitary vasculature is the neural crest (NC), as SOX9 is strongly involved in NC migration (Cheung & Briscoe 2003; Theveneau & Mayor 2012). It is generally accepted that the neural crest contributes to blood vessels and connective tissue throughout the embryonic head. Quail-chick transplantation experiments showed that neural crest cells indeed contribute to the pituitary vasculature and connective tissue (Etchevers et al. 2001; Le Douarin et al. 2004). More recently, a NC-lineage reporter line (*Wnt1*^{Cre}*)* was shown to label cells migrating into the pituitary anterior lobe at 14.5 dpc, similar to the EMCN+/SOX9+ cells observed in WT pituitaries (Fig. 3.20). Moreover, ablation of β-catenin in NC cells disrupted the pituitary vasculature due to complete loss of pericytes (Davis et al. 2016). Besides the NC, other candidate lineages worth investigating are: the *Vav1*-lineage, as EMCN also represents a marker of haematopoietic progenitors throughout development (Matsubara et al. 2005; Brachtendorf et al. 2001) and the *Tie2* lineage, which represents the endothelial cell lineage (Kisanuki et al. 2001).

6.3.4 Differences in ACP pathogenesis between mouse models and humans

Contrary to the murine models, exome-sequencing of different compartments of human ACP (i.e. clusters, stellate reticulum, palisaded epithelium) revealed that they all contained equal frequencies of CTNNB1 mutations, indicating human ACPs are clonal in origin and that they follow a cell-autonomous origin . Further differences between human ACP and the murine model are exemplified by the expression pattern of EMCN. Although the expression pattern of EMCN and SOX9 did not resemble that found during *Hesx1*$^{Cre/+}$*;Ctnnb1*$^{lox(ex3)/+}$ tumourigenesis, human EMCN+ cells rarely formed part of a developed vascular system in human ACP. Instead, they were often present as single cells or large cell agglomerations within microcysts, suggesting active remodelling/migration (Fig. 3.21g,h). Additionally, some ACP cases contained vast numbers of EMCN+ cells which occupied most of the extra-tumoural tissue (Fig. 3.21d,e,f,I,j,k,l), otherwise known as reactive glial-tissue, and intermingled with the tumour in a pattern reminiscent of the EMCN+/SOX9+ swarms from the mouse ACP model. Because β-catenin clusters are often located to the tumour invasion front, it is possible that signalling occurs with the extra-tumoural space in order to recruit large numbers of EMCN+ cells. In conclusion, although the cell of origin and mechanisms underlying ACP formation might differ between mice and humans, the paracrine activities of the β-catenin clusters through the SASP might lead to similar pathogenic mechanisms such as remodelling of the microenvironment and recruitment of endothelial progenitors with pro-tumourigenic activities.

Of interest, preliminary RNAseq results suggest that the β-catenin clusters from both mouse and human ACP share a transcriptional profile reminiscent of the enamel knot (John Apps, unpublished results). The enamel knot is a transient signalling centre of great importance for proper tooth development. It shares indeed many features with the senescent β-catenin clusters, such as the secretion of signalling

factors (SHH, FGFs, BMPs) and p21 accumulation (Li et al. 2016). Coincidentally, the similarities between human ACP and odontogenic tumours had previously been noted such as enamel protein expression and presence of ghost cells (Sekine et al. 2004; Mehendiratta et al. 2012). Further understanding of the role of key genes and signalling pathways involved in the crosstalk between signalling centres, such as the enamel knot, and the microenvironment could provide novel targets leading to the ablation of senescent β-catenin clusters in mouse and human ACP.

6.4 Chemokine signalling promotes further cell recruitment into the tumourigenic microenvironment

In chapter 4, conditional knockout of the chemokine receptor CXCR4 was performed to deprive the β-catenin clusters from a crucial growth/survival factor. However, CXCR4 knockout did not affect cluster survival or their secretory phenotype (Figs. 4.14 and 4.15) and remodelling of the microenvironment was unchanged as evidenced by the recruitment EMCN+ swarms (Fig. 4.17e), while pituitary tumours still developed (Fig. 4.16). These results warn against further attempts targeting the cluster's survival through a single growth factor/trophic pathway, as it is possible that multiple signalling pathways converge on the same downstream effectors of cell survival and compensate for the loss of a single receptor. Resistance of the β-catenin clusters to cell death could be a result of the senescent phenotype itself, as senescent cells are known to be resistant to apoptosis induced by nutrient-deprivation (Sasaki et al. 2001; Burton & Faragher 2015). Additionally, the main pro-survival pathway activated by CXCR4/SDF-1 is NF-κB signalling (Rehman & Wang 2009; Teicher & Fricker 2010) and in chapter 3 it is demonstrated that the clusters themselves are the source of a plethora of pro-survival factors such as IL1A, and IL1B which are crucial activators of NF-κB signalling (Lawrence, 2009).

Another issue to discuss is the possibility that deletion of CXCR4 might result detrimental to tumour formation, as the survival curve of *Hesx1*$^{Cre/+;}$*Ctnnb1*$^{lox(ex3)/+}$*;Cxcr4*$^{fl/fl}$ mice crossed that of their heterozygous controls, giving the impression they might die sooner than expected (Figure 4.16e). Although this result was not statistically significant, there were not enough animal numbers to reach any conclusion. However, it must be noted that the goal of these experiments was to ablate the clusters themselves and to prevent tumour formation, not to evaluate rate of tumour growth (data on tumour size was not collected for these genotypes).

Besides showing that CXCR4/SDF-1 signalling is not necessary for β-catenin cluster survival, results presented in chapter 4 provide insight into the crosstalk occurring across the evolving tumourigenic microenvironment. Notably, CXCR4+ cells were found to interact closely with the clusters in both mouse and human ACP (Figs. 4.8 and 4.10). However, the source of SDF-1in both mouse and humans was not the clusters themselves (Figs. 4.9a-c and 4.11a-c). In the mouse, the source of SDF-1 was found to be stromal cells invading the pituitary anterior lobe (Fig. 4.9c). This discrepancy suggests that CXCR4 might be instead involved in long distance migration of cells from a different compartment to the tumourigenic pituitary gland. This is supported by the finding of CXCR4+ tip cells displaying filopodial processes, observed even after CXCR4 conditional knockout in the *Hesx1* lineage (Fig. 4.17a-d) and that these were also present within the EMCN+ swarms (demonstrated to not belong to the *Hesx1* lineage) (Fig. 4.17). Moreover, analysis of postnatal mutant pituitaries at different stages revealed that the pre-neoplastic regions contain large numbers of non-*Hesx1*-derived CXCR4+ cells also displaying filopodia (Fig. 4.18a-d,g-h). Finally, end-point tumours (which were non-cell autonomous in origin) displayed extensive presence of CXCR4+ mesenchymal cells and profuse CXCR4+ vascularisation (Fig. 4.18e,f,i,j). Because EMCN+/SOX9+ cells occupy the whole

stromal compartment in *Hesx1*$^{Cre/+}$*;Ctnnb1*$^{lox(ex3)/+}$ pituitaries, it is likely that they are also the invasive cells that become the source of SDF-1. Additionally, preliminary experiments show that *Hesx1*$^{Cre/+}$*;Apc*$^{fl/fl}$ pituitaries do not have an expanded SDF-1-expressing population and it has been shown that they also do not display swarms of EMCN+/SOX9+ cells (Fig. 7g). Indeed, endothelial cells and perivascular stromal cells are the most commonly described sources of SDF-1 in normal and pathogenic contexts (Pitt et al. 2015; Ding & Morrison 2013).

Although CXCR4 and SOX9 share a similar expression pattern in cells that appear to interact with the β-catenin clusters, it was never shown that these proteins are co-expressed in the same cells. Therefore, this would be a necessary demonstration. If indeed CXCR4+/SOX9+ cells are shown to be present throughout pituitary development and interacting with the clusters, then chemical targeting of CXCR4 could potentially prevent the recruitment of these cells to the clusters.

Chapter 4 additionally provides evidence of active signalling mediated by SASP, as the CXCR2 ligands CXCL1, CXCL2 and CXCL3 (all SASP factors) have been shown to be highly overexpressed by the mouse clusters (Andoniadou et al. 2012). Instead, the expression of the chemokine receptor CXCR2 was upregulated in non-cluster cells in *Hesx1*$^{Cre/+}$*;Ctnnb1*$^{lox(ex3)/+}$ pituitaries and tumours, as well as in human ACP (Figs. 4.9g-i and 4.11d-f).

Together, these observations allow to envision a mechanism by which the senescent β-catenin clusters initially recruit and maintain EMCN+/SOX9+ swarms which contain a future tumour cell-of-origin. EMCN+/SOX9+ cells in turn secrete SDF-1 which allows further recruitment of other cell types into the microenvironment which might also respond to local cluster signalling (e.g. CXCR2+ cells) and reinforce the paracrine tumourigenesis process (e.g. tumour-associated fibroblasts, pro-inflammatory immune cells, endothelial cells, etc.) (Fig. 6.1).

In summary, the results presented in chapters 3 and 4 provide the basis for future research on the role of the tumourigenic microenvironment in the non-cell autonomous formation of pituitary tumours. Characterisation of the immune response is particularly encouraged as SASP factors are inherently pro-inflammatory and chronic inflammation is intimately associated with tumourigenesis (Crusz & Balkwill 2015). Additionally, a better understanding of the inflammatory process occurring in mouse models of ACP will provide support for the use of small-molecule inhibitors for CXCR4 or CXCR2. The use CXCR4 antagonist AMD3100 (Plerixafor) has shown promising results as a chemosensitizer in the treatment of different types of leukaemias (Burger & Peled 2009; Uy et al. 2012) and it is currently being evaluated in clinical trials for the treatment of solid tumours such as pancreatic ductal adenocarcinoma, high grade ovarian, colorectal adenocarcinoma and breast cancers (Liu et al. 2015). Additionally, inhibition of CXCR2 has demonstrated to effectively impair tumour growth by preventing trafficking of myeloid-derived suppressor cells (MDSCs) in colorectal adenocarcinoma, pancreatic adenocarcinoma and rhabdomyosarcoma models (Highfill et al. 2014; Steele et al. 2016; Jamieson et al. 2012).

6.5 The role of p53 in WNT-driven tumourigenesis in the pituitary gland

The demonstration of a senescent phenotype and the activation of the SASP in the β-catenin clusters, as well as their involvement in the modification of the tumourigenic microenvironment prompted the hypothesis that targeting the onset of senescence in these structures would prevent SASP activation and therefore abrogate non-cell autonomous tumourigenesis. As presented in the general introduction, the onset and maintenance of senescence has been demonstrated to depend on p53 in many contexts, including *in vivo* cancer studies (Muñoz-Espín &

Serrano 2014). Therefore, chapter 5 introduced the characterisation of a Hesx*1*$^{Cre/+}$*; Ctnnb1*$^{lox(ex3)/+}$;*Trp53*$^{fl/fl}$ mice, in which expression of the tumour suppressor p53 was ablated in embryonic pituitary progenitors and therefore, in the clusters (Fig. 5.1).

6.5.1 p53 is not required for inducing senescence and the SASP in the embryonic β-catenin clusters

Unexpectedly, embryonic *Hesx1*$^{Cre/+}$*;Ctnnb1*$^{lox(ex3)/+}$;*Trp53*$^{fl/fl}$ clusters lacked the expression of proliferation markers (Fig. 5.2), did not undergo apoptosis (Fig 5.3), maintained the expression of p21 and p16 (Fig. 5.4) and activated the DDR (Fig. 5.5). Moreover, analysis of the clusters' secretory phenotype by qRT-PCR and ISH revealed no significant changes in the expression of mitogenic factors *Shh, Bmp4, Fgf3* and *Wnt6*; nor of key SASP factors *Il1a, Il1b, Il6, Cxcl1, Cxcl2* and *Ccl20*. Finally, analysis of the stromal compartment revealed that 18.5 dpc *Hesx1*$^{Cre/+}$*;Ctnnb1*$^{lox(ex3)/+}$;*Trp53*$^{fl/fl}$ pituitaries also contained an expanded EMCN+/SOX9+ population (Fig. 5.8). Together, this evidence indicates that p53 is not required for the induction and maintenance of senescence in β-catenin clusters and their SASP during embryonic pituitary development and therefore, a different pathway must mediate this process.

A number of studies have demonstrated the dispensability of p53 in oncogene-induced senescence and identified other pathways responsible for mediating this process. Although the p53-dependent cell cycle arrest occurs mainly through activation of p21, it has been shown senescence can be achieved in the absence of p53 through the induction of p21 by other pathways. It has been demonstrated that p21 activation can occur through the DDR-related kinase Chk2 (Aliouat-Denis et al. 2005), downregulation of protein arginine methyltransferase 6 (PRMT6) (Phalke et al. 2012) or inactivation of the E3 ligase complex component *Skp2* (Lin et al. 2010). p53-independent OIS has also been reported to be mediated by products of the CDKN2A

locus ($p16^{INK4A}$ and $p19^{ARF}$) (Christoffersen et al. 2010; Ha et al. 2007; Haferkamp et al. 2009) or the p38 MAPK pathway (Kwong et al. 2009). Additionally, it has been revealed that developmentally programmed senescence is mediated by p21 through TGF-β/SMAD signalling, independently of p53 and p16/ARF (Muñoz-Espín et al. 2013). Further examples have shown that OIS can even be induced without the requirement of p53, p21 and p16 (Cipriano et al. 2011; Prieur et al. 2011). Finally, certain isoforms of p63, a member of the p53-family, were demonstrated to induce OIS *in vivo* by activation of p21, also independently of p53 (Guo et al. 2009). Interestingly, p63 is highly expressed in human ACP (Cao et al. 2010; Esheba & Hassan 2015) and preliminary data has also identified its expression in the human β-catenin clusters (John Apps, unpublished results).

Therefore, the induction of senescence in β-catenin clusters might depend on one or more of the pathways just described. Also worth of discussion is the fact that the expression of several SASP factors was not affected after p53 knockout of in *Hesx1*$^{Cre/+}$*;Ctnnb1*$^{lox(ex3)/+}$;*Trp53*$^{fl/fl}$ embryonic pituitaries (Figs. 5.6 and 5.7), while the expansion of EMCN+/SOX9+ cell swarms remained unchanged (Fig. 5.8). This was also an unexpected result, as it has been observed that p53-deficient senescent cells display a significant increase in the secretion of SASP factors and exacerbation of the pro-tumourigenic effects of the SASP in the microenvironment (Coppé et al. 2008; Rodier et al. 2009; Freund et al. 2011). Future experiments aiming at characterising the transcriptional profile of targeted cells isolated from *Sox2*$^{CreERT2/+}$*;Ctnnb1*$^{lox(ex3)/+}$*;Trp53*$^{fl/fl}$*;R26*$^{YFP/+}$ pituitaries are being conducted to gain further insight into the pathways that mediate the senescence induction in p53-deficient β-catenin clusters and to confirm that the SASP remains unchanged in these structures.

6.5.2 Complete absence of p53 promotes cell-autonomous tumourigenesis postnatally and associates with higher malignancy phenotypes

Chapter 5 also demonstrates that, in the absence of p53, WNT-driven pituitary tumours arise in cell-autonomous fashion, despite the onset of senescence and the SASP in embryonic p53-deficient β-catenin clusters (Fig. 5.10). Indeed, lineage tracing experiments demonstrated that 100% of *Hesx1*$^{Cre/+}$*;Ctnnb1*$^{lox(ex3)/+}$*;Trp53*$^{fl/fl}$*;R26*$^{YFP/+}$ tumours were mostly formed by oncogenic β-catenin-targeted YFP+ cells. Conversely, the number of YFP+ tumours observed in p53-wild-type and p53-heterozygous mice was 35.3% and 44.4%, respectively (further discussed below). Notably, complete inactivation of p53 led to a significant increase in mortality rate and tumour size in comparison to heterozygous controls. (Fig. 5.9). In this regard, it is important to discuss that the *Trp53*$^{fl/fl}$ survival curve is very similar to that of *Hesx1*$^{Cre/+}$*;Ctnnb1*$^{lox(ex3)/+}$ mice (John Apps, personal communication). Although this would suggest that loss of only one *Trp53* allele might have a positive effect in survival, care must be taken as comparison between different genetic backgrounds might render confounding results. For example, the *Hesx1*$^{Cre/+;}$*Ctnnb1*$^{lox(ex3)/+}$;*Cxcr4*$^{fl/fl}$ curve is displaced far to the left compared to *Hesx1*$^{Cre/+;}$*Ctnnb1*$^{lox(ex3)/+}$. However, it was shown that these tumours do not differ in their phenotype and size (data not shown), while *Hesx1*$^{Cre/+}$*;Ctnnb1*$^{lox(ex3)/+}$*;Trp53*$^{fl/fl}$*;R26*$^{YFP/+}$ tumours are clearly different in phenotype and size. In conclusion, there is a high possibility that point of death does not correlate well with changes in tumour size or phenotype and is possibly more related to hydrocephalus formation and should be considered in future experiments.

Trp53$^{fl/fl}$ tumours displayed distinct histopathological features indicating a higher malignancy grade (Fig. 5.11) and a much higher proliferative index compared to tumours derived non-cell autonomously (Fig. 5.12). This increase in proliferation

and malignancy upon complete abrogation of p53 falls in line with previous experiments conducted in mouse models of WNT-driven carcinogenesis (Kuo et al. 2015; Méniel et al. 2014). Also of note, a small proportion of *Hesx1*$^{Cre/+}$*;Ctnnb1*$^{lox(ex3)/+}$*;Trp53*$^{fl/fl}$*;R26*$^{YFP/+}$ tumours displayed a novel epithelial-histology (Fig. 5.11d,h). Therefore, complete absence of p53 in the context of oncogenic β-catenin generates a full bias for the cell-autonomous formation of pituitary tumours with increased proliferation and enhanced malignancy phenotypes. Importantly, some of the features acquired by p53 KO tumours are highly reminiscent of human ACP, such as the presence of epithelium (completely absent from classic *Hesx1*$^{Cre/+}$*;Ctnnb1*$^{lox(ex3)/+}$ tumours) and acellular, keratinized deposits resembling human ACP "wet keratin". Together with a drastic increase in proliferative and mitotic indexes, p53 KO tumours could provide a model in which to study malignant ACP pathogenesis. Although it was attempted, such tumours are extremely rare and no samples could be obtained during the course of this work. However, transcriptomic and genomic analysis of such tumours is recommended as it could shine light into the role of p53 in human ACP pathogenesis. This will be particularly important in the improvement of current therapies, as irradiation is still a main therapeutic approach and it is under debate if its use underlies tumour recurrence and malignant transformation in human ACP (Rodriguez et al. 2007; Sofela et al. 2014)

The molecular and mutational landscapes that distinguish tumours derived by cell-autonomous (YFP+) and non-cell autonomous (YFP-) mechanisms, as well as the identity of their respective cells-of-origin remain to be determined. Interestingly, some YFP+ tumours displayed high expression of E-cadherin, which in the wild-type postnatal pituitary gland is only expressed in the stem cell-rich marginal zone (MZ). E-cadherin expression is also maintained in the YFP+ epithelia of the pre-neoplastic regions that precede tumour formation, which also include the β-catenin clusters (Fig. 5.14), suggesting that YFP+ tumours may arise from embryonic pituitary remnants.

6.5.3 Cell-autonomous tumourigenesis also occurs in the context of p53 haploinsufficiency and wild type p53

Pituitary tumours developed cell-autonomously in 35.3% of mice carrying a wild type p53 locus (*Hesx1*$^{Cre/+}$*;Ctnnb1*$^{lox(ex3)/+}$*;R26*$^{YFP/+}$) and in 44.4% of those carrying one intact copy of p53 (*Hesx1*$^{Cre/+}$*;Ctnnb1*$^{lox(ex3)/+}$*;Trp53*$^{fl/+}$*;R26*$^{YFP/+}$) (Fig. 5.10). This observation is difficult to explain with current data, as YFP+ tumours of these control strains were not analysed due to time constraints. It will be important to increase sample numbers to clarify if there is a significant difference in the proportion of YFP+ tumours that develop in each of these backgrounds. If there is a significant increase in the number of YFP+ tumours in the p53 heterozygous background, this would suggest that p53 haploinsufficiency also gives a competitive advantage to targeted cells. In this case, it could be that that haploinsufficiency can promote WNT-driven tumour formation by itself or that targeted cells undergo loss of heterozygosity (LOH). In the case of lymphomas and multiple myeloma, it has been shown that expression of the remaining p53 allele can be further downregulated or completely silenced by promoter hypermethylation leading to decreased survival in mice and humans (van der Weyden et al. 2012; Teoh et al. 2014). Additionally, *Trp53* haploinsufficiency has been proved to be sufficient for enhancing tumourigenesis, by cooperating with the expression of oncogenes such as EGFR (Rahrmann et al. 2014) and oncogenic β-catenin (Ridgeway et al. 2006). It is also important to remark that the results presented in chapter 5 fall in line with thorough characterisation of tumours spontaneously formed in *Trp53*$^{-/-}$, *Trp53*$^{+/-}$ and *Trp53*$^{+/+}$ mice, where the level of p53 inactivation also correlated positively with a drastic acceleration in tumour growth and decrease in survival. Intriguingly, *Trp53*$^{-/-}$, *Trp53*$^{+/-}$ and *Trp53*$^{+/+}$ mice developed distinct types of cancer with different frequencies. While *Trp53*$^{-/-}$ developed mostly lymphomas of T-cell origin and some soft-tissue sarcomas, *Trp53*$^{+/-}$ mice developed an almost equal mix of osteosarcomas, B-cell lymphomas and soft-tissue sarcomas

(Donehower & Lozano 2009). Interestingly, while half of the *Trp53*$^{+/-}$ tumours retained one functional copy of *Trp53*, (i.e. p53 is haploinsufficient), the rest of the tumours displayed LOH of the other allele (Venkatachalam et al. 1998; Venkatachalam et al. 2001). Further transcriptomic and exome-sequencing studies will be necessary in order to determine the status of the *Trp53* locus in *Hesx1*$^{Cre/+}$*;Ctnnb1*$^{lox(ex3)/+}$*;R26*$^{YFP/+}$ and *Hesx1*$^{Cre/+}$*;Ctnnb1*$^{lox(ex3)/+}$*;Trp53*$^{fl/+}$*;R26*$^{YFP/+}$ tumours and to correlate it with their YFP expression and phenotype.

An exciting possibility arising from the development of YFP+ tumours in *Hesx1*$^{Cre/+}$*;Ctnnb1*$^{lox(ex3)/+}$*;R26*$^{YFP/+}$ and *Hesx1*$^{Cre/+}$*;Ctnnb1*$^{lox(ex3)/+}$*;Trp53*$^{fl/+}$*;R26*$^{YFP/+}$ mice is that the paracrine activities of the SASP could also be required for cell-autonomous tumourigenesis. Evidence for this could be obtained by generating *Hesx1*$^{Cre/+}$*;Trp53*$^{fl/fl}$*;Apc*$^{fl/fl}$*;R26*$^{YFP/+}$ mice. In this model, it could be expected that absence of p53 in the context of WNT signalling would allow the β-catenin clusters to bypass or escape senescence, leading to cell-autonomous tumour formation. However, and as previously mentioned, *Hesx1*$^{Cre/+}$*;Apc*$^{fl/fl}$ β-catenin clusters display a dampened SASP, absence of micro-environmental alterations and do not form tumours. If YFP+ tumours also do not develop in *Hesx1*$^{Cre/+}$*;Trp53*$^{fl/fl}$*;Apc*$^{fl/fl}$*;R26*$^{YFP/+}$, this would provide evidence for a role of the SASP also in pituitary cell-autonomous tumourigenesis.

6.5.4 Non-cell autonomous and cell-autonomous mechanisms might coexist and compete during pituitary tumourigenesis

Because senescence and the SASP remained unaltered in the embryonic β-catenin clusters of *Hesx1*$^{Cre/+}$*;Ctnnb1*$^{lox(ex3)/+}$*;Trp53*$^{fl/fl}$*;R26*$^{YFP/+}$ mice and they also appeared to modify their microenvironment, it would be expected that there is a point where both YFP+ and YFP-tumourigenic populations compete before tumour formation. This situation might also occur during the tumourigenic process in

Hesx1$^{Cre/+}$*;Ctnnb1*$^{lox(ex3)/+}$*;R26*$^{YFP/+}$ and *Hesx1*$^{Cre/+}$*;Ctnnb1*$^{lox(ex3)/+}$*;Trp53*$^{fl/+}$*;R26*$^{YFP/+}$ backgrounds, albeit with different dynamics and leading to different outcomes.

In this case, inactivation of p53 in the context of oncogenic β-catenin would be regarded as an advantage if it allowed a YFP+ cell to bypass (or escape) senescence, avoid apoptosis, accelerate their cell cycle or impair DNA damage-repair checkpoints (Meek 2009; Cornel et al. 2014; Frank et al. 2011; Méniel et al. 2014; Lozano 2010). Conversely, in the context of p53 hemizygosity or wild type loci these advantages would be diminished enabling YFP- tumours to arise occasionally, as observed in 55.6% of *Hesx1*$^{Cre/+}$*;Ctnnb1*$^{lox(ex3)/+}$*;Trp53*$^{fl/+}$*;R26*$^{YFP/+}$ and 64.7% of *Hesx1*$^{Cre/+}$*;Ctnnb1*$^{lox(ex3)/+}$*;R26*$^{YFP/+}$ tumours (Fig. 5.10). Notably, in a mouse model of lymphoma driven either by oncogenic β-catenin or loss of *Apc*, cancer cells undergo p53-independent OIS but require inactivation of p53 for tumourigenesis to proceed by evasion of apoptosis. *Trp53*$^{-/-}$ lymphomas displayed diminished latency and also a distinct molecular phenotype than those from a *Trp53*$^{+/-}$ background (Xu et al. 2008; Sharma & Sen 2013). Although end-point *Hesx1*$^{Cre/+}$*;Ctnnb1*$^{lox(ex3)/+}$*;Trp53*$^{fl/fl}$*;R26*$^{YFP/+}$ YFP+ tumours indeed displayed a proliferative advantage (Fig. 5.12), further experiments should aim at analysing proliferation, apoptosis and senescence markers in targeted and non-targeted cells at intermediate stages before the onset of tumour growth. This will allow identification of essential biological processes that determine which mechanism of tumourigenesis is to prevail in this context. In this regard, exome-sequencing and expression profiling of tumours from each different genotype will provide crucial insight into additional mutations and molecular alterations required to shift the balance in favour of cell-autonomous or non-cell autonomous tumourigenesis.

The concomitant occurrence of cell-autonomous and paracrine mechanisms of tumourigenesis in murine ACP are also supported by findings shown where inducible ablation of p53 and activation of oncogenic β-catenin occurs in adult SOX2+ cells.

Strikingly, both *Sox2*$^{CreERT2/+}$;*Ctnnb1*$^{lox(ex3)/+}$;*Trp53*$^{fl/fl}$;*R26*$^{YFP/+}$ and *Sox2*$^{CreERT2/+}$;*Ctnnb1*$^{lox(ex3)/+}$;*Trp53*$^{fl/+}$;*R26*$^{YFP/+}$ pituitaries developed pre-tumoural lesions in cell-autonomous and non-cell autonomous fashions (Fig. 5.16); contrary to *Sox2*$^{CreERT2/+}$;*Ctnnb1*$^{lox(ex3)/+}$ mice, which were previously reported to only develop YFP- tumours (Andoniadou et al. 2013). Although thorough analysis of full-grown tumours was not possible in this model, it is encouraging that YFP+ tumours only developed in complete absence of p53, while YFP- tumours developed in *Trp53*$^{fl/+}$ pituitaries. This further supports the idea that the YFP+ population expressing oncogenic β-catenin holds a significant advantage over paracrinally-induced cells only when p53 expression is completely abrogated. Further experiments conducting laser-capture microdissection (LCM) and expression profiling of YFP+/YFP- lesions and tumours will also reveal pathways involved in the selective promotion of paracrine versus non-paracrine mechanisms of carcinogenesis.

The results here presented give way to a number of interesting questions of relevance for the study of senescence in cancer: are p53-deficient cell-autonomously-formed tumours derived from a β-catenin cluster cell? (i.e. an already senescent cell escapes senescence). Are they derived from another *Hesx1*-lineage cell? (i.e. a non-senescent cell bypasses senescence). The same questions can be asked for non-cell autonomous tumourigenesis and cells not carrying the initial oncogenic hit. Also, is the SASP also necessary to generate a pro-tumourigenic environment necessary for cell-autonomous tumourigenesis? Currently, a genetic strategy allowing to both lineage-trace and to ablate senescent cells *in vivo* is being developed by the host lab. Application of this strategy in *Hesx1*$^{Cre/+}$;*Ctnnb1*$^{lox(ex3)/+}$;*Trp53*$^{fl/fl}$ and *Sox2*$^{Cre/+}$;*Ctnnb1*$^{lox(ex3)/+}$;*Trp53*$^{fl/fl}$ mice will allow to ablate senescent β-catenin clusters and help dissect the mechanisms underlying both paracrine and cell-autonomously derived tumourigenesis.

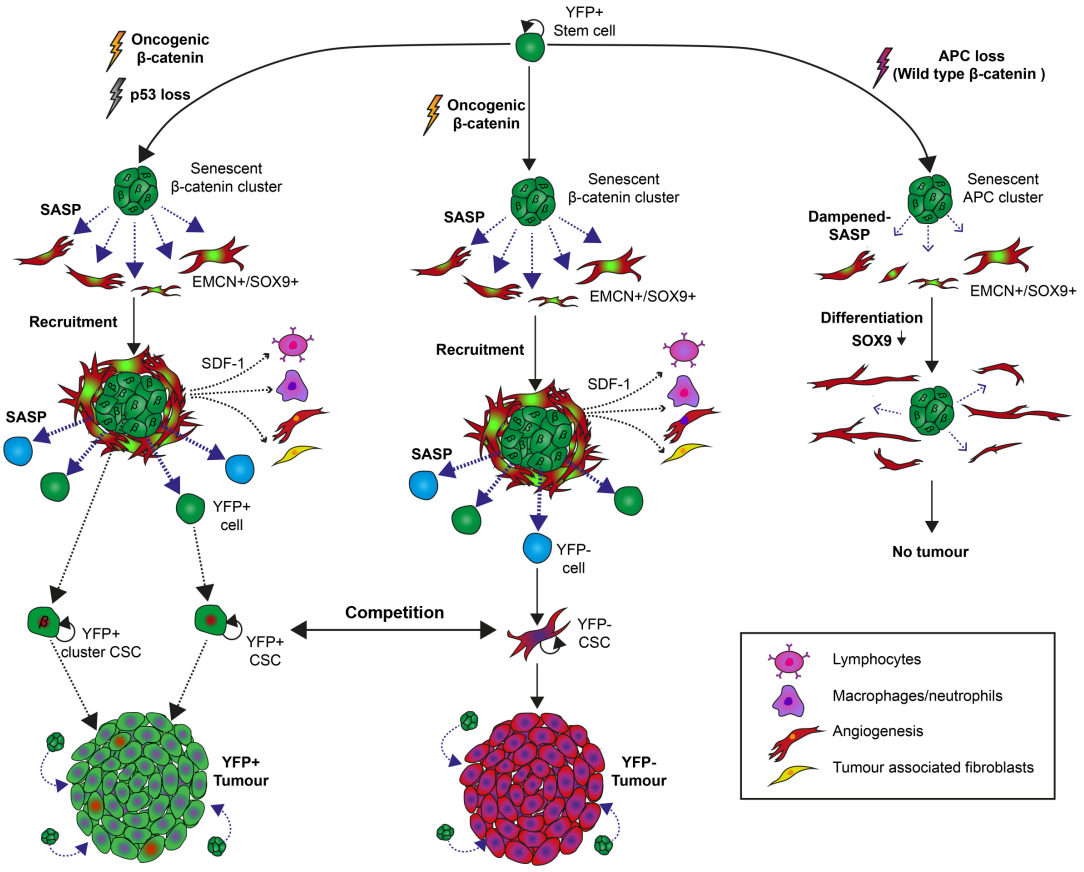

Fig. 6.1 Proposed model for the role of senescence and the Senescence-Associated Secretory Phenotype (SASP) in the non-cell autonomous formation of pituitary tumours.

(Centre) Activation of oncogenic β-catenin in YFP+ embryonic pituitary progenitors of *Hesx1*$^{Cre/+}$;*Ctnnb1*$^{lox(ex3)/+}$;*R26*$^{YFP/+}$ mice leads to WNT pathway overactivation and the formation of senescent β-catenin clusters. The clusters activate a SASP which recruit swarms of EMCN+/SOX9+ embryonic endothelial progenitors not derived from the *Hesx1*-lineage (YFP-). Throughout pituitary development, the SASP maintains the undifferentiated phenotype of EMCN+/SOX9+ cells, which further interact with the clusters by forming nests around them. EMCN+/SOX9+ express the chemokine SDF-1 which can recruit different cell types to the microenvironment such as lymphocytes, macrophages, neutrophils, fibroblasts and angiogenic progenitors. Continuous pro-tumourigenic signalling from the SASP and from recruited cells eventually lead to the transformation of a cell-of-origin, possibly derived from the EMCN+/SOX9+ population, which acquires a cancer stem cell (CSC) phenotype and forms a YFP- tumour. **(Left)** In the context of p53 loss (and possibly in a proportion of *Hesx1*$^{Cre/+}$;*Ctnnb1*$^{lox(ex3)/+}$;*R26*$^{YFP/+}$ cases), senescent β-catenin clusters with an active

SASP also form and recruit cells to the microenvironment. Absence of p53 and the SASP provide the advantages necessary for a YFP+ cell to outcompete their YFP- counterpart and to give rise to a YFP+ tumour. This YFP+ CSC could derive either from a cluster cell that escapes senescence or a non-cluster YFP+ cell that bypasses senescence. **(Right)** Loss of tumour suppressor *Apc* also leads to WNT pathway overactivation and the formation of senescent β-catenin-accumulating clusters, albeit with a dampened SASP. Lower SASP levels are not sufficient to recruit and maintain the undifferentiated phenotype of EMCN+/SOX9+ progenitors, which eventually downregulate SOX9 and become part of the normal pituitary vasculature. These differentiated cells are unable to respond to further SASP signals and cannot be primed to become the cell-of-origin. The absence of an expanded EMCN+/SOX9+ population also leads to reduced SDF-1 levels and thus, other inflammatory and pro-tumourigenic cell-types are not recruited into the microenvironment. Altogether, the absence of a primed cell-of-origin and the lack of a tumour-permissive microenvironment prevent tumour formation, either cell-autonomous or paracrine in origin.

6.6 Concluding remarks regarding non-cell autonomous tumourigenesis

In summary, this thesis provides strong evidence arguing that the mechanism of tumour formation occurring in mouse models of ACP does not fall in line with the cancer stem cell paradigm and follows instead a paracrine model of tumourigenesis.

Particularly, evidence is provided indicating that the β-catenin accumulating clusters present in *Hesx1*$^{Cre/+}$*;Ctnnb1*$^{lox(ex3)/+}$ mice and human ACP undergo senescence and accumulate DNA-damage, leading to the activation of NF-κB signalling and the SASP, a potent pro-tumourigenic signalling mechanism. Additionally, it is shown that the clusters in the mouse model and humans are similar structures both functionally and biologically, which makes a case for challenging the key pathways identified in this work to gain further insight into the mechanisms driving the development of ACP in humans, with the aim of identifying novel therapeutic targets in the future.

Altogether, evidence obtained through experiments conducted in *Hesx1*$^{Cre/+}$*;Ctnnb1*$^{lox(ex3)/+}$ (Chapter 3), *Hesx1*$^{Cre/+}$*;Ctnnb1*$^{lox(ex3)/+}$*;Trp53*$^{fl/fl}$ (Chapter 5) and *Hesx1*$^{Cre/+}$*;Apc*$^{fl/fl}$ mice (Chapter 7) suggests that acquisition of senescence in a targeted cell and a robust activation of the SASP are involved in the modification of the pituitary microenvironment that precedes non-cell autonomous tumourigenesis and the transformation of a non-targeted cell of origin. Possible underlying mechanisms could be: 1) the modification of the microenvironment is sufficient for paracrine tumourigenesis to proceed; 2) the SASP itself possesses transformation capabilities or 3) both a modified microenvironment and a direct effect of the SASP are necessary for tumour development. Current understanding of the role of chronic inflammation in carcinogenesis argues for the third option.

A great number of the cytokines recognised as hallmark SASP factors are known to act as growth factors, which can activate oncogenic pathways that lead to hyper proliferation and replicative stress. This replicative stress will inevitably lead to genomic instability, DNA damage and the acquisition of novel mutations. Additionally, recent research has uncovered the ability of the SASP to promote cell reprogramming, particularly through IL-6, (Mosteiro et al. 2016) and to increase intrinsic cellular plasticity and regeneration (Ritschka et al. 2017). In both cases, the SASP would cause the expansion of a pool of stem cell/progenitor cells and the likelihood of accumulating mutations. This would certainly be aided by the well described generation of a proinflammatory microenvironment. In such an environment, abnormal amounts of reactive-oxygen and nitrogen species would be produced, leading to DNA-damage either directly or through the activation of signalling pathways that also lead to hyper proliferation, such as the NF-κB pathway, and reinforcing replicative stress on the cell. Finally, the SASP could also affect the ability of the immune system to clear these stressed cells, further promoting the accumulation of pro tumourigenic mutations.

The data here collected argues that acquisition of senescence in a targeted cell and the robust activation of the SASP are potentially involved in the recruitment and paracrine transformation of a non-targeted cell-of-origin. In this sense, no studies to date have described this exact mechanism for the origin of tumours, although there is evidence indicating its applicability in other types of cancers. In a hepatocellular carcinoma model, the SASP was shown to remodel the immune response in order to induce tumours formed by non-targeted cells (Lujambio et al. 2013). Another study reported that expression of PDGF, a validated SASP factor (Demaria et al. 2014), lead to the formation of gliomas by non-targeted recruited cells, which eventually became transformed and formed gliomas even after transplantation (Fomchenko et al. 2011). Additionally, non-dividing epidermal cells carrying a MAPK transgene

induced non-targeted infiltrative cells to form skin papillomas upon injury. Importantly, this effect was mediated by the secretion of the hallmark SASP factor IL1A from targeted cells (Arwert et al. 2010). More recently, the SASP was shown to induce the emergence of cancer stem like cells in a multiple myeloma model (Cahu et al. 2012), while the SASP of senescent melanoma cells induced the reprogramming of naïve melanoma cells in order to form tumours (Ohanna et al. 2013).

In view of the potential applicability of the paracrine model to other cancers, it will be particularly interesting to study the role of senescence and the SASP in models where the non-cell autonomous origin of tumours/cancers has been described, especially those driven by oncogenic β-catenin/WNT signalling (Kode et al. 2014; Deschene et al. 2014; Xavier et al. 2015; Kretzschmar et al. 2016). Also, the results obtained in this thesis warn against the idea that OIS has exclusively beneficial roles in tumourigenesis, which derived from the simple observation that premalignant cancers display high levels of senescence markers, while fully malignant cancers do not (Braig et al. 2005; Chen et al. 2005; Collado et al. 2005; Michaloglou et al. 2005). Therefore, further study of the role of OIS and the SASP in cancer development is encouraged in light of lineage-tracing experiments, as senescent cells carrying driver mutations might not be related to the cell that eventually generates a tumour. A re-evaluation of the origin of tumours in different models of cancer by using lineage tracing strategies, while keeping in mind paracrine mechanisms of tumour development and the detrimental effects the SASP will allow the development of better targeted therapies for human cancers, as this study and several others (Campisi 2013) suggest that senescence is, indeed, a double edged-sword.

7. APPENDIX: THE ROLE OF SENESCENCE AND THE SASP IN THE CONTEXT OF WILD-TYPE β-CATENIN

In the following appendix, ongoing research and preliminary data regarding *Hesx1*$^{Cre/+;}$*Apc*$^{fl/fl}$ mice will be presented in order to facilitate the discussion of the results presented in this thesis.

7.1 Ablation of the tumour suppressor APC leads to WNT pathway activation and senescence induction in β-catenin clusters, but not to tumour formation.

Previously, the host lab generated *Hesx1*$^{Cre/+;}$*Apc*$^{fl/fl}$ mice, in which expression of the tumour suppressor *Apc* is ablated in pituitary embryonic progenitors (*Hesx1* cell-lineage). These experiments aimed to answer the following research question: Does ACP tumorigenesis require the activation of the WNT pathway or the expression of oncogenic β-catenin?

As described in the introduction chapter, APC is a crucial component of the β-catenin destruction complex and mutations in *Apc* lead to stabilization and accumulation of β-catenin, resulting in overall activation of the WNT-signalling pathway. Therefore, *Hesx1*$^{Cre/+;}$*Apc*$^{fl/fl}$ mice activate the WNT pathway, as the *Hesx1*$^{Cre/+;}$*Ctnnb1*$^{lox(ex3)/+}$ mice do, but this activation is caused by wild-type β-catenin rather than its oncogenic version (i.e. lacking the amino acids encoded by exon 3).

Similarly to *Hesx1*$^{Cre/+;}$*Ctnnb1*$^{lox(ex3)/+}$ mice, the embryonic pituitaries of *Hesx1*$^{Cre/+;}$*Apc*$^{fl/fl}$ at 18.5 dpc displayed nucleo-cytoplasmic β-catenin accumulating clusters (Fig. 7.2a). which also displayed WNT pathway activation as shown by increased expression of WNT-target gene *Axin2* (Fig. 7.1b). The clusters found in *Hesx1*$^{Cre/+;}$*Apc*$^{fl/fl}$ pituitaries were of smaller size relative to the *Hesx1*$^{Cre/+;}$*Ctnnb1*$^{lox(ex3)/+}$ (i.e. composed by less cells) at all observed stages (10.5, 12.5 and 18.5 dpc). At 18.5 dpc, there was a significant difference in cluster cell number (t test, $p<0.0001$), as *Hesx1*$^{Cre/+;}$*Ctnnb1*$^{lox(ex3)/+}$ clusters had in average 5.9 cells (126 clusters counted), while *Hesx1*$^{Cre/+;}$*Apc*$^{fl/fl}$ clusters had 1.9 cells (108 clusters counted).

Litters born from *Hesx1*$^{Cre/+}$;*Apc*$^{fl/+}$ and *Hesx1*$^{+/+}$;*Apc*$^{fl/fl}$ breeding pairs displayed normal Mendelian ratios, indicating absence of perinatal lethality. Additionally, all mice displayed normal size and weight (Neda Mousavy, unpublished results), in contrast to the perinatal dwarfism found in *Hesx1*$^{Cre/+;}$*Ctnnb1*$^{lox(ex3)/+}$ mice (Gaston-Massuet, 2011). ISH on 12.5 dpc embryos demonstrated normal expression patterns between mutants and controls for pituitary fate determination factor *Lhx3,* and pituitary lineage commitment genes *Pit1* and *Prop1* (Fig. 7.1d). At 18.5 dpc *Hesx1*$^{Cre/+;}$*Apc*$^{fl/fl}$ pituitaries were hyperplastic, similarly to *Hesx1*$^{Cre/+;}$*Ctnnb1*$^{lox(ex3)/+}$ pituitaries. However, differentiation of the hormone-producing cells was normal, as determined by the expression of GH, PIT1, and ACTH (Fig. 7.1e). This is in contrast with *Hesx1*$^{Cre/+;}$*Ctnnb1*$^{lox(ex3)/+}$ pituitaries at the same stage, where the *Pit1* lineage was severely affected (Gaston-Massuet et al. 2011).

Intriguingly, no *Hesx1*$^{Cre/+;}$*Apc*$^{fl/fl}$ animals developed tumours postnatally (Fig. 7.1f, n= 39) and were fertile and viable up to almost 2 years follow-up (n= 17) . In fact, the colony was maintained through *Hesx1*$^{Cre/+;}$*Apc*$^{fl/fl}$ animals. Additionally, examination of the early postnatal pituitary revealed they did not contain β-catenin accumulating clusters (Neda Mousavy, unpublished results) nor pre-neoplastic regions as in the case of *Hesx1*$^{Cre/+;}$*Ctnnb1*$^{lox(ex3)/+}$ mice (Fig. 7.1f).

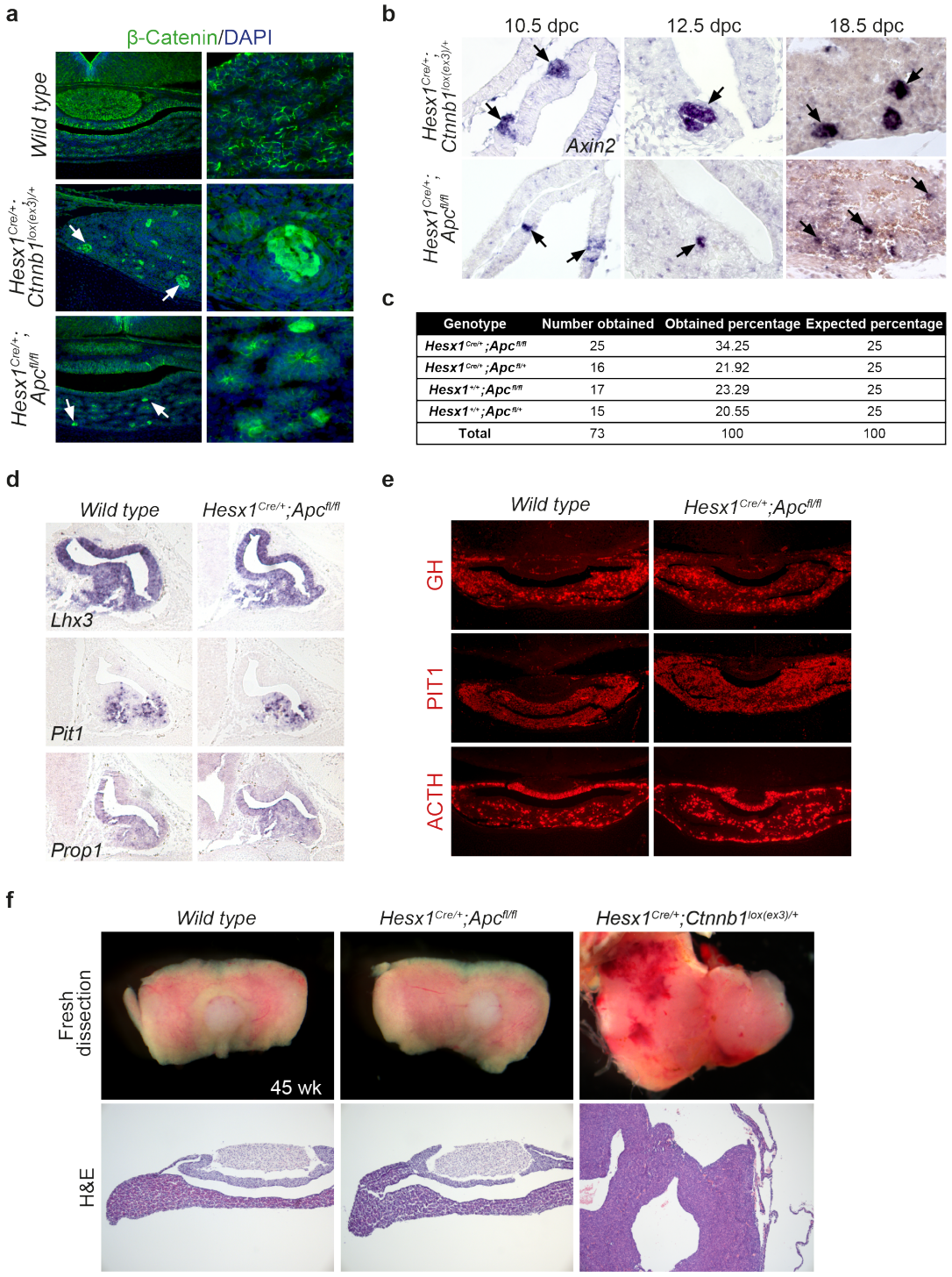

Genotype	Number obtained	Obtained percentage	Expected percentage
Hesx1$^{Cre/+}$;*Apc*$^{fl/fl}$	25	34.25	25
Hesx1$^{Cre/+}$;*Apc*$^{fl/+}$	16	21.92	25
Hesx1$^{+/+}$;*Apc*$^{fl/fl}$	17	23.29	25
Hesx1$^{+/+}$;*Apc*$^{fl/+}$	15	20.55	25
Total	73	100	100

Fig 7.1 Phenotypic characterisation of *Hesx1*$^{Cre/+}$;*Apc*$^{fl/fl}$ mice and pituitaries.

(a) Immunofluorescence for β-catenin in wild type, *Hesx1*$^{Cre/+}$;*Ctnnb1*$^{lox(ex3)/+}$ and *Hesx1*$^{Cre/+}$;*Apc*$^{fl/fl}$ pituitaries at 18.5 dpc. Nucleo-cytoplasmic β-catenin accumulating clusters are also observed in *Hesx1*$^{Cre/+}$;*Apc*$^{fl/fl}$ mutants but in lower numbers and of smaller size than *Hesx1*$^{Cre/+}$;*Ctnnb1*$^{lox(ex3)/+}$ clusters. **(b)** *In situ* hybridisation (ISH)

showing overexpression of the WNT pathway target gene, *Axin2,* at different stages of development in clusters of both *Hesx1*$^{Cre/+}$*;Ctnnb1*$^{lox(ex3)/+}$ and *Hesx1*$^{Cre/+}$*;Apc*$^{fl/fl}$ pituitaries. **(c)** Table showing normal Mendelian ratios for crosses between *Hesx1*$^{Cre/+}$*;Apc*$^{fl/+}$ and *Hesx1*$^{+/+}$*;Apc*$^{fl/fl}$ mice (Chi-square test, P>0.05, N=73). **(d)** ISH shows normal expression of pituitary lineage determination and differentiation factors *Lhx3*, *Pit1* and *Prop1* in *Hesx1*$^{Cre/+}$*;Apc*$^{fl/fl}$ *pituitaries at* 12.5 dpc. (e) Immunofluorescence for growth hormone (GH), PIT1 and Adrenocorticotropic (ACTH) shows normal terminal differentiation of *Hesx1*$^{Cre/+}$*;Apc*$^{fl/fl}$ pituitaries at 18.5 dpc. **(f)** Wild type and *Hesx1*$^{Cre/+}$*;Apc*$^{fl/fl}$ pituitaries at 45 weeks of age show normal morphology and histology (H&E staining shown) unlike *Hesx1*$^{Cre/+}$*;Ctnnb1*$^{lox(ex3)/+}$ specimens of the same age which already showed developing tumours.

Further characterisation of the embryonic *Hesx1*$^{Cre/+;}$*Apc*$^{fl/fl}$ clusters revealed they are similar to their *Hesx1*$^{Cre/+;}$*Ctnnb1*$^{lox(ex3)/+}$ counterparts as they were also negative for proliferation and apoptosis markers. Additionally, they were also found to contain SOX2+ cells and to not express SOX9+ (Fig. 7.2a), suggesting the clusters present in *Hesx1*$^{Cre/+;}$*Apc*$^{fl/fl}$ and *Hesx1*$^{Cre/+;}$*Ctnnb1*$^{lox(ex3)/+}$ pituitaries share some features in their cellular and molecular phenotype.

A thorough analysis for molecular markers of senescence revealed that *Hesx1*$^{Cre/+;}$*Apc*$^{fl/fl}$ clusters also accumulate markers of the senescent phenotype such as those related to cell cycle inhibition (p21 and p16) and the DNA-Damage Response (phospho-DNA-PKCs and PARP-1). Moreover, *Hesx1*$^{Cre/+;}$*Apc*$^{fl/fl}$ clusters displayed accumulation of phospho-Iκ-Bα, indicating activation of the NF-κB pathway (Fig. 7.2b). Therefore, *Hesx1*$^{Cre/+;}$*Apc*$^{fl/fl}$ embryonic pituitaries also contain nucleo-cytoplasmic β-catenin accumulating clusters which become senescent and activate the NF-κB pathway.

In order to explain the absence of oncogenic potential, the strength of the SASP induction was compared between *Hesx1*$^{Cre/+;}$*Apc*$^{fl/fl}$ and *Hesx1*$^{Cre/+;}$*Ctnnb1*$^{lox(ex3)/+}$clusters. The expression of key senescence markers and secreted factors was analysed by qRT-PCR in *Hesx1*$^{Cre/+;}$*Ctnnb1*$^{lox(ex3)/+}$ and *Hesx1*$^{Cre/+}$*;Apc*$^{fl/fl}$ pituitaries at 18.5 dpc (Fig. 7.2c). Markers analysed were *Axin2, Trp53, Cdkn1a, Cdkn2a, Shh, Bmp4, Il1a, Il1b, Cxcl1* and *Tgfb1*. Although *Hesx1*$^{Cre/+;}$*Ctnnb1*$^{lox(ex3)/+}$ pituitaries displayed higher expression for all markers when compared to *Hesx1*$^{Cre/+}$*;Apc*$^{fl/fl}$, only *Cdkn2a, Shh, Bmp4, Il1a* and *Il1b* displayed statistically significant differences. The expression of secretory factors such as *Shh* and *Bmp4* was previously shown to be upregulated in the β-catenin clusters of *Hesx1*$^{Cre/+;}$*Ctnnb1*$^{lox(ex3)/+}$ pituitaries (Andoniadou et al. 2012). *In situ* hybridisation in 14.5 dpc *Hesx1*$^{Cre/+;}$*Ctnnb1*$^{lox(ex3)/+}$ pituitaries showed that *Axin2*-overexpressing clusters corresponded with the overexpression of *Bmp4, Fgf3* and *Shh* in consecutive sections. Conversely, *Hesx1*$^{Cre/+}$*;Apc*$^{fl/fl}$ pituitaries also displayed *Axin2* overexpressing clusters, but *Bmp4, Fgf3* and *Shh* signal could not be detected at the 14.5 dpc stage (Fig. 7.2d), while they were barely expressed at 18.5 dpc (not shown). These results suggest that *Hesx1*$^{Cre/+}$*;Apc*$^{fl/fl}$ clusters display a dampened SASP signature. Additionally, their reduced numbers and smaller individual size might result in an overall diminished presence of secretory factors.

In chapter 3 it was shown that a population of EMCN+/SOX9^{high} cells interacts closely with the β-catenin clusters early in development, expand profusely and occupy most of the pituitary stroma up to 18.5 dpc. Interestingly, triple immunostaining for EMCN, SOX9 and β-catenin at 14.5 and 18.5 dpc showed that *Hesx1*$^{Cre/+}$*;Apc*$^{fl/fl}$ pituitaries lack this EMCN+/SOX9^{high} population. Instead, the stroma of *Hesx1*$^{Cre/+}$*;Apc*$^{fl/fl}$ pituitaries resembled more that of the wild-type pituitary, as EMCN+ cells were located only in the developing vasculature, did not form rings around the clusters and few expressed SOX9 (Fig. 7.2e). Additionally, quantification of the total

area occupied by EMCN+ cells (3 sections per pituitary, n=3) showed the absence of statistical difference in EMCN+ area between wild type and *Hesx1*$^{Cre/+}$;*Apc*$^{fl/fl}$ pituitaries, while a statistically significant difference was found when compared to *Hesx1*$^{Cre/+;}$*Ctnnb1*$^{lox(ex3)/+}$ and *Hesx1*$^{Cre/+;}$*Ctnnb1*$^{lox(ex3)/+}$;*Trp53*$^{fl/fl}$ pituitaries, which develop tumours postnatally (Fig. 7.2f). These results further support a role for the SASP in the remodelling of the microenvironment, including recruiting and maintaining large numbers of EMCN+/SOX9^{high} cells in early stages of tumourigenesis. Of note, β-catenin accumulating clusters of larger size were found occasionally in *Hesx1*$^{Cre/+}$;*Apc*$^{fl/fl}$ pituitaries (2-3 clusters, n=6 pituitaries). These clusters resembled more their *Hesx1*$^{Cre/+;}$*Ctnnb1*$^{lox(ex3)/+}$ counterparts and interestingly, were surrounded by rings of SOX9+^{high} cells, suggesting that cluster size might also determine an effect of the microenvironment (Fig. 7.2g).

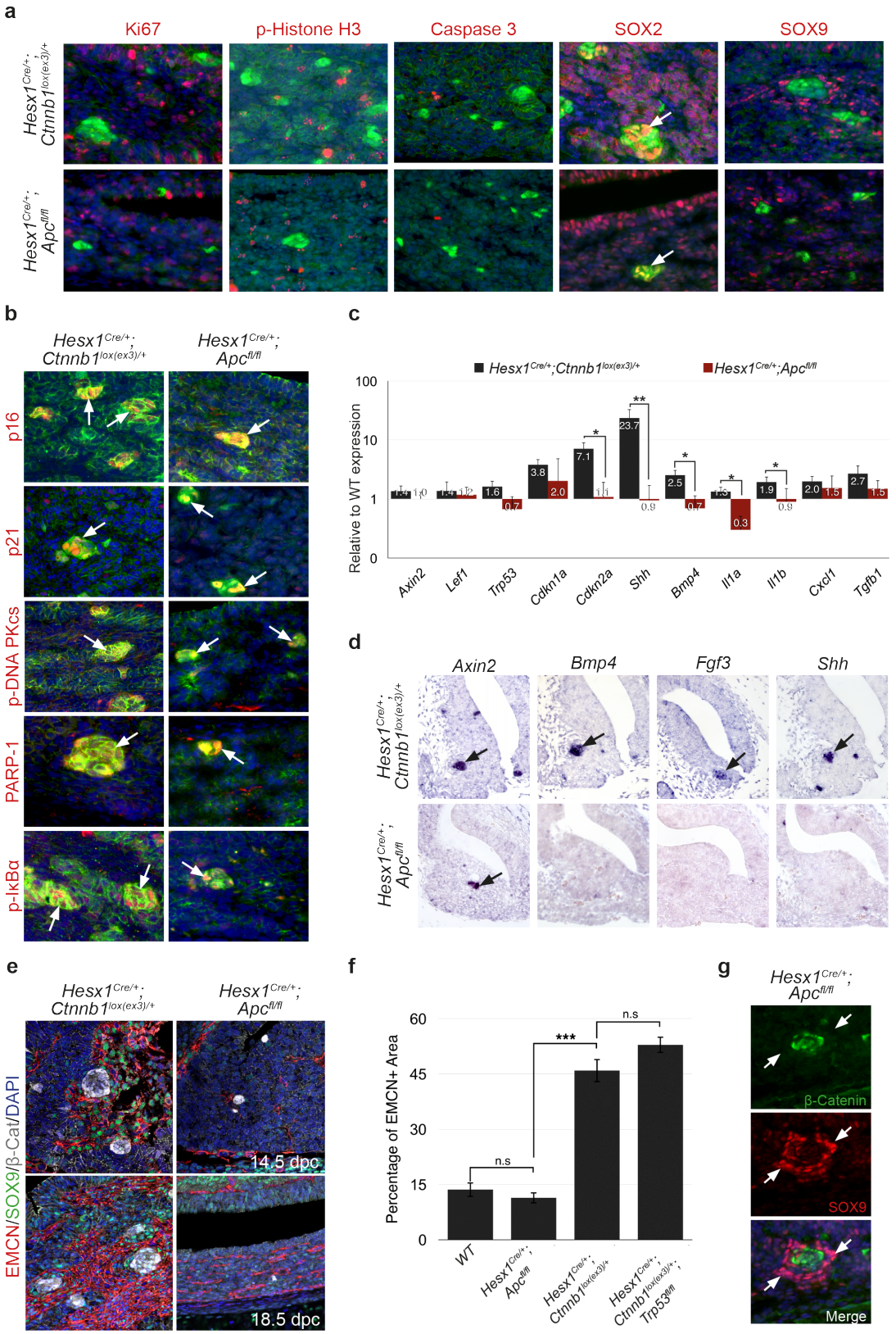

Fig. 7.2 Characterisation of the β-catenin clusters of *Hesx1*$^{Cre/+}$;*Apc*$^{fl/fl}$ embryos.

(a) Double immunostaining for β-catenin together with Ki67, phosphorylated Histone H3 and cleaved Caspase 3, shows that the *Hesx1*$^{Cre/+}$;*Apc*$^{fl/fl}$ clusters are also do not proliferate and do not undergo apoptosis. Additionally, the clusters from

Hesx1$^{Cre/+}$*;Ctnnb1*$^{lox(ex3)/+}$ and *Hesx1*$^{Cre/+}$*;Apc*$^{fl/fl}$ share the expression of stem cell marker SOX2 but rarely express SOX9. **(b)** Double fluorescent immunostaining for β-catenin and markers of senescence activation. *Hesx1*$^{Cre/+}$*;Apc*$^{fl/fl}$ clusters also display accumulation of p21, p16, phosphorylated DNA-PKcs, PARP-1 and phosphorylated Iκ-Bα, indicating cell cycle arrest, an active DNA-damage-response and activation of the NF-κB pathway, respectively. **(c)** qRT-PCR comparing the expression of senescence and SASP markers in *Hesx1*$^{Cre/+}$*;Ctnnb1*$^{lox(ex3)/+}$ and *Hesx1*$^{Cre/+}$*;Apc*$^{fl/fl}$ pituitaries at 18.5 dpc in comparison to wild types. **(d)** *In situ* hybridisation for secretory growth factors in 14.5 dpc *Hesx1*$^{Cre/+}$*;Ctnnb1*$^{lox(ex3)/+}$ and *Hesx1*$^{Cre/+}$*;Apc*$^{fl/fl}$ pituitaries. *Axin2* is a target of the WNT pathway and therefore is overexpressed in β-catenin clusters. Consecutive sections are shown. **(e)** Triple immunostaining for EMCN, SOX9 and β-catenin in 14.5 and 18.5 dpc pituitaries showing the absence of EMCN/SOX9^{high} swarms around the β-catenin in *Hesx1*$^{Cre/+}$*;Apc*$^{fl/fl}$ pituitaries at both stages. **(f)** Quantification of the total area occupied by EMCN+ cells (3 different sections per pituitary analyses, n=3, ANOVA, *** denotes $p<0.001$). **(g)** Double immunostaining for β-catenin and SOX9 shows the rare presence of larger clusters in *Hesx1*$^{Cre/+}$*;Apc*$^{fl/fl}$ pituitaries which were also surrounded by SOX9+^{high} cells (~2 of such clusters observed in 6 pituitaries).

BIBLIOGRAPHY

Aaronson, S.A., 1991. Growth factors and cancer. *Science (New York, N.Y.)*, 254(5035), pp.1146–53. Available at: http://www.ncbi.nlm.nih.gov/pubmed/1659742 [Accessed August 11, 2016].

Acosta, J.C. et al., 2013. A complex secretory program orchestrated by the inflammasome controls paracrine senescence. *Nature cell biology*, 15(8), pp.978–90. Available at: http://www.pubmedcentral.nih.gov/articlerender.fcgi?artid=3732483&tool=pmcentrez&rendertype=abstract [Accessed August 6, 2013].

Acosta, J.C. et al., 2008. Chemokine signaling via the CXCR2 receptor reinforces senescence. *Cell*, 133(6), pp.1006–18. Available at: http://www.ncbi.nlm.nih.gov/pubmed/18555777 [Accessed February 1, 2013].

Acosta, J.C. & Gil, J., 2009. A role for CXCR2 in senescence, but what about in cancer? *Cancer research*, 69(6), pp.2167–70. Available at: http://www.ncbi.nlm.nih.gov/pubmed/19276354 [Accessed February 1, 2013].

Adam, R.C. et al., 2015. Pioneer factors govern super-enhancer dynamics in stem cell plasticity and lineage choice. *Nature*, 521(7552), pp.366–370. Available at: http://www.nature.com/doifinder/10.1038/nature14289 [Accessed September 5, 2016].

Aird, K.M. et al., 2015. ATM Couples Replication Stress and Metabolic Reprogramming during Cellular Senescence. *Cell reports*, 11(6), pp.893–901. Available at: http://www.sciencedirect.com/science/article/pii/S2211124715003897.

Akiyama, H. et al., 2004. Essential role of Sox9 in the pathway that controls formation of cardiac valves and septa. *Proceedings of the National Academy of Sciences of the United States of America*, 101(17), pp.6502–7. Available at: http://www.ncbi.nlm.nih.gov/pubmed/15096597 [Accessed August 5, 2016].

Aliouat-Denis, C.C.-M. et al., 2005. p53-Independent Regulation of p21 Expression and Senescence by Chk2. *Mol Cancer Res*, 3(11), pp.627–34.

Anastas, J.N. & Moon, R.T., 2013. WNT signalling pathways as therapeutic targets in cancer. *Nature Reviews Cancer*, 13(1), pp.11–26. Available at: http://www.ncbi.nlm.nih.gov/pubmed/23258168%5Cnhttp://www.nature.com/doifinder/10.1038/nrc3419.

Ancrile, B., Lim, K.-H. & Counter, C.M., 2007. Oncogenic Ras-induced secretion of IL6 is required for tumorigenesis. *Genes & development*, 21(14), pp.1714–9. Available at: http://www.ncbi.nlm.nih.gov/pubmed/17639077 [Accessed August 18, 2016].

Andoniadou, C.L. et al., 2011. HESX1- and TCF3-mediated repression of Wnt/ B-catenin targets is required for normal development of the anterior forebrain. *Development*, 4942, pp.4931–4942. Available at: http://dev.biologists.org/cgi/doi/10.1242/dev.066597 [Accessed October 18, 2011].

Andoniadou, C.L. et al., 2012. Identification of novel pathways involved in the pathogenesis of human adamantinomatous craniopharyngioma. *Acta neuropathologica*. Available at: http://www.ncbi.nlm.nih.gov/pubmed/22349813 [Accessed March 17, 2012].

Andoniadou, C.L. et al., 2013. The Sox2 + population of the adult murine pituitary includes progenitor / stem cells with tumour-inducing potential. *Cell stem cell*, 13(433–445).

Aquilina, K. et al., 2010. Malignant transformation of irradiated craniopharyngioma in children: report of 2 cases. *Journal of neurosurgery. Pediatrics*, 5(2), pp.155–61. Available at: http://www.ncbi.nlm.nih.gov/pubmed/20121363 [Accessed August 10, 2016].

Ara, T. et al., 2003. Impaired colonization of the gonads by primordial germ cells in mice lacking a chemokine, stromal cell-derived factor-1 (SDF-1). *Proceedings of the National Academy of Sciences of the United States of America*, 100(9), pp.5319–23. Available at: http://www.pubmedcentral.nih.gov/articlerender.fcgi?artid=154343&tool=pmcentrez&rendertype=abstract.

Arwert, E.N. et al., 2010. Tumor formation initiated by nondividing epidermal cells via an inflammatory infiltrate. *Proceedings of the National Academy of Sciences of the United States of America*, 107(46), pp.19903–19908. Available at: http://www.ncbi.nlm.nih.gov/pubmed/21041641 [Accessed July 10, 2016].

Austinat, M. et al., 2008. Correlation between β-catenin mutations and expression of Wnt-signaling target genes in hepatocellular carcinoma. *Molecular Cancer*, 7(1), p.21. Available at: http://molecular-cancer.biomedcentral.com/articles/10.1186/1476-4598-7-21 [Accessed September 5, 2016].

Bajoghli, B., 2013. Evolution and function of chemokine receptors in the immune system of lower vertebrates. *European Journal of Immunology*, 43(7), pp.1686–1692. Available at: http://doi.wiley.com/10.1002/eji.201343557 [Accessed August 16, 2016].

Baker, D.J. et al., 2011. Clearance of p16Ink4a-positive senescent cells delays ageing-associated disorders. *Nature*, 479(7372), pp.232–236. Available at: http://www.nature.com/doifinder/10.1038/nature10600 [Accessed August 17, 2016].

Baker, D.J. et al., 2016. Naturally occurring p16 Ink4a -positive cells shorten healthy lifespan. *Nature*, pp.1–20. Available at: http://dx.doi.org/10.1038/nature16932.

Balabanian, K. et al., 2012. Proper desensitization of CXCR4 is required for lymphocyte development and peripheral compartmentalization in mice. *Blood*, 119(24), pp.5722–30. Available at: http://www.ncbi.nlm.nih.gov/pubmed/22438253 [Accessed August 19, 2013].

Barbieri, F. et al., 2014. Emerging targets in pituitary adenomas: Role of the CXCL12/CXCR4-R7 system. *International Journal of Endocrinology*, 2014.

Barbieri, F. et al., 2008. Overexpression of stromal cell-derived factor 1 and its receptor CXCR4 induces autocrine/paracrine cell proliferation in human pituitary adenomas. *Clinical cancer research : an official journal of the American Association for Cancer Research*, 14(16), pp.5022–32. Available at: http://www.ncbi.nlm.nih.gov/pubmed/18698020 [Accessed November 3, 2011].

Barbieri, F. et al., 2007. Role of stromal cell-derived factor 1 (SDF1/CXCL12) in regulating anterior pituitary function. *Journal of molecular endocrinology*, 38(3), pp.383–9. Available at: http://www.ncbi.nlm.nih.gov/pubmed/17339401 [Accessed June 15, 2011].

Bartkova, J. et al., 2006. Oncogene-induced senescence is part of the tumorigenesis barrier imposed by DNA damage checkpoints. *Nature*, 444(November), pp.633–637.

Bavik, C. et al., 2006. The gene expression program of prostate fibroblast senescence modulates neoplastic epithelial cell proliferation through paracrine mechanisms. *Cancer research*, 66(2), pp.794–802. Available at: http://www.ncbi.nlm.nih.gov/pubmed/16424011 [Accessed November 12, 2014].

Beauséjour, C.M. et al., 2003. Reversal of human cellular senescence: roles of the p53 and p16 pathways. *The EMBO journal*, 22(16), pp.4212–22. Available at: http://www.pubmedcentral.nih.gov/articlerender.fcgi?artid=175806&tool=pmcentrez&rendertype=abstract.

Beck, B. & Blanpain, C., 2013. Unravelling cancer stem cell potential. *Nature Reviews Cancer*, 13(10), pp.727–738. Available at: http://www.nature.com/doifinder/10.1038/nrc3597.

Bieging, K.T., Mello, S.S. & Attardi, L.D., 2014. Unravelling mechanisms of p53-mediated tumour suppression. *Nature Reviews Cancer*, 14(5), pp.359–370. Available at: http://www.nature.com/doifinder/10.1038/nrc3711.

Bilodeau, S., Roussel-Gervais, A. & Drouin, J., 2009. Distinct developmental roles of cell cycle inhibitors p57Kip2 and p27Kip1 distinguish pituitary progenitor cell cycle exit from cell cycle reentry of differentiated cells. *Molecular and cellular biology*, 29(7), pp.1895–908. Available at: http://www.pubmedcentral.nih.gov/articlerender.fcgi?artid=2655618&tool=pmcentrez&rendertype=abstract [Accessed July 21, 2011].

Bodmer, W.F. et al., 1987. Localization of the gene for familial adenomatous polyposis on

chromosome 5. *Nature*, 328(6131), pp.614–6. Available at: http://www.ncbi.nlm.nih.gov/pubmed/3039373 [Accessed August 15, 2016].

Bodnar, A.G. et al., 1998. Extension of life-span by introduction of telomerase into normal human cells. *Science (New York, N.Y.)*, 279(5349), pp.349–52. Available at: http://www.ncbi.nlm.nih.gov/pubmed/9454332 [Accessed September 5, 2016].

Bonner, W.M. et al., 2008. γH2AX and cancer. *Nature Reviews Cancer*, 8(12), pp.957–967.

Brachtendorf, G. et al., 2001. Early expression of endomucin on endothelium of the mouse embryo and on putative hematopoietic clusters in the dorsal aorta. *Developmental dynamics : an official publication of the American Association of Anatomists*, 222(3), pp.410–9. Available at: http://www.ncbi.nlm.nih.gov/pubmed/11747076 [Accessed September 26, 2013].

Braig, M. et al., 2005. Oncogene-induced senescence as an initial barrier in lymphoma development. *Nature*, 436(August).

Brastianos, P.K. et al., 2014. Exome sequencing identifies BRAF mutations in papillary craniopharyngiomas. *Nature genetics*, 46(2), pp.161–5. Available at: http://www.nature.com/doifinder/10.1038/ng.2868.

Bunin, G.R. et al., 1998. The descriptive epidemiology of craniopharyngioma. *Journal of neurosurgery*, 89(4), pp.547–51. Available at: http://www.ncbi.nlm.nih.gov/pubmed/9761047 [Accessed August 9, 2016].

Burd, C.E. et al., 2013. Monitoring Tumorigenesis and Senescence In Vivo with a p16INK4a-Luciferase Model. *Cell*, 152(1), pp.340–351.

Burger, J.A. & Kipps, T.T.J., 2006. CXCR4: a key receptor in the crosstalk between tumor cells and their microenvironment. *Blood*, 107(5), pp.1761–1767. Available at: http://www.ncbi.nlm.nih.gov/pubmed/16269611 [Accessed June 20, 2011].

Burger, J.A. & Peled, A., 2009. CXCR4 antagonists: targeting the microenvironment in leukemia and other cancers. *Leukemia*, 23(1), pp.43–52. Available at: http://www.nature.com/doifinder/10.1038/leu.2008.299 [Accessed September 1, 2016].

Burton, D.G.A. & Faragher, R.G.A., 2015. Cellular senescence: from growth arrest to immunogenic conversion. *AGE*, 37(2), p.27. Available at: http://link.springer.com/10.1007/s11357-015-9764-2 [Accessed September 1, 2016].

Busillo, J.M. & Benovic, J.L., 2007. Regulation of CXCR4 Signaling. *Biochimica et Biophysica Acta*, 1768(4), pp.952–963.

Buslei, R. et al., 2005. Common mutations of beta-catenin in adamantinomatous craniopharyngiomas but not in other tumours originating from the sellar region. *Acta neuropathologica*, 109(6), pp.589–97. Available at: http://www.ncbi.nlm.nih.gov/pubmed/15891929 [Accessed July 10, 2016].

Buslei, R. et al., 2007. Nuclear beta-catenin accumulation associates with epithelial morphogenesis in craniopharyngiomas. *Acta neuropathologica*, 113(5), pp.585–90. Available at: http://www.ncbi.nlm.nih.gov/pubmed/17221204 [Accessed June 4, 2014].

Bussmann, J., Wolfe, S. a & Siekmann, A.F., 2011. Arterial-venous network formation during brain vascularization involves hemodynamic regulation of chemokine signaling. *Development (Cambridge, England)*, 138(9), pp.1717–26. Available at: http://www.pubmedcentral.nih.gov/articlerender.fcgi?artid=3074448&tool=pmcentrez&rendertype=abstract [Accessed March 17, 2013].

Cahu, J., Bustany, S. & Sola, B., 2012. Senescence-associated secretory phenotype favors the emergence of cancer stem-like cells. *Cell death & disease*, 3(12), p.e446. Available at: http://www.pubmedcentral.nih.gov/articlerender.fcgi?artid=3542619&tool=pmcentrez&rendertype=abstract [Accessed November 24, 2014].

Campisi, J., 2013. Aging, Cellular Senescence, and Cancer. *Annual Review of Physiology*, 75(1), pp.685–705. Available at: http://www.annualreviews.org/doi/abs/10.1146/annurev-physiol-030212-183653.

Canino, C. et al., 2012. SASP mediates chemoresistance and tumor-initiating-activity of mesothelioma cells. *Oncogene*, 31(26), pp.3148–63. Available at: http://www.ncbi.nlm.nih.gov/pubmed/22020330 [Accessed July 16, 2014].

Cano, D. a., Soto-Moreno, A. & Leal-Cerro, A., 2014. Genetically Engineered Mouse Models of Pituitary Tumors. *Frontiers in Oncology*, 4(August), pp.1–10. Available at: http://journal.frontiersin.org/article/10.3389/fonc.2014.00203/abstract.

Cao, J. et al., 2010. Expression of aberrant beta-catenin and impaired p63 in craniopharyngiomas. *British journal of neurosurgery*, 24(3), pp.249–56. Available at: http://www.ncbi.nlm.nih.gov/pubmed/20128632.

Castilho, R.M. et al., 2009. mTOR mediates Wnt-induced epidermal stem cell exhaustion and aging. *Cell stem cell*, 5(3), pp.279–89. Available at: http://www.sciencedirect.com/science/article/pii/S1934590909003014 [Accessed July 25, 2014].

Castinetti, F. et al., 2011. Pituitary stem cell update and potential implications for treating hypopituitarism. *Endocrine reviews*, 32(4), pp.453–71. Available at: http://www.ncbi.nlm.nih.gov/pubmed/21493869 [Accessed October 29, 2011].

Cavallero, S. et al., 2015. CXCL12 Signaling Is Essential for Maturation of the Ventricular Coronary Endothelial Plexus and Establishment of Functional Coronary Circulation. *Developmental Cell*, 33(4), pp.469–477.

Chan, C.-H.H. et al., 2011. Novel ARF/p53-independent senescence pathways in cancer repression. *Journal of Molecular Medicine*, 89(9), pp.857–867. Available at: http://www.ncbi.nlm.nih.gov/pubmed/21594579 [Accessed July 25, 2016].

Chang, J. et al., 2016. Clearance of senescent cells by ABT263 rejuvenates aged hematopoietic stem cells in mice. *Nature Medicine*, 22(1), pp.78–83. Available at: http://www.ncbi.nlm.nih.gov/pubmed/26657143.

Chauvet, N. et al., 2009. Characterization of adherens junction protein expression and localization in pituitary cell networks. *The Journal of endocrinology*, 202(3), pp.375–87. Available at: http://www.ncbi.nlm.nih.gov/pubmed/19505949 [Accessed February 1, 2013].

Chen, J. et al., 2009. Pituitary progenitor cells tracked down by side population dissection. *Stem Cells*, 27(5), pp.1182–1195. Available at: http://www.ncbi.nlm.nih.gov/pubmed/19418455 [Accessed July 10, 2016].

Chen, Z. et al., 2005. Crucial role of p53-dependent cellular senescence in suppression of Pten-deficient tumorigenesis. *Nature*, 436(7051), pp.725–30. Available at: http://www.pubmedcentral.nih.gov/articlerender.fcgi?artid=1939938&tool=pmcentrez&rendertype=abstract [Accessed August 18, 2013].

Cheung, M. & Briscoe, J., 2003. Neural crest development is regulated by the transcription factor Sox9. *Development (Cambridge, England)*, 130(23), pp.5681–93. Available at: http://www.ncbi.nlm.nih.gov/pubmed/14522876 [Accessed August 5, 2016].

Chien, Y. et al., 2011. Control of the senescence-associated secretory phenotype by NF-κB promotes senescence and enhances chemosensitivity. *Genes & development*, 25(20), pp.2125–36. Available at: http://www.pubmedcentral.nih.gov/articlerender.fcgi?artid=3205583&tool=pmcentrez&rendertype=abstract [Accessed May 30, 2014].

Choo, A.Y. et al., 2008. Rapamycin differentially inhibits S6Ks and 4E-BP1 to mediate cell-type-specific repression of mRNA translation. *Proceedings of the National Academy of Sciences*, 105(45), pp.17414–17419. Available at: http://www.pnas.org/cgi/doi/10.1073/pnas.0809136105 [Accessed August 30, 2016].

Christoffersen, N.R. et al., 2010. p53-independent upregulation of miR-34a during oncogene-induced senescence represses MYC. *Cell Death and Differentiation*, 17, pp.236–245. Available at: http://www.nature.com/doifinder/10.1038/cdd.2009.109 [Accessed September 2, 2016].

Cipriano, R. et al., 2011. TGF-β signaling engages an ATM-CHK2-p53–independent RAS-induced senescence and prevents malignant transformation in human mammary epithelial cells. *Proceedings of the National Academy of Sciences*, 108(21), pp.8668–8673. Available at: http://www.pnas.org/cgi/doi/10.1073/pnas.1015022108 [Accessed July 25, 2016].

Clarke, M.F. & Fuller, M., 2006. Stem cells and cancer: two faces of eve. *Cell*, 124(6), pp.1111–5. Available at: http://www.ncbi.nlm.nih.gov/pubmed/16564000 [Accessed July 10, 2016].

Clevers, H., 2011. The cancer stem cell: premises, promises and challenges. *Nature medicine*, 17(3), pp.313–9. Available at: http://www.ncbi.nlm.nih.gov/pubmed/21386835 [Accessed July 10, 2016].

Clevers, H., Loh, K.M. & Nusse, R., 2014. Stem cell signaling. An integral program for tissue renewal and regeneration: Wnt signaling and stem cell control. *Science (New York, N.Y.)*, 346(6205), p.1248012. Available at: http://www.ncbi.nlm.nih.gov/pubmed/25278615.

Colavitti, R. & Finkel, T., 2005. Reactive oxygen species as mediators of cellular senescence. *IUBMB life*, 57(4–5), pp.277–281.

Collado, M. et al., 2005. Senescence in premalignant tumours. *Nature*, 436(August), p.642.

Collado, M. & Serrano, M., 2010. Senescence in tumours: evidence from mice and humans. *Nature reviews. Cancer*, 10(1), pp.51–7. Available at: http://www.pubmedcentral.nih.gov/articlerender.fcgi?artid=3672965&tool=pmcentrez&rendertype=abstract [Accessed July 11, 2014].

Coppé, J.-P., Patil, C.K., et al., 2010. A human-like senescence-associated secretory phenotype is conserved in mouse cells dependent on physiological oxygen. *PloS one*, 5(2), p.e9188. Available at: http://www.pubmedcentral.nih.gov/articlerender.fcgi?artid=2820538&tool=pmcentrez&rendertype=abstract [Accessed March 8, 2013].

Coppé, J.-P. et al., 2008. Senescence-associated secretory phenotypes reveal cell-nonautonomous functions of oncogenic RAS and the p53 tumor suppressor. *PLoS biology*, 6(12), pp.2853–68. Available at: http://www.pubmedcentral.nih.gov/articlerender.fcgi?artid=2592359&tool=pmcentrez&rendertype=abstract [Accessed December 13, 2013].

Coppé, J.-P., Desprez, P.-Y., et al., 2010. The senescence-associated secretory phenotype: the dark side of tumor suppression. *Annual review of pathology*, 5(1), pp.99–118. Available at: http://www.annualreviews.org/doi/abs/10.1146/annurev-pathol-121808-102144 [Accessed July 10, 2014].

Cornel, A. et al., 2014. The cytoplasmic side of p53's oncosuppressive activities. *FEBS letters*, 588(16), pp.1–10. Available at: http://dx.doi.org/10.1016/j.febslet.2014.04.015 [Accessed April 28, 2014].

Crescenzi, E. et al., 2011. NF-κB-dependent cytokine secretion controls Fas expression on chemotherapy-induced premature senescent tumor cells. *Oncogene*, 30(24), pp.2707–2717. Available at: http://www.nature.com/doifinder/10.1038/onc.2011.1 [Accessed September 5, 2016].

Crusz, S.M. & Balkwill, F.R., 2015. Inflammation and cancer: advances and new agents. *Nature Reviews Clinical Oncology*, 12(10), pp.1–13. Available at: http://www.nature.com/doifinder/10.1038/nrclinonc.2015.105.

Dai, C.Y. & Enders, G.H., 2000. p16 INK4a can initiate an autonomous senescence program. *Oncogene*, 19(13), pp.1613–22. Available at: http://www.ncbi.nlm.nih.gov/pubmed/10763818 [Accessed August 17, 2016].

Dankort, D. et al., 2007. A new mouse model to explore the initiation, progression, and therapy of BRAFV600E-induced lung tumors. *Genes & Development*, 21(4), pp.379–384. Available at: http://www.genesdev.org/cgi/doi/10.1101/gad.1516407 [Accessed August 19, 2016].

Dattani, M.T. et al., 1998. Mutations in the homeobox gene HESX1/Hesx1 associated with septo-optic dysplasia in human and mouse. *Nature genetics*, 19(2), pp.125–33. Available at: http://www.ncbi.nlm.nih.gov/pubmed/9620767 [Accessed August 14, 2012].

Davalos, A.R. et al., 2010. Senescent cells as a source of inflammatory factors for tumor progression. *Cancer metastasis reviews*, 29(2), pp.273–83. Available at: http://www.pubmedcentral.nih.gov/articlerender.fcgi?artid=2865636&tool=pmcentrez&rendertype=abstract [Accessed September 3, 2014].

Davis, S.W. et al., 2009. Genetics, gene expression and bioinformatics of the pituitary gland. *Hormone research*, 71(suppl 2), pp.101–115. Available at: http://www.pubmedcentral.nih.gov/articlerender.fcgi?artid=3140954&tool=pmcentrez&rendertype=abstract [Accessed October 25, 2011].

Davis, S.W. et al., 2016. ß-Catenin Is Required in the Neural Crest and Mesencephalon for Pituitary Organogenesis. *BMC Developmental Biology*, 16(16), pp.1–17. Available at: http://dx.doi.org/10.1186/s12861-016-0118-9.

Deaconess, B.I. et al., 1998. Impaired B-lymphopoiesis, myelopoiesis, and derailed cerebellar neuron migration in CXCR4- and SDF-1-deficient mice. *Proceedings of the National Academy of Sciences of the United States of America*, 95(16), pp.9448–53. Available at: http://www.pubmedcentral.nih.gov/articlerender.fcgi?artid=21358&tool=pmcentrez&rendertype=abstract.

Debacq-Chainiaux, F. et al., 2009. Protocols to detect senescence-associated beta-galactosidase (SA-betagal) activity, a biomarker of senescent cells in culture and in vivo. *Nature protocols*, 4(12), pp.1798–806. Available at: http://www.ncbi.nlm.nih.gov/pubmed/20010931 [Accessed January 28, 2014].

Debies, M.T. et al., 2008. Tumor escape in a Wnt1-dependent mouse breast cancer model is enabled by p19Arf/p53 pathway lesions but not p16 Ink4a loss. *The Journal of clinical investigation*, 118(1), pp.51–63. Available at: http://www.ncbi.nlm.nih.gov/pubmed/18060046 [Accessed August 30, 2016].

Décaillot, F.M. et al., 2011. CXCR7/CXCR4 heterodimer constitutively recruits beta-arrestin to enhance cell migration. *The Journal of biological chemistry*, 286(37), pp.32188–97. Available at: http://www.pubmedcentral.nih.gov/articlerender.fcgi?artid=3173186&tool=pmcentrez&rendertype=abstract [Accessed November 23, 2012].

Dekkers, O.M. et al., 2006. Quality of life in treated adult craniopharyngioma patients. *European Journal of Endocrinology*, 154, pp.483–489.

Demaria, M. et al., 2014. An Essential Role for Senescent Cells in Optimal Wound Healing through Secretion of PDGF-AA. *Developmental Cell*, 31(6), pp.722–733. Available at: http://linkinghub.elsevier.com/retrieve/pii/S1534580714007291 [Accessed December 12, 2014].

Denef, C., 2008. Paracrinicity: the story of 30 years of cellular pituitary crosstalk. *Journal of neuroendocrinology*, 20(1), pp.1–70. Available at: http://www.pubmedcentral.nih.gov/articlerender.fcgi?artid=2229370&tool=pmcentrez&rendertype=abstract [Accessed July 21, 2012].

Deschene, E.R. et al., 2014. Beta-Catenin Activation Regulates Tissue Growth Non-Cell Autonomously in the Hair Stem Cell Niche. *Science*, 343(6177), pp.1353–1356. Available at: http://www.ncbi.nlm.nih.gov/pubmed/24653033 [Accessed March 21, 2014].

Dimri, G.P. et al., 1995. A biomarker that identifies senescent human cells in culture and in aging skin in vivo. *Proceedings of the National Academy of Sciences of the United States of America*, 92(20), pp.9363–7. Available at: http://www.pubmedcentral.nih.gov/articlerender.fcgi?artid=40985&tool=pmcentrez&rendertype=abstract.

Dimri, G.P., 2005. What has senescence got to do with cancer? *Cancer cell*, 7(6), pp.505–12. Available at:

http://www.pubmedcentral.nih.gov/articlerender.fcgi?artid=1769521&tool=pmcentrez&rendertype=abstract [Accessed January 2, 2014].

Ding, L. & Morrison, S.J., 2013. Haematopoietic stem cells and early lymphoid progenitors occupy distinct bone marrow niches. *Nature*, 495(7440), pp.231–5. Available at: http://www.nature.com/doifinder/10.1038/nature11885 [Accessed March 26, 2014].

Donehower, L.A. & Lozano, G., 2009. 20 Years Studying P53 Functions in Genetically Engineered Mice. *Nature reviews. Cancer*, 9(11), pp.831–841.

Donehower, L. a, 2009. Using mice to examine p53 functions in cancer, aging, and longevity. *Cold Spring Harbor perspectives in biology*, 1(6), p.a001081. Available at: http://www.pubmedcentral.nih.gov/articlerender.fcgi?artid=2882127&tool=pmcentrez&rendertype=abstract.

Dörr, J.R. et al., 2013. Synthetic lethal metabolic targeting of cellular senescence in cancer therapy. *Nature*, 501(7467), pp.421–5. Available at: http://www.ncbi.nlm.nih.gov/pubmed/23945590 [Accessed November 6, 2013].

Le Douarin, N.M. et al., 2004. Neural crest cell plasticity and its limits. *Development (Cambridge, England)*, 131(19), pp.4637–50. Available at: http://www.ncbi.nlm.nih.gov/pubmed/15358668 [Accessed September 1, 2016].

Drury, L.J. et al., 2011. Monomeric and dimeric CXCL12 inhibit metastasis through distinct CXCR4 interactions and signaling pathways. *Proceedings of the National Academy of Sciences of the United States of America*, 108(43), pp.17655–17660. Available at: http://www.ncbi.nlm.nih.gov/pubmed/21990345 [Accessed October 18, 2011].

Du, Q. & Geller, D.A., 2010. Cross-Regulation Between Wnt and NF-κB Signaling Pathways. *Forum on immunopathological diseases and therapeutics*, 1(3), pp.155–181. Available at: http://www.ncbi.nlm.nih.gov/pubmed/21686046 [Accessed September 6, 2016].

Durinck, S. et al., 2009. Mapping identifiers for the integration of genomic datasets with the R/Bioconductor package biomaRt. *Nature protocols*, 4(8), pp.1184–91. Available at: http://www.ncbi.nlm.nih.gov/pubmed/19617889 [Accessed September 6, 2016].

Eash, K.J. et al., 2010. CXCR2 and CXCR4 antagonistically regulate neutrophil trafficking from murine bone marrow. *The Journal of Clinical Investigation*, 120(7), pp.30–33.

Escot, S. et al., 2013. Misregulation of SDF1-CXCR4 signaling impairs early cardiac neural crest cell migration leading to conotruncal defects. *Circulation research*, 113(5), pp.505–16. Available at: http://www.ncbi.nlm.nih.gov/pubmed/23838132 [Accessed November 30, 2013].

Esheba, G.E. & Hassan, A.A., 2015. Comparative immunohistochemical expression of β-catenin, EGFR, ErbB2, and p63 in adamantinomatous and papillary craniopharyngiomas. *Journal of the Egyptian National Cancer Institute*, 27(3), pp.139–145. Available at: http://www.sciencedirect.com/science/article/pii/S1110036215000576.

Etchevers, H.C. et al., 2001. The cephalic neural crest provides pericytes and smooth muscle cells to all blood vessels of the face and forebrain. *Development (Cambridge, England)*, 128(7), pp.1059–68. Available at: http://www.ncbi.nlm.nih.gov/pubmed/11245571.

Ewald, J.A. et al., 2010. Therapy-induced senescence in cancer. *Journal of the National Cancer Institute*, 102(20), pp.1536–46. Available at: http://www.ncbi.nlm.nih.gov/pubmed/20858887 [Accessed August 16, 2016].

Fang, L. et al., 1999. p21Waf1/Cip1/Sdi1 induces permanent growth arrest with markers of replicative senescence in human tumor cells lacking functional p53. *Oncogene*, 18(18), pp.2789–2797. Available at: http://www.nature.com/doifinder/10.1038/sj.onc.1202615 [Accessed August 17, 2016].

Fauquier, T. et al., 2008. SOX2-expressing progenitor cells generate all of the major cell types in the adult mouse pituitary gland. *Proceedings of the National Academy of Sciences of the United States of America*, 105(8), pp.2907–12. Available at: http://www.pnas.org/content/105/8/2907.long [Accessed August 5, 2016].

Fearon, E.R., 2011. Molecular genetics of colorectal cancer. *Annu Rev Pathol*, 6, pp.479–507. Available at: http://www.ncbi.nlm.nih.gov/pubmed/21090969.

Feldser, D.M. et al., 2010. Stage-specific sensitivity to p53 restoration during lung cancer progression. *Nature*, 468(7323), pp.572–575. Available at: http://www.nature.com/doifinder/10.1038/nature09535.

Filomeni, G., De Zio, D. & Cecconi, F., 2015. Oxidative stress and autophagy: the clash between damage and metabolic needs. *Cell Death and Differentiation*, 22(3), pp.377–388. Available at: http://www.nature.com/doifinder/10.1038/cdd.2014.150.

Fischer, T. et al., 2008. Reassessment of CXCR4 chemokine receptor expression in human normal and neoplastic tissues using the novel rabbit monoclonal antibody UMB-2. *PloS one*, 3(12), p.e4069. Available at: http://www.pubmedcentral.nih.gov/articlerender.fcgi?artid=2605258&tool=pmcentrez&rendertype=abstract [Accessed December 15, 2011].

Fitzgerald, A.L. et al., 2015. Reactive oxygen species and p21Waf1/Cip1 are both essential for p53-mediated senescence of head and neck cancer cells. *Cell Death and Disease*, 6(3), p.e1678. Available at: http://www.nature.com/doifinder/10.1038/cddis.2015.44 [Accessed August 16, 2016].

Flores, I., Benetti, R. & Blasco, M.A., 2006. Telomerase regulation and stem cell behaviour. *Current Opinion in Cell Biology*, 18, pp.254–260.

Florio, T., 2011. Adult pituitary stem cells: From pituitary plasticity to adenoma development. *Neuroendocrinology*, 94(4), pp.265–277. Available at: http://www.ncbi.nlm.nih.gov/pubmed/22116388 [Accessed July 15, 2012].

Fomchenko, E.I. et al., 2011. Recruited Cells Can Become Transformed and Overtake PDGF-Induced Murine Gliomas Progression M. S. Lesniak, ed. *PloS one*, 6(7), p.e20605. Available at: http://www.ncbi.nlm.nih.gov/pubmed/21754979 [Accessed July 10, 2016].

Franceschi, C. & Campisi, J., 2014. Chronic Inflammation (Inflammaging) and Its Potential Contribution to Age-Associated Diseases. *The Journals of Gerontology Series A: Biological Sciences and Medical Sciences*, 69(Suppl 1), pp.S4–S9. Available at: http://biomedgerontology.oxfordjournals.org/cgi/doi/10.1093/gerona/glu057 [Accessed August 17, 2016].

Frank, A.K. et al., 2011. Wild-type and mutant p53 proteins interact with mitochondrial caspase-3. *Cancer Biology & Therapy*, 11(8), pp.740–745.

Freund, A., Patil, C.K. & Campisi, J., 2011. p38MAPK is a novel DNA damage response-independent regulator of the senescence-associated secretory phenotype. *The EMBO journal*, 30(8), pp.1536–48. Available at: http://www.pubmedcentral.nih.gov/articlerender.fcgi?artid=3102277&tool=pmcentrez&rendertype=abstract [Accessed November 14, 2013].

Fu, Q. et al., 2012. The adult pituitary shows stem/progenitor cell activation in response to injury and is capable of regeneration. *Endocrinology*, 153(7), pp.3224–35. Available at: http://www.ncbi.nlm.nih.gov/pubmed/22518061 [Accessed June 3, 2013].

Fujita, T. et al., 2015. Identification and Characterization of CXCR4-Positive Gastric Cancer Stem Cells M. Seno, ed. *PLOS ONE*, 10(6), p.e0130808. Available at: http://dx.plos.org/10.1371/journal.pone.0130808 [Accessed July 10, 2016].

Fumagalli, M. et al., 2014. Stable Cellular Senescence Is Associated with Persistent DDR Activation. *PloS one*, 9(10), p.e110969. Available at: http://www.pubmedcentral.nih.gov/articlerender.fcgi?artid=4207795&tool=pmcentrez&rendertype=abstract [Accessed November 10, 2014].

Gaillard, H., García-Muse, T. & Aguilera, A., 2015. Replication stress and cancer. *Nature Reviews Cancer*, 15(5), pp.276–289. Available at: http://www.nature.com/doifinder/10.1038/nrc3916.

Gao, S. et al., 2011. Malignant transformation of craniopharyngioma: Case report and review of the literature. *Journal of Neuro-Oncology*, 103(3), pp.719–725. Available at:

http://link.springer.com/10.1007/s11060-010-0407-2 [Accessed August 10, 2016].

Garcia-Lavandeira, M. et al., 2009. A GRFa2/Prop1/stem (GPS) cell niche in the pituitary. *PloS one*, 4(3), p.e4815. Available at: http://www.ncbi.nlm.nih.gov/pubmed/19283075 [Accessed December 3, 2011].

Garcia-Lavandeira, M. et al., 2011. Craniopharyngiomas Express Embryonic Stem Cell Markers (SOX2, OCT4, KLF4, and SOX9) as Pituitary Stem Cells but Do Not Coexpress RET/GFRA3 Receptors. *The Journal of clinical endocrinology and metabolism*, 97(January), pp.1–8. Available at: http://www.ncbi.nlm.nih.gov/pubmed/22031517 [Accessed December 10, 2011].

García-Prat, L. et al., 2016. Autophagy maintains stemness by preventing senescence. *Nature*, 529(7584), pp.37–42. Available at: http://www.nature.com/doifinder/10.1038/nature16187 [Accessed September 5, 2016].

Gaston-Massuet, C. et al., 2008. Genetic interaction between the homeobox transcription factors HESX1 and SIX3 is required for normal pituitary development. *Developmental biology*, 324(2), pp.322–33. Available at: http://www.ncbi.nlm.nih.gov/pubmed/18775421 [Accessed September 28, 2011].

Gaston-Massuet, C. et al., 2011. Increased Wingless (Wnt) signaling in pituitary progenitor/stem cells gives rise to pituitary tumors in mice and humans. *Proceedings of the National Academy of Sciences of the United States of America*, 1088(3), pp.11482–7. Available at: http://www.pnas.org/content/108/28/11482.short [Accessed October 29, 2011].

Gire, V. & Dulic, V., 2015. Senescence from G2 arrest, revisited. *Cell cycle (Georgetown, Tex.)*, 14(3), pp.297–304. Available at: http://www.ncbi.nlm.nih.gov/pubmed/25564883 [Accessed July 25, 2016].

Glaser, S., Anastassiadis, K. & Stewart, a F., 2005. Current issues in mouse genome engineering. *Nature genetics*, 37(11), pp.1187–93. Available at: http://www.ncbi.nlm.nih.gov/pubmed/16254565 [Accessed July 30, 2011].

Gleiberman, A.S. et al., 2008. Genetic approaches identify adult pituitary stem cells. *Proceedings of the National Academy of Sciences of the United States of America*, 105(17), pp.6332–7. Available at: http://www.pubmedcentral.nih.gov/articlerender.fcgi?artid=2359820&tool=pmcentrez&rendertype=abstract [Accessed August 5, 2016].

Gong, J. et al., 2014. High expression levels of CXCL12 and CXCR4 predict recurrence of adamanti-nomatous craniopharyngiomas in children. *Cancer biomarkers : section A of Disease markers*, 14(4), pp.241–51. Available at: http://www.ncbi.nlm.nih.gov/pubmed/24934367 [Accessed August 18, 2014].

Gonzalez-Meljem, J.M., 2012. *A Study of the Expression Pattern and Function of the CXCR4 Gene During Pituitary Development*. University College London.

Grymula, K. et al., 2010. Overlapping and distinct role of CXCR7-SDF-1/ITAC and CXCR4-SDF-1 axes in regulating metastatic behavior of human rhabdomyosarcomas. *International journal of cancer. Journal international du cancer*, 127(11), pp.2554–68. Available at: http://www.pubmedcentral.nih.gov/articlerender.fcgi?artid=2907445&tool=pmcentrez&rendertype=abstract [Accessed February 1, 2013].

Gu, Z. et al., 2014. Wnt/β-catenin signaling mediates the senescence of bone marrow-mesenchymal stem cells from systemic lupus erythematosus patients through the p53/p21 pathway. *Molecular and cellular biochemistry*, 387(1–2), pp.27–37. Available at: http://www.ncbi.nlm.nih.gov/pubmed/24130040 [Accessed August 11, 2014].

Guo, X. et al., 2009. TAp63 induces senescence and suppresses tumorigenesis in vivo. *Nature cell biology*, 11(12), pp.1451–7. Available at: http://www.pubmedcentral.nih.gov/articlerender.fcgi?artid=2920298&tool=pmcentrez&rendertype=abstract.

Ha, L. et al., 2007. ARF functions as a melanoma tumor suppressor by inducing p53-

independent senescence. *Proceedings of the National Academy of Sciences*, 104(26), pp.10968–10973. Available at: http://www.pnas.org/cgi/doi/10.1073/pnas.0611638104 [Accessed September 2, 2016].

Haege, S. et al., 2012. CXC chemokine receptor 7 (CXCR7) regulates CXCR4 protein expression and capillary tuft development in mouse kidney. *PloS one*, 7(8), p.e42814. Available at: http://www.pubmedcentral.nih.gov/articlerender.fcgi?artid=3412803&tool=pmcentrez&rendertype=abstract [Accessed November 2, 2012].

Haferkamp, S. et al., 2009. The relative contributions of the p53 and pRb pathways in oncogene-induced melanocyte senescence. *Aging*, 1(6), pp.542–556.

Halazonetis, T.D., Gorgoulis, V.G. & Bartek, J., 2008. An Oncogene-Induced DNA Damage Model for Cancer Development. *Science*, 319(5868), pp.1352–1355. Available at: http://www.ncbi.nlm.nih.gov/pubmed/18323444 [Accessed August 17, 2016].

Hall, B.M. et al., 2016. Aging of mice is associated with p16(Ink4a)- and β-galactosidase-positive macrophage accumulation that can be induced in young mice by senescent cells. *Aging*, 8(7), pp.1294–315. Available at: http://www.ncbi.nlm.nih.gov/pubmed/27391570 [Accessed August 18, 2016].

Harada, N. et al., 1999. Intestinal polyposis in mice with a dominant stable mutation of the beta-catenin gene. *The EMBO journal*, 18(21), pp.5931–5942. Available at: http://emboj.embopress.org/cgi/doi/10.1093/emboj/18.21.5931 [Accessed August 11, 2016].

Hashimoto, H., Ishikawa, H. & Kusakabe, M., 1998. Three-Dimensional Analysis of the Developing Pituitary. *Scanning Electron Microscopy*, 166(January), pp.157–166.

Hasty, P. et al., 2013. mTORC1 and p53: Clash of the gods? *Cell Cycle*, 12(1), pp.20–25.

Hattori, T. et al., 2010. SOX9 is a major negative regulator of cartilage vascularization, bone marrow formation and endochondral ossification. *Development (Cambridge, England)*, 137(6), pp.901–11. Available at: http://www.ncbi.nlm.nih.gov/pubmed/20179096 [Accessed September 20, 2013].

Hayden, M.S. & Ghosh, S., 2012. NF- B, the first quarter-century: remarkable progress and outstanding questions. *Genes & Development*, 26(3), pp.203–234. Available at: http://genesdev.cshlp.org/cgi/doi/10.1101/gad.183434.111 [Accessed September 5, 2016].

Hayden, M.S., West, A.P. & Ghosh, S., 2006. NF-κB and the immune response. *Oncogene*, 25(51), pp.6758–6780. Available at: http://www.nature.com/doifinder/10.1038/sj.onc.1209943 [Accessed September 5, 2016].

Hayflick, L., 1965. The limited in vitro lifetime of human diploid cell strains. *Experimental cell research*, 37, pp.614–36. Available at: http://www.ncbi.nlm.nih.gov/pubmed/14315085 [Accessed September 5, 2016].

Hayflick, L. & Moorhead, P.S., 1961. The serial cultivation of human diploid cell strains. *Experimental cell research*, 25, pp.585–621.

He, C. & Klionsky, D.J., 2009. Regulation Mechanisms and Signaling Pathways of Autophagy. *Annual review of genetics*, 43, pp.67–93.

Heckmann, D. et al., 2013. The disparate twins: A comparative study of CXCR4 and CXCR7 in SDF-1α-induced gene expression, invasion and chemosensitivity of colon cancer. *Clinical cancer research : an official journal of the American Association for Cancer Research*. Available at: http://www.ncbi.nlm.nih.gov/pubmed/24255072 [Accessed November 27, 2013].

Herbig, U. et al., 2006. Cellular senescence in aging primates. *Science (New York, N.Y.)*, 311(5765), p.1257. Available at: http://www.ncbi.nlm.nih.gov/pubmed/16456035 [Accessed August 17, 2016].

Hermann, P.C. et al., 2007. Distinct Populations of Cancer Stem Cells Determine Tumor

Growth and Metastatic Activity in Human Pancreatic Cancer. *Cell Stem Cell*, 1(3), pp.313–323.

Hermesz, E., Mackem, S. & Mahon, K.A., 1996. Rpx : a novel anterior-restricted homeobox gene progressively activated in the prechordal plate , anterior neural plate and Rathke ' s pouch of the mouse embryo. *Development*, 52, pp.41–52.

Hernandez, L. et al., 2011. Opposing roles of CXCR4 and CXCR7 in breast cancer metastasis. *Breast cancer research : BCR*, 13(6), p.R128. Available at: http://breast-cancer-research.com/content/13/6/R128 [Accessed January 11, 2012].

Herranz, N. et al., 2015. mTOR regulates MAPKAPK2 translation to control the senescence-associated secretory phenotype. *Nature Cell Biology*, 17(9). Available at: http://www.nature.com/doifinder/10.1038/ncb3225.

Highfill, S.L. et al., 2014. Disruption of CXCR2-mediated MDSC tumor trafficking enhances anti-PD1 efficacy. *Science translational medicine*, 6(237), p.237ra67. Available at: http://www.ncbi.nlm.nih.gov/pubmed/24848257 [Accessed September 1, 2016].

Holland, J.D. et al., 2006. Differential functional activation of chemokine receptor CXCR4 is mediated by G proteins in breast cancer cells. *Cancer research*, 66(8), pp.4117–24. Available at: http://www.ncbi.nlm.nih.gov/pubmed/16618732 [Accessed November 11, 2011].

Holland, J.D. et al., 2013. Wnt signaling in stem and cancer stem cells. *Current Opinion in Cell Biology*, 25(2), pp.254–264. Available at: http://dx.doi.org/10.1016/j.ceb.2013.01.004.

Hölsken, A. et al., 2013. Adamantinomatous craniopharyngiomas express tumor stem cell markers in cells with activated Wnt signaling: further evidence for the existence of a tumor stem cell niche? *Pituitary*, 17(6), pp.546–56. Available at: http://www.ncbi.nlm.nih.gov/pubmed/24356780 [Accessed May 8, 2014].

Huang, B. et al., 1999. Autosomal XX sex reversal caused by duplication of SOX9. *American journal of medical genetics*, 87(4), pp.349–53. Available at: http://www.ncbi.nlm.nih.gov/pubmed/10588843 [Accessed August 5, 2016].

Hubackova, S. et al., 2012. IL1-alpha and TGFβ-Nox4 signaling, oxidative stress and DNA damage response are shared features of replicative, oncogene-induced, and drug-induced paracrine "Bystander senescence." *Aging*, 4(12), pp.932–951. Available at: http://impactaging.com/papers/v4/n12/full/100520.html [Accessed August 17, 2016].

Huff, V., 2011. Wilms' tumours: about tumour suppressor genes, an oncogene and a chameleon gene. *Nature Reviews Cancer*, 11(2), pp.111–121. Available at: http://www.nature.com/doifinder/10.1038/nrc3002 [Accessed August 16, 2016].

Hüsken, U. & Carl, M., 2012. The Wnt/beta-catenin signaling pathway establishes neuroanatomical asymmetries and their laterality. *Mechanisms of development*, 130(6–8), pp.330–5. Available at: http://linkinghub.elsevier.com/retrieve/pii/S0925477312000871 [Accessed May 1, 2014].

Iannello, A. et al., 2013. p53-dependent chemokine production by senescent tumor cells supports NKG2D-dependent tumor elimination by natural killer cells. *The Journal of experimental medicine*, 210(10), pp.2057–69. Available at: http://www.ncbi.nlm.nih.gov/pubmed/24043758 [Accessed August 17, 2016].

Ikeda, T. et al., 2004. The combination of SOX5, SOX6, and SOX9 (the SOX trio) provides signals sufficient for induction of permanent cartilage. *Arthritis and rheumatism*, 50(11), pp.3561–73. Available at: http://www.ncbi.nlm.nih.gov/pubmed/15529345 [Accessed August 5, 2016].

Inomata, M. et al., 1996. Alteration of beta-catenin expression in colonic epithelial cells of familial adenomatous polyposis patients. *Cancer research*, 56(9), pp.2213–7. Available at: http://www.ncbi.nlm.nih.gov/pubmed/8616874 [Accessed August 15, 2016].

Isaacs, H., 2009. Fetal Brain Tumors: A Review of 154 Cases. *American Journal of Perinatology*, 26(6), pp.453–466. Available at: http://www.thieme-

connect.de/DOI/DOI?10.1055/s-0029-1214245 [Accessed August 10, 2016].

Ivanov, a. et al., 2013. Lysosome-mediated processing of chromatin in senescence. *The Journal of Cell Biology*, 202(1), pp.129–143. Available at: http://www.jcb.org/cgi/doi/10.1083/jcb.201212110.

Ivins, S. et al., 2015. The CXCL12/CXCR4 Axis Plays a Critical Role in Coronary Artery Development. *Developmental cell*, 33(4), pp.455–68. Available at: http://www.ncbi.nlm.nih.gov/pubmed/26017770 [Accessed September 6, 2016].

Jacobs, J.J.L. et al., 2004. Significant role for p16INK4a in p53-independent telomere-directed senescence. *Current biology : CB*, 14(24), pp.2302–8. Available at: http://www.ncbi.nlm.nih.gov/pubmed/15620660 [Accessed July 25, 2016].

Jaisser, F., 2000. Inducible gene expression and gene modification in transgenic mice. *Journal of the American Society of Nephrology : JASN*, 11 Suppl 1, pp.S95–S100.

Jamieson, T. et al., 2012. Inhibition of CXCR2 profoundly suppresses inflammation-driven and spontaneous tumorigenesis. *The Journal of Clinical Investigation*, 122(9), pp.3127–3144. Available at: http://www.jci.org/articles/view/61067 [Accessed September 1, 2016].

Janzer, R. et al., 2000. Craniopharyngioma. *World Health Organization classification of tumours of the central nervous system*, pp.244–246. Available at: https://scholar.google.co.uk/scholar?hl=en&q=janzer+craniopharyngioma+&btnG=&as_sdt=1%2C5&as_sdtp=#0 [Accessed December 12, 2015].

Jayakody, S.A. et al., 2012. SOX2 regulates the hypothalamic-pituitary axis at multiple levels. *The Journal of Clinical Investigation*, 122(10), pp.3635–3646.

Jo, A. et al., 2014. The versatile functions of Sox9 in development, stem cells, and human diseases. *Genes & Diseases*, 1(2), pp.149–161.

Joa, A. et al., 2012. The versatile functions of Sox9 in development, stem cells, and human diseases. *Genes and Diseases*, 29(6), pp.997–1003.

Joo, J.G. et al., 2009. Foetal craniopharyngioma diagnosed by prenatal ultrasonography and confirmed by histopathological examination. *Prenatal diagnosis*, 29, pp.160–163.

Jung, M.-J. et al., 2013. Upregulation of CXCR4 is functionally crucial for maintenance of stemness in drug-resistant non-small cell lung cancer cells. *Oncogene*, 32(2), pp.209–221. Available at: http://www.nature.com/doifinder/10.1038/onc.2012.37 [Accessed July 10, 2016].

Junttila, M.R. et al., 2010. Selective activation of p53-mediated tumour suppression in high-grade tumours. *Nature*, 468(7323), pp.567–71. Available at: http://www.pubmedcentral.nih.gov/articlerender.fcgi?artid=3011233&tool=pmcentrez&rendertype=abstract.

Jurk, D. et al., 2014. Chronic inflammation induces telomere dysfunction and accelerates ageing in mice. *Nature communications*, 2(May), p.4172. Available at: http://www.nature.com/doifinder/10.1038/ncomms5172 [Accessed July 11, 2014].

Jurkiewicz, E. et al., 2010. Antenatal diagnosis of the congenital craniopharyngioma. *Polish journal of radiology / Polish Medical Society of Radiology*, 75(1), pp.98–102. Available at: http://www.ncbi.nlm.nih.gov/pubmed/22802769 [Accessed August 10, 2016].

Kamijo, T. et al., 1997. Tumor Suppression at the Mouse INK4a Locus Mediated by the Alternative Reading Frame Product p19 ARF. *Cell*, 91(5), pp.649–659.

Kang, C. et al., 2015. The DNA damage response induces inflammation and senescence by inhibiting autophagy of GATA4. *Science (New York, N.Y.)*, 349(6255), p.aaa5612. Available at: http://www.ncbi.nlm.nih.gov/pubmed/26404840.

Kang, C. & Elledge, S.J., 2016. How autophagy both activates and inhibits cellular senescence. *Autophagy*, 12(5), pp.898–899. Available at: http://www.ncbi.nlm.nih.gov/pubmed/27129029%5Cnhttp://www.tandfonline.com/doi/full/10.1080/15548627.2015.1121361.

Kang, P. et al., 2012. Sox9 and NFIA Coordinate a Transcriptional Regulatory Cascade during the Initiation of Gliogenesis. *Neuron*, 74(1), pp.79–94.

Kang, T.-W. et al., 2011. Senescence surveillance of pre-malignant hepatocytes limits liver cancer development. *Nature*, 479(7374), pp.547–51. Available at: http://www.ncbi.nlm.nih.gov/pubmed/22080947 [Accessed August 17, 2016].

Kasemeier-Kulesa, J.C. et al., 2010. CXCR4 controls ventral migration of sympathetic precursor cells. *The Journal of neuroscience : the official journal of the Society for Neuroscience*, 30(39), pp.13078–88. Available at: http://www.ncbi.nlm.nih.gov/pubmed/20881125 [Accessed November 29, 2012].

Kasperczyk, H. et al., 2009. Characterization of sonic hedgehog as a novel NF-kappaB target gene that promotes NF-kappaB-mediated apoptosis resistance and tumor growth in vivo. *FASEB journal : official publication of the Federation of American Societies for Experimental Biology*, 23(1), pp.21–33. Available at: http://www.ncbi.nlm.nih.gov/pubmed/18772349 [Accessed August 31, 2016].

Kato, K. et al., 2004. Possible linkage between specific histological structures and aberrant reactivation of the Wnt pathway in adamantinomatous craniopharyngioma. *The Journal of pathology*, 203(3), pp.814–21. Available at: http://www.ncbi.nlm.nih.gov/pubmed/15221941 [Accessed August 13, 2012].

Katsumoto, K. & Kume, S., 2011. Endoderm and mesoderm reciprocal signaling mediated by CXCL12 and CXCR4 regulates the migration of angioblasts and establishes the pancreatic fate. *Development (Cambridge, England)*, 138(10), pp.1947–55. Available at: http://www.ncbi.nlm.nih.gov/pubmed/21490062 [Accessed July 18, 2011].

Kawai, T. et al., 2016. SOX9 is a novel cancer stem cell marker surrogated by osteopontin in human hepatocellular carcinoma. *Scientific Reports*, 6, p.30489. Available at: http://www.nature.com/articles/srep30489 [Accessed August 2, 2016].

Kelberman, D. et al., 2009. Genetic regulation of pituitary gland development in human and mouse. *Endocrine reviews*, 30(7), pp.790–829. Available at: http://www.pubmedcentral.nih.gov/articlerender.fcgi?artid=2806371&tool=pmcentrez&rendertype=abstract [Accessed July 30, 2011].

Kelberman, D. et al., 2006. Mutations within Sox2/SOX2 are associated with abnormalities in the hypothalamo- pituitary-gonadal axis in mice and humans. *The Journal of Clinical Investigation*, 116(9), pp.2442–2455.

Kikuchi, M. et al., 2007. Changes in E- and N-cadherin expression in developing rat adenohypophysis. *Anatomical Record*, 290(5), pp.486–490.

Kim, J.M. et al., 2011. The Cyclic Pentapeptide d-Arg3FC131, a CXCR4 Antagonist, Induces Apoptosis of Somatotrope Tumor and Inhibits Tumor Growth in Nude Mice. *Neuroendocrinology*, 152(February), pp.536–544. Available at: http://www.ncbi.nlm.nih.gov/pubmed/21147876 [Accessed October 29, 2011].

Kinoshita, M. et al., 2001. Identification of human endomucin-1 and -2 as membrane-bound O-sialoglycoproteins with anti-adhesive activity. *FEBS letters*, 499(1–2), pp.121–6. Available at: http://www.ncbi.nlm.nih.gov/pubmed/11418125 [Accessed September 26, 2013].

Kinzler, K.W. & Vogelstein, B., 1996. Lessons from Hereditary Colorectal Cancer. *Cell*, 87(2), pp.159–170.

Kisanuki, Y.Y. et al., 2001. Tie2-Cre transgenic mice: a new model for endothelial cell-lineage analysis in vivo. *Developmental biology*, 230(2), pp.230–42. Available at: http://www.ncbi.nlm.nih.gov/pubmed/11161575 [Accessed September 1, 2016].

Klaus, A. & Birchmeier, W., 2008. Wnt signalling and its impact on development and cancer. *Nature reviews. Cancer*, 8(5), pp.387–398.

Klionsky, D.J. et al., 2016. Guidelines for the use and interpretation of assays for monitoring autophagy (3rd edition). *Autophagy*, 8627.

Kode, A. et al., 2014. Leukaemogenesis induced by an activating β-catenin mutation in

osteoblasts. *Nature*, 506(7487), pp.240–4. Available at: http://www.ncbi.nlm.nih.gov/pubmed/24429522 [Accessed February 20, 2014].

Koesters, R. et al., 1999. Mutational activation of the beta-catenin proto-oncogene is a common event in the development of Wilms' tumors. *Cancer research*, 59(16), pp.3880–2. Available at: http://www.ncbi.nlm.nih.gov/pubmed/10463574 [Accessed September 5, 2016].

Korinek, V. et al., 1997. Constitutive transcriptional activation by a beta-catenin-Tcf complex in APC-/- colon carcinoma. *Science (New York, N.Y.)*, 275(5307), pp.1784–7. Available at: http://www.ncbi.nlm.nih.gov/pubmed/9065401 [Accessed August 15, 2016].

Kostadinov, S. et al., 2014. Fetal craniopharyngioma: management, postmortem diagnosis, and literature review of an intracranial tumor detected in utero. *Pediatric and developmental pathology : the official journal of the Society for Pediatric Pathology and the Paediatric Pathology Society*, 17(5), pp.409–12. Available at: http://www.ncbi.nlm.nih.gov/pubmed/25020160 [Accessed August 10, 2016].

Kreso, A. & Dick, J.E.J., 2014. Evolution of the cancer stem cell model. *Cell Stem Cell*, 14(3), pp.275–291. Available at: http://www.ncbi.nlm.nih.gov/pubmed/24607403 [Accessed July 9, 2016].

Kretzschmar, K. et al., 2016. Compartmentalized Epidermal Activation of β-Catenin Differentially Affects Lineage Reprogramming and Underlies Tumor Heterogeneity. *Cell Reports*, 14, pp.269–281. Available at: http://dx.doi.org/10.1016/j.celrep.2015.12.041.

Kristopaitis, T. et al., 2000. Malignant craniopharyngioma. *Archives of pathology & laboratory medicine*, 124(9), pp.1356–60. Available at: http://www.ncbi.nlm.nih.gov/pubmed/10975938 [Accessed August 10, 2016].

Krizhanovsky, V. et al., 2008. Senescence of Activated Stellate Cells Limits Liver Fibrosis. *Cell*, 134(4), pp.657–667.

Krtolica, A. et al., 2001. Senescent fibroblasts promote epithelial cell growth and tumorigenesis: a link between cancer and aging. *Proceedings of the National Academy of Sciences of the United States of America*, 98(21), pp.12072–7. Available at: http://www.pubmedcentral.nih.gov/articlerender.fcgi?artid=59769&tool=pmcentrez&rendertype=abstract.

Kuilman, T. et al., 2008. Oncogene-induced senescence relayed by an interleukin-dependent inflammatory network. *Cell*, 133(6), pp.1019–31. Available at: http://www.ncbi.nlm.nih.gov/pubmed/18555778 [Accessed April 30, 2014].

Kuo, T.-L. et al., 2015. APC haploinsufficiency coupled with p53 loss sufficiently induces mucinous cystic neoplasms and invasive pancreatic carcinoma in mice. *Oncogene*, (October 2014), pp.1–12. Available at: http://www.nature.com/doifinder/10.1038/onc.2015.284.

Kurz, D.J. et al., 2000. Senescence-associated (beta)-galactosidase reflects an increase in lysosomal mass during replicative ageing of human endothelial cells. *Journal of cell science*, 113 (Pt 2, pp.3613–22. Available at: http://www.ncbi.nlm.nih.gov/pubmed/11017877.

Kwong, J. et al., 2009. p38 and p38 Mediate Oncogenic ras-induced Senescence through Differential Mechanisms. *Journal of Biological Chemistry*, 284(17), pp.11237–11246. Available at: http://www.jbc.org/cgi/doi/10.1074/jbc.M808327200 [Accessed September 2, 2016].

Laberge, R.-M. et al., 2015. MTOR regulates the pro-tumorigenic senescence-associated secretory phenotype by promoting IL1A translation. *Nature cell biology*, Advance On(November 2014), pp.1–15. Available at: http://www.nature.com/doifinder/10.1038/ncb3195.

Labeur, M. et al., 2010. Pituitary tumors: Cell type-specific roles for BMP-4. *Molecular and Cellular Endocrinology*, 326(1), pp.85–88.

Larsimont, J.C.J.-C. et al., 2015. Sox9 Controls Self-Renewal of Oncogene Targeted Cells

and Links Tumor Initiation and Invasion. *Cell Stem Cell*, 17(1), pp.60–73. Available at: http://linkinghub.elsevier.com/retrieve/pii/S1934590915002179 [Accessed August 2, 2016].

Lawrence, T., 2009. The nuclear factor NF-kappaB pathway in inflammation. *Cold Spring Harbor perspectives in biology*, 1(6), p.a001651. Available at: http://www.ncbi.nlm.nih.gov/pubmed/20457564 [Accessed September 1, 2016].

Le, O.N.L. et al., 2010. Ionizing radiation-induced long-term expression of senescence markers in mice is independent of p53 and immune status. *Aging cell*, 9(3), pp.398–409. Available at: http://www.ncbi.nlm.nih.gov/pubmed/20331441 [Accessed August 16, 2016].

Lee, B.Y. et al., 2006. Senescence-associated beta-galactosidase is lysosomal beta-galactosidase. *Aging cell*, 5(2), pp.187–95. Available at: http://www.ncbi.nlm.nih.gov/pubmed/16626397 [Accessed July 12, 2014].

Lee, Y. et al., 2010. Absence of activating mutations of CXCR4 in pituitary tumours. *Clinical endocrinology*, 72(2), pp.209–13. Available at: http://www.ncbi.nlm.nih.gov/pubmed/19473177 [Accessed November 3, 2011].

Lee, Y., Kim, J.M. & Lee, E.J., 2008. Functional expression of CXCR4 in somatotrophs: CXCL12 activates GH gene, GH production and secretion, and cellular proliferation. *The Journal of endocrinology*, 199(2), pp.191–9. Available at: http://www.ncbi.nlm.nih.gov/pubmed/18753332 [Accessed October 27, 2011].

Lefranc, F. et al., 2003. Characterization of the levels of expression of retinoic acid receptors, galectin-3, macrophage migration inhibiting factor, and p53 in 51 adamantinomatous craniopharyngiomas. *Journal of neurosurgery*, 98(1), pp.145–53. Available at: http://www.ncbi.nlm.nih.gov/pubmed/12546363 [Accessed May 19, 2014].

Leppert, M. et al., 1987. The gene for familial polyposis coli maps to the long arm of chromosome 5. *Science (New York, N.Y.)*, 238(4832), pp.1411–3. Available at: http://www.ncbi.nlm.nih.gov/pubmed/3479843 [Accessed August 15, 2016].

Levoye, A. et al., 2009. CXCR7 heterodimerizes with CXCR4 and regulates CXCL12-mediated G protein signaling. *Blood*, 113(24), pp.6085–93. Available at: http://www.ncbi.nlm.nih.gov/pubmed/19380869 [Accessed August 31, 2011].

Li, C.-Y. et al., 2016. αE-catenin inhibits YAP/TAZ activity to regulate signalling centre formation during tooth development. *Nature Communications*, 7, p.12133. Available at: http://www.nature.com/doifinder/10.1038/ncomms12133 [Accessed February 8, 2017].

Li, W. et al., 2013. Peripheral Nerve-Derived CXCL12 and VEGF-A Regulate the Patterning of Arterial Vessel Branching in Developing Limb Skin. *Developmental cell*, 24(4), pp.359–71. Available at: http://dx.doi.org/10.1016/j.devcel.2013.01.009 [Accessed February 27, 2013].

Liang, Z. et al., 2007. CXCR4/CXCL12 axis promotes VEGF-mediated tumor angiogenesis through Akt signaling pathway. *Biochemical and Biophysical Research Communications*, 359(3), pp.716–722.

Liao, E.-C. et al., 2014. Radiation induces senescence and a bystander effect through metabolic alterations. *Cell Death and Disease*, 5(5), p.e1255. Available at: http://www.nature.com/doifinder/10.1038/cddis.2014.220 [Accessed August 16, 2016].

Lin, H.-K. et al., 2010. Skp2 targeting suppresses tumorigenesis by Arf-p53-independent cellular senescence. *Nature*, 464(7287), pp.374–379. Available at: http://www.nature.com/doifinder/10.1038/nature08815 [Accessed September 2, 2016].

Lines, K.E., Stevenson, M. & Thakker, R. V., 2016. Animal models of pituitary neoplasia. *Molecular and Cellular Endocrinology*, 421, pp.68–81. Available at: http://dx.doi.org/10.1016/j.mce.2015.08.024.

Lippitz, B.E., 2013. Cytokine patterns in patients with cancer: a systematic review. *The lancet oncology*, 14(6), pp.e218-28. Available at: http://www.ncbi.nlm.nih.gov/pubmed/23639322 [Accessed June 11, 2013].

Liu, C. et al., 2013. CXCL12/CXCR4 signal axis plays an important role in mediating bone morphogenetic protein 9-induced osteogenic differentiation of mesenchymal stem cells. *International journal of medical sciences*, 10(9), pp.1181–92. Available at: http://www.ncbi.nlm.nih.gov/pubmed/23935395 [Accessed June 30, 2016].

Liu, C. et al., 2016. Sox9 regulates self-renewal and tumorigenicity by promoting symmetrical cell division of cancer stem cells in hepatocellular carcinoma. *Hepatology (Baltimore, Md.)*, 64(1), pp.117–29. Available at: http://www.ncbi.nlm.nih.gov/pubmed/26910875 [Accessed September 1, 2016].

Liu, K. et al., 2013. The multiple roles for Sox2 in stem cell maintenance and tumorigenesis. *Cellular signalling*, 25(5), pp.1264–71. Available at: http://www.pubmedcentral.nih.gov/articlerender.fcgi?artid=3871517&tool=pmcentrez&rendertype=abstract [Accessed July 31, 2014].

Liu, T. et al., 2015. Effectiveness of AMD3100 in treatment of leukemia and solid tumors: from original discovery to use in current clinical practice. *Experimental hematology & oncology*, 5, p.19. Available at: http://www.ncbi.nlm.nih.gov/pubmed/27429863 [Accessed September 6, 2016].

Löbrich, M. & Jeggo, P. a, 2007. The impact of a negligent G2/M checkpoint on genomic instability and cancer induction. *Nature reviews. Cancer*, 7(11), pp.861–869.

Love, M.I. et al., 2014. Moderated estimation of fold change and dispersion for RNA-seq data with DESeq2. *Genome Biology*, 15(12), p.550. Available at: http://genomebiology.biomedcentral.com/articles/10.1186/s13059-014-0550-8 [Accessed September 6, 2016].

Lozano, G., 2010. Mouse models of p53 functions. *Cold Spring Harbor perspectives in biology*, 2(4), p.a001115. Available at: http://www.ncbi.nlm.nih.gov/pubmed/20452944 [Accessed September 6, 2016].

Lu, M., Grove, E. a & Miller, R.J., 2002. Abnormal development of the hippocampal dentate gyrus in mice lacking the CXCR4 chemokine receptor. *Proceedings of the National Academy of Sciences of the United States of America*, 99(10), pp.7090–5. Available at: http://www.pubmedcentral.nih.gov/articlerender.fcgi?artid=124533&tool=pmcentrez&rendertype=abstract.

Luan, J. et al., 2001. Developmental expression of two CXC chemokines, MIP-2 and KC, and their receptors. *Cytokine*, 14(5), pp.253–63. Available at: http://www.ncbi.nlm.nih.gov/pubmed/11444905 [Accessed July 17, 2013].

Lughetti, L. & Bruzzi, P., 2011. Obesity and craniopharyngioma. *Italian journal of Pedriatics*, 37(38), pp.2–7.

Lujambio, A. et al., 2013. Non-cell-autonomous tumor suppression by p53. *Cell*, 153(2), pp.449–60. Available at: http://www.ncbi.nlm.nih.gov/pubmed/23562644 [Accessed August 12, 2013].

Luo, X. et al., 2016. Stromal-Initiated Changes in the Bone Promote Metastatic Niche Development Article Stromal-Initiated Changes in the Bone Promote Metastatic Niche Development. *CellReports*, 14(1), pp.82–92. Available at: http://dx.doi.org/10.1016/j.celrep.2015.12.016.

Luo, Y. et al., 2005. Functional SDF1 alpha/CXCR4 signaling in the developing spinal cord. *Journal of neurochemistry*, 93(2), pp.452–62. Available at: http://www.ncbi.nlm.nih.gov/pubmed/15816868 [Accessed October 3, 2011].

Maciel-Barón, L.A. et al., 2016. Senescence associated secretory phenotype profile from primary lung mice fibroblasts depends on the senescence induction stimuli. *AGE*, 38(1), p.26. Available at: http://link.springer.com/10.1007/s11357-016-9886-1 [Accessed September 5, 2016].

Mainwaring, L. a & Kenney, A.M., 2011. Divergent functions for eIF4E and S6 kinase by sonic hedgehog mitogenic signaling in the developing cerebellum. *Oncogene*, 30(15), pp.1784–97. Available at: http://www.pubmedcentral.nih.gov/articlerender.fcgi?artid=3583293&tool=pmcentrez&r

endertype=abstract [Accessed August 30, 2016].

Mallette, F.A., Ferbeyre, G. & Mallette, F.A., 2007. The DNA damage signaling pathway is a critical mediator of oncogene-induced senescence. *Genes & development*, 21(514), pp.43–48.

Maretto, S. et al., 2003. Mapping Wnt/beta-catenin signaling during mouse development and in colorectal tumors. *Proceedings of the National Academy of Sciences of the United States of America*, 100(6), pp.3299–304. Available at: http://www.ncbi.nlm.nih.gov/pubmed/12626757 [Accessed September 9, 2016].

Marino, S. et al., 2000. Induction of medulloblastomas in p53-null mutant mice by somatic inactivation of Rb in the external granular layer cells of the cerebellum. *Genes & development*, 14(8), pp.994–1004. Available at: http://www.pubmedcentral.nih.gov/articlerender.fcgi?artid=316543&tool=pmcentrez&rendertype=abstract.

Markakis, E.A., 2002. Development of the neuroendocrine hypothalamus. *Frontiers in Neuroendocrinology*, 23(3), pp.257–291.

Martin, C. et al., 2003. Chemokines Acting via CXCR2 and CXCR4 Control the Release of Neutrophils from the Bone Marrow and Their Return following Senescence. *Immunity*, 19, pp.583–593.

Martin, D. et al., 2014. Accumulation of dephosphorylated 4EBP after mTOR inhibition with rapamycin is sufficient to disrupt paracrine transformation by the KSHV vGPCR oncogene. *Oncogene*, 33(18), pp.2405–2412. Available at: http://www.nature.com/doifinder/10.1038/onc.2013.193 [Accessed August 11, 2016].

Martinez-Barbera, J.P., 2015. Biology of human craniopharyngioma: lessons from mouse models. *The Journal of endocrinology*, 14, pp.161–172.

Martinez-Barbera, J.P. & Andoniadou, C.L., 2016. Concise Review: Paracrine Role of Stem Cells in Pituitary Tumors: A Focus on Adamantinomatous Craniopharyngioma. *Stem Cells*, 34(2), pp.268–276.

Massa, A. et al., 2006. SDF-1 controls pituitary cell proliferation through the activation of ERK1/2 and the Ca2+-dependent, cytosolic tyrosine kinase Pyk2. *Annals of the New York Academy of Sciences*, 1090, pp.385–98. Available at: http://www.ncbi.nlm.nih.gov/pubmed/17384283 [Accessed November 10, 2011].

Matos, L., Gouveia, A.M. & Almeida, H., 2015. ER Stress Response in Human Cellular Models of Senescence. *The journals of gerontology. Series A, Biological sciences and medical sciences*, 70(8), pp.924–35. Available at: http://www.ncbi.nlm.nih.gov/pubmed/25149687 [Accessed August 16, 2016].

Matsubara, A. et al., 2005. Endomucin, a CD34-like sialomucin, marks hematopoietic stem cells throughout development. *The Journal of experimental medicine*, 202(11), pp.1483–92. Available at: http://www.pubmedcentral.nih.gov/articlerender.fcgi?artid=2213340&tool=pmcentrez&rendertype=abstract [Accessed September 26, 2013].

McGrath, K.E. et al., 1999. Embryonic expression and function of the chemokine SDF-1 and its receptor, CXCR4. *Developmental biology*, 213(2), pp.442–56. Available at: http://www.ncbi.nlm.nih.gov/pubmed/10479460.

Meek, D.W., 2009. Tumour suppression by p53: a role for the DNA damage response? *Nature reviews. Cancer*, 9(10), pp.714–723. Available at: http://dx.doi.org/10.1038/nrc2716.

Mehendiratta, M. et al., 2012. Ghost cells: A journey in the dark…. *Dental research journal*, 9(Suppl 1), pp.S1-8. Available at: http://www.pubmedcentral.nih.gov/articlerender.fcgi?artid=3692186&tool=pmcentrez&rendertype=abstract.

Mellado, M. et al., 2007. Disrupted cardiac development but normal hematopoiesis in mice deficient in the second CXCL12/SDF-1 receptor, CXCR7. *Proceedings of the National Academy of Sciences of the United States of America*, 104(37), pp.14759–64. Available

at:
http://www.pubmedcentral.nih.gov/articlerender.fcgi?artid=1976222&tool=pmcentrez&rendertype=abstract.

Menendez, D., Inga, A. & Resnick, M. a, 2009. The expanding universe of p53 targets. *Nature reviews. Cancer*, 9(10), pp.724–737. Available at: http://dx.doi.org/10.1038/nrc2730.

Méniel, V. et al., 2014. Apc and p53 interaction in DNA damage and genomic instability in hepatocytes. *Oncogene*, (February), pp.1–12. Available at: http://www.ncbi.nlm.nih.gov/pubmed/25347740 [Accessed November 27, 2014].

Mertens, F. et al., 2015. Pituitary tumors contain a side population with tumor stem cell-associated characteristics. *Endocrine-Related Cancer*, 22(4), pp.481–504. Available at: http://erc.endocrinology-journals.org/lookup/doi/10.1530/ERC-14-0546.

Di Micco, R. et al., 2006. Oncogene-induced senescence is a DNA damage response triggered by DNA hyper-replication. *Nature*, 444(7119), pp.638–42. Available at: http://www.ncbi.nlm.nih.gov/pubmed/17136094 [Accessed November 23, 2014].

Michaloglou, C. et al., 2005. BRAFE600-associated senescence-like cell cycle arrest of human naevi. *Nature*, 436(7051), pp.720–724. Available at: http://www.nature.com/doifinder/10.1038/nature03890.

Mikels, a J. & Nusse, R., 2006. Wnts as ligands: processing, secretion and reception. *Oncogene*, 25(57), pp.7461–7468.

Mithal, D.S., Banisadr, G. & Miller, R.J., 2012. CXCL12 Signaling in the Development of the Nervous System. *Journal of Neuroimmune Pharmacology*, 7(4), pp.820–834. Available at: http://link.springer.com/10.1007/s11481-011-9336-x [Accessed August 16, 2016].

Mo, W. et al., 2013. CXCR4/CXCL12 Mediate Autocrine Cell- Cycle Progression in NF1-Associated Malignant Peripheral Nerve Sheath Tumors. *Cell*, pp.1–14. Available at: http://linkinghub.elsevier.com/retrieve/pii/S0092867413001451 [Accessed February 25, 2013].

Momota, H. et al., 2003. Immunohistochemical analysis of the p53 family members in human craniopharyngiomas. *Brain tumor pathology*, 20(2), pp.73–7. Available at: http://www.ncbi.nlm.nih.gov/pubmed/14756444 [Accessed May 19, 2014].

Moniot, B. et al., 2004. SOX9 specifies the pyloric sphincter epithelium through mesenchymal-epithelial signals. *Development (Cambridge, England)*, 131(15), pp.3795–804. Available at: http://www.ncbi.nlm.nih.gov/pubmed/15240557 [Accessed August 5, 2016].

Morin, P.J. et al., 1997. Activation of beta-catenin-Tcf signaling in colon cancer by mutations in beta-catenin or APC. *Science (New York, N.Y.)*, 275(5307), pp.1787–90. Available at: http://www.ncbi.nlm.nih.gov/pubmed/9065402 [Accessed August 15, 2016].

Mosteiro, L. et al., 2016. Tissue damage and senescence provide critical signals for cellular reprogramming in vivo. *Science*, 354(6315).

Müller, H.L., 2014. Childhood craniopharyngioma: treatment strategies and outcomes. *Expert review of neurotherapeutics*, 14(2), pp.187–97. Available at: http://www.ncbi.nlm.nih.gov/pubmed/24428758 [Accessed July 10, 2016].

Müller, H.L., 2013. Childhood craniopharyngioma. *Pituitary*, 16(1), pp.56–67. Available at: http://www.ncbi.nlm.nih.gov/pubmed/22678820 [Accessed August 4, 2012].

Müller, H.L. et al., 2004. Longitudinal study on growth and body mass index before and after diagnosis of childhood craniopharyngioma. *The Journal of clinical endocrinology and metabolism*, 89(December), pp.3298–3305. Available at: http://www.ncbi.nlm.nih.gov/pubmed/15240606 [Accessed August 9, 2016].

Muñoz-Espín, D. et al., 2013. Programmed cell senescence during mammalian embryonic development. *Cell*, 155(5), pp.1104–18. Available at: http://linkinghub.elsevier.com/retrieve/pii/S0092867413012956 [Accessed November 15, 2013].

Muñoz-Espín, D. & Serrano, M., 2014. Cellular senescence : from physiology to pathology.

Nature reviews. Molecular cell biology, 15(7), pp.482–496. Available at: http://dx.doi.org/10.1038/nrm3823.

Nakamura, M., Ohsawa, S. & Igaki, T., 2014. Mitochondrial defects trigger proliferation of neighbouring cells via a senescence-associated secretory phenotype in Drosophila. *Nature Communications*, 5, p.5264. Available at: http://www.nature.com/doifinder/10.1038/ncomms6264.

Nakanishi, Y. et al., 2013. Dclk1 distinguishes between tumor and normal stem cells in the intestine. *Nature genetics*, 45(1), pp.98–103. Available at: http://www.ncbi.nlm.nih.gov/pubmed/23202126.

Narita, M. et al., 2011. Spatial coupling of mTOR and autophagy augments secretory phenotypes. *Science (New York, N.Y.)*, 332(6032), pp.966–70. Available at: http://www.ncbi.nlm.nih.gov/pubmed/21512002 [Accessed September 5, 2016].

Negoto, T. et al., 2015. Sequential pathological changes during malignant transformation of a craniopharyngioma : A case report and review of the literature. *Surgical Neurology International*, 6(50).

Nguyen, L. V et al., 2012. Cancer stem cells: an evolving concept. *Nature reviews. Cancer*, 12(2), pp.133–43. Available at: http://www.ncbi.nlm.nih.gov/pubmed/22237392 [Accessed July 10, 2016].

Nicolas, M. et al., 2003. Notch1 functions as a tumor suppressor in mouse skin. *Nature genetics*, 33(3). Available at: http://www.ncbi.nlm.nih.gov/pubmed/12590261 [Accessed July 10, 2016].

Nie, Y. et al., 2004. The role of CXCR4 in maintaining peripheral B cell compartments and humoral immunity. *The Journal of experimental medicine*, 200(9), pp.1145–56. Available at: http://www.pubmedcentral.nih.gov/articlerender.fcgi?artid=2211858&tool=pmcentrez&rendertype=abstract [Accessed August 9, 2011].

Nielsen, E.H. et al., 2011. Incidence of craniopharyngioma in Denmark (n = 189) and estimated world incidence of craniopharyngioma in children and adults. *Journal of Neuro-Oncology*, 104(3), pp.755–763. Available at: http://link.springer.com/10.1007/s11060-011-0540-6 [Accessed August 9, 2016].

Nochols, K.E. et al., 2001. Germ-line p53 mutations predispose to a wide spectrum of early-onset cancers. *Cancer Epidemiology Biomarkers and Prevention*, 10(2), pp.83–87.

Nomiyama, H., Osada, N. & Yoshie, O., 2013. Systematic classification of vertebrate chemokines based on conserved synteny and evolutionary history. *Genes to cells : devoted to molecular & cellular mechanisms*, 18(1), pp.1–16. Available at: http://www.pubmedcentral.nih.gov/articlerender.fcgi?artid=3568907&tool=pmcentrez&rendertype=abstract [Accessed September 28, 2013].

Nomura, R., Yoshida, D. & Teramoto, A., 2009. Stromal cell-derived factor-1 expression in pituitary adenoma tissues and upregulation in hypoxia. *Journal of neuro-oncology*, 94(2), pp.173–81. Available at: http://www.ncbi.nlm.nih.gov/pubmed/19280118 [Accessed November 5, 2011].

Norbury, C.J. & Zhivotovsky, B., 2004. DNA damage-induced apoptosis. *Oncogene*, 23(16), pp.2797–2808. Available at: http://www.nature.com/doifinder/10.1038/sj.onc.1207532 [Accessed August 19, 2016].

Nozaki, M. et al., 1998. Rare occurrence of inactivating p53 gene mutations in primary non-astrocytic tumors of the central nervous system: reappraisal by yeast functional assay. *Acta neuropathologica*, 95(3), pp.291–6. Available at: http://www.ncbi.nlm.nih.gov/pubmed/9542595 [Accessed December 8, 2015].

Nusse, R. & Varmus, H.E., 1982. Many tumors induced by the mouse mammary tumor virus contain a provirus integrated in the same region of the host genome. *Cell*, 31(1), pp.99–109. Available at: http://www.ncbi.nlm.nih.gov/pubmed/6297757 [Accessed August 15, 2016].

Ohanna, M. et al., 2013. Secretome from senescent melanoma engages the STAT3 pathway to favor reprogramming of naive melanoma towards a tumor-initiating cell phenotype . *Oncotarget*, 4(12), pp.2012–2224. Available at: http://www.pubmedcentral.nih.gov/articlerender.fcgi?artid=3926821&tool=pmcentrez&rendertype=abstract.

Ohanna, M. et al., 2011. Senescent cells develop a PARP-1 and nuclear factor- k B-associated secretome (PNAS). *Genes & Development*, 25, pp.1245–1261.

Ohtani, N. & Hara, E., 2013. Roles and mechanisms of cellular senescence in regulation of tissue homeostasis. *Cancer Science*, 104(5), pp.525–530.

Oikonomou, E. et al., 2005. Beta-catenin mutations in craniopharyngiomas and pituitary adenomas. *Journal of neuro-oncology*, 73(3), pp.205–9. Available at: http://www.ncbi.nlm.nih.gov/pubmed/15980970 [Accessed September 5, 2016].

Olivier, M., Hollstein, M. & Hainaut, P., 2010. TP53 Mutations in Human Cancers: Origins, Consequences, and Clinical Use. *Cold Spring Harbor Perspectives in Biology*, 2(1), pp.a001008–a001008. Available at: http://cshperspectives.cshlp.org/lookup/doi/10.1101/cshperspect.a001008 [Accessed August 19, 2016].

Oshima, H. et al., 2014. TNF-α/TNFR1 signaling promotes gastric tumorigenesis through induction of Noxo1 and Gna14 in tumor cells. *Oncogene*, 33(29), pp.3820–9. Available at: http://www.ncbi.nlm.nih.gov/pubmed/23975421 [Accessed August 11, 2016].

Pankiv, S. et al., 2007. p62/SQSTM1 Binds Directly to Atg8/LC3 to Facilitate Degradation of Ubiquitinated Protein Aggregates by Autophagy. *Journal of Biological Chemistry*, 282(33), pp.24131–24145. Available at: http://www.jbc.org/lookup/doi/10.1074/jbc.M702824200 [Accessed September 5, 2016].

Park, W.-Y. et al., 2016. H3K27 Demethylase JMJD3 Employs the NF-κB and BMP Signaling Pathways to Modulate the Tumor Microenvironment and Promote Melanoma Progression and Metastasis. *Cancer research*, 76(1), pp.161–70. Available at: http://www.ncbi.nlm.nih.gov/pubmed/26729791 [Accessed August 31, 2016].

Parrinello, S. et al., 2005. Stromal-epithelial interactions in aging and cancer: senescent fibroblasts alter epithelial cell differentiation. *Journal of cell science*, 118(Pt 3), pp.485–96. Available at: http://www.ncbi.nlm.nih.gov/pubmed/15657080 [Accessed August 17, 2016].

Perez-Castro, C. et al., 2012. Cellular and molecular specificity of pituitary gland physiology. *Physiological Reviews*, 92(1), pp.1–38. Available at: http://www.ncbi.nlm.nih.gov/pubmed/22298650.

Perkins, N.D., 2007. Integrating cell-signalling pathways with NF-κB and IKK function. *Nature Reviews Molecular Cell Biology*, 8(1), pp.49–62. Available at: http://www.nature.com/doifinder/10.1038/nrm2083 [Accessed September 5, 2016].

Phalke, S. et al., 2012. p53-Independent regulation of p21Waf1/Cip1 expression and senescence by PRMT6. *Nucleic acids research*, 40(19), pp.9534–42. Available at: http://www.ncbi.nlm.nih.gov/pubmed/22987071 [Accessed July 25, 2016].

Pitt, L.A. et al., 2015. CXCL12-Producing Vascular Endothelial Niches Control Acute T Cell Leukemia Maintenance. *Cancer Cell*, 27(6), pp.755–768. Available at: http://linkinghub.elsevier.com/retrieve/pii/S1535610815001786 [Accessed September 1, 2016].

Pluquet, O. et al., 2015. The unfolded protein response and cellular senescence. A review in the theme: cellular mechanisms of endoplasmic reticulum stress signaling in health and disease. *American journal of physiology. Cell physiology*, 308(6), pp.C415-25. Available at: http://www.ncbi.nlm.nih.gov/pubmed/25540175 [Accessed August 16, 2016].

Polakis, P., 2007. The many ways of Wnt in cancer. *Current Opinion in Genetics & Development*, 17(1), pp.45–51.

Polaskis, P., 2012. Wnt signaling in cancer. *Cold Spring Harbor Perscpetives in Biology*, 4(5),

pp.1–14.

Pollina, E.A. & Brunet, A., 2011. Epigenetic regulation of aging stem cells. *Oncogene*, 30(28), pp.3105–3126. Available at: http://www.nature.com/doifinder/10.1038/onc.2011.45 [Accessed August 17, 2016].

Potok, M.A. et al., 2008. WNT signaling affects gene expression in the ventral diencephalon and pituitary gland growth. *Developmental dynamics : an official publication of the American Association of Anatomists*, 237(4), pp.1006–20. Available at: http://www.pubmedcentral.nih.gov/articlerender.fcgi?artid=2799114&tool=pmcentrez&rendertype=abstract [Accessed December 3, 2012].

Prieur, A. et al., 2011. p53 and p16(INK4A) independent induction of senescence by chromatin-dependent alteration of S-phase progression. *Nature communications*, 2(May), p.473. Available at: http://www.nature.com/doifinder/10.1038/ncomms1473 [Accessed July 25, 2016].

Qi, S. et al., 2013. Growth and weight of children with craniopharyngiomas based on the tumour location and growth pattern. *J Clin Neurosci*, 20(12), pp.1702–1708. Available at: http://dx.doi.org/10.1016/j.jocn.2012.12.030.

Rahrmann, E.P. et al., 2014. Trp53 haploinsufficiency modifies EGFR-driven peripheral nerve sheath tumorigenesis. *Am J Pathol*, 184(7), pp.2082–2098. Available at: http://ac.els-cdn.com/S0002944014002302/1-s2.0-S0002944014002302-main.pdf?_tid=fa9371ac-a257-11e4-92e3-00000aacb361&acdnat=1421946127_1d248289d74a6f990a59990e53237cb6.

Rajagopal, S. et al., 2010. Beta-arrestin- but not G protein-mediated signaling by the "decoy" receptor CXCR7. *Proceedings of the National Academy of Sciences of the United States of America*, 107(2), pp.628–32. Available at: http://www.pubmedcentral.nih.gov/articlerender.fcgi?artid=2818968&tool=pmcentrez&rendertype=abstract [Accessed March 25, 2012].

Reddy, R.K., 2011. *Characterisation of Gene Expression Patterns in a Mouse Model for Adamantinomatous Craniopharyngioma*. University College London.

Rehman, A.O. & Wang, C., 2009. CXCL12/SDF-1 alpha activates NF-kappaB and promotes oral cancer invasion through the Carma3/Bcl10/Malt1 complex. *International journal of oral science*, 1(3), pp.105–18. Available at: http://www.ncbi.nlm.nih.gov/pubmed/20695076 [Accessed September 1, 2016].

Reya, T. & Clevers, H., 2005. Wnt signalling in stem cells and cancer. *Nature*, 434(7035), pp.843–50. Available at: http://www.ncbi.nlm.nih.gov/pubmed/15829953.

Ridgeway, a G., McMenamin, J. & Leder, P., 2006. P53 levels determine outcome during beta-catenin tumor initiation and metastasis in the mammary gland and male germ cells. *Oncogene*, 25(25), pp.3518–27. Available at: http://www.ncbi.nlm.nih.gov/pubmed/16434961.

Ritschka, B. et al., 2017. The senescence-associated secretory phenotype induces cellular plasticity and tissue regeneration. *Genes and Development*, 31, pp.1–12.

Rizzoti, K., 2015. Genetic regulation of murine pituitary development. *Journal of Medical Endocrinology*, (January), pp.1–37.

Rizzoti, K., Akiyama, H. & Lovell-Badge, R., 2013. Mobilized Adult Pituitary Stem Cells Contribute to Endocrine Regeneration in Response to Physiological Demand. *Cell Stem Cell*, 13(4), pp.419–432. Available at: http://www.pubmedcentral.nih.gov/articlerender.fcgi?artid=3793864&tool=pmcentrez&rendertype=abstract [Accessed May 27, 2014].

Robertson, E.J. & Soriano, P., 1999. Generalized lacZ expression with the ROSA26 Cre reporter strain. *Nature genetics*, 21(1), pp.70–1. Available at: http://www.ncbi.nlm.nih.gov/pubmed/9916792.

Rodier, F. et al., 2009. Persistent DNA damage signalling triggers senescence-associated inflammatory cytokine secretion. *Nature cell biology*, 11(8), pp.973–9. Available at:

http://dx.doi.org/10.1038/ncb1909 [Accessed December 14, 2013].

Rodriguez, F.J. et al., 2007. The spectrum of malignancy in craniopharyngioma. *The American journal of surgical pathology*, 31(7), pp.1020–8. Available at: http://www.ncbi.nlm.nih.gov/pubmed/17592268.

Rogelj, S. et al., 1988. Basic fibroblast growth factor fused to a signal peptide transforms cells. *Nature*, 331(6152). Available at: http://www.nature.com/doifinder/10.1038/331173a0 [Accessed July 10, 2016].

Rostène, W. et al., 2011. Chemokines and chemokine receptors: new actors in neuroendocrine regulations. *Frontiers in neuroendocrinology*, 32(1), pp.10–24. Available at: http://www.ncbi.nlm.nih.gov/pubmed/20624414 [Accessed June 25, 2011].

Rovillain, E. et al., 2011. Activation of nuclear factor-kappa B signalling promotes cellular senescence. *Oncogene*, 30(20), pp.2356–2366. Available at: http://dx.doi.org/10.1038/onc.2010.611.

Rubinfeld, B. et al., 1993. Association of the APC gene product with beta-catenin. *Science (New York, N.Y.)*, 262(5140), pp.1731–4. Available at: http://www.ncbi.nlm.nih.gov/pubmed/8259518 [Accessed August 15, 2016].

Rubinfeld, B. et al., 1997. Stabilization of beta-catenin by genetic defects in melanoma cell lines. *Science (New York, N.Y.)*, 275(5307), pp.1790–2. Available at: http://www.ncbi.nlm.nih.gov/pubmed/9065403 [Accessed August 15, 2016].

Ruhland, M.K. et al., 2016. Stromal senescence establishes an immunosuppressive microenvironment that drives tumorigenesis. *Nature communications*, 7, p.11762. Available at: http://www.ncbi.nlm.nih.gov/pubmed/27272654 [Accessed August 17, 2016].

Rusten, T.E. & Stenmark, H., 2010. P62, an Autophagy Hero or Culprit? *Nature cell biology*, 12(3), pp.207–209. Available at: http://dx.doi.org/10.1038/ncb0310-207.

Sagiv, A. et al., 2013. Granule exocytosis mediates immune surveillance of senescent cells. *Oncogene*, 32(15), pp.1971–1977. Available at: http://www.nature.com/doifinder/10.1038/onc.2012.206 [Accessed August 17, 2016].

Sajedi, E. et al., 2013. Analysis of mouse models carrying the I26T and R160C substitutions in the transcriptional repressor HESX1 as models for septo-optic dysplasia and hypopituitarism. *Disease models & mechanisms*, 1(4–5), pp.241–54. Available at: http://www.pubmedcentral.nih.gov/articlerender.fcgi?artid=2590837&tool=pmcentrez&rendertype=abstract [Accessed April 2, 2013].

Salama, R. et al., 2014. Cellular senescence and its effector programs. *Genes & development*, 28(2), pp.99–114. Available at: http://genesdev.cshlp.org/cgi/doi/10.1101/gad.235184.113 [Accessed May 27, 2014].

Saland, L.C., 2001. The mammalian pituitary intermediate lobe : An update on innervation and regulation. *Brain Reseach Bulletin*, 54(6), pp.587–593.

Salminen, A. et al., 2008. Activation of innate immunity system during aging: NF-kB signaling is the molecular culprit of inflamm-aging. *Ageing Research Reviews*, 7(2), pp.83–105.

Salminen, A., Kauppinen, A. & Kaarniranta, K., 2012. Emerging role of NF-κB signaling in the induction of senescence-associated secretory phenotype (SASP). *Cellular signalling*, 24(4), pp.835–45. Available at: http://www.ncbi.nlm.nih.gov/pubmed/22182507 [Accessed May 30, 2014].

Samulowitz, U. et al., 2002. Human Endomucin. , 160(5), pp.1669–1681.

Sánchez-Alcañiz, J.A. et al., 2011. Cxcr7 controls neuronal migration by regulating chemokine responsiveness. *Neuron*, 69(1), pp.77–90. Available at: http://www.ncbi.nlm.nih.gov/pubmed/21220100 [Accessed July 26, 2011].

Sarkar, S., 2013. Regulation of autophagy by mTOR-dependent and mTOR-independent pathways: autophagy dysfunction in neurodegenerative diseases and therapeutic application of autophagy enhancers. *Biochemical Society Transactions*, 41(5), pp.1103–

30. Available at: http://www.ncbi.nlm.nih.gov/pubmed/24059496.

Sarkisian, C.J. et al., 2007. Dose-dependent oncogene-induced senescence in vivo and its evasion during mammary tumorigenesis. *Nature Cell Biology*, 9(5), pp.493–505. Available at: http://www.nature.com/doifinder/10.1038/ncb1567 [Accessed August 19, 2016].

Sasaki, M. et al., 2001. Senescent cells are resistant to death despite low Bcl-2 level. *Mechanisms of ageing and development*, 122(15), pp.1695–706. Available at: http://www.ncbi.nlm.nih.gov/pubmed/11557274 [Accessed September 1, 2016].

Sato, S. et al., 2015. Ablation of the p16INK4a tumour suppressor reverses ageing phenotypes of klotho mice. *Nature Communications*, 6, p.7035. Available at: http://www.nature.com/doifinder/10.1038/ncomms8035 [Accessed July 25, 2016].

Sauer, B. & Henderson, N., 1988. Site-specific DNA recombination in mammalian cells by the Cre recombinase of bacteriophage P1. *Proceedings of the National Academy of Sciences of the United States of America*, 85(14), pp.5166–70. Available at: http://www.pubmedcentral.nih.gov/articlerender.fcgi?artid=281709&tool=pmcentrez&rendertype=abstract.

Scagliotti, V. et al., 2015. Histopathology and molecular characterisation of intrauterine-diagnosed congenital craniopharyngioma. *Pituitary*, 19(1), pp.50–56.

Schepers, A.G. et al., 2012. Lineage Tracing Reveals Lgr5+ Stem Cell Activity in Mouse Intestinal Adenomas. *Science*, 337(October), pp.449–452.

Schindelin, J. et al., 2012. Fiji: an open-source platform for biological-image analysis. *Nature methods*, 9(7), pp.676–82. Available at: http://www.ncbi.nlm.nih.gov/pubmed/22743772 [Accessed September 6, 2016].

Scott, C.E. et al., 2010. SOX9 induces and maintains neural stem cells. *Nature Neuroscience*, 13(10), pp.1181–1189. Available at: http://www.nature.com/doifinder/10.1038/nn.2646 [Accessed September 1, 2016].

Seaberg, R.M. & Van Der Kooy, D., 2003. Stem and progenitor cells: the premature desertion of rigorous definitions. *Trends in neurosciences*, 26(3).

Sekine, S. et al., 2002. *Craniopharyngiomas of Adamantinomatous Type Harbor β-Catenin Gene Mutations*,

Sekine, S. et al., 2004. Expression of enamel proteins and LEF1 in adamantinomatous craniopharyngioma: evidence for its odontogenic epithelial differentiation. *Histopathology*, 45(6), pp.573–9. Available at: http://www.ncbi.nlm.nih.gov/pubmed/15569047.

Sengupta, R. et al., 2012. CXCR4 activation defines a new subgroup of Sonic hedgehog-driven medulloblastoma. *Cancer research*, 72(1), pp.122–32. Available at: http://www.ncbi.nlm.nih.gov/pubmed/22052462 [Accessed October 10, 2012].

Serrano, M. et al., 1997. Oncogenic ras provokes premature cell senescence associated with accumulation of p53 and p16(INK4a). *Cell*, 88(5), pp.593–602.

Serrano, M. et al., 1996. Role of the INK4a locus in tumor suppression and cell mortality. *Cell*, 85(1), pp.27–37. Available at: http://www.ncbi.nlm.nih.gov/pubmed/8620534 [Accessed August 19, 2016].

Serrano, M., Hannon, G.J. & Beach, D., 1993. A new regulatory motif in cell-cycle control causing specific inhibition of cyclin D/CDK4. *Nature*, 366(6456), pp.704–7. Available at: http://www.ncbi.nlm.nih.gov/pubmed/8259215 [Accessed December 7, 2015].

Seymour, P.A. et al., 2007. SOX9 is required for maintenance of the pancreatic progenitor cell pool. *Proceedings of the National Academy of Sciences of the United States of America*, 104(6), pp.1865–70. Available at: http://www.ncbi.nlm.nih.gov/pubmed/17267606 [Accessed August 5, 2016].

Sharma, a & Sen, J.M., 2013. Molecular basis for the tissue specificity of β-catenin oncogenesis. *Oncogene*, 32(15), pp.1901–9. Available at:

http://www.pubmedcentral.nih.gov/articlerender.fcgi?artid=3534820&tool=pmcentrez&rendertype=abstract [Accessed May 29, 2014].

Sharpless, N.E. & Sherr, C.J., 2015. Forging a signature of in vivo senescence. *Nature Reviews Cancer*, 15(7), pp.397–408. Available at: http://www.nature.com/doifinder/10.1038/nrc3960.

Shaw, A.C. et al., 2010. Aging of the innate immune system. *Current Opinion in Immunology*, 22(4), pp.507–513.

Shelton, D.N. et al., 1999. Microarray analysis of replicative senescence. *Current Biology*, 9(17), pp.939–945.

Shlomo Melmed, 2011. Hypothalamic Regulation of Anterior Pituitary Function. In *The Pituitary*. London: Elsevier, pp. 21–41.

Singh, A.P. et al., 2012. CXCL12/CXCR4 signaling axis induces SHH expression in pancreatic cancer cells via ERK- and Akt- mediated activation of NF-κB: implications for bidirectional tumor-stromal interactions. *The Journal of biological chemistry*, 287(46), pp.39115–39124. Available at: http://www.ncbi.nlm.nih.gov/pubmed/22995914 [Accessed November 1, 2012].

Slack, J.M.W., 2008. Origin of stem cells in organogenesis. *Science (New York, N.Y.)*, 322(5907), pp.1498–501. Available at: http://www.ncbi.nlm.nih.gov/pubmed/19056975 [Accessed August 3, 2016].

Sofela, A.A. et al., 2014. Malignant transformation in craniopharyngiomas. *Neurosurgery*, 75(3), p.306–14; discussion 314. Available at: http://www.ncbi.nlm.nih.gov/pubmed/24978859.

Spike, B.T. & Wahl, G.M., 2011. p53, Stem Cells, and Reprogramming: Tumor Suppression beyond Guarding the Genome. *Genes & cancer*, 2(4), pp.404–19. Available at: http://www.pubmedcentral.nih.gov/articlerender.fcgi?artid=3135646&tool=pmcentrez&rendertype=abstract [Accessed August 28, 2014].

Stache, C., Hölsken, A., Schlaffer, S.-M., et al., 2014. Insights into the infiltrative behavior of adamantinomatous craniopharyngioma in a new xenotransplant mouse model. *Brain pathology (Zurich, Switzerland)*, pp.1–25. Available at: http://www.ncbi.nlm.nih.gov/pubmed/24716541 [Accessed May 8, 2014].

Stache, C., Hölsken, A., Fahlbusch, R., et al., 2014. Tight junction protein claudin-1 is differentially expressed in craniopharyngioma subtypes and indicates invasive tumor growth. *Neuro-oncology*, 16(2), pp.256–264.

Stamos, J.L. & Weis, W.I., 2013. The beta-Catenin Destruction Complex. *Cold Spring Harbor Perscpetives in Biology*, 5, pp.1–16.

Steele, C.W. et al., 2016. CXCR2 Inhibition Profoundly Suppresses Metastases and Augments Immunotherapy in Pancreatic Ductal Adenocarcinoma. *Cancer Cell*, 29, pp.832–845. Available at: http://dx.doi.org/10.1016/j.ccell.2016.04.014 [Accessed September 1, 2016].

Stolt, C.C. et al., 2003. The Sox9 transcription factor determines glial fate choice in the developing spinal cord. *Genes & development*, 17(13), pp.1677–89. Available at: http://www.ncbi.nlm.nih.gov/pubmed/12842915 [Accessed August 5, 2016].

Storer, M. et al., 2013. Senescence Is a Developmental Mechanism that Contributes to Embryonic Growth and Patterning. *Cell*, 155(5), pp.1119–1130. Available at: http://www.ncbi.nlm.nih.gov/pubmed/24238961 [Accessed November 15, 2013].

Stumm, R.K. et al., 2003. CXCR4 regulates interneuron migration in the developing neocortex. *The Journal of neuroscience : the official journal of the Society for Neuroscience*, 23(12), pp.5123–30. Available at: http://www.ncbi.nlm.nih.gov/pubmed/12832536.

Su, L.K. et al., 1992. Multiple intestinal neoplasia caused by a mutation in the murine homolog of the APC gene. *Science (New York, N.Y.)*, 256(5057), pp.668–70. Available at: http://www.ncbi.nlm.nih.gov/pubmed/1350108 [Accessed August 15, 2016].

Su, L.K., Vogelstein, B. & Kinzler, K.W., 1993. Association of the APC tumor suppressor protein with catenins. *Science (New York, N.Y.)*, 262(5140), pp.1734–7. Available at: http://www.ncbi.nlm.nih.gov/pubmed/8259519 [Accessed August 15, 2016].

Subramanian, A. et al., 2005. Gene set enrichment analysis: A knowledge-based approach for interpreting genome-wide expression profiles. *Proceedings of the National Academy of Sciences*, 102(43), pp.15545–15550. Available at: http://www.pnas.org/cgi/doi/10.1073/pnas.0506580102 [Accessed September 6, 2016].

Sugrue, M.M. et al., 1997. Wild-type p53 triggers a rapid senescence program in human tumor cells lacking functional p53. *Proceedings of the National Academy of Sciences of the United States of America*, 94(18), pp.9648–53. Available at: http://www.ncbi.nlm.nih.gov/pubmed/9275177 [Accessed August 17, 2016].

Sun, D. et al., 2013. Sox9-related signaling controls zebrafish juvenile ovary-testis transformation. *Cell death & disease*, 4, p.e930. Available at: http://www.ncbi.nlm.nih.gov/pubmed/24263104 [Accessed August 5, 2016].

Sun, X. et al., 2010. CXCL12/CXCR4/CXCR7 Chemokine Axis and Cancer Progression. *Cancer Metastasis Reviews*, 29(4), pp.709–722.

Swartling, F.J. et al., 2012. Distinct Neural Stem Cell Populations Give Rise to Disparate Brain Tumors in Response to N-MYC. *Cancer Cell*, 21(5), pp.601–613. Available at: http://linkinghub.elsevier.com/retrieve/pii/S153561081200164X [Accessed September 1, 2016].

Takuma, N. et al., 1998. Formation of Rathke's pouch requires dual induction from the diencephalon. *Development (Cambridge, England)*, 125(23), pp.4835–40. Available at: http://www.ncbi.nlm.nih.gov/pubmed/9806931 [Accessed August 3, 2016].

Tanida, I., Ueno, T. & Kominami, E., 2010. LC3 and Autophagy. *Methods in molecular biology (Clifton, N.J.)*, 648.

Tasdemir, N. et al., 2016. BRD4 connects enhancer remodeling to senescence immune surveillance. *Cancer Discovery*. Available at: http://cancerdiscovery.aacrjournals.org/cgi/doi/10.1158/2159-8290.CD-16-0217.

Tateyama, H. et al., 2001. Different keratin profiles in craniopharyngioma subtypes and ameloblastomas. *Pathology, research and practice*, 197(11), pp.735–42. Available at: http://www.ncbi.nlm.nih.gov/pubmed/11770017 [Accessed November 1, 2012].

Tchkonia, T. et al., 2013. Cellular senescence and the senescent secretory phenotype: therapeutic opportunities. *The Journal of clinical investigation*, 123(3), pp.966–72. Available at: http://www.jci.org/articles/view/64098 [Accessed January 7, 2014].

Teicher, B. a & Fricker, S.P., 2010. CXCL12 (SDF-1)/CXCR4 pathway in cancer. *Clinical cancer research : an official journal of the American Association for Cancer Research*, 16(11), pp.2927–31. Available at: http://www.ncbi.nlm.nih.gov/pubmed/20484021 [Accessed July 25, 2011].

Tena-Suck, M.L. et al., 2006. Clinico-pathological and immunohistochemical characteristics associated to recurrence/regrowth of craniopharyngiomas. *Clinical Neurology and Neurosurgery*, 108(7), pp.661–669.

Teoh, P.J. et al., 2014. P53 Haploinsufficiency and Functional Abnormalities in Multiple Myeloma. *Leukemia*, 28(10), pp.2066–74. Available at: http://www.ncbi.nlm.nih.gov/pubmed/24625551.

The Cancer Genome Atlas Network, 2012. Comprehensive molecular characterization of human colon and rectal cancer. *Nature*, 487(7407), pp.330–337. Available at: http://dx.doi.org/10.1038/nature11252%5Cnhttp://www.pubmedcentral.nih.gov/articlerender.fcgi?artid=3401966&tool=pmcentrez&rendertype=abstract%5Cnhttp://adsabs.harvard.edu/abs/2012natur.487..330t.

Theveneau, E. et al., 2010. Collective Chemotaxis Requires Contact-Dependent Cell Polarity. *Developmental Cell*, 19(1), pp.39–53. Available at: http://www.springerlink.com/index/n3m2217446178852.pdf [Accessed November 3,

2011].

Theveneau, E. & Mayor, R., 2012. Neural crest delamination and migration: from epithelium-to-mesenchyme transition to collective cell migration. *Developmental biology*, 366(1), pp.34–54. Available at: http://www.ncbi.nlm.nih.gov/pubmed/22261150 [Accessed October 30, 2012].

Thomas, P. et al., 1996. Anterior primitive endoderm may be responsible for patterning the anterior neural plate in the mouse embryo. *Current Biology*, 6(11), pp.1487–1496. Available at: http://linkinghub.elsevier.com/retrieve/pii/S0960982296007531 [Accessed September 5, 2016].

Thomas Kuilman et al., 2010. The essence of senescence. *Genes and Development*, 24, pp.2463–2479.

Trautmann, F. et al., 2014. CXCR4 as biomarker for radioresistant cancer stem cells. *International journal of radiation biology*, 90(8), pp.687–99. Available at: http://www.ncbi.nlm.nih.gov/pubmed/24650104 [Accessed July 7, 2016].

Treier, M. et al., 2001. Hedgehog signaling is required for pituitary gland development. *Development (Cambridge, England)*, 128(3), pp.377–86. Available at: http://www.ncbi.nlm.nih.gov/pubmed/11152636 [Accessed August 3, 2016].

Treier, M. et al., 1998. Multistep signaling requirements for pituitary organogenesis in vivo. *Genes & Development*, 12(11), pp.1691–1704. Available at: http://www.genesdev.org/cgi/doi/10.1101/gad.12.11.1691 [Accessed August 7, 2012].

Tu, T.C. et al., 2016. A Chemokine Receptor, CXCR4, Which Is Regulated by Hypoxia-Inducible Factor 2α, Is Crucial for Functional Endothelial Progenitor Cells Migration to Ischemic Tissue and Wound Repair. *Stem cells and development*, 25(3), pp.266–76. Available at: http://www.ncbi.nlm.nih.gov/pubmed/26620723 [Accessed August 16, 2016].

Uy, G.L. et al., 2012. A phase 1/2 study of chemosensitization with the CXCR4 antagonist plerixafor in relapsed or refractory acute myeloid leukemia. *Blood*, 119(17), pp.3917–24. Available at: http://www.ncbi.nlm.nih.gov/pubmed/22308295 [Accessed September 1, 2016].

Valent, P. et al., 2012. Cancer stem cell definitions and terminology: the devil is in the details. *Nature reviews. Cancer*, 12(11), pp.767–75. Available at: http://www.ncbi.nlm.nih.gov/pubmed/23051844 [Accessed July 10, 2016].

Vankelecom, H., 2010. Pituitary stem/progenitor cells: embryonic players in the adult gland? *The European journal of neuroscience*, 32(12), pp.2063–81. Available at: http://www.ncbi.nlm.nih.gov/pubmed/21143661 [Accessed July 30, 2011].

Vankelecom, H. & Gremeaux, L., 2010. Stem cells in the pituitary gland: A burgeoning field. *General and comparative endocrinology*, 166(3), pp.478–88. Available at: http://dx.doi.org/10.1016/j.ygcen.2009.11.007 [Accessed August 1, 2012].

Venkatachalam, S. et al., 2001. Is p53 Haploinsufficient for Tumor Suppression? Implications for the p53+/+ Mouse Model in Carcinogenicity Testing. *Toxicologic pathology*, 29(4), pp.147–154.

Venkatachalam, S. et al., 1998. Retention of wild-type p53 in tumors from p53 heterozygous mice: reduction of p53 dosage can promote cancer formation. *The EMBO Journal*, 17(16), pp.4657–4667.

Ventura, A. et al., 2007. Restoration of p53 function leads to tumour regression in vivo. *Nature*, 445(7128), pp.661–665. Available at: http://www.nature.com/doifinder/10.1038/nature05541 [Accessed August 19, 2016].

Virgintino, D. et al., 2013. The CXCL12/CXCR4/CXCR7 ligand-receptor system regulates neuro-glio-vascular interactions and vessel growth during human brain development. *Journal of inherited metabolic disease*, 36(3), pp.455–66. Available at: http://www.ncbi.nlm.nih.gov/pubmed/23344887 [Accessed August 30, 2013].

Visvader, J.E. et al., 2012. Cancer stem cells: current status and evolving complexities. *Cell*

stem cell, 10(6), pp.717–28. Available at: http://www.ncbi.nlm.nih.gov/pubmed/22704512 [Accessed July 10, 2016].

Vital, P. et al., 2014. The senescence-associated secretory phenotype promotes benign prostatic hyperplasia. *American Journal of Pathology*, 184(3), pp.721–731. Available at: http://dx.doi.org/10.1016/j.ajpath.2013.11.015.

Vousden, K.H. & Ryan, K.M., 2009. P53 and Metabolism. *Nature reviews. Cancer*, 9(10), pp.691–700.

Wagner, J. et al., 2015. Overexpression of the novel senescence marker β-galactosidase (GLB1) in prostate cancer predicts reduced PSA recurrence. *PloS one*, 10(4), p.e0124366. Available at: http://www.ncbi.nlm.nih.gov/pubmed/25876105 [Accessed August 19, 2016].

Wajapeyee, N. et al., 2008. Oncogenic BRAF induces senescence and apoptosis through pathways mediated by the secreted protein IGFBP7. *Cell*, 132(3), pp.363–74. Available at: http://www.ncbi.nlm.nih.gov/pubmed/18267069 [Accessed August 17, 2016].

Wang, C. et al., 2009. DNA damage response and cellular senescence in tissues of aging mice. *Aging Cell*, 8(3), pp.311–323. Available at: http://doi.wiley.com/10.1111/j.1474-9726.2009.00481.x [Accessed August 17, 2016].

Wang, Y. et al., 2011. CXCR4 and CXCR7 have distinct functions in regulating interneuron migration. *Neuron*, 69(1), pp.61–76. Available at: http://dx.doi.org/10.1016/j.neuron.2010.12.005 [Accessed July 14, 2011].

Ward, R.D. et al., 2006. Cell proliferation and vascularization in mouse models of pituitary hormone deficiency. *Molecular endocrinology (Baltimore, Md.)*, 20(6), pp.1378–90. Available at: http://www.ncbi.nlm.nih.gov/pubmed/16556738 [Accessed August 11, 2012].

Weaver, A.N. & Yang, E.S., 2013. Beyond DNA Repair: Additional Functions of PARP-1 in Cancer. *Frontiers in oncology*, 3(November), p.290. Available at: http://www.pubmedcentral.nih.gov/articlerender.fcgi?artid=3841914&tool=pmcentrez&rendertype=abstract [Accessed October 20, 2014].

Wesche, J. et al., 2011. Fibroblast growth factors and their receptors in cancer. *The Biochemical journal*, 437(2), pp.199–213. Available at: http://www.ncbi.nlm.nih.gov/pubmed/21711248 [Accessed August 11, 2016].

van der Weyden, L. et al., 2012. Jdp2 downregulates Trp53 transcription to promote leukaemogenesis in the context of Trp53 heterozygosity. *Oncogene*, 32(3), pp.397–402. Available at: http://dx.doi.org/10.1038/onc.2012.56.

White, E., 2012. Deconvoluting the context-dependent role for autophagy in cancer. *Nat Rev Cancer*, 12(6), pp.401–410.

White, R.R. et al., 2015. Controlled induction of DNA double-strand breaks in the mouse liver induces features of tissue ageing. *Nature communications*, 6, p.6790. Available at: http://www.ncbi.nlm.nih.gov/pubmed/25858675.

Wirawan, E. et al., 2012. Autophagy: for better or for worse. *Cell research*, 22(1), pp.43–61. Available at: http://www.pubmedcentral.nih.gov/articlerender.fcgi?artid=3351915&tool=pmcentrez&rendertype=abstract [Accessed January 21, 2014].

Wood, L.D. et al., 2007. The Genomic Landscapes of Human Breast and Colorectal Cancers. *Science*, 318(5853), pp.1108–1113. Available at: http://www.sciencemag.org/cgi/content/abstract/318/5853/1108.

Wu, Y. et al., 2012. A chemokine receptor CXCR2 macromolecular complex regulates neutrophil functions in inflammatory diseases. *The Journal of biological chemistry*, 287(8), pp.5744–55. Available at: http://www.pubmedcentral.nih.gov/articlerender.fcgi?artid=3285346&tool=pmcentrez&rendertype=abstract [Accessed April 18, 2013].

Würth, R. et al., 2014. CXCL12 modulation of CXCR4 and CXCR7 activity in human

glioblastoma stem-like cells and regulation of the tumor microenvironment. *Frontiers in cellular neuroscience*, 8, p.144. Available at: http://www.ncbi.nlm.nih.gov/pubmed/24904289 [Accessed July 7, 2016].

Xavier, G.M. et al., 2015. Activated WNT signaling in postnatal SOX2-positive dental stem cells can drive odontoma formation. *Scientific Reports*, 5(April), p.14479. Available at: http://www.nature.com/doifinder/10.1038/srep14479.

Xu, M. et al., 2008. Beta-catenin expression results in p53-independent DNA damage and oncogene-induced senescence in prelymphomagenic thymocytes in vivo. *Molecular and cellular biology*, 28(5), pp.1713–1723. Available at: http://mcb.asm.org/cgi/doi/10.1128/MCB.01360-07.

Xue, W. et al., 2007. Senescence and tumour clearance is triggered by p53 restoration in murine liver carcinomas. *Nature*, 445(7128), pp.656–60. Available at: http://www.nature.com/doifinder/10.1038/nature05529 [Accessed July 21, 2014].

Yauch, R.L. et al., 2008. A paracrine requirement for hedgehog signalling in cancer. *Nature*, 455(7211), pp.406–410. Available at: http://www.nature.com/doifinder/10.1038/nature07275 [Accessed August 11, 2016].

Yoshida, D. et al., 2010. The CXCR4 antagonist AMD3100 suppresses hypoxia-mediated growth hormone production in GH3 rat pituitary adenoma cells. *Journal of neuro-oncology*, 100(1), pp.51–64. Available at: http://www.ncbi.nlm.nih.gov/pubmed/20309720 [Accessed July 27, 2011].

Young, A.R.J. et al., 2009. Autophagy mediates the mitotic senescence transition. *Genes & development*, 23(7), pp.798–803. Available at: http://www.ncbi.nlm.nih.gov/pubmed/19279323 [Accessed September 5, 2016].

Yu, Y.-C. et al., 2013. Radiation-induced senescence in securin-deficient cancer cells promotes cell invasion involving the IL-6/STAT3 and PDGF-BB/PDGFR pathways. *Scientific Reports*, 3, pp.378–383. Available at: http://www.nature.com/articles/srep01675 [Accessed August 18, 2016].

Yun, M.H., Davaapil, H. & Brockes, J.P., 2015. Recurrent turnover of senescent cells during regeneration of a complex structure. *eLife*, 4. Available at: http://www.ncbi.nlm.nih.gov/pubmed/25942455 [Accessed September 5, 2016].

Zhang, C.-F. et al., 2014. Suppression of Autophagy Dysregulates the Antioxidant Response and Causes Premature Senescence of Melanocytes. *The Journal of investigative dermatology*, (April), pp.1–27. Available at: http://www.ncbi.nlm.nih.gov/pubmed/25290687 [Accessed October 10, 2014].

Zhang, D., Wang, H. & Tan, Y., 2011. Wnt/β-Catenin Signaling Induces the Aging of Mesenchymal Stem Cells through the DNA Damage Response and the p53/p21 Pathway A. J. Cooney, ed. *PLoS ONE*, 6(6), p.e21397. Available at: http://dx.plos.org/10.1371/journal.pone.0021397 [Accessed August 30, 2016].

Zhang, S. & Cui, W., 2014. Sox2, a key factor in the regulation of pluripotency and neural differentiation. *World journal of stem cells*, 6(3), pp.305–11. Available at: http://www.ncbi.nlm.nih.gov/pubmed/25126380 [Accessed July 10, 2016].

Zheng, Z.-Y. et al., 2015. Wild-Type N-Ras, Overexpressed in Basal-like Breast Cancer, Promotes Tumor Formation by Inducing IL-8 Secretion via JAK2 Activation. *Cell Reports*, 12(3), pp.511–524.

Zhu, J. & You, C., 2015. Craniopharyngioma: Survivin expression and ultrastructure. *Oncology Letters*, 9(1), pp.75–80.

Zhu, X., Gleiberman, A.S. & Rosenfeld, M.G., 2007. Molecular Physiology of Pituitary Development : Signaling and Transcriptional Networks. *Physiological Reviews*, 87(1), pp.933–963.

Zhu, Y. et al., 2015. The Achilles' Heel of Senescent Cells: From Transcriptome to Senolytic Drugs. *Aging Cell*, p.n/a--n/a. Available at: http://dx.doi.org/10.1111/acel.12344.

Zoicas, F. & Schöfl, C., 2012. Craniopharyngioma in Adults. *Frontiers in Endocrinology*, 3.

Available at: http://journal.frontiersin.org/article/10.3389/fendo.2012.00046/abstract [Accessed February 14, 2017].

Zomer, A. et al., 2013. Brief report: Intravital imaging of cancer stem cell plasticity in mammary tumors. *Stem Cells*, 31(3), pp.602–606.

Zou, Y.R. et al., 1998. Function of the chemokine receptor CXCR4 in haematopoiesis and in cerebellar development. *Nature*, 393(6685), pp.595–9. Available at: http://www.ncbi.nlm.nih.gov/pubmed/9634238.